PhD degree in Systems Medicine (curriculum in Molecular Oncology)

European School of Molecular Medicine (SEMM),

University of Milan and University of Naples "Federico II"

Settore disciplinare: BIO/11

New findings into target-directed microRNA degradation mechanism

Carmela Rubolino

Italian Institute of Technology

Tutor: Dr. Francesco Nicassio

Italian Institute of Technology

PhD Coordinator: Prof. Saverio Minucci

Anno accademico 2021-2022

Table of Contents

Table of Figures

List of Abbreviations

ACPL2 (acid phosphatase-like 2)

AGO (Argonaute)

AMO (anti-miRNA oligonucleotides)

ANGPTL4 (Angiopoietin Like 4)

ATM (ATM Serine/Threonine Kinase)

BARD1 (BRCA1-associated RING domain protein 1)

BC (breast cancer)

BCL2L11 (BCL2 Like 11)

B-CLL (B-cell chronic lymphocytic leukemia)

BRCA1 (BReast CAncer gene 1)

BRCA2 (BReast CAncer gene 2)

C8orf58 (Chromosome 8 Open Reading Frame 58)

CCR4 (C-C Motif Chemokine Receptor 4)

CDH1 (epithelial cadherin)

CHEK2 (Checkpoint kinase 2)

circRNAs (circular RNAs)

CLDN1 (Claudin 1)

CNV (Copy number variation)

CPC (Copies per cell)

CPM (counts per million)

CRISPR (Clustered Regularly Interspaced Short Palindromic Repeats)

CRISPRi (CRISPR interference)

CRKL (CRK Like Proto-Oncogene, Adaptor Protein)

CRL (Cullin-RING E3 ubiquitin ligase)

CS (conserved)

CSC (Cancer stem cells)

CTGF (connective tissue growth factor)

DDX6 (DEAD-Box Helicase 6)

DGCR8 (DiGeorge Syndrome Critical Region 8)

DIS3L2 (DIS3 Like 3'-5' Exoribonuclease 2)

DMEM (Dulbecco's Modified Eagle Medium)

DNMT1 (DNA Methyltransferase 1)

EBAX-1 (Elongin BC-binding axon regulator)

eIF4E (eukaryotic Initiation Factor 4E)

ELOB (Elongin B)

ELOC (Elongin C)

EMT (Epithelial-Mesenchymal transition)

ER (Estrogen receptor)

ERK (extracellular signal regulated kinase)

EZH2 (Enhancer of Zeste Homolog 2)

FACS (Fluorescence-activated cell sorting)

FBS (Fetal Bovine Serum)

FLT3 (fms related receptor tyrosine kinase 3)

FOXO1 (Forkhead Box O1)

FOXO3a (Forkhead Box O3)

GATA3 (Gata-binding protein 3)

GFP (Green fluorescent protein)

GO (Gene Ontologies)

GTEx (Genotype-Tissue Expression)

GW (growing)

HC (High Confidence)

HCMV (Human cytomegalovirus)

HER2 (Human epithelial receptor 2)

HER2+ (Human epithelial receptor 2 amplified)

HGF (Hepatocyte growth factor)

HMGA2 (High Mobility Group AT-Hook 2)

HSF2 (heat shock transcription factor 2)

HSURs (*Herpesvirus saimiri* U RNAs)

HVS (*Herpesvirus saimiri*)

IQSEC1 (IQ Motif And Sec7 Domain ArfGEF 1)

ITGB3 (Integrin b3)

Kb (Kilobase)

kDa (kilodaltons)

KO (knock-out)

KRAS (Kirsten rat sarcoma)

LIN28A (Lin-28 Homolog A)

LIN28B (Lin-28 Homolog B)

LNA (locked - nucleic - acid antisense oligonucleotides)

lncRNA (long non-coding RNA)

LOX (Lysyl Oxidase)

MAP3K9 (Mitogen-Activated Protein Kinase Kinase Kinase 9)

MAPKAPK2 (Mitogen-activated protein kinase-activated protein kinase 2)

MBC (metaplastic breast cancer)

MCF-7 (Michigan Cancer Foundation-7)

MCMV (Murine cytomegalovirus)

MDE (MiRNA Degradation Element)

MEFs (Mouse embryonic fibroblasts)

MFE (minimal free energy)

miRNAs (microRNAs)

MMP9 (Matrix Metallopeptidase 9)

MRE (miRNA responsive element)

MRP1 (multidrug-resistance associated protein 1)

MYOD1 (Myogenic Differentiation 1)

NCS (Non-conserved)

NGFR (Nerve Growth Factor Receptor)

NK-AML (Normal karyotype acute myeloid leukemia)

NOT (Negative regulator of transcription)

NREP (Neuronal regeneration related protein)

PABPC (Polyadenylate-binding protein)

PAI-1 (Plasminogen activator inhibitor-1)

PALB2 (Partner and localizer of BRCA2)

PAN (Poly-A specific ribonuclease subunit)

PARN (Poly-A specific ribonuclease)

PDAC (Pancreatic ductal adenocarcinoma)

PDCD4 (Programmed Cell Death 4)

PDGF (Platelet derived growth factor)

PNPase^{old-35} (Polyribonucleotide Phosphorylase)

Pol II (RNA polymerase II)

PR (Progesterone receptor)

PTEN (Phosphatase and Tensin homolog)

PTMs (Post-translational modifications)

RAD51C (RAD51 homolog C)

Ras (Rat Sarcoma Protein)

RBM4 (RNA Binding Motif Protein 4)

REEP4 (Receptor Accessory Protein 4)

RFP (Red fluorescent protein)

RING (Really Interesting New Gene)

RISC (RNA-induced silencing complex)

RLU (Relative Light Unit)

Robo (Roundabout)

RPKM (Reads Per Kilobase of exon per Million mapped reads)

RPLP0 (Ribosomal Protein Lateral Stalk Subunit P0)

RRP41 (Ribosomal RNA-processing protein 41)

RT-qPCR (Quantitative reverse transcription PCR)

SEM (Standard Error of the Mean)

SERPINE1 (Serpin Family E Member 1)

sgRNAs (single guide RNAs)

shRNAs (short-hairpin RNAs)

SMAD2 (Mothers against decapentaplegic homolog 2)

SNAI1 (Snail Family Transcriptional Repressor 1)

SNORD72 (Small Nucleolar RNA, C/D Box 72)

SNPs (Single nucleotide polymorphisms)

sRNA (small RNA)

sRNA-seq (small RNA-sequencing)

TCGA (The Cancer Genome Atlas)

TDMD (Target-directed miRNA Degradation)

TDTT (Tailing and target-directed trimming)

TGF-β (Transforming Growth Factor-β)

TGFβR2 (Transforming growth factor, beta receptor II)

TMEM196 (Transmembrane Protein 196)

TNBC (Triple-negative breast cancer)

TNRC6 (Trinucleotide repeat-containing gene 6 protein)

TNTases (Terminal nucleotidyl transferases)

TPM (Target per miRNA)

TRBP (TAR RNA-binding protein)

TSBs (Target Site Blockers)

Tsp-1 (thrombospondin-1)

TUT1 (Terminal Uridylyl Transferase 1)

TUT2 (Terminal Uridylyl Transferase 2)

TWF1 (Twinfilin 1)

TWIST1 (Twist-related protein 1)

TWIST2 (Twist-related protein 2)

TYRP1 (Tyrosinase related protein 1)

Ubc9 (Ubiquitin conjugating enzyme 9)

UTR (Untranslated region)

VEGFA (Vascular Endothelial Growth Factor A)

XPO5 (Exportin 5)

XRN (5'-3' exonuclease I)

ZEB1 (Zinc Finger E-Box Binding Homeobox 1)

ZEB2 (Zinc Finger E-Box Binding Homeobox 2)

ZFYVE26 (Zinc Finger FYVE-Type Containing 26)

ZSWIM8 (Zinc Finger SWIM-Type Containing 8)

Abstract

MiRNAs are a class of small non-coding RNAs that function in post-transcriptional gene silencing by interacting with target RNAs. A novel mechanism in control of miRNA levels, called Target-Directed miRNA degradation (TDMD), has been described, which involves specific transcripts able to interact with miRNAs and induce miRNA degradation. We showed that an endogenous RNA transcript, Serpine1, uses TDMD to control levels and activity of miR:30b/c in murine fibroblasts. It is unknown how many other TDMD transcripts exist; therefore, we developed TDMD*finder*, a computational pipeline and free webtool, that identifies "high confidence" TDMD interactions in the Human and Mouse transcriptomes by combining sequence alignment and feature selection approaches. Our predictions suggested that TDMD is widespread, with potentially every miRNA controlled by endogenous targets. We experimentally tested 37 TDMD*finder* predictions, of which 17 showed TDMD effects as measured by RT-qPCR and small RNA sequencing, linking the miR-17, miR-19, miR-30, miR-221, miR-26 and miR-23 families to novel endogenous TDMD triggers. Computational analyses performed using the multiomic TCGA platform substantiated the possible involvement of many TDMD transcripts in human cancer and highlighted 36 highly significant pan-cancer interactions, suggesting TDMD as a new potential oncogenic mechanism. Focusing on the SERPINE1:miR30b/c pair as a model, we applied molecular and genetic approaches to manipulate TDMD and investigate the effects afforded by miRNA degradation in breast cancer. Our results suggested that TDMD is used by breast cancer cells to keep low miRNA activity and provide a selective advantage in various cancer phenotypes. In order to identify all TDMD-regulated miRNAs in breast cancer, we inhibited the TDMD mechanism by knocking down a critical player of the pathway, the ZSWIM8 culling-RING ubiquitin ligase substrate adapter. We repressed ZSWIM8 by CRISPR interference in a set of 8 different breast cancer (BC) cell lines, representing the entire spectrum of BC subtypes. Our analyses showed that loss of ZSWIM8 caused significantly increased accumulation of 31 miRNAs, without any evidence of transcriptional regulation, thus expanding the role of endogenous TDMD in sculpting miRNA levels. Finally, to identify the TDMD triggers in BC, we designed a strategy based on the combined use of TDMD*finder* predictions and experimental CRISPR-based tools. We performed a proof-of-concept validation of the approach by identifying the endogenous TDMD trigger (NREP) for miR-29b-3p in SUM159PT and BT549, proving that this can be an effective strategy to quickly identify TDMD substrates and triggers.

1. Introduction

1.1 MicroRNAs

1.1.1 MicroRNA biogenesis

MicroRNAs (miRNAs) are a class of small non-coding RNAs that act in post-transcriptional regulation of gene expression (Akiyoshi S. et al., 2001, Bartel, 2009). They have evolutionary conserved sequences about 18-25 nt long, which function at post-transcriptional level as guide molecules in RNA silencing through different mechanisms, including target degradation and protein synthesis inhibition (Eulalio et al. 2008; Bartel et al., 2018; Jonas and Izaurralde 2015).

MiRNAs have been initially discovered in invertebrate organisms. In particular, Lee et al. (1993) identified noncoding RNAs (ncRNAs), lin-4 and let-7, required for the proper timing of *C. elegans* development. Subsequently, hundreds of other short RNAs, characterized by highly conserved sequences, were found in worms, flies, plants and mammals, and they were called microRNAs (miRNAs) (Pasquinelli et al., 2000; Lagos-Quintana et al., 2001; Lau et al., 2001; Lee and Ambros, 2001).

MiRNA genes are located all over the genome, both in intergenic and intragenic regions. “Intragenic miRNAs” can be encoded from intron or exon sequences of coding and non-coding genes, while "intergenic miRNAs" can be found in genome areas that are far from transcribed genes (**Figure 1**). Furthermore, miRNA genes could be arranged in the genome as independent transcriptional units or in close proximity to other miRNAs creating a multicistronic primary transcript (Lagos-Quintana et al., 2001; Lau et al., 2001; Lee and Ambros, V., 2001; Ha and Kim 2014). In this case, the transcript consists of multiple hairpins and is processed to generate more miRNAs that are clustered together.

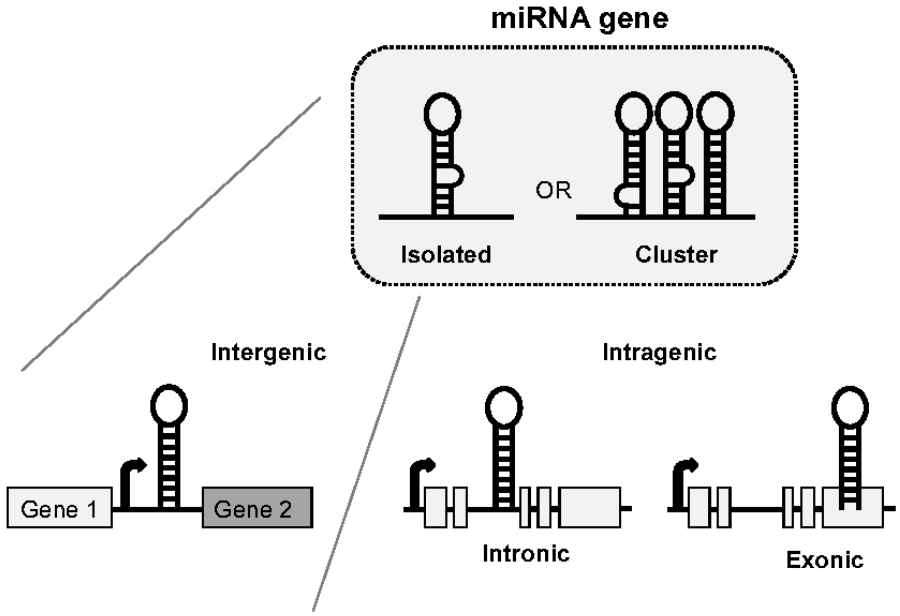

Figure 1. Genomic locations of miRNAs. MiRNA genes are organized as single units or in clusters, and are located in intergenic or intragenic genome regions, including intronic and exonic sequences (Figure from Role of non-coding in Cystic Fibrosis, Chapter 12 Varilh et al, book edited by Dennis Wat, 2015).

The transcription process is coordinated by different transcription factors (i.e. Myc, ZEB1 and ZEB2, MYOD1, p53) that modulate gene expression (Chang et al. 2008; Kim et al. 2009). Also, histone modifications and DNA methylation can regulate the transcription factors recruitment thus promoting or inhibiting miRNA transcription (Davis-Dusenbery and Hata, 2010).

MiRNAs are transcribed by RNA polymerase II (Pol II) which recognizes a promoter region and generates primary transcripts, called pri-miRNAs (Cai et al., 2004; Lee et al., 2004, 2002). These precursors (typically 1kb long) are characterized by a capped single-stranded RNA portion at its 5' followed by a stem and loop region (33-35 nt of length) and a poly-A tail at its 3' end (Ha and Kim, 2014).

Subsequently, each pri-miRNA is processed in the nucleus by Microprocessor, a 364 KDa heterotrimeric complex composed by three proteins: two molecules of the RNA binding protein DiGeorge Syndrome Critical Region 8 (DGCR8) and a ribonuclease III enzyme called Drosha (Denli et al., 2004) (**Figure 2**). In particular, the stem and loop region of the pri-miRNA is recognized by the Microprocessor complex and this allows the cleavage of the primary transcript by the two RNase III domains of Drosha that cut each strand of the stem with a 2 bp offset, and generate a ~60 nt stem-loop called pre-miRNA (Lee et al., 2003). Interestingly, sometimes the Microprocessor complex can trigger the termination of the transcription and this anticipates the 3' end maturation generating transcript without a

poly-A tail (Ballarino et al., 2009).

Microprocessor activity is highly conserved among animal species, and both Drosha and DGCR8 are essential miRNA biogenesis. In fact, the knockout of these genes results in mouse lethality during embryogenesis (Ha and Kim, 2014).

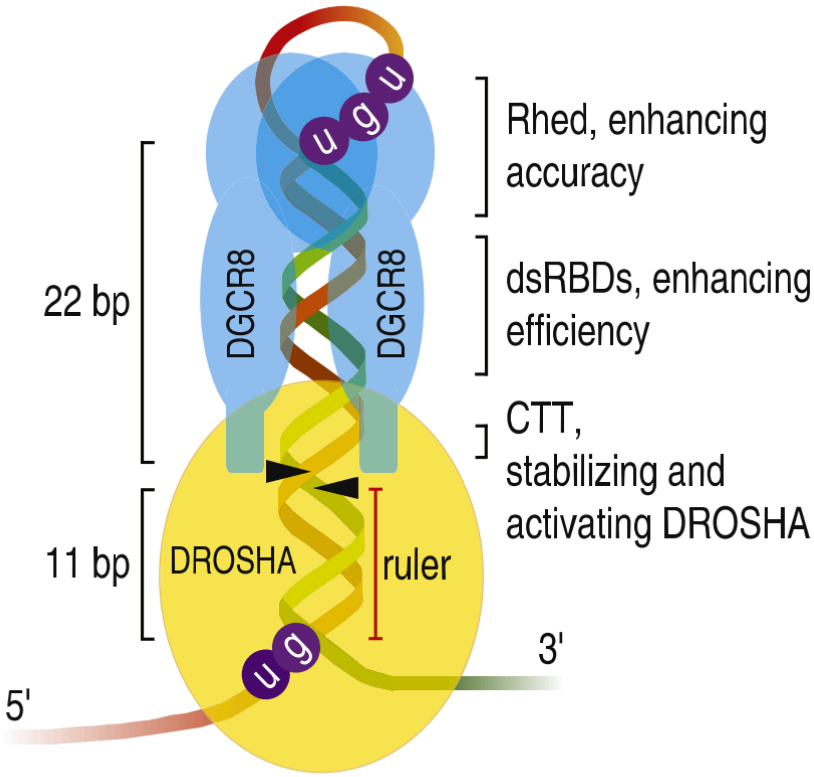

Figure 2. Model of Microprocessor. DGCR8 recognizes an apical UGU motif in Pri-miRNAs which are bound then by Drosha and DGCR8 (Figure from Nguyen et al., 2015).

After this first processing step, the pre-miRNA is exported to the cytoplasm thanks to the formation of a ternary complex with Exportin 5 (XPO5) and Ran-GTP, which diffuses through a nuclear pore. XPO5 seems to protect the pre-miRNA from the nuclease activity of cellular RNases (Yi et al., 2003), while the GTP hydrolysis of Ran-GTP causes conformational changes that releases the pre-miRNA into the cytoplasm. (Bohnsack et al., 2004; Lund et al., 2004). Here, a 200 kDa endonuclease with two RNase III domains, Dicer, cuts both strands near the loop to generate a small miRNA duplex with unmatched ends (2 nt 3' overhang), containing the miRNA paired to its passenger strand (Grishok et al., 2001; Hutvágner et al., 2001) (**Figure 3**).

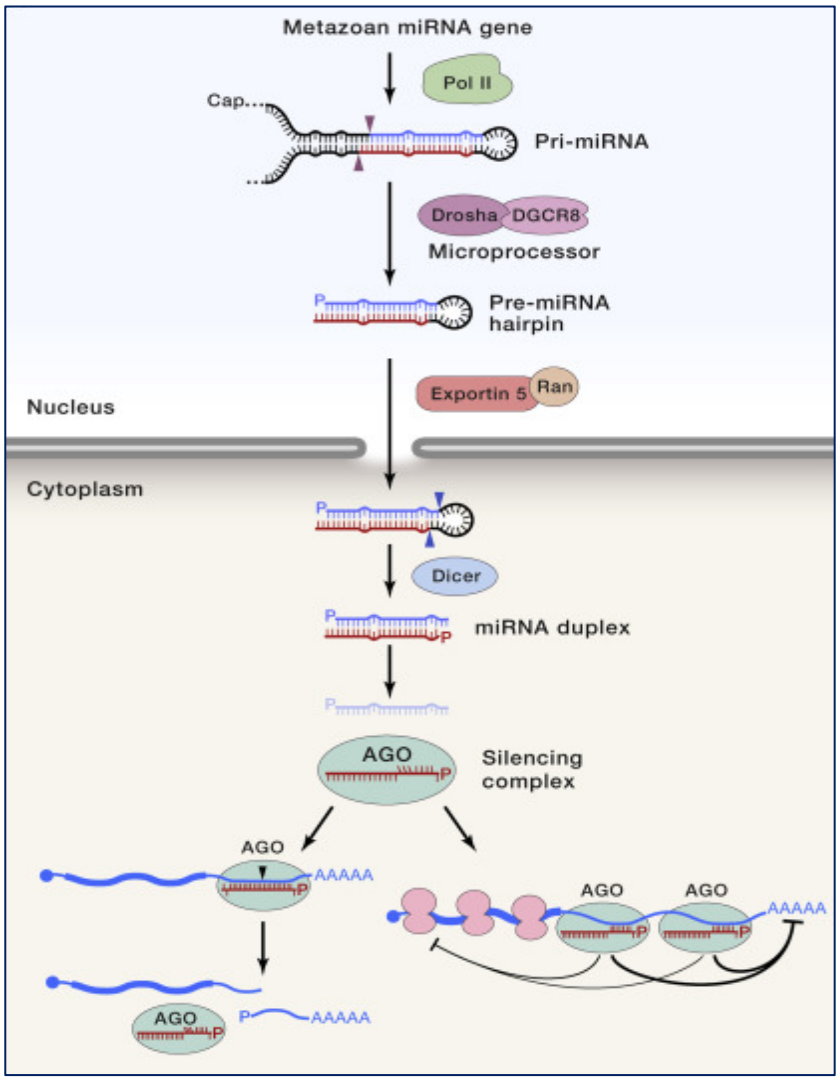

Figure 3. Schematic representation of miRNA biogenesis and function. The canonical pathway of miRNA biogenesis begins with the transcription of a pri-miRNA which is processed by the Microprocessor complex. After exiting the nucleus, a second processing step takes place by Dicer, before the formation of the silencing complex together with the AGO protein. (Figure from Bartel, 2018).

Recently, "non-canonical" miRNAs, with an alternative biogenesis pathway, have been discovered (Bartel, 2018) (**Figure 4**). In particular, some intronic primary miRNA transcripts, called "mirtrons", are processed by the spliceosome which debranches pre-miRNA hairpins (Okamura et al., 2007; Ruby et al., 2007) (**Figure 4B**). Moreover, also endogenous short-hairpin RNAs (shRNAs) and chimeric hairpins have a Drosha-independent processing, bypassing the Microprocessor complex (Andersson et al., 2005; Babiarz et al., 2008; Bellutti et al., 2015) (**Figure 4C, Figure 4D**). Conversely, it has been observed that miR-451 undergoes to Microprocessor-mediated cleavage bypassing Dicer processing (Bartel, 2018) (**Figure 4E**).

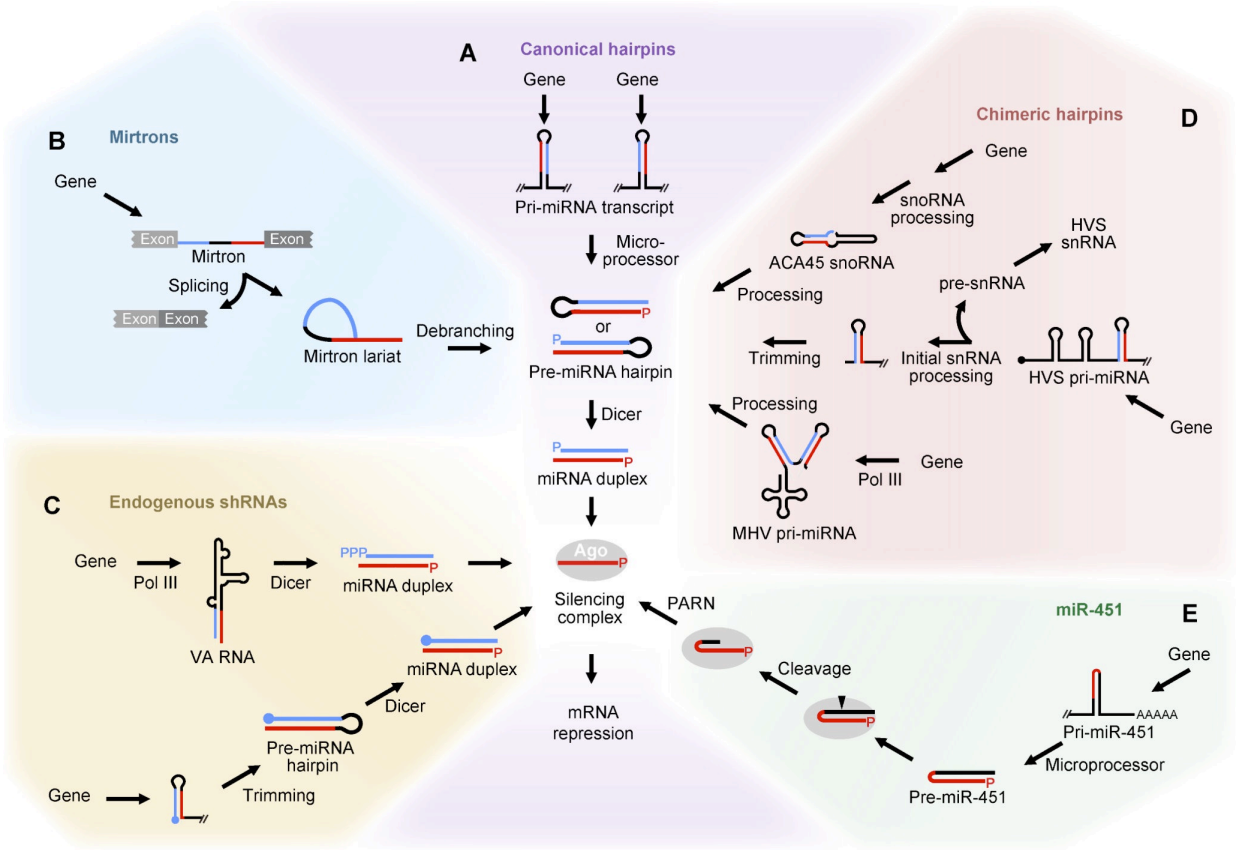

Figure 4. Canonical and non-canonical miRNA biogenesis pathways. In addition to the canonical pathway (A), miRNAs can follow alternative biogenesis. Mirtrons (B), endogenous shRNAs (C) and chimeric hairpins (D) are processed bypassing Microprocessor. The biogenesis of miR-451 (E) is an exception as Dicer is bypassed (Figure from Bartel, 2018).

The Microprocessor activity is regulated by post-translational modifications (PTMs) that consequently miRNA processing (Treiber et al., 2019). The complex is extensively methylated most at the level of arginine residues and this event regulates microRNA biogenesis (Spadotto et al., 2020). In humans, the Dicer action can be modulated by the TAR RNA-binding protein (TRBP), a cofactor which regulates the processing efficiency, tuning the length of mature miRNAs (Ha and Kim, 2014).

Once formed, the duplex is loaded into an Argonaute (AGO) protein to form the pre-RNA-induced silencing complex (pre-miRISC) (**Figure 5**). The loading process requires ATP and the intervention of molecular chaperones (HSC70/HSP90) (Yoda et al., 2010), that mediate AGO conformational opening and the binding of the dsRNA (Iwasaki et al. 2010). Four AGO proteins are known in humans (AGO1-4) and they can bind indistinguishably all human miRNAs (Dueck et al. 2012), As shown in **Figure 5**, AGO proteins are characterized by a bilobar structure formed by different domains. One lobe contains the MID-PIWI domains involved in the binding of the guide strand. The PIWI domain has also a cleavage site important for the slicing activity. The second lobe contains the PAZ domain which

functions as a pocket for the recognition and binding of the 3'complementary site of the miRNA to targets (Kim et al. 2009; Elkayam et al. 2012).

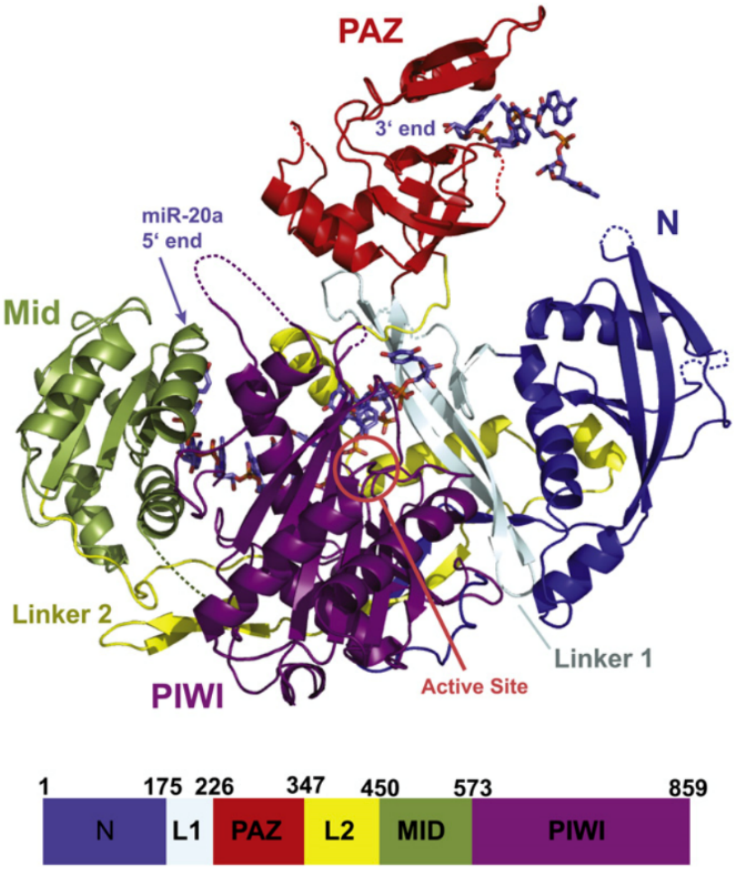

Figure 5. AGO protein structure. The two lobes formed by the MID-PIWI and N-PAZ domains can be observed (Figure from Elkayam et al., 2012).

After the duplex binding has occurred, one of the two strands (passenger strand) is usually released and quickly degraded, while the other will become the final miRNA (guide strand). Probably, the unwinding of the passenger strand is due to the falling of AGO tension during the protein conformational opening (O'Brien et al., 2018).

The choice on which strand will be eliminated and which one will be kept depends on how the duplex bond to the AGO occurs. In particular, it depends on thermodynamic stability of the two ends of the dsRNA. In fact, AGO protein has a pocket that binds the duplex with a preferred orientation. Specifically, the pocket binds either a 5'-terminal pU or pA of the guide strand (Frank et al., 2010; Suzuki et al., 2015) or a 5'-nucleoside monophosphate of the strand with a lower 5' stability (Khvorova et al., 2003; Schwarz et al., 2003).

The activity of AGO proteins is subjected to a fine regulation. Specifically, hydroxylation enhances AGO2 stability and promotes its localization in the processing bodies (p-bodies),

which are distinct foci in the cytoplasm where enzymes involved in mRNA turnover are located. (Ha and Kim, 2014).

Another post-translational modification that AGO can undergo is phosphorylation that can be carried out by different proteins such as MAPKAPK2 and AKT3. In the first case, MAPKAPK2 leads AGO localization to p-bodies, while the phosphorylation by AKT3 stimulates translational repression activity.

Conversely, the phosphorylation of Tyr393 upon hypoxia causes Dicer dissociation from the RISC complex and the pre-miRNAs processing inhibition. AGO activity can be also inhibited due to cellular stress or viral infection. AGO stability is enhanced by miRNA loading. In fact, AGO is more suitable to proteasome degradation when its pocket is empty (Ha and Kim, 2014).

The miRNA loaded into AGO generates an effector complex called RNA-induced silencing complex (RISC) which promote mRNA repression at post-transcriptional level (Hammond et al., 2001; Mourelatos et al., 2002).

1.1.2 MicroRNA mechanism of action

Once the RISC complex is constituted, the target RNAs can be recognized thanks to a pairing of their sequence with sequence of the miRNA loaded on AGO (**Figure 6**). Precisely, the target recognition sequence is called "miRNA responsive elements" (MREs), and is generally located at the 3'-UTR. MRE consists in a region of 6 nucleotides complementary to the miRNA seed sequence, which includes miRNA nucleotides 2-7 (**Figure 6A**).

In some cases, atypical canonical sites, consisting in a supplementary pairing of the miRNA 3'-region involving nucleotides 13-16, can take place (Grimson et al., 2007; Wee et al., 2012; Salomon et al., 2015) (**Figure 6B**).

Similarly, also non-canonical sites have been highlighted. These sites have incomplete pairing to the seed region and extensive pairing to the 3' of the miRNA at nucleotides 13-16. (Bartel, 2009) (**Figure 6C**).

The complementarity between miRNAs and RNA targets is limited, so a very high number of RNAs could interact with a single miRNA.

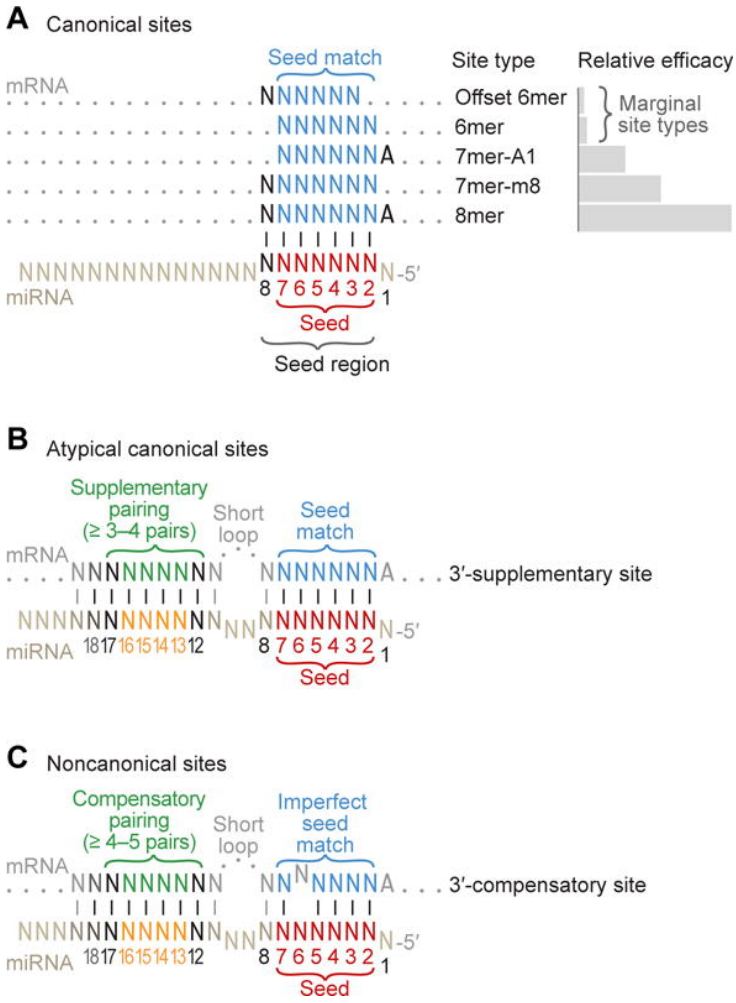

Figure 6. MicroRNA Target Sites. MiRNAs bind target through seed interaction. Different types of interaction are possible, based on the presence of canonical (A), atypical canonical (B) and noncanonical (C) sites (Figure from Bartel, 2018).

After the recognition between the target RNA and the miRNA, the transcript repression process can take place in two alternative ways.

In the first way, if the pairing between miRNA and its target is extensive, the miRNA carries on the slicing process by AGO (Hutwagner et al., 2002; Yekta et al., 2004). This mechanism is common in plants (Jones-Rhoades et al., 2006), while in humans and other mammals it has only been observed for 20 cellular transcripts (Davis et al., 2005; Shin et al., 2010), a circular RNA (Hansen et al., 2011) and a few viral mRNAs (Sullivan et al., 2005; Barth et al., 2008).

The second method of repression, typical of humans and many animals, causes mRNA destabilization and translational repression, without mRNA cleavage, and does not require a complete pairing miRNA-target (Carthew and Sontheimer, 2009) (**Figure 7**). To take place, AGO recruits the adapter protein TNRC6, which interacts with the poly(A)-binding protein PABPC associated with the mRNA poly (A) tail. This interaction leads to the recruitment of the PAN2 – PAN3 and CCR4 – NOT complexes (Jonas and Izaurralde, 2015), two

deadenylases that shorten the poly (A) tail causing destabilization of the mRNA with decapping and 5′-to-3′ exonucleolytic decay (Chen and Shyu, 2011).

Furthermore, CCR4 – NOT inhibits translation recruiting DDX6, a helicase that binds the decapping complex and interacts with eIF4E transporter (4E-T) which enhances both the decay and translational repression of miRNA targets (Kamenska et al., 2014, 2016; Nishimura et al., 2015).

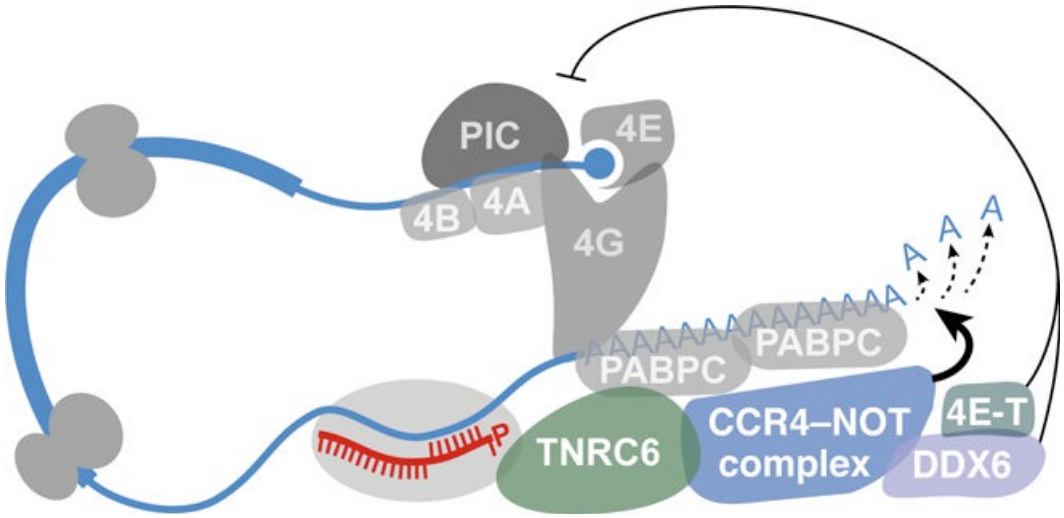

Figure 7. The silencing complex. The main mechanism of mRNA repression by miRNAs requires the interaction of different proteins in order to cause mRNA decay (Figure from Bartel, 2018).

1.2 MiRNA degradation

Cellular levels of miRNA are the result of a balance between biogenesis and decay processes. The latter mechanisms are certainly less known than the biosynthetic ones.

Several approaches have been used to study miRNA decay. In particular, it is possible to block the enzymes involved in the processing of miRNAs. For example, after knock-down of the DICER1 gene, the pre-miRNAs no longer undergo the maturation process and it is possible to evaluate how the levels of pre-existing miRNAs vary over time. Using this approach, Gantier et al. (2011) calculated that miRNAs have a mean half-life of 5 days, with a range from 4 to 9 days for most miRNAs.

Another approach uses actinomycin-D, a molecule that binds to DNA in the transcription initiation complex, preventing RNA elongation and inhibiting transcription (Sobell 1985). In this way, it is possible to calculate the decay rates of miRNAs present using different techniques. Bail et al. (2010) measured miRNA levels using microarrays and found that most miRNAs have a long half-life. Similarly, Guo et al. (2015) used RNA sequencing and

confirmed that miRNAs decay slowly. However, they also observed the presence of a subset of miRNAs, mostly containing passenger strands, with high turnover.

So, most miRNAs are very stable and have a long half-life in the cell probably thanks to AGO proteins, which hide both 5' and 3' ends of miRNAs from the degradation by cellular RNases.

However, it has recently been shown that not all miRNAs exhibit remarkable stability and their turnover can rapidly increase based on cellular context, with short half-lives ranging from <2 h to 10 h (Marzi et al., 2016; Kingston and Bartel, 2019; Reichholf et al., 2019).

Krol et al. (2010) observed in neural cells that some miRNAs show highly variable stability with low half-lives. Rissland et al. (2011) observed similar results in *Schizosaccharomyces pombe* pointing out also how some miRNAs can respond rapidly to transcriptional changes.

In particular, Hwang et al., (2007) demonstrated how the expression of different miRNAs is regulated through the cell cycle. For example, miR-29b exhibits higher levels and a longer half-life in mitotically arrested cells, unlike in cycling cells, where miRNA levels are lower. Obviously, miRNA levels are generally reduced after cell division as the miRNA pool is split between the two newly born cells (Marzi et al., 2016).

Furthermore, it has been observed that growth factors and serum can downregulate miRNA levels (Avraham et al., 2010; Zhu et al., 2012).

Another particular mechanism of regulation of miRNA levels occurs through the "miRNA sponges" represented by circular RNAs (circRNAs), which are produced through a backsplicing process by the splicing machinery (Chen and Yang, 2015). Hansen et al. (2013) discovered that the circRNA CDR1as is capable of decreasing miR-7 levels through a sponging effect, thereby causing the loss of its repressive activity on its mRNA targets.

In addition, in the cytoplasmic environment there are many 3-to-5 'RNA-exonucleases which help to reduce the levels of miRNAs. The action on miRNAs of RNA-exonuclease XRN (5'-3' exonuclease I), RRP41 (Ribosomal RNA-processing protein 41) and PNPase-old-35 (Polyribonucleotide Phosphorylase) has been demonstrated in humans (Bail et al., 2010; Das et al., 2010).

However, since the binding of miRNAs to AGO increases their stability and protects them from degradation, it is necessary that the miRNAs undergo modifications to decrease their affinity to AGO so that they can then be attacked by cytosolic exonucleases.

These modifications may be the result of a miRNA degradation process, called tailing and target-directed trimming (TDTT), favored by highly complementary miRNA targets. In this mechanism, these targets bind to the miRNA in the RISC complex and promote the addition of nucleotides at the 3 'end of the miRNA (tailing) and the elimination of nucleotides at both

the 5' and 3 'ends (trimming), thus promoting its decay (Ameres et al., 2010; Baccarini et al., 2011; Xie et al., 2012).

Finally, miRNA levels can also be regulated by target. This mechanism was first studied in plants (Rüegger and Großhans, 2012), but it has recently been observed in mammals. In particular, it has been described to act on miR-29b, miR-7 and miR-30c/ b by the endogenous RNAs libra / Nrep, Cyrano and Serpine1, respectively (Bitetti et al., 2018; Ghini, Rubolino et al., 2018; Kleaveland et al., 2018).

Specifically, the increased instability of these miRNAs is due to their pairing with a highly complementary target that triggers the decay of the miRNA. This process, called target-directed miRNA degradation (TDMD), is described in detail in the next paragraph.

1.2.1 Target-Directed MicroRNA Degradation (TDMD)

TDMD determines an active degradation of mature miRNAs after their loading on the AGO proteins and the mechanism does not alter either the biogenesis or their processing (Cazalla et al., 2010; de la Mata et al., 2015; Kleaveland et al., 2018).

Interestingly, although the silencing action by miRNAs and its TDMD-dependent decay are opposite processes, both require a miRNA:RNA target pairing.

The difference in the activation of one of the two mechanisms lies in the different miRNA:RNA target interaction, which allows the target to evade the silencing in favor of a destabilization of the bound miRNA (Bartel, 2018).

More precisely, a partial pairing involving the seed region at the 5’-end is able to determine the silencing through mRNA inhibition of translation and degradation.

Conversely, a more extensive and stable pairing at the level of the 3’-end region of the miRNA induces TDMD (**Figure 8**).

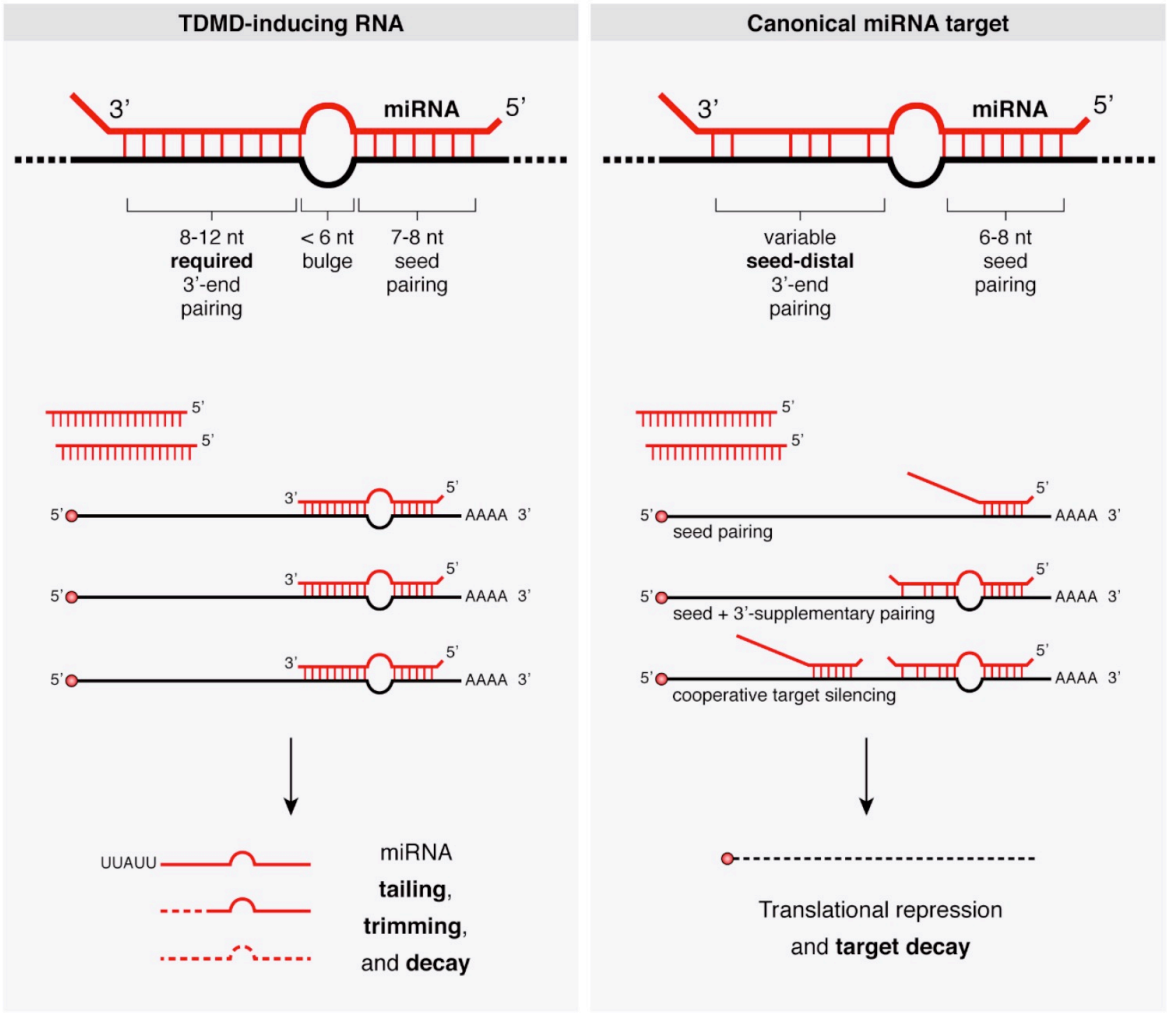

Figure 8. Target binding architectures define the outcomes of miRNA binding. On the right it is shown the typical miRNA-mRNA interaction that leads to translational repression and target decay. On the left, Target-miRNA conformations defining TDMD are displayed. Target RNAs bind to their cognate miRNAs promoting their tailing, trimming and decay (Figure from Fuchs Wightman et al., 2018).

The first insight that RNA sequences could promote miRNA decay is based on artificial target RNA studies in Drosophila. These synthetic RNAs, unlike the target mRNAs, had a large nucleotide pairing with miRNAs and triggered the tailing and trimming processes with subsequent degradation (Ameres et al., 2010). Baccarini et al. (2011) confirmed these observations and highlighted an increase in the decay rate of miRNAs in the presence of the corresponding artificial targets.

It was initially thought that these artificial RNAs could act through the "miRNA sponges" mechanism by sequestering miRNAs and blocking their activity (Carè et al., 2007; Gentner et al., 2009) (**Figure 9A**). However, this mechanism, while blocking miRNAs, did not affect their stability, contrary to TDMD (Ebert et al., 2007).

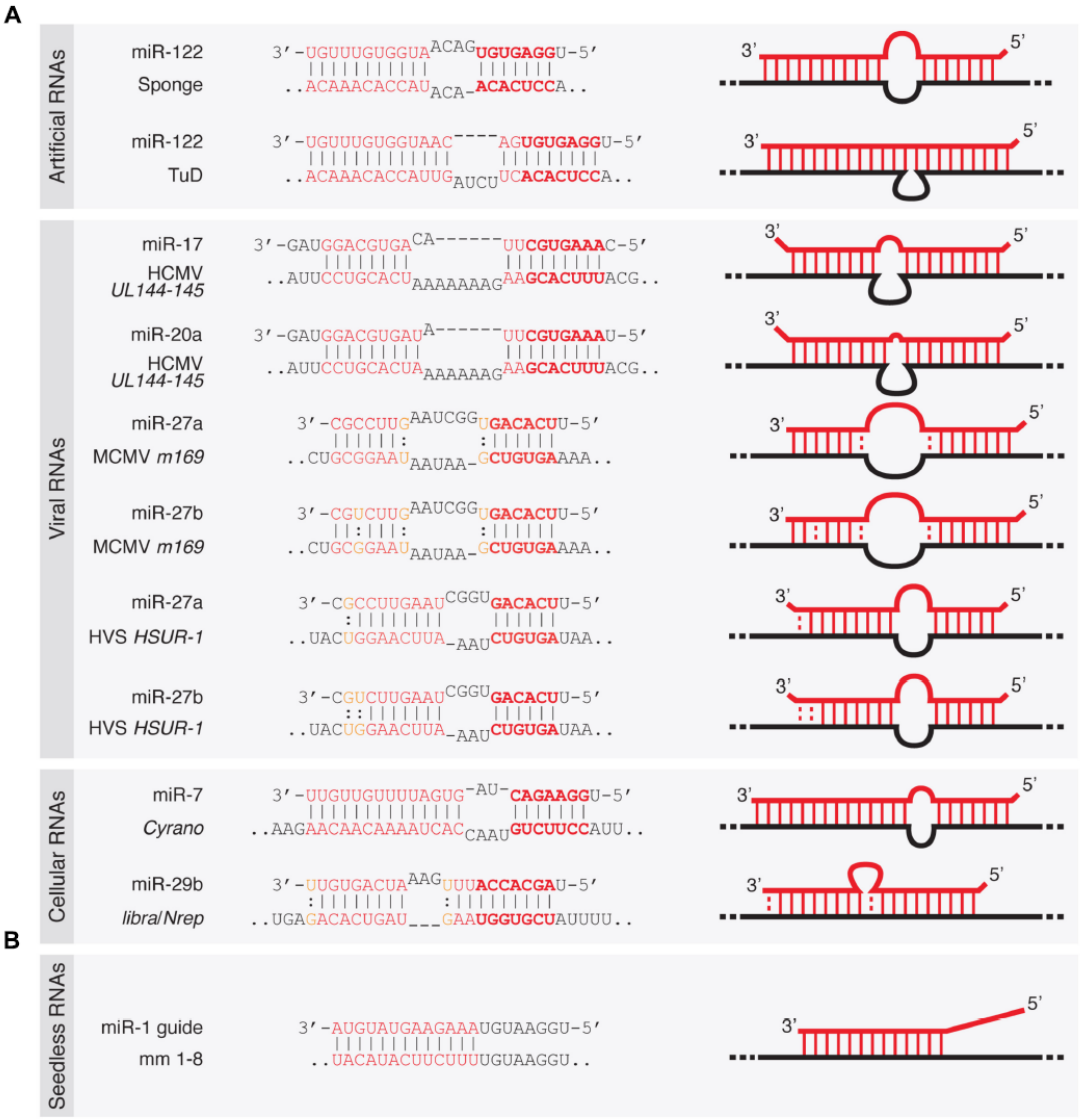

Figure 9. Architecture of TDMD-inducing miRNA binding sites. (A) RNA targets (artificial RNAs, viral RNAs, cellular RNAs) that interact with their cognate miRNAs through the seed region, the bulge and the extended 3' complementarity to induce TDMD. (B) A seedless, non-canonical target is also able to destabilize a miRNA (Figure from Fuchs Wightman et al., 2018).

Subsequent studies noted a variable efficacy of TDMD based on different cell lines. For example, certain artificial targets resulted in modest TDMD-dependent degradation in mammalian non-neuronal cell lines, while on the contrary they induced a more potent effect in neuronal cells (de la Mata et al., 2015; Kleaveland et al., 2018).

The TDMD mechanism can also be used by some viruses which are able to block the miRNAs of the infected host cells (Guo and Steitz, 2014) (**Figure 9A**).

Cazalla et al. (2010) observed this behavior in *Herpesvirus saimiri* (HVS), infecting primate T cells. Here the virus produces seven small non-coding RNAs called HSURs that show complementarity with different cellular miRNAs. Among these, miR-27 creates the most extensive nucleotide pairing which leads to its decay.

Similarly, the murine cytomegalovirus (MCMV) expresses a transcript called m169 which, through its 3'-UTR, pairs with miR-27, stimulating its degradation by the host's TDMD (Libri et al., 2012; Marcinowski et al. al., 2012).

Viruses take advantage of this machinery since eliminating certain miRNAs allows the expression of host genes useful for viral development. After all, many cellular miRNAs are known to interfere with the various stages of viral infection and replication, so viruses may have developed TDMD to counter these cellular defenses (McCaskill et al., 2015).

For example, the human cytomegalovirus (HCMV) activates TDMD mainly against miR-17 and miR-20a, whose elimination determines an increased proliferation of the virus through a greater synthesis of viral DNA (Lee et al., 2013).

Unlike viruses, in metazoans the physiological goal of TDMD is theoretically not completely clear. Despite this, several cellular transcripts, capable of activating the miRNA degradation machinery, have been identified.

Specifically, the *libra* transcript, a long non-coding RNA (lncRNA), was observed in the zebrafish cerebellum to induce the elimination of miR-29b through TDMD.

Similarly, the same miRNA is negatively regulated in mice, as well as in humans, by the *libra* homologous Nrep, an mRNA encoding a small protein. This transcript contains a 20-base sequence in the 3'-UTR complementary to miR-29b. The complementarity site creates an extensive pairing from the 5 'to the 3'-end, except for a mismatch of 3 nucleotides in a central position (**Figure 9A**). If the miR-29b degradation process is altered in mice and zebrafish, for instance by modifying the Nrep pairing site, these organisms show behavioral dysfunctions, thus demonstrating the importance of the process (Bitetti et al., 2018).

Subsequently, Kleaveland et al. (2018) discovered another target RNA, Cyrano, which is able to initiate the decay process of miR-7 (**Figure 9A**). Cyrano is a lncRNA correlated with miR-7 regulation in brain development and brain differentiation (Ulitsky et al., 2011; Smith et al., 2017). However, it was observed that Cyrano KO mice show no relevant abnormalities. On the other hand, however, deletions affecting Cyrano:miR-7 pairing sequence determine in different tissues an increase in miR-7 levels and in its inhibitory action (Kleaveland et al., 2018).

In particular, one of the biological targets of miR-7 that is affected by its repressive action after Cyrano depletion, is Cdr1as, a circRNA, which contains multiple pairing sites with miR-7 and also shows a complementarity with another miRNA, miR-671 (Hansen et al., 2011).

Although Cdr1as is capable of interacting at different sites with both miR-7 and miR-671, however, the observed effects are different. The Cdr1as:miR-7 interaction does not induce

TDMD against miR-7. In fact, in Cdr1as KO mice it has been noted that the levels of miR-7 are also reduced.

Instead, the Cdr1as:miR-671 interaction seems to trigger the TDMD-dependent degradation of the miRNA. As confirmation of this, Piwecka et al. (2017) noted that Cdr1as depletion results in a slight increase in miR-671.

The discovery of the TDMD machinery is very recent and several aspects of this mechanism are still not understood.

The first aspect that must be considered concerns the type of interaction between the miRNA and the RNA target and therefore what characteristics exactly the RNA transcript must have to induce TDMD.

As already described above, TDMD occurs in the presence of an extensive complementarity between miRNA and the transcript, higher than that existing between miRNA and the mRNAs. On the other hand, if an RNA target binds to miRNA in the same way as a mRNA, TDMD would not be triggered (**Figure 10**).

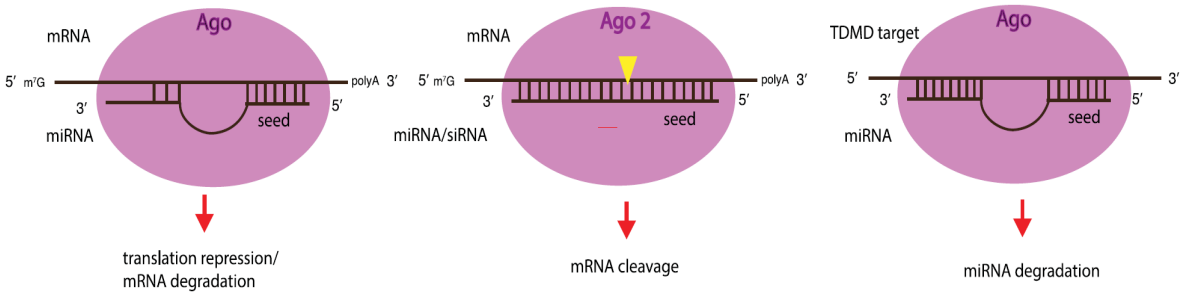

Figure 10. Three known modes of miRNA–target interaction on Ago proteins. Based on the different interactions between miRNA and an RNA target, different outcomes are possible (Figure from Pawlica et al., 2019).

The pairing takes place both in the seed region at the 5' end and in a large region at the 3' end of the miRNA. In the central part there is instead a small bulge.

In vitro and cell cultures studies have attempted to evaluate the number of maximum tolerated mismatches that are still able to initiate the degradation process. Specifically, it has been shown that the presence of a maximum of 8 mismatches at the 3 'end of the miRNA still allow the activation of TDMD (de la Mata et al., 2015).

On the contrary, however, the m169 transcript of HCMV does not tolerate any mismatch in its pairing with miR-27. This could be caused by the presence of a very large bulge in the central region, that would not allow further mismatches (Haas et al., 2016).

Furthermore, although the interaction at the level of the seed region is important, Park et al. (2017) demonstrated that miRNAs can also be destabilized by seedless, non-canonical targets with an extensive 3' end pairing (**Figure 9B**).

Thus, the number of tolerated mismatches varies according to the cell type and the conditions considered. This makes it difficult to identify a single and precise type of binding architecture between miRNA and the target able to trigger TDMD (Fuchs Wightman et al. 2018).

The degradation of miRNAs is closely related to the tailing and trimming processes at the 3' ends of the miRNAs and TDMD is almost always associated with these remodelling modifications.

Terminal nucleotidyl transferase (TNTase), an enzyme belonging to the superfamily of DNA polymerase-beta, intervenes in tailing by adding nucleotides, especially adenosines and uridines, to the 3 'ends of different RNAs, including miRNAs (Martin and Keller, 2017).

Tailing is a process capable of regulating various aspects of the life of an RNA. In addition to the contribution to miRNA degradation, TNTases are also able to regulate the maturation and function of several non-coding RNAs.

A TNTase directly implicated in TDMD seems to be TUT1, although Haas et al. (2016) observed that TUT1 knockdown does not alter the TDMD process, probably due to the presence of other TNTases as well.

Instead, the trimming process starting from the 3'end involves several 3'-to-5' exoribonucleases. Although the PARN enzyme is well known to degrade 3'-tailed miRNAs (Boele et al., 2014; Katoh et al., 2015), currently the exoribonuclease capable of degrading miRNAs after binding to a RNA target appears to be DIS3L2 (Haas et al., 2016).

However, when activated by Cyrano, TDMD proceeds independently of the action of DIS3L2 (Kleaveland et al., 2018). The reason may be due to the action of the enzyme on uridylated targets (Gallouzi and Wilusz, 2013), while in the presence of Cyrano an adenylation of the miRNA is favored.

DIS3L2 was copurified in HeLa cells together with other proteins such as TUT1, the XRN2 exoribonuclease and proteins of the RISC complex (AGO1, 2 and 3, TNRC6B and RBM4), which suggests their connection to the TDMD machinery. Actually, the pairing of the RNA target favors the 3 'tailing of the miRNA when the latter is associated with AGO. Therefore, the TDMD acts in proximity or in association with the RISC complex (de la Mata et al., 2015; Haas et al., 2016).

Particular attention should be paid to the AGO protein which binds miRNAs at the level of the central sequence protecting their two ends. The subsequent binding of the target

determines the exposure of the 3'-end guide strand to the attack of TNTases and 3'-to-5' exoribonucleases.

Several studies have tried to investigate the structure of AGO to better understand its role in the TDMD process. Schirle et al. (2014) noted that AGO adapts its pocket to favor the binding and creates two distinct portions separated by a central one (**Figure 11**).

The first part, the seed chamber, is immediately generated for the association with the seed-paired target RNAs. The second portion, the additional chamber, identified in hAGO2, hosts additional nucleotides and creates the energetically most favorable environment for initiating the early interactions with the guide 3' half (Sheu-Gruttadauria et al., 2019). The central part between the two chambers, consisting of the PIWI and L2 loops, acts as a central gate that blocks the central region of the miRNA. The open gate allows access to the duplex inside an additional central room. The miRNA tail passes inside a narrow channel structure formed by the N and PAZ domains and in the latter, it binds with its 3'-end.

In this way, AGO creates separate chambers inside its pocket that favor the connection with the different functional domains of the guide RNA.

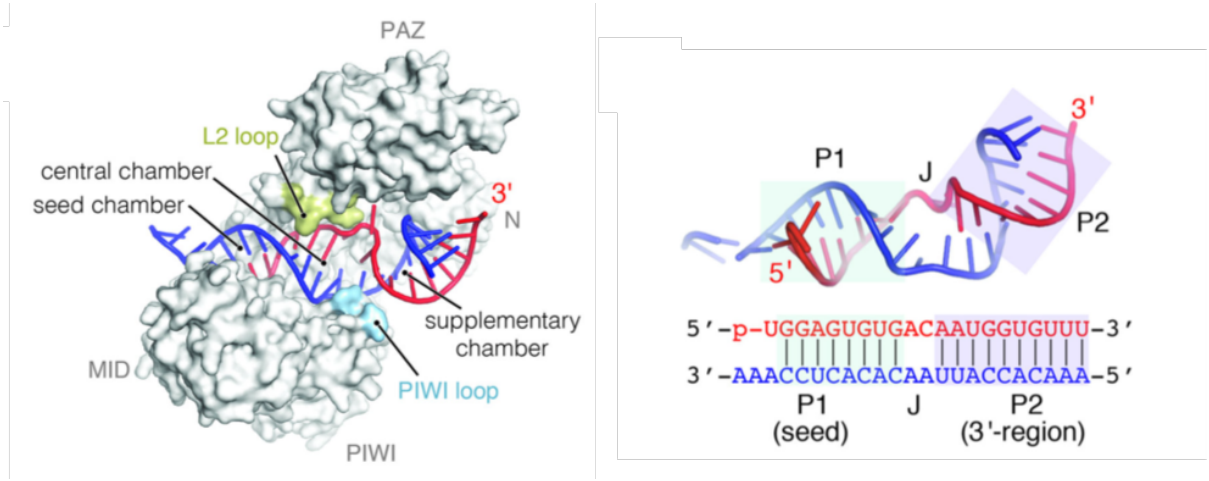

Figure 11. Representation of the hAGO2 structure interacting with the miRNA-RNA target duplex. On the right it is shown a hypothetical miRNA paired with its TDMD target. On the left, the different domains of the hAGO2 protein create chambers to accommodate the duplex (adapted by Sheu-Gruttadauria et al., 2019).

Sheu-Gruttadauria et al. (2019) generated a crystal structure of hAgo2 bound to both miRNAs and TDMD targets. They observed that the complex assumes a conformation in which the central gate is open, while the guide RNA and the target are wrapped around each other. When this happens, the 3' end of the miRNA detaches from the hydrophobic portion of the binding pocket and is exposed to the hydrophilic cellular environment where it can undergo remodeling by tailing and trimming enzymes (**Figure 12**).

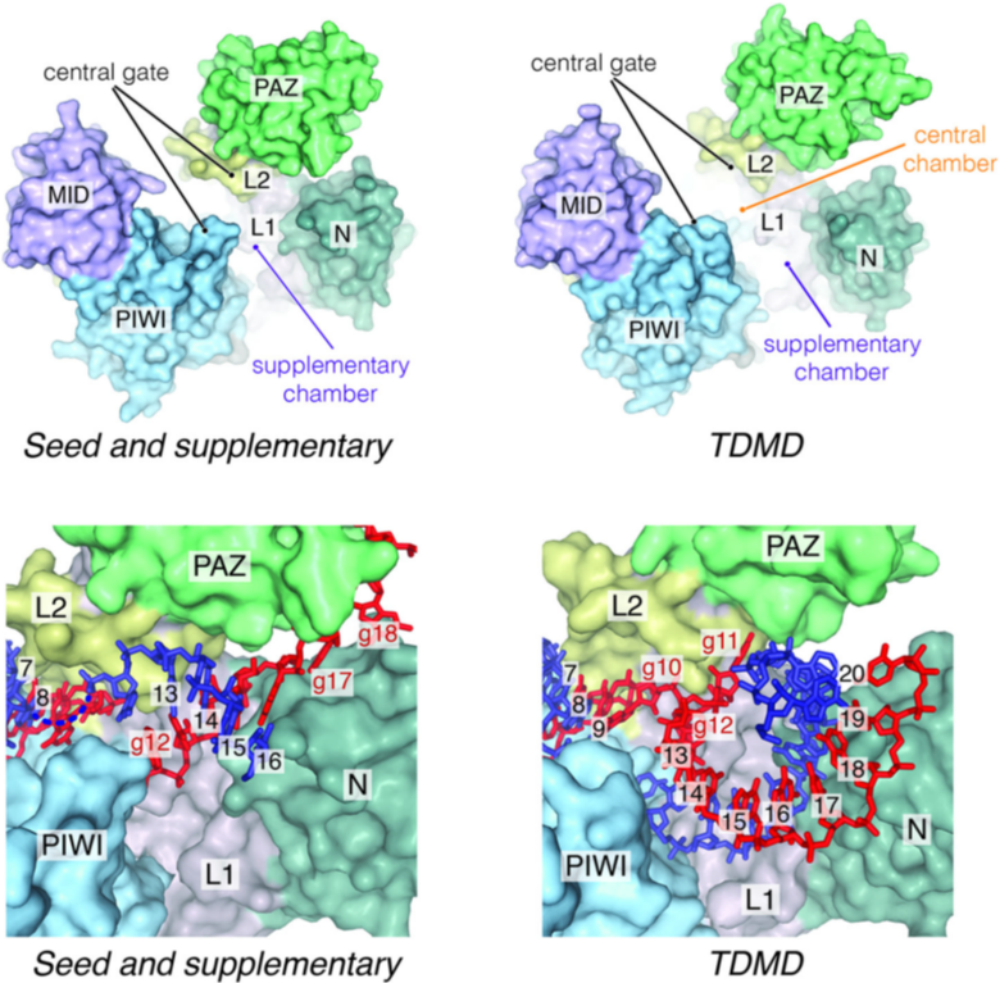

Figure 12. The structural model for extended miRNA-target pairing. On the top, the representations of the seed and supplementary (left) and TDMD (right) conformations are shown. Below, the supplementary chambers of the seed and supplementary (left) and TDMD (right) conformations are zoomed in to show the duplex bond. The numeric labels represent the RNA base-pairs, while the red alphanumeric labels describe non-paired miRNA nucleotides (Adapted by Sheu-Gruttadauria et al., 2019).

Confirmations of this model also derive from target RNA mutagenesis experiments which prove the importance of pairing with miRNA to create a flexible bipartite duplex.

Probably, the entire process proceeds in a discontinuous manner and is regulated by various checkpoints that correspond to the achievement of low-energy conformations, starting from the pairing with the seed region. Passing each checkpoint allows the passage to the next phases. Furthermore, before reaching the slicing phase, an extension of the central and additional chamber is necessary to accommodate the paired duplex. Therefore, a further movement of the N domain is required. This domain also serves to facilitate the unwinding of the guide-passenger RNA duplex during miRNA loading (Faehnle et al., 2013; Hauptmann et al., 2013; Nakanishi et al., 2013).

1.2.2 ZSWIM8 protein

The work of Sheu-Gruttadauria et al. (2019) underlines the importance of extensive pairing at the 3' end which promotes conformational changes both in the AGO protein and the miRNA. Consequently, the separation of the miRNA 3'end from its binding pocket in the PAZ domain takes place, making the 3' region vulnerable to exposure to tailing and trimming. These processes both occur while the miRNA is still bound by AGO (de la Mata et al., 2015; Haas et al., 2016).

Therefore, the study of this system leads to a TDMD model whereby tailing marks the miRNA for trimming and, subsequently, degradation by cellular nucleases is favored (Wyers et al., 2005; Rissland and Norbury, 2009; Lim et al., 2014).

However, there are still some inconsistencies in linking TDTT to TDMD. For example, in some cases, TDTT may be stimulated without a detectable degradation of the miRNA, or, on the contrary, TDMD activation has been described without having tailing and trimming processes.

In fact, Kleaveland et al. (2018) observed that blocking the tailing of miR-7 through deletion of the PAPD4 enzyme (TENT2 / TUT2 / GLD2) did not alter the Cyrano-dependent miR-7 degradation, demonstrating that the tailing process is not essential for trigger the decay.

So, it is clear that additional factors are needed to perfect the TDMD machinery.

Two recent studies carried out by Shi et al. (2020) and Han et al. (2020) performed a CRISPR screen to identify the protein-coding genes needed to reduce the level of miR-7 in K562 cells. The authors identified the ZSIWM8 protein, whose depletion determines a significant increase in miR-7 levels.

Furthermore, small RNA-seq (sRNA-seq) experiments showed that the increase in miR-7 corresponded to an increase only in the guide strand and not in the passenger strand. This effect has also been observed with CYRANO knockdown and is consistent with the fact that TDMD acts after the miRNA loading on AGO and therefore the change of the content affects only the guide strand.

In contrast, transcription and processing, that are two other processes that affect miRNA levels, have an effect on both the guide and the passenger strand.

It was also observed that a certain variability in the length of the miR-7 guide strand in the 3' end, demonstrating the presence of the tailing and trimming processes. Further experiments identified many other ZSWIM8-sensitive miRNAs in different cell lines, such as Drosophila S2 cells, mouse embryonic fibroblasts (MEFs), and HeLa and MCF-7 tumor lines Shi et al. (2020). Also, in HCT116 cells, Han et al. (2020) showed the induction of ZSWIM8-mediated TDMD for the miR-29b, after pairing with the Nrep transcript.

ZSWIM8 is a Cullin-RING E3 ubiquitin ligase (CRL), made up of 1837 amino acids in humans (**Figure 13**). CRLs are involved in the protein ubiquitin-dependent degradation by the 26S proteasome (Schreiner et al., 2019). Structurally these ligases contain a Cullin protein, which acts as a scaffold to link the substrate receptor with a RING-finger protein. The latter is associated with ubiquitin-binding E2 enzymes, thus promoting substrate ubiquitination (Hua and Vierstra, 2011).

ZSWIM8 belongs to a subclass of CRLs that use Elongin B (ELOB / TCEB2) and Elongin C (ELOC / TCEB1) as adapter proteins to link the substrate receptor to the Cullin protein (Mahrour et al., 2008).

Consequently, ZSWIM8 possesses a domain to bind Cullin, a BC domain to bind two Elongin proteins and also a zinc finger domain whose precise function is not known (Wang et al., 2013). These three domains correspond to the first 208 amino acids of the protein which is highly conserved in different organisms.

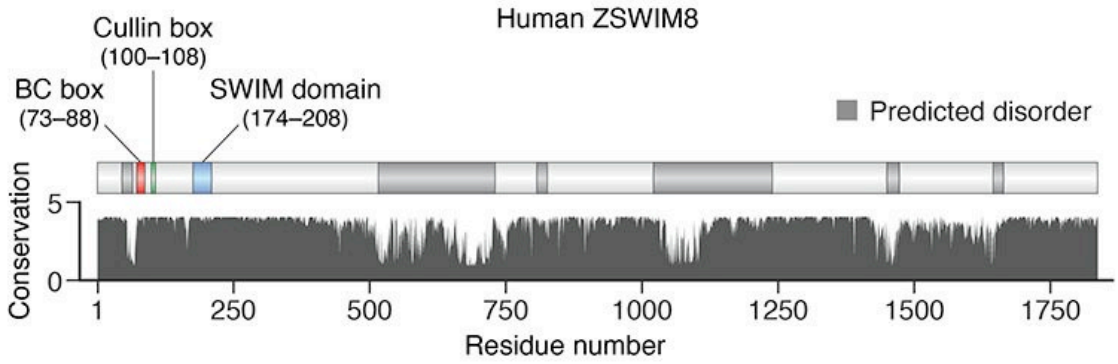

Figure 13. The domain structure and conservation of human ZSWIM8. Most of the protein is highly conserved. The three functional domains are located near the N-terminus in the first 208 amino acids (adapted by Shi et al., 2020).

The biological functions of ZSWIM8 have been studied in different animal models.

In flies, the presence of point mutations in the gene leads to lethality (Yamamoto et al., 2014). In *C. elegans*, EBAX-1 (Elongin BC-binding axon regulator), an ortholog of ZSWIM8, is needed in developing neurons to determine the degradation of the SAX-3 / Robo receptor when it is not properly folded (Wang et al., 2013).

In human cells, similarly to what has been observed in C. elegans, ZSWIM8 contributes to the degradation of Robo. Further studies performed in tumor lines show that ZSWIM8 is not required for cell viability, but generally confers a fitness advantage (Shi et al., 2020).

1.2.3 TDMD E3 model

The mechanism of action of ZSWIM8 within the TDMD pathway is not completely know. It was hypothesized that ZSWIM8 could act by regulating the expression of Cyrano, but it was observed that ZSWIM8 knockdown has no significant effects on Cyrano levels and vice versa. However, both require the presence of the other to influence miRNA levels and, more precisely, Cyrano is located upstream in the pathway (Shi et al., 2020).

A new TDMD model, called E3 model, is therefore defined, according to which ZSWIM8 senses the conformational changes that occur when the target RNA pairs with the 3' region of the miRNA (**Figure 14**).

Subsequently, the polyubiquitination of AGO is stimulated and lead to its degradation by the proteasome. The destruction of AGO exposes the miRNA to the action of some not yet identified cellular exonucleases, with consequent degradation and release of the undamaged trigger, as it is protected by the presence of the 5 'cap and the 3' poly (A) tail. Then the RNA target can act again by associating itself with a new miRNA (Kleaveland et al., 2018).

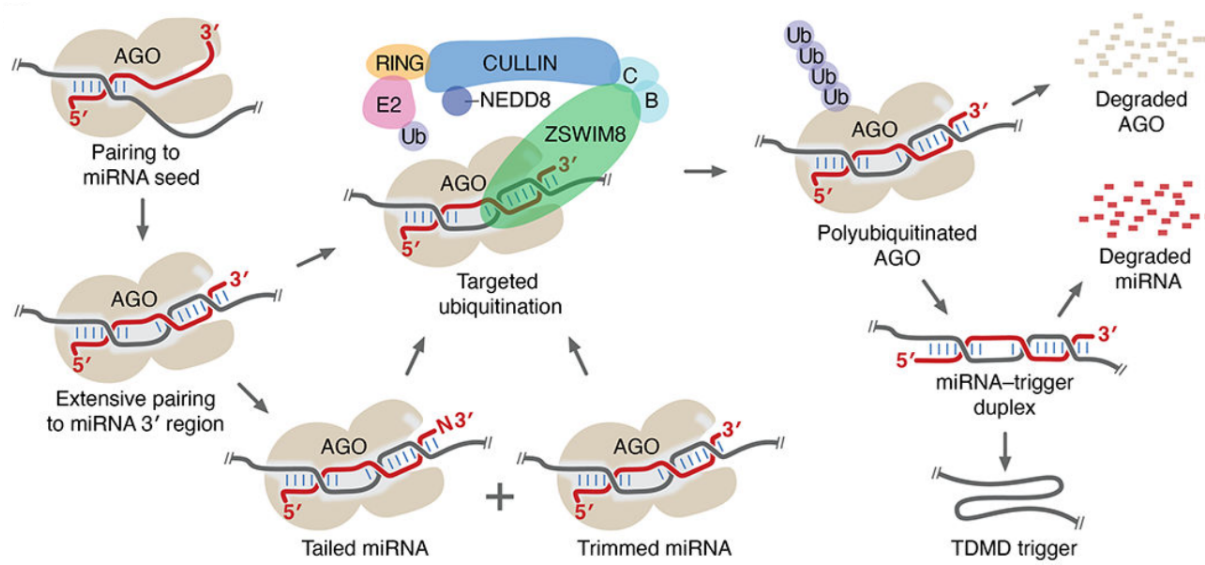

Figure 14. The E3 model of TDMD and its interplay with TDTT. After the pairing to miRNA seed and 3' region, ZWIM8 activates the polyubiquitination of AGO leading to its degradation. The loss of AGO causes miRNA decay, while the RNA target is recovered. Tailing and trimming processes can take place but are not indispensable (adapted by Shi et al., 2020).

Polyubiquitination of AGO occurs at the level of lysine residues. 25 lysine residues have been identified on the surface of human AGO2 and they are conserved in the four isoforms of the protein. By mutating each of these 25 lysines into arginines, lysine K493 was identified as a critical site for TDMD activity (Han et al., 2020) (**Figure 15**).

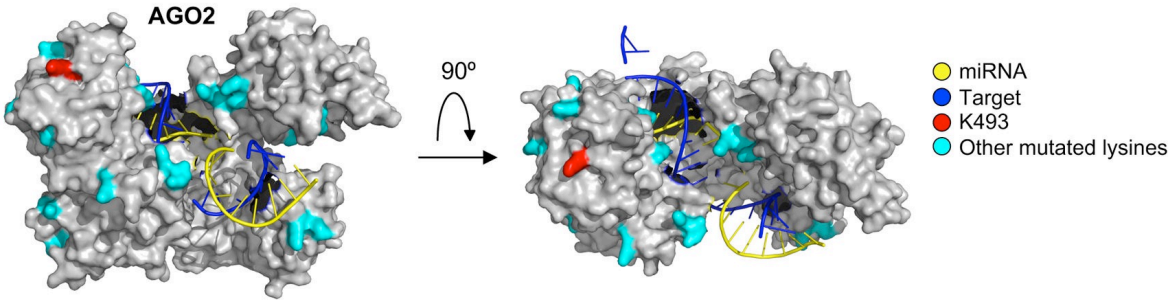

Figure 15. Lysines distribution on the surface of AGO2. The 25 lysines exposed on the AGO2 surface are highlighted in cyan. The red lysine is critical for TDMD (Figure from Han et al., 2020).

This model differs from the previous one which did not propose AGO degradation and considered tailing as a key event to mark miRNA for trimming (Ameres et al., 2010).
Similarly, the E3 model confirms the importance of the conformational changes that occur at the miRNA 3' end and that determine its detachment from the PAZ domain. Conformational changes also occur on the protein complex and determine the enlargement of the internal chamber to facilitate pairing (Sheu-Gruttadauria et al., 2019). ZSWIM8 is able to take advantage of these movements to associate with the complex and create a degron, i.e. a region that regulates protein degradation.
The 3' end of the miRNA is thus exposed and can undergo tailing and trimming processes although these are not essential. Therefore, TDMD does not depend on TDTT, but the two processes can be decoupled. Indeed, inhibiting tailing and trimming by modifying the 2'-OH end of the miRNA does not reduce the miRNA decay rate (Ameres et al., 2010) (**Figure 16**).
Further confirmations of the ZSWIM8-dependent degradation derive from knockdown experiments of genes encoding the accessory proteins ELOB, ELOC and Cullin that determine miRNA accumulation and reduction of its degradation. Furthermore, through coimmunoprecipitation experiments, the ability of ZSWIM8 to polyubiquitinate AGO has been confirmed (Shi et al., 2020).

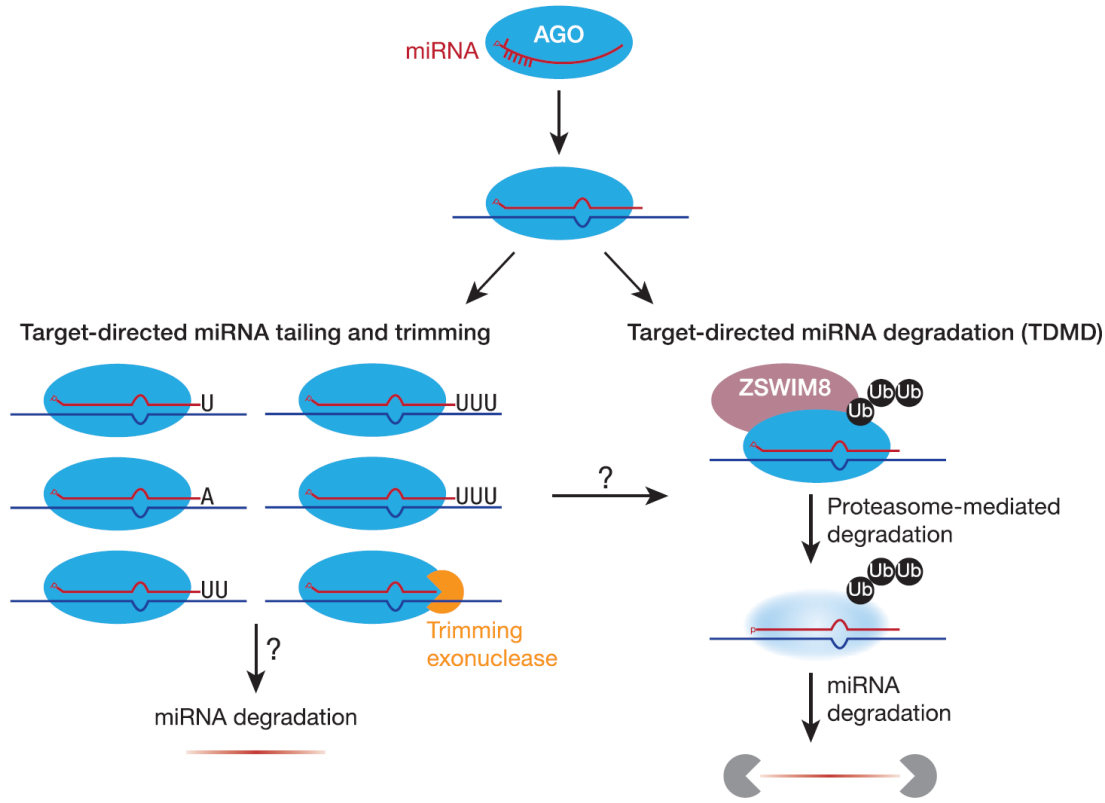

Figure 16. Target-dependent miRNA turnover. MiRNA degradation can occur through two target-dependent mechanisms. TDMD can be decoupled from TDTT, which can take place independently of the former (Figure from Wu and Zamore, 2021).

1.3 MiRNA and Cancer

1.3.1 OncomiR and tumor suppressor miRNAs

Due to their role as cellular regulators, miRNAs are able to modulate the activity of approximately 50% of all protein-coding genes. Consequently, they are implicated in most cellular processes such as proliferation, differentiation, apoptosis, DNA damage and repair, etc. (Krol et al., 2010). Furthermore, miRNAs have been linked to several human pathologies, including viral diseases, immune-related diseases, neurodegenerative diseases and cancers (Li and Kowdley, 2012).

The involvement of microRNAs in tumors has been known for a short time, and precisely from the discovery of genetic deletions and translocations involving the genes of miR-15 and miR-16, in the 70% of patients with B-cell chronic lymphocytic leukemia (B-CLL) (Calin et al., 2002)

Subsequently, it was noted that in many tumor cells the miRNA expression profiles were significantly altered compared to normal cells, demonstrating that certain miRNAs are involved in tumor development and growth (Calin and Croce, 2006).

Based on their altered expression, miRNAs have been classified into oncogenic miRNAs (oncomiR, Onc) and tumor suppressor miRNAs.

In tumors, oncogenic miRNAs are overexpressed and act by repressing tumor suppressor target mRNAs. Known examples of oncomiR are miR125b (Croce, 2009) and the miR-17-92 cluster which is amplified in many solid tumors and lymphomas (Esquela-Kerscher and Slack, 2006; Mogilyansky et al., 2013).

Conversely, tumor suppressor miRNAs, which physiologically suppress the translation of mRNAs encoding oncogenes, are under-regulated in tumors and therefore their oncogenic targets are overexpressed.

Among the tumor suppressors, the families of let-7, miR-30, miRNA-34, miR-200 and miRNA-16 were highlighted, as well as miR-133a, miR-145, miR-143 (Qiu et al., 2013, 2014).

Let-7 is highly expressed with thousands of copies in most cell types, while other tumor suppressor miRNAs may have a more specific expression in certain cells than others. The regulatory action of let-7 is observed at the level of oncogenes, such as Myc, KRAS and HMGA2 (Balzeau et al., 2017). There are 12 members of the let-7 family which are all regulated by two RNA-binding proteins, LIN28A and LIN28B. These proteins bind let-7 pre-miRNA to prevent mature miRNA production (Hagan et al., 2009).

The tumor suppressor role of the miR-30 family is well studied. In colorectal cancer it suppresses cell chemoresistance and stemness (Jiang et al., 2018). In the endothelium, McCann et al. (2019) identified the presence of a pathway, including TGF-β, miR-30c and Serpine1, involved in fibrin production. Alteration of the expression of miR-30c determines the formation of hyperfibrinolytic, dysmorphic vessels that develop in a disorderly manner and contribute to tumor progression.

Regarding miR-34, it plays the role of tumor suppressor in many types of cancer, such as intestinal (Jiang and Hermeking, 2017) and lung (Okada et al., 2018) tumors. Furthermore, some studies have shown its efficacy as a therapeutic agent in preclinical mouse models of breast and prostate cancer (Cheng et al., 2014; Adams et al., 2016).

Instead, the miR-200 family is able to reduce chemoresistance and limit the metastases development. It works by blocking the expression of the transcription factors ZEB1 and ZEB2, thus avoiding the epithelial-mesenchymal transition (EMT) and the action of factors involved in migration and invasiveness (Shimono et al., 2009).

Furthermore, miR-374b, under-expressed in cervical cancer, acts in the p38 / ERK signaling pathway determining a key role in the inhibition of cell proliferation and migration (Li et al., 2018).

However, the subdivision of miRNAs into oncogenics and tumor suppressors is not always so clear-cut and defined. Indeed, in some cases, certain miRNAs can play both roles (Svoronos et al., 2016).

For example, miR-125b has a predominantly oncomiR action in many blood cancers, while it acts as a tumor suppressor in several solid tumors. While it may seem paradoxical, the explanation may lie in the fact that this miRNA has several different targets, including both proapoptotic and antiapoptotic factors, both proliferative and differentiation, and both prometastatic and antimetastatic factors. Thus, probably, the effect of miR-125b will depend on how the balance of expression of these factors is oriented in each tumor. (Shaham et al., 2012; Sun et al., 2013).

Another notable case is miR-155 which is generally considered an oncomiR and is upregulated in many aggressive tumors, where it acts by blocking TGFβR2 expression and promoting cell proliferation and migration, as observed in gastric cancer (Qu et al., 2018).

On the other hand, however, despite its evident oncogenic effects, some authors have observed its ability to act as a tumor suppressor in certain tumors. In particular, by repressing the SKI oncogene, miR-155 is able to inhibit proliferation in various melanoma cell lines (Levati et al., 2011). In FLT3-wildtype normal karyotype acute myeloid leukemia (NK-AML), it plays a proapoptotic role and can stimulate differentiation (Palma et al., 2014). Similarly, it can limits the development of ovarian cancer by acting on SMAD2 and CLDN1, two transcripts encoding a proliferation and differentiation pathway protein and a tight junction protein, respectively (Qin et al., 2013). The same effect can also be observed in stomach cancer (Li et al., 2012), a clearly paradoxical condition considering, as described above, that miR-155 is known to be a potent oncomiR in this tumor.

Another particular case is given by miR-7, which also manifests opposite behaviors. Specifically, it can promote tumorigenesis by stimulating the Ras / ERK / Myc pathway (Chou et al., 2010), but on the contrary it acts as a tumor suppressor, for example preventing the development of chemoresistance through the silencing of the drug efflux transporter MRP1 (multidrug-resistance associated protein 1) (Kalinowski et al., 2014).

The difficulty in many cases of uniquely classifying the behavior of miRNAs in cancer is probably due to the enormous heterogeneity of tumors, in which the presence of innumerable mutations and polymorphisms could alter the pairings between miRNA and mRNA target giving rise to a variability of effects. Furthermore, the fact that miRNAs can have a large number of targets makes the situation even more complicated. Even though it has not yet been demonstrated, it could be hypothesized that some miRNAs may exert opposite effects in different regions of a given tumor (Svoronos et al., 2016).

1.3.2 Aspects of tumor biology regulated by miRNAs

Currently, it can be stated that most cancer hallmarks are subject to miRNA-mediated regulation which are implicated in all steps of tumorigenesis from tumor initiation to metastasis (Goodall and Wickramasinghe, 2021).

The cell cycle is regulated by various oncogenic and tumor suppressor factors. For example, p27 (Kip1) is a cell cycle inhibitor and its levels are very low in several cancers. This tumor suppressor is under the control of miR-221 and miR-222, which are generally overexpressed in many cancers and promote proliferation after targeting with p27 (Kip1) (Galardi et al., 2007; Gillies et al., 2007).

Another very important tumor suppressor is p53, which is mutated in about 50% of human cancers. Several miRNAs have been related to this protein, such as the miR-34 family which is upregulated after induction of p53 through direct activation of the pri-miRNAs of this family (Chang et al., 2007) (**Figure 17**).

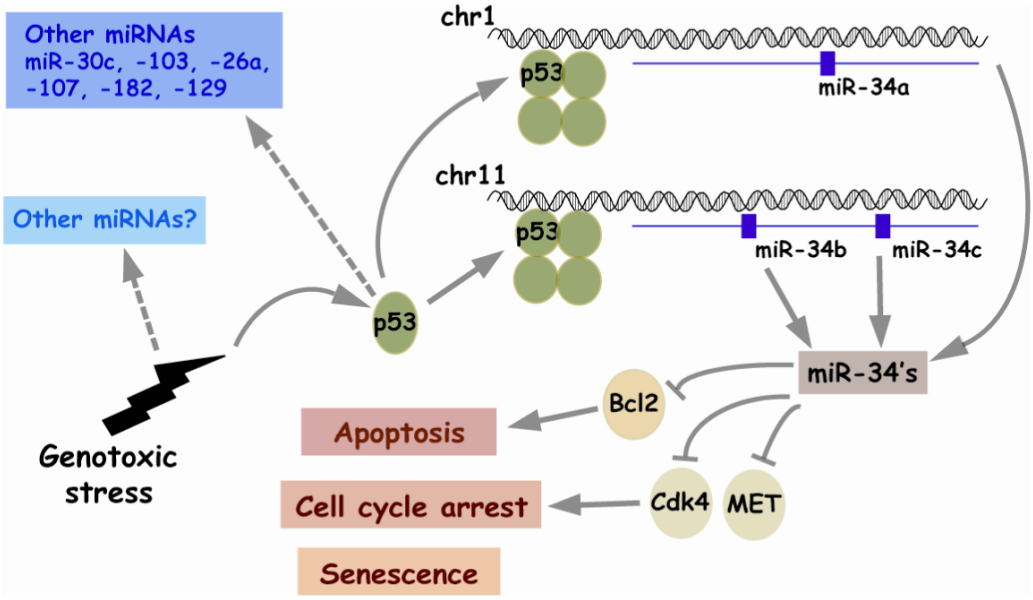

Figure 17. p53 and miR-34 pathway. The miR-34 family acts as a tumor suppressor and is induced by p53 (Figure from Lee and Dutta, 2009).

Other miRNAs that are induced by p53 following DNA damage are miR-30c, miR-103, miR-26a, miR-107 and miR -182 (Lee and Dutta, 2009).

p53 also stimulates apoptosis, a complex and regulated process of programmed cell death. Some miRNAs are involved in this process, such as miR-29b which regulates the expression of the antiapoptotic factor Mcl-1 (Mott et al., 2007). This miRNA is also closely correlated with p53, as it acts targeting the suppressors of p53 and thus stabilizing the tumor suppressor protein (Park et al. 2009)

The distinctive signs of malignant tumors include the ability to invasive and metastasize, and the stimulation of angiogenesis. These processes can also be regulated by miRNAs. In particular, several studies have focused on miR-10b and miR-21. The latter above all is highly upregulated in many tumors and promotes motility and invasion by acting directly on PTEN, a tumor suppressor that is involved in the regulation of the cell cycle and is able to inhibit cell invasion (Meng et al., 2007). PTEN is not the only target of miR-21, which can interact with many other transcripts such as Pdcd4, whose repression determines intravasation and metastasis (Asangani et al., 2007).

As regards tumor angiogenesis, the miR-17-92 cluster appears to be strongly active in this process, due to the Myc stimulation (Fiedler and Thum, 2016). Two cluster members, miR-18 and miR-19 act on CTGF (connective tissue growth factor) and anti-angiogenic factor Tsp-1 (thrombospondin-1) respectively by repressing their expression.

1.3.3 Mechanisms of miRNA dysregulation in cancer

The overexpression and downregulation of different miRNAs in cancer are associated with various dysregulation mechanisms that can intervene in both biogenesis and degradation.

Genetic mutations and epigenetic modifications of miRNA genes by DNA promoter histone hypoacetylation or hypermethylation have been demonstrated in different cancer types (Saito et al., 2006; Hackanson et al., 2008).

Methylation of CpG islands at the level of promoters of miR-34 genes and of some members of the miR-200 family results in a block of their expression and is associated with the development of cancers, such as colorectal and breast cancers (Toyota et al., 2008; Lim et al., 2013).

Furthermore, many tumors correlate with the development of hypoxia, which induces a reduction in the expression of Drosha and Dicer, and post-translational modifications in AGO2 (Rupaimoole et al., 2014; Golden et al., 2017). These events result in an inhibition of the maturation of miRNAs, such as let-7a, miR-16 and miR-200 (van den Beucken et al., 2014).

Despite this, not all miRNAs are affected by hypoxia. For example, the reduction in the hypoxia-dependent processing is overcome by miR-210 due to a greater induction of transcription (Huang et al., 2009). On the contrary, hypoxia increases the levels of miR-630 since the target of this miRNA is precisely DICER1 mRNA (Rupaimoole et al., 2016).

Moreover, the export step of miRNAs from the nucleus can be altered in tumors due to mutations or post-translational modifications of XPO5 that contribute to the downregulation

of mature miRNAs, as observed by an accumulation in the nucleus of miRNA precursors in gastric, colorectal and endometrial cancers (Melo et al., 2010).
The dysregulation of the levels of some miRNAs could also be due to an altered degradation process. In this case, the TDMD mechanism could play a key role, for example through an upregulation of target RNAs directed against miRNAs.

1.3.4 Clinical applications

Due to their correlation with certain cancers, some miRNAs could be exploited as molecular markers in the diagnostic and prognostic field, and could be good indicators of the origin and stage of cancer. For example, miR-196a is overexpressed in pancreatic ductal adenocarcinoma (PDAC), while miR-217 is repressed. Thus, measuring the miR-196a / miR-217 ratio is a good marker of PDAC (Yu et al., 2017).
In recent years, thanks to the improvement of molecular biology techniques for the extraction and detection of nucleic acids, it is possible to evaluate miRNA levels with greater sensitivity and specificity even starting from biopsies and low amounts of RNA.
Similarly, the study of tumor development-related miRNAs could lead to their use in a therapeutic approach. In fact, recently various miRNA-based therapies have been developed (Petrovic and Ergun, 2018). Since miRNAs can be dysregulated and intervene in the cancer pathway in two different ways (as oncomiR or tumor suppressors), two different therapeutic strategies can be developed.
Regarding oncomiRs, which are upregulated in cancer, it is necessary to intervene by inhibiting their biogenesis or blocking them, in order to reduce their levels. This goal can be achieved in particular by antagomiR (anti-miR) (Kong et al., 2012), miRNA sponges (Ebert and Sharp, 2010; Bak and Mikkelsen, 2014), anti-miRNA oligonucleotides (AMO) (Amodeo et al., 2013), locked - nucleic - acid antisense oligonucleotides (LNA) (Nedaeinia et al., 2016), etc. (**Figure 18**).

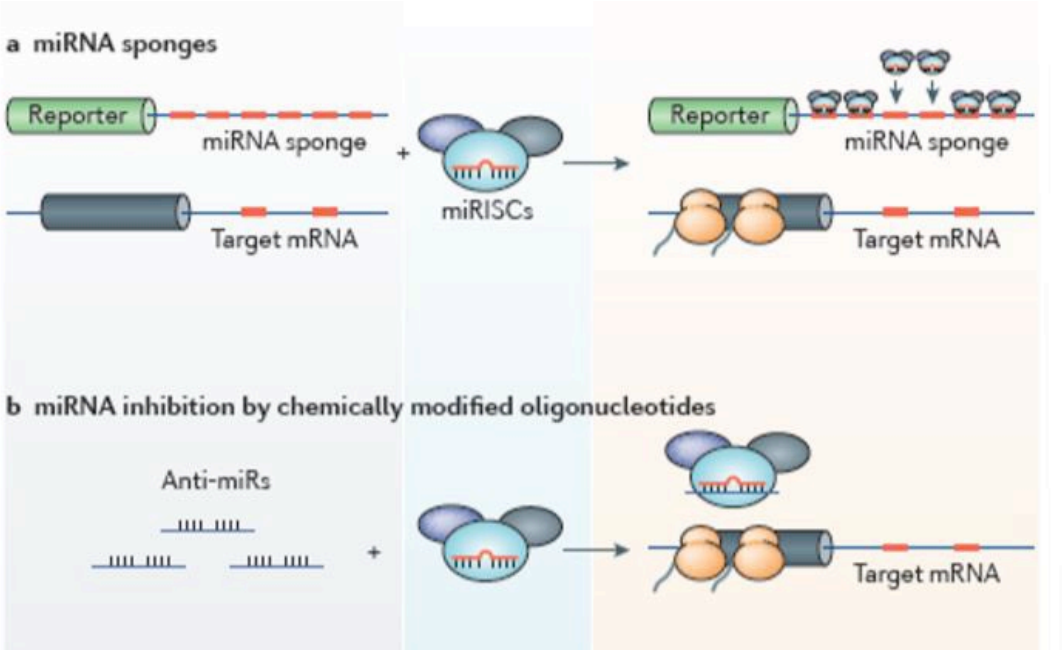

Figure 18. MiRNA inhibition strategies. Several strategies can be applied to block the activity of a miRNA. MiRNA sponges (A) consist of RNAs containing complementary binding sites to a specific miRNA. Several modified oligonucleotides (B) can be created against a miRNA preventing it from interacting with its target transcript (Figure adapted by Mekuria et al., 2018).

Various anti-miRs have been created against different miRNAs such as miR-10b, miR-221, miR-155, miR-122, miR-21 and have shown therapeutic potential against cancer (Nguyen and Chang, 2017).

On the other hand, as regards miRNA tumor suppressors, which are downregulated in cancer, it is necessary to increase their levels through restoration and replacement mechanisms (Henry et al., 2011; Barger and Nana-Sinkam, 2015).

This type of approach is not easy to implement, since either the biogenesis of the suppressed endogenous miRNA has to be stimulated, or an exogenous miRNA has to be introduced into the cell. However, the latter strategy requires efficient means for the transfer of synthetic miRNA into the cell, for example through electroporation or carriers (Terasawa et al., 2011; Hosseinahli et al., 2018) (**Figure 19**).

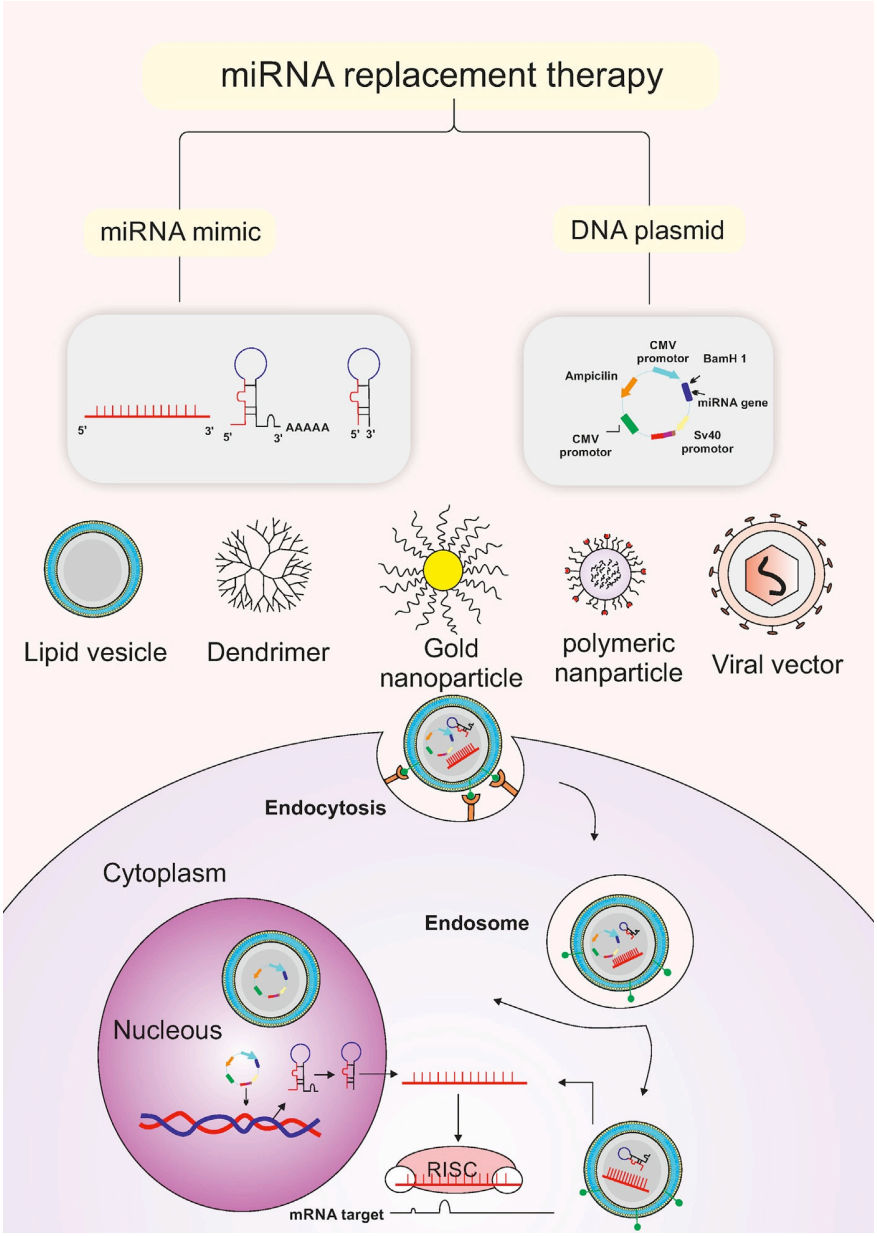

Figure 19. Different strategies used in miRNA replacement therapy. A range of vectors is used to deliver these miRNA mimics or DNA plasmids to the tumor cell nucleus or cytoplasm (Figure from Hosseinahli et al., 2018).

Synthetic miRNAs or mimics are chemically modified double-stranded RNA molecules designed to endogenous miRNAs and contain 17-26 nucleotides with sequences highly equivalent to those of their endogenous counterpart. For this reason, they follow the same biogenesis, once they enter the cell (Shah et al., 2016). Long et al. (2009) used a let-7a mimic in laryngeal cancer cells to restore the expression of let-7a that was highly reduced in this tumor. Similar results were obtained in liver cancer cells where the action of a miR-7 mimic resulted in a reduction in cell proliferation and invasiveness (Wu et al., 2017). One of the most studied miRNAs for mimic strategy is miR-34, which have been used to increase the miRNA level and are currently being tested in phase I clinical trials in various solid and hematological neoplasms. Studies in murine models of lung cancer with these mimics

encapsulated in lipid nanoparticles based on viral vectors, showed a reduction in tumorigenesis and no side effects related to the vector used (Saliminejad et al., 2018). The liposomal mimic of miR-34a, MRX34, had a positive therapeutic result in patients with advanced-stage resistant solid tumors (Beg et al., 2017).

Another particular approach to upregulate tumor suppressor miRNAs was developed by Gilot et al. (2017), who discovered in metastatic melanoma cell lines that the mRNA of TYRP1, encoding the tyrosinase-related protein 1, also exhibits a non-coding function in miR-16 sequestering, thus limiting its tumor suppressor activity. The authors designed LNA Target Site Blockers (TSBs) based on the miRNA sequence in order to block TYRP1 and increase the availability of miR-16.

1.3.5 miRNA and Breast Cancer

Breast cancer (BC) represents one of the main invasive cancers among women, about 30% worldwide, with a mortality / incidence ratio of 15% (Siegel et al., 2020).

On average, about 10% of cases are associated with a genetic predisposition, mainly linked to mutations in the BRCA1 and BRCA2 genes (Kuchenbaecker et al., 2017). Recently, additional genes have been identified that could play a key role in the development and progression of BC. In particular, this group includes: PALB2, ATM, CHEK2, RAD51C, BARD1 and TP53 (Loibl et al., 2021).

In addition to genetic predisposition, environmental factors and incorrect lifestyles can also have a great impact on the development of this tumor (Nur et al., 2019).

Histologically, the most common BCs are invasive ductal carcinoma (also called no special type) and invasive lobular breast cancer, characterized by epithelial cadherin (CDH1) mutations and a dissociated growth pattern.

From a biological point of view, breast cancer is a very heterogeneous tumor and can be divided into at least three main subtypes based on the status of three receptors: estrogen receptor (ER), progesterone receptor (PR), and human epithelial receptor 2 (HER2). The classification includes: luminal ER-positive and PR-positive, which is further subdivided into luminal A and B; HER2-positive; and triple-negative breast cancer (TNBC) (Denkert et al., 2017). Triple negative subtype can be further subclassified generally into basal, claudin-low, MBC (metaplastic breast cancer) and interferon-rich (**Figure 20**).

Luminal subtypes are associated with a better prognosis, while TNBC subtypes are more aggressive.

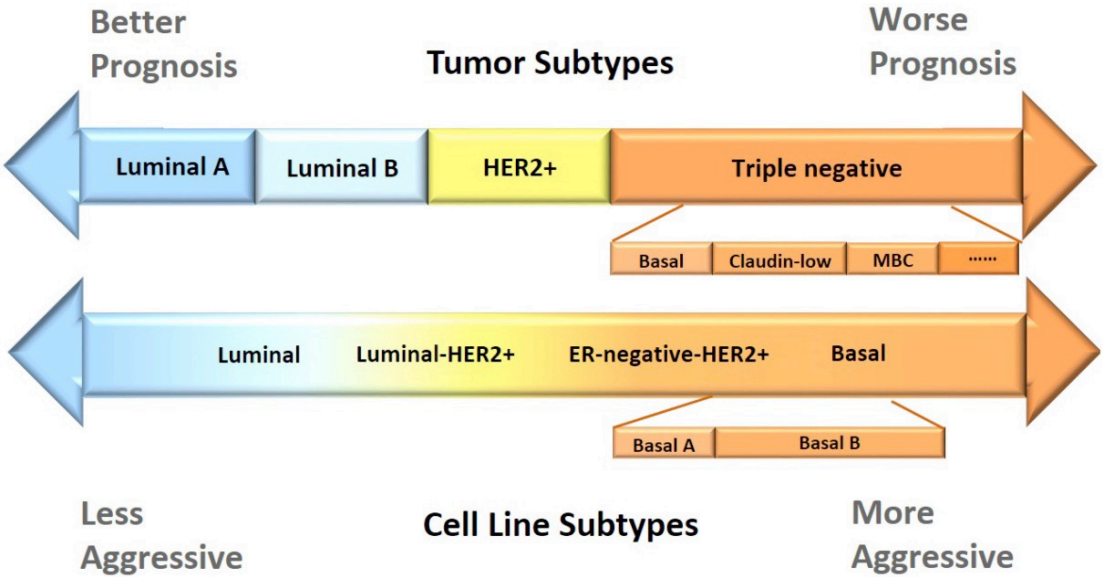

Figure 20. Comparison of the current subtyping classification between breast cancer cell lines and tumors. Based on the expression of ER, PR, HER2, BC is classified as luminal A, luminal B, HER2 positive, and triple negative. A similar subdivision is made for BC cell lines (Figure from Dai et al., 2017)

Similarly to the BC classification, it is also possible to subdivide the BC cell lines used in the various studies (Dai et al., 2017) (**Figure 20**).

Luminal breast cancer cell lines express ER and / or PR and are characterized by a more differentiated phenotype with a lower propensity to migrate thanks to the presence of strong tight junctions.

HER2 positive cell lines express HER2 but not ER and show more heterogeneous features ranging between luminal and TNBC subtypes. For this reason, they can be divided into luminal-HER2+ and ER-negative-HER2+ based on their closest proximity to luminal and TNBC, respectively.

Cell lines belonging to this subtype are more aggressive than the luminal one and with a greater invasive capacity. On the other hand, however, they appear to be more responsive to certain drugs and represent a good study model for evaluating the Herceptin response.

Finally, the Triple Negative cell lines are characterized by low or no expression of all three receptors and can be divided into two very heterogeneous categories: Triple Negative A (or basal A) and Triple Negative B (or basal B).

Basal A lines may have either luminal-like or basal-like morphologies, while basal B lines are the most undifferentiated and invasive, and show a more mesenchymal-like appearance. Understanding the molecular mechanisms underlying this tumor, identifying molecular markers important for diagnosis and prognosis and intervening with increasingly targeted therapies, represents a great challenge.

The study of miRNAs in BC falls within these objectives as the dysregulation of several miRNAs has now been associated with the pathophysiology of this cancer (Cantini et al., 2019, Moi et al., 2019).

Different miRNAs have been observed to be upregulated or downregulated in cell lines, animal models and in BC patients. **Figure 21** summarizes the main ones and describes their role in the invasion-metastasis cascade (Fridrichova and Zmetakova, 2019).

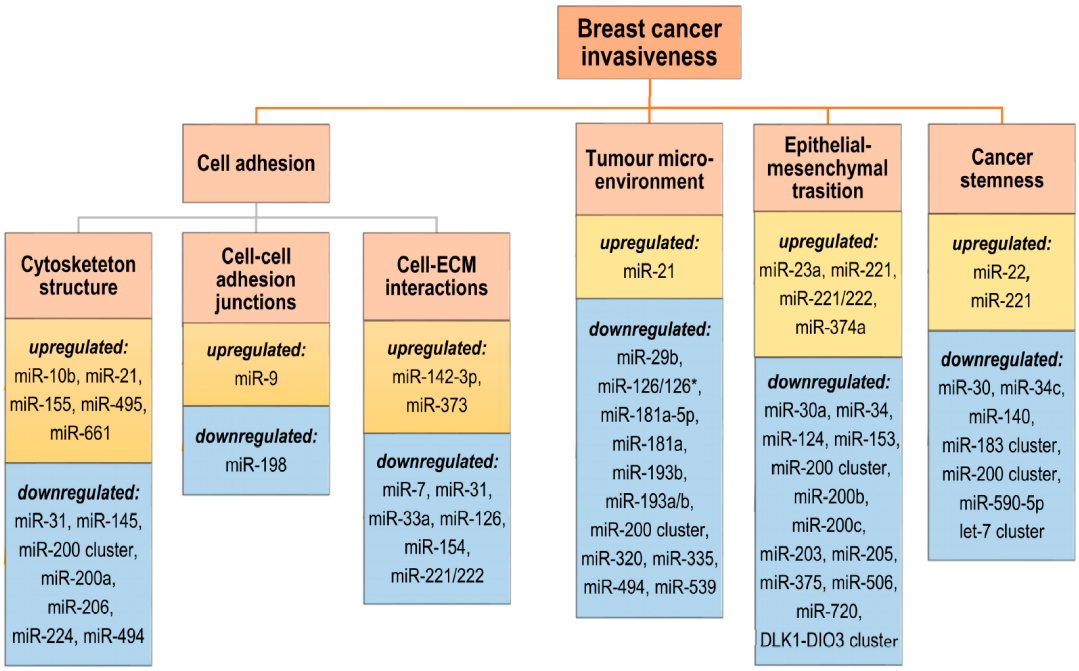

Figure 21. Up-regulated and down-regulated miRNAs in BC. The schematic describes the different processes associated with breast cancer invasiveness and stemness, and shows the main dysregulated mirNAs involved (Figure from Fridrichova and Zmetakova, 2019).

Dysregulation can be associated with different causes and determines effects on the tumor at various levels.

Several large-scale studies have shown that in BC cells the promoters of many miRNA clusters (e.g. miR-335, miR-106a, miR-363, miR-20b, miR-296, miR-298, miR-212, mir - 200b, miR-200c / 141) show an altered methylation pattern which can be associated with an altered expression, as previously described.

Yu et al. (2013) demonstrated that Kindlin 2, a protein capable of interacting with DNMT1 (DNA Methyltransferase 1), stimulates the hypermethylation of the miR-200 family promoter, inducing its silencing.

The altered expression of various miRNAs, such as miR-125b-1 and miR-31, can also occur following dysregulation of histone methylation in BC. Specifically, as regards miR-31, EZH2 (Enhancer of Zeste Homolog 2), a histone-lysine N-methyltransferase enzyme, is

upregulated and consequently determines a hypermethylation of histones with a transcriptional stop of the miRNA gene (Kandettu et al., 2020). EZH2 can also determine epigenetic silencing of the genes of two tumor suppressor miRNAs: miR-29b and miR-30d. Furthermore, the presence of significant chromosomal aberrations and mutations in BC may also contribute to altering the genes encoding miRNAs (Sharma et al., 2014).

For example, the amplification of genomic regions could involve the locus of miR-191/425 which is upregulated and can promote cell proliferation and metastasis (Zhang et al., 2018). A similar effect is observed following the amplification of the miR-130a locus (Riaz et al., 2013).

Even simple single nucleotide polymorphisms (SNPs) have a significant impact on the expression and activity of miRNAs, and therefore on the predisposition to disease (Sun et al., 2009). Certain SNPs in miR-146a, miR-499, miR-125a, miR-605, and miR-182 pre-miRNAs have been correlated with an increased risk of developing BC (Morales et al., 2018). Chacon-Cortes et al. (2015) and Hu et al. (2009) identified specific SNPs in miR-145 and miR-499a associated with the development of breast cancer.

The alterations can also affect the genes encoding the miRNA processing proteins, as confirmed by Passon et al. (2012) who found low levels of Dicer and Drosha in triple-negative breast cancer.

Furthermore, the upregulation of a miRNA may be the result of the overexpression of a transcription factor in BC, such as the case of ZEB1 and HSF2 (heat shock transcription factor 2) which stimulate the miR-183/96/182 cluster. These miRNAs then determine the repression of oncorepressive transcription factors, such as FOXO3a (Forkhead Box O3) and FOXO1 (Forkhead Box O1) (Li et al., 2014).

Another cluster that plays a critical role in BC is the miR-200b / 200a / 429 cluster, implicated in the inhibition of migration and metastasis processes. In fact, in MDA-MB-231, an epithelial cell line isolated from the breast tissue of an adenocarcinoma patient, the induction of miR200b determines a silencing effect against the mRNA of WAVE3, a protein that activates the invasion capacity of tumor cells (Sossey-Alaoui et al., 2009). Similar studies on other BC cell lines have also shown silencing activity against other protumor factors, such as SNAI1, TWIST1, TWIST2 and ZEB1 (Watson et al., 2018).

In particular, the TWIST family basic helix-loop-helix transcription factor induces the expression of miR-10b which is upregulated in metastatic breast cancer. In non-metastatic breast cancer cell lines, the ectopic expression of miR-10b induced the processes of invasion, intravasation and metastasis (Ma et al., 2007).

In contrast to miR-10b, the anti-metastatic role of miR-29b has been highlighted: it is induced by the transcription factor gata-binding protein 3 (GATA3) and is more present in

luminal breast cancers where it limits the invasive power of this subtype. In fact, the loss of miR-29b in these tumors causes an increase in pathogenicity and malignancy. The direct targets of this miRNA include a number of pro-metastatic factors involved in angiogenesis and remodeling of the tumor microenvironment, such as VEGFA, ANGPTL4, PDGF, LOX and MMP9 (Chou et al., 2013).

GATA3 also regulates miR-30c expression binding directly to its promoter. Many studies have highlighted an important role of this miRNA in BC, as it intervenes in the tumor progression and chemoresistance, thanks to its ability to regulate the EMT. Specifically, it acts on the transcript of the TWF1 gene which encodes a cytoskeleton actin-binding protein (called Twinfilin 1), implicated in morphological and motile processes, and also in EMT and chemoresistance in cancer cells (Bockhorn et al., 2013). Therefore, miR-30c acts as an important tumor suppressor and could be used to enhance the action of anti-tumor drugs. Yu et al. (2010) observed that downregulation of the miR-30 family enhances tumorigenesis due to the upregulation of two other targets, ubiquitin conjugating enzyme 9 (Ubc9) and integrin b3 (ITGB3). By inducing the expression of miR-30 in BC cell lines, there is a reduction in their ability of self-renewal and an increased apoptosis. Recently, Jamshidi et al. (2021) confirmed these data, highlighting that a high expression of the miR-30 family is associated with a greater effect of drug treatment and with an improved BC patient survival.

Aim of the project

miRNAs activity relies on the regulation of their cellular levels, which is the result of the balance between biosynthesis and decay. A novel mechanism, called Target-Directed miRNA degradation (TDMD), has emerged where targets with extended complementarity can induce the decay of their miRNAs. When we started the study of TDMD, in 2017, little was known about the miRNA decay. The evidence for TDMD was derived from studies on viral RNA targets (Cazalla et al., 2010; Marcinowski et al., 2012) and on artificial transcripts (Denzler et al., 2014; Baccarini et al., 2011). At that time, several aspects related to TDMD mechanisms needed to be investigated:

i) the existence of endogenous RNA transcripts implicated in TDMD in mammalian cells and their impact in modulating miRNA activity in physiology (addressed in chapter 1);
   - published on Nature Communication (Ghini, Rubolino et al., 2018)

ii) a systematic prediction of mammalian transcripts involved in the TDMD mechanism (addressed in chapter 2);
   - published on NAR (Simeone, Rubolino et al., 2022)

iii) a proof-of-concept study on the relevance of the TDMD mechanism in modulating human cancer phenotypes (addressed in chapter 3);

iv) a systematic identification of miRNAs controlled by TDMD in cancer (addressed in chapter 4).

The results obtained during my PhD work are here presented, organized in four chapters. In each of these chapters we tried to provide new evidence about the open questions reported above, respectively. More specifically, in chapter 1, with the aim of identifying endogenous TDMD transcripts, we focused on a candidate TDMD trigger, Serpine1, and we discovered that it was able to degrade miR-30b/c in 3T9 mouse fibroblasts (Ghini, Rubolino et al., 2018). In the same period, other two research groups had independently proven the existence of endogenous TDMD transcripts in mammalian cells: CYRANO able to induce degradation of miR-7 in mouse and NREP shown to degrade miR-29b-3p in mouse cerebellum (Kleaveland et al. 2018; Bitetti et al. 2018). In chapter 2, in order to unveil new RNA transcripts able to induce TDMD of their miRNAs, we developed a computational pipeline and free webtool, named TDMD*finder*. In order to verify the accuracy of our predictions, we experimentally tested 37 predicted TDMD*finder*, of which 17 showed TDMD effects

(Simeone, Rubolino et al., 2022). Therefore, TDMD*finder* represented the first inventory of TDMD interactions.

In chapter 3, in order to identify all the TDMD interactions potentially involved in cancer, we performed computational analyses using the multiomic TCGA platform (Simeone, Rubolino et al., 2022). Moreover, to gain a deeper understanding about the possible role of TDMD mechanism in human cancer, we provided a proof-of-principle validation of the involvement of TDMD in tumorigenesis, using breast cancer as model and focusing on a candidate TDMD-transcript (unpublished data).

In 2020, the ZSWIM8 Cullin-RING E3 ubiquitin ligase substrate adaptor has been shown as an essential component of the TDMD mechanism (Shi et al., 2020; Han et al., 2020). In chapter 4, we exploited ZSWIM8 knock-down as a tool to gain a deeper understanding of TDMD involvement in breast cancer, identifying multiple novel TDMD miRNA substrates (unpublished data). In the near future, by combining ZSWIM8 manipulation, TDMD*finder* predictions and experimental validation of candidate TDMD triggers, we aim at providing a complete molecular map of all the TDMD players (miRNAs and targets) involved in breast tumors.

2. Results

2.1 Selection of TDMD candidate transcripts in mammalian genomes

At the time we started our investigation into the TDMD mechanism, in 2017, the mechanism has been associated with an extensive complementarity between target and miRNA which involved a region in addition to the seed that is complementary to the 3' end of the miRNA named 3' complementary site (Bartel, 2009). In order to search TDMD candidate targets in mammalian cells, we retrieved, by using TargetScan database, RNA transcripts that could be able to degrade their miRNAs (**Figure 22A**). Based on the 3' pairing contribution (3C-score), we divided the 3C targets into three classes: 1) Low with 3C scores between -0.01 and -0.03; 2) Mid with 3C scores between -0.03 and -0.05; 3) High with 3c scores lower than -0.05 (Examples in **Figure 22B**). The High class, with the highest complementarity, includes only the 0.8% of all predicted miRNA:target interactions (**Figure 22C**).

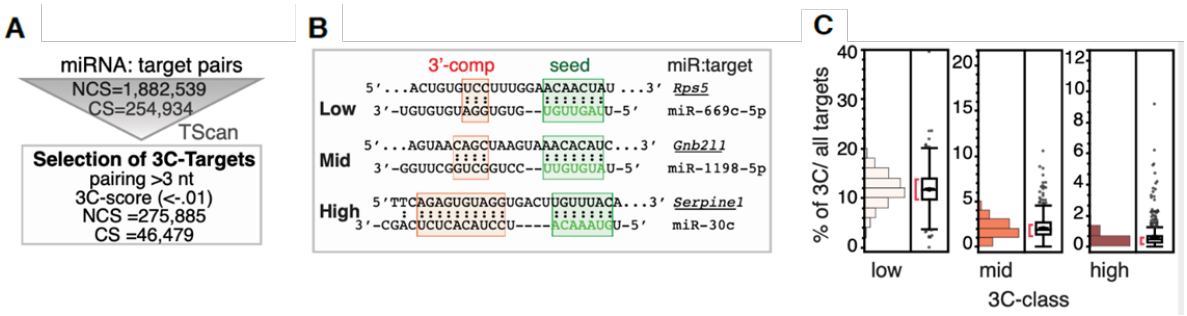

Figure 22. Candidate TDMD transcripts in 3T9 cells. (A) Scheme summarizing filtering criteria for the selection of 3C-targets from all miRNA:target interactions in the TargetScan database (NCS: non-conserved sequence, CS: conserved sequence). All 3C-targets were further classified according to their 3C score. (B) Three classes of 3C scores were identified: low (from –0.01 to –0.03); mid (from –0.03 to –0.05); and high (lower than –0.05). Three examples are shown. (C) The fraction of 3C-targets over the number of all predicted targets was calculated for each miRNA and plotted as distribution, with box-plots and whiskers for each class of targets.

2.1.1 Serpine1 is a candidate transcript for miR-30b/c in 3T9 fibroblasts

The TDMD occurrence also depend on miRNA:target relative expression levels (Bosson et al., 2014; Denzler et al., 2014) in a specific cellular context. We decided to focus on mouse 3T9 fibroblasts. The selected cellular system is apt to study transcriptional changes

associated with the cell cycle; in fact, fibroblasts can be induced to quiescence by serum starvation and then induced to cell cycle re-entry by adding serum (Iyer et al.; 1999) (**Figure 23A**). The choice of this fibroblast serum model to study TDMD was substantiated by two reasons: i) changes in gene expression related to cell cycle re-entry occur in few hours by avoiding miRNAs dilution by cell division; ii) data of gene and miRNA expression, transcription and decay were already available (Marzi et al.; 2016). We matched RNA and miRNA expression data to select the target:miRNA 3C pairs that could be studied in our cellular system. We found 18.856 pairs, in particular 1083 of them falling in the 3C-high class (**Figure 23A**).

Then, to select a "putative" target able to degrade its miRNA, we considered two parameters: 1) the maximum change in expression of all 3C-transcripts during the cell cycle re-entry (**Figure 23B**); 2) the maximum contribution of each target to the total 3C target pool of a given miRNA over the time course (**Figure 23B**). We found that Serpine1 showed the highest change in expression (maximum log2 fold change=6.92), a really high 3C score for miR-30b-5p and miR-30c-5p and a contribution to the 3C-target pool of 33.8% for miR-30b-5p and 35% for miR-30c-5p.

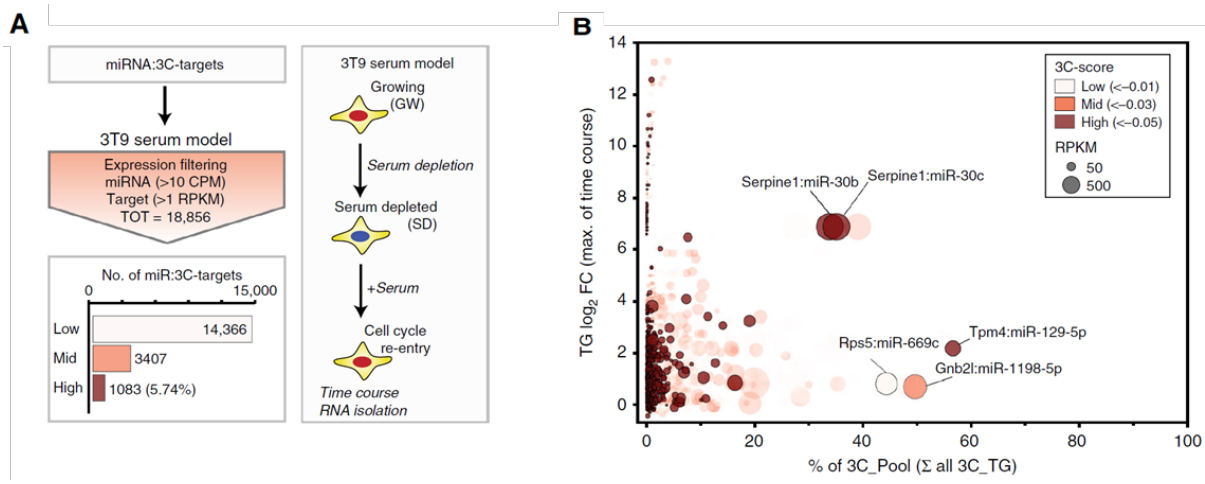

Figure 23. Strategy to select TDMD 3C pairs. (A) 3C-targets have been screened to determine which of them were eligible for 3T9 serum model (scheme on the right). Only the pairs that were found expressed in at least one condition (growing, absence of serum or time course upon serum stimulation) were maintained. The distribution of filtered couples based on the 3C-score is showed. (B) Bubble plot reporting all the filtered miRNA:target pairs stratified according to the target max contribution (percentage, x-axis) to the 3C-targets pool of a miRNA (RPKMtarget/RPKMSum_all_3C-targets) and to the target max regulation (log2 fold change, y-axis) across the time course. Bubble size is proportional to target abundance (RPKMtarget), and target colour reflects the class of 3C-score.

2.1.2 miR-30b/c expression is fastly downregulated during cell cycle re-entry

Serpine1 (PAI-1) encodes a serine protease inhibitor protein able to inhibits fibrinolysis and also plays an important role in the early G0>G1 transcriptional program (Iyer et al.; 1999). miR-30 family consists in five members that can interact with Serpine1 transcript, since it has a high-affinity 8-mer seed match (**Figure 24**).

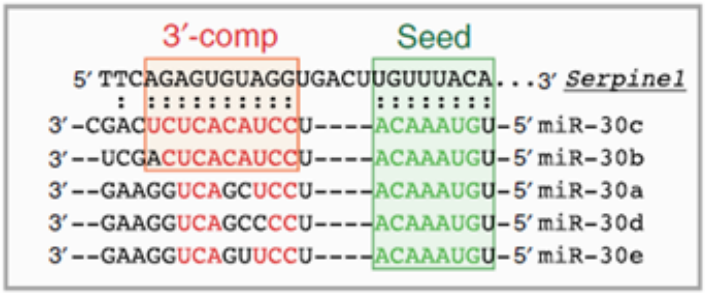

Figure 24. Alignment of the MRE of Serpine1 with miR-30 family components. The seed match is the same for all miR-30 family members and it is shown in green. The bases of the 3′ complementarity, which is extensive only for miR-30b (9 nt) and miR-30c (11 nt) are showed in red.

Anyway, only when Serpine1 interacts with miR-30b-5p and miR-30c-5p, it forms an internal bulge of 5 nucleotides and an extended 3' base pairing of 9 nucleotides in the case of miR-30b and 11 nucleotides for miR-30c-5p. So, Serpine1 is a candidate decay target only for miR-30b/c and not for miR-30a/d/e. To asses this point, we starved the 3T9 fibroblasts and we performed a time course experiment. Upon serum stimulation of 3T9 fibroblasts we found that Serpine1 was highly and quickly induced, by reaching a peak at 2h (>1000 RPKM, **Figure 25**). The contribution of Serpine1 to the total target pool was maximum at this level, indeed it represented > 90% of the entire pool of 3C high targets for miR-30b/c (**Figure 25**).

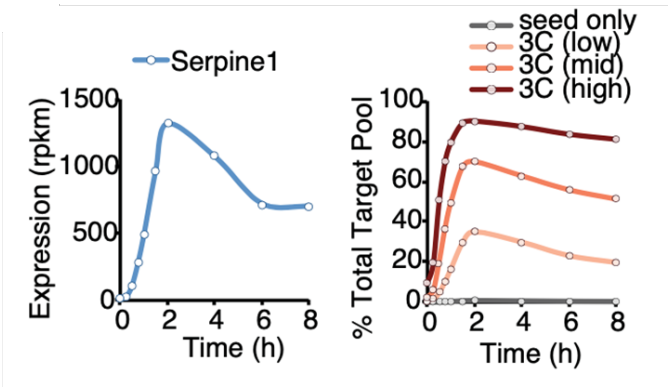

Figure 25. Regulation of Serpine1 during serum stimulation. Expression of Serpine1 after serum stimulation of starved 3T9 fibroblasts (left panel). In the Right panel has been reported the contribution of Serpine1 expression to the entire target pool, evaluated over different 3C score classes.

We performed small RNA library preparation and small RNA sequencing (sRNA-seq) results over the time course of stimulation revealed that miR-30b/c expression levels decreased after 4 hours upon serum addition, while the levels of other members of the miR-30 family (miR-30a/d/e) remained unchanged (**Figure 26**).

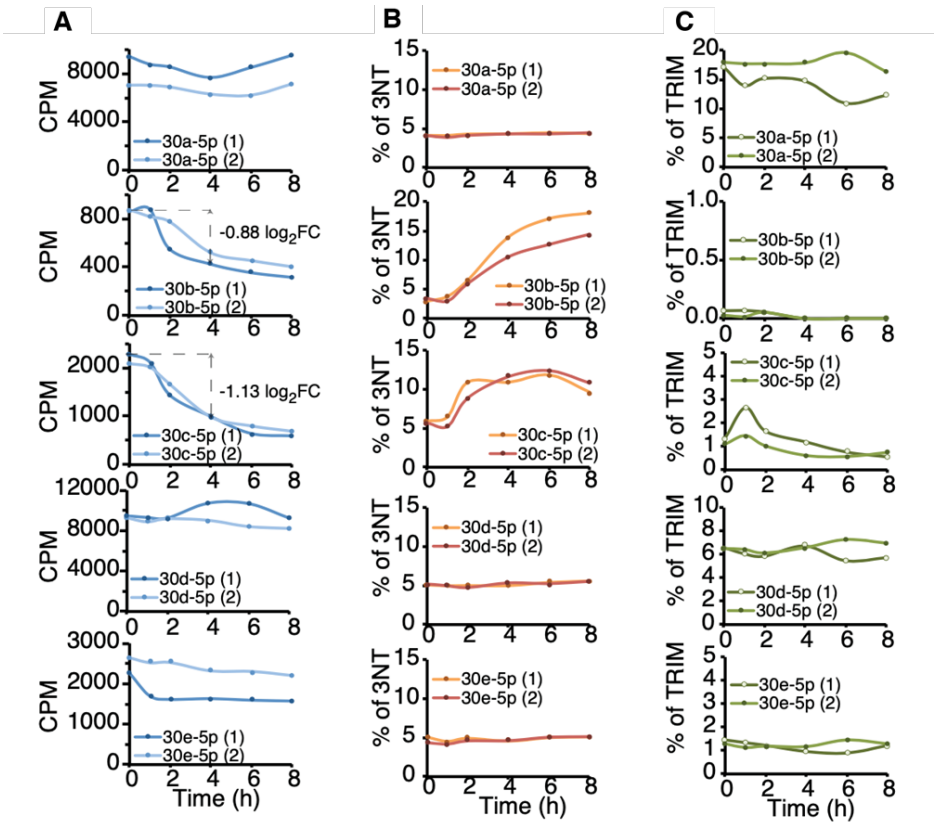

Figure 26. Regulation of miR-30 family members during serum stimulation. Expression of miR-30 family members after serum stimulation of starved 3T9 fibroblasts. Shown for each miRNA are: A) the expression level (CPM, counts per million), B) tailing events (% of 3NT, 3′-nontemplated isomiRs) and C) trimming events (% of TRIM, trimmed forms) in two biological replicates.

These sRNA-seq results also provided us the opportunity to monitor the effect of Serpine1 on the level of miR-30b/c passenger strand: the expression of miR-30b/c passenger strand did not significantly change (**Figure 27**).

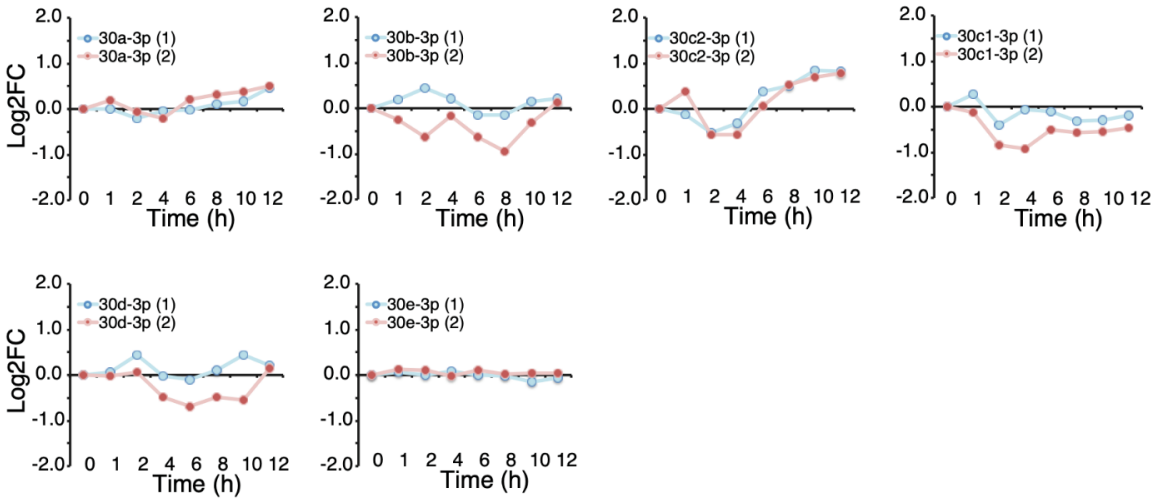

Figure 27. Regulation of passenger miRNAs during serum stimulation. Expression of passenger miRNAs of the miR-30 family after serum stimulation of starved 3T9 fibroblasts was measured by sRNA-seq.

TDMD has also associated with the addition of non-templated nucleotides to the miRNA 3' terminus and/or removal of nucleotides at the 3'end. These processes are known as tailing and trimming. We used the IsomiRage tool to map tailing and trimming isomiRs (Muller et al., 2014). We found that the 3' tailing of miR-30b/c was significantly increased (**Figure 26B**), instead the trimming variants were slightly affected (**Figure 26C**). The prevalent modifications were adenylation and uridylation (around the 40% being A-forms) (**Figure 28**).

The abundance of miR-30a/d/e tailed and trimmed isoforms remained substantially unchanged throughout time (**Figure 26B**, **Figure 26C**).

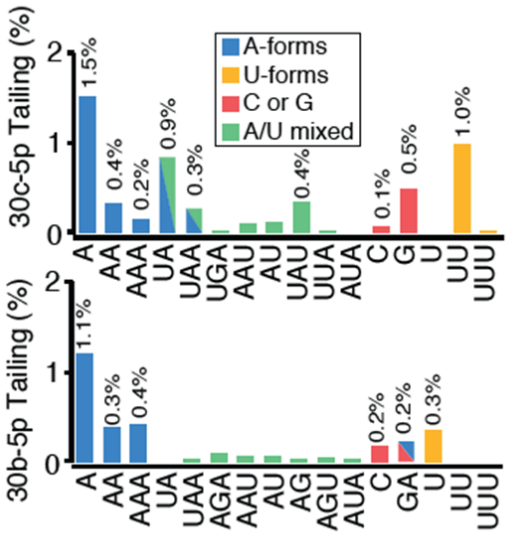

Figure 28. Representation of the 3' tailing modifications. Frequency of tailing for both miR-30c (top panel) and miR-30b (bottom panel) in growing 3T9 fibroblasts.

We measured the synthesis rate of primary transcripts (pri-miRNAs) during serum stimulation through a pulse labeling approach (Rabani et al., 2011). Interestingly, miR-30b and -30c (which consists into two copies, 30c-1 and 30c-2) do not belong to the same gene unit, but correspond to three different genes, transcribed separately (**Figure 29**).

No significant changes were observed in the synthesis rates of pri-miR-30b-30d and pri-miR-30e-30c-1, while the pri-miR-30a-30c-2 undergoes an initial decrease followed by a slow increase **Figure 29**).

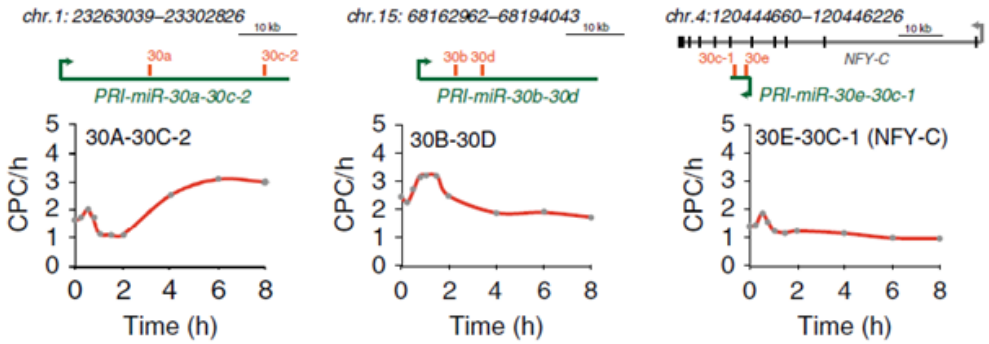

Figure 29. Regulation of pri-miRNAs during serum stimulation. Synthesis rate of the pri-miRNAs of the miR-30 family after serum stimulation, as measured by a short pulse of 4SU.

Therefore, during the serum induced cycle re-entry of quiescent fibroblasts, Serpine1 reached a very high concentration. Concomitantly with the target induction, the rapid and specific reduction of miR-30b/c levels was observed and it could be due to a direct degradation of the miRNA related to post-transcriptional events.

2.1.3 Serpine1 controls miR-30b/c abundance in the cell

By performing absolute quantification, we investigated the expression range of Serpine1 and miR-30 in the cell. To do this, we created a titration curve by using synthetic miR-30 RNA oligonucleotides and a Serpine1 plasmid DNA template (**Figure 30**).

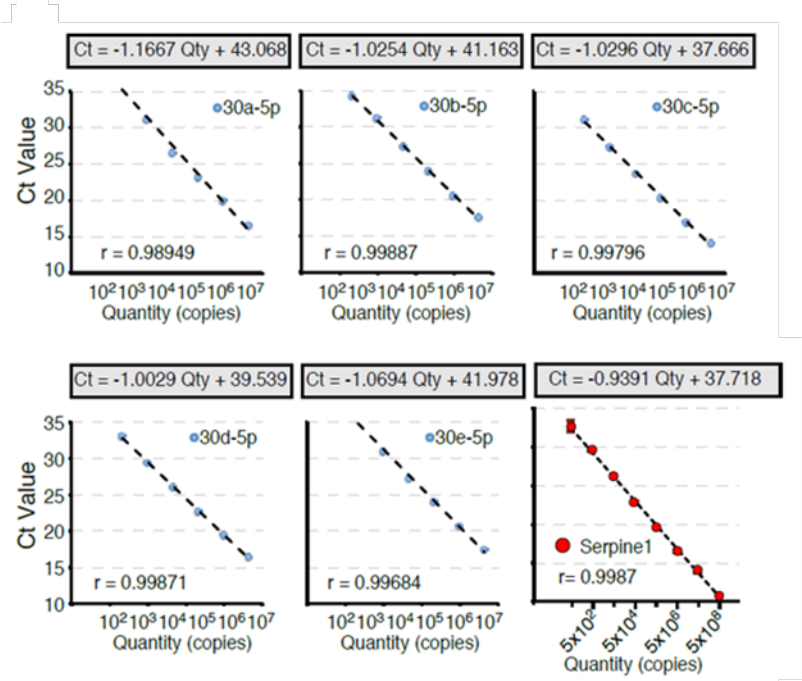

Figure 30. Absolute quantification of miR-30 family members and Serpine1. Standard curves for the absolute quantification are reported. In the case of miR-30 members, the cDNA obtained by spiking synthetic miRNAs in 3T9 RNA was serially diluted (10^9 copies of the synthetic miRNAs were reverse transcribed and serially diluted from 10^7 to 10^2 copies for the qPCR). For Serpine1, a plasmid where the 3'UTR of Serpine1 was cloned downstream of mCherry protein was serially diluited. Results were fitted into linear correlation. The coefficient of determination of fitting (r) and linear equation is showed.

The results showed that miR-30c was expressed at approximately 70 CPC (copies per cell) in exponentially growing (GW) cells. In addition, miR-30b/c accounted for nearly 40% of the total copies of miR-30 (**Figure 31A**).

The expression levels of miR-30c and Serpine1 are comparable in growing cells and in quiescent fibroblasts. Specifically, Serpine1 reaches values of 170 CPC in GW cells and 88 CPC in quiescent cells (**Figure 31B**) with a target for miRNA (TPM) value of approximately 1 (**Figure 31C**).

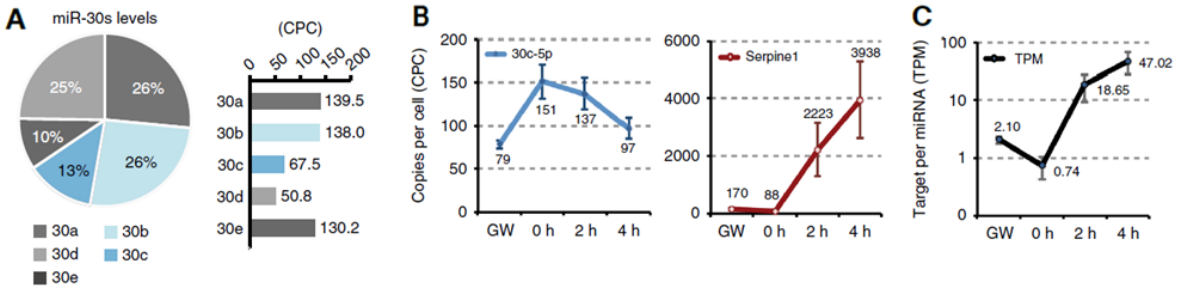

Figure 31. Quantitative analysis of Serpine1 and miR:30 family members. (A) Percentage contribution and copies per cell (CPC) for all members of the miR-30 family in growing cells are reported, using absolute quantification data. (B) Absolute quantification of miR-30c and Serpine1 in 3T9 cells. Data refer to three different biological experiments (average and SEM) (C) A target-per-miRNA (TPM) value was calculated using absolute quantification.

Serum stimulation determines a notable increase in Serpine1 expression, which reaches about 4000 cpc after 4 hours and reaches a TPM ratio > 40 (**Figure 31C**). So, Serpine1 showed both molecular and quantitative requirements to induce degradation of miR-30b/c through TDMD.

To confirm the role of Serpine1 in the occurrence of the TDMD, we decided to use the CRISPR / Cas9 system to manipulate Serpine1 MRE. Therefore, sgRNAs were designed to ensure the biallelic genomic deletion of a minimal region of about 160 nt within the Serpine1 3'UTR (**Figure 32A**), including miR-30 MRE. Poorly conserved MREs for miR-224 and miR-320 are also found in this deleted region, but these miRNAs are not expressed at elevated levels in 3T9 cells.

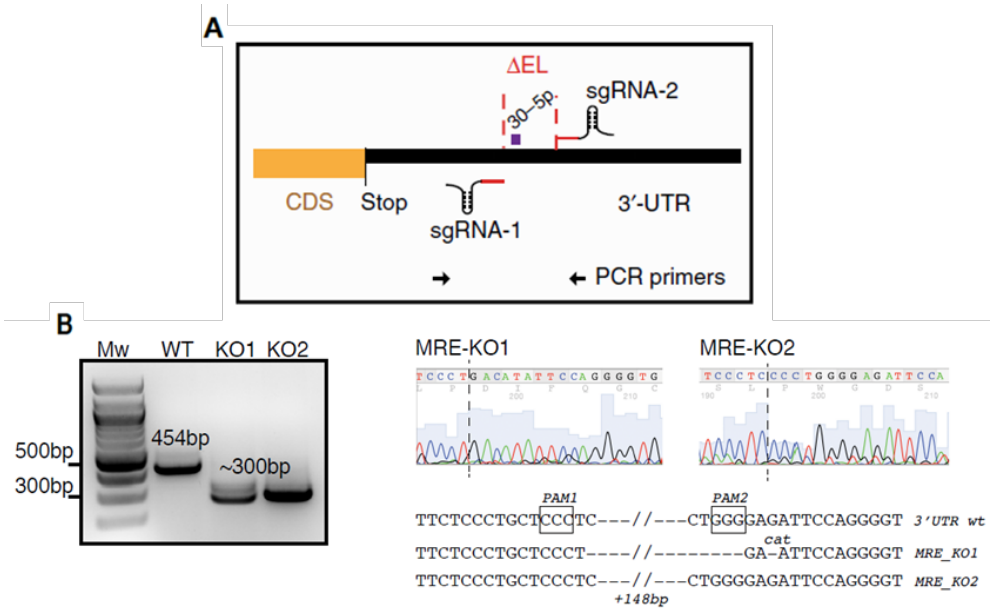

Figure 32. Strategy for the removal of miR-30 MRE from 3′UTR of Serpine1 by using CRISPR-Cas9 technology. (A) Scheme of the CRISPR-Cas9 strategy used to remove the miR-30 MRE from 3'UTR of Serpine1. The positions of the sgRNAs and the PCR primers used have been reported. (B) Characterization of MRE-KO (Knock out) clones. On the left, genomic PCR was used to screen for MRE-KO clones. A region which comprises the deletion was amplified, producing a 454 bp band in case of wild-type cells or a ~300 bp band in case of KO clones. Two independent MRE-KO clones were shown on the left in the figure; on the right, the products of PCR were sequenced to confirm the MRE deletions. Chromatograms (top) and sequences (bottom) with the expected deletion in the Serpine1 locus have been reported (dashed lines mark deletion junctions).

Two independent mutant clones were created, Serpine1: miR-30 MRE-KO1 and Serpine1: miR-30 MRE-KO2 (**Figure 32B**). Importantly, Serpine1 protein and mRNA expression were not altered by the deletion of the 3 ' UTR gene (**Figure 33A**).

Furthermore, we found that, for both clones, the proliferation rates and the cell cycle profiles were similar to those of the corresponding parental cells (**Figure 33B**).

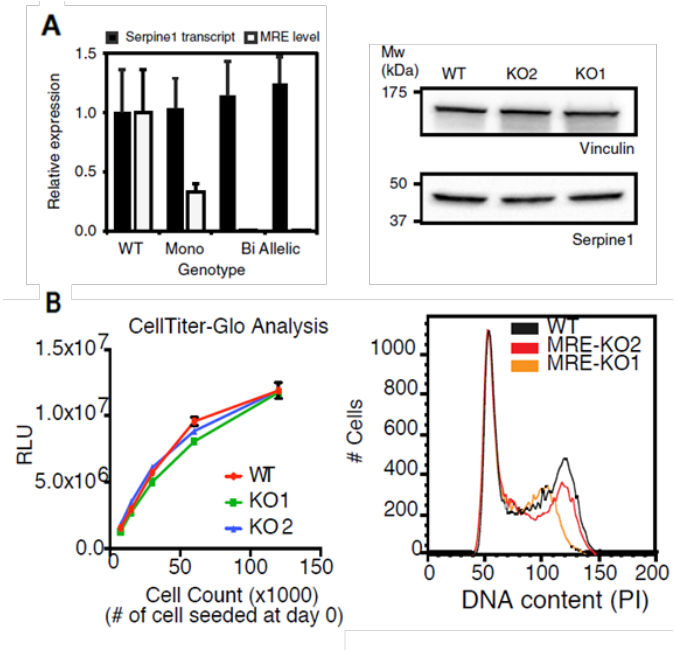

Figure 33. Characterization of MRE KO clones. (A) On the left, Serpine1 expression by RT-qPCR in wild-type (WT) 3T9 murine fibroblasts and in clones with mono-allelic (N=3) or bi-allelic deletion (MRE-KO1 and MRE-KO2) of the miR-30 MRE. On the right, Serpine1 protein level in WT or MRE-KO clones. Vinculin was used as normalizer. (B) On the left, cell viability of 3T9 WT and MRE-KO clones was investigated by measuring the ATP quantity by CellTiter-Glo assay (Promega). Luminescence (RLU, y-axis) was read after 24hrs. On the right, cell cycle profile of growing WT and MRE-KO cells was evaluated performing propidium iodide staining by FACS.

Then, we measured the global expression levels of miRNAs and their isoforms through sRNA-seq. The results showed that in both clones only a few miRNAs, including miR-30c-5p (1.03 log2FC, p = 0.0013) and 30b-5p (0.92 log2FC, p = 0.0180), were significantly induced (**Figure 34**).

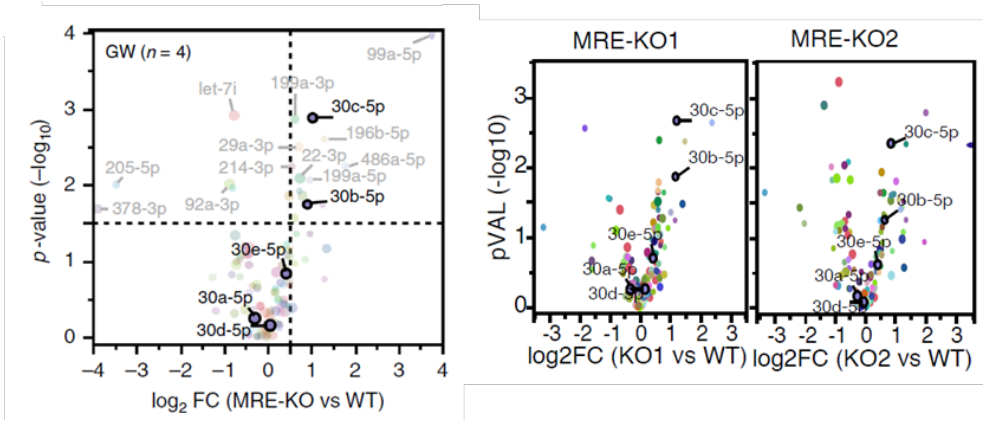

Figure 34. Serpine1 control miR-30b/c degradation. sRNA-seq was performed to measure miRNA expression in WT (n = 4) and MRE-KO clones in growing conditions. The graphs show the log2 FC (MRE-KO cells compared to WT, x-axis) and the p-value (–log10, y-axis), by Welch's t-test. On the left, the average log2FC of both MRE KO clones has been reported, instead on the right the two MRE KO clones were analyzed separately. Colour coding represents various miRNA families.

Notably, the expression levels of the other members of the family (30a-d-e), as well as of passenger miRNAs, did not show any change. Primary transcript levels for the three miR-30 loci were measured by RT-qPCR without observing significant differences between clones and parental cells (**Figure 35A**). Consequently, it can be assumed that the increase in miR-30b/c was not attributable to an increased transcriptional activity, but to a reduction in their degradation rate. Also, the tailing process of miR-30b/c was reduced in both MRE-KO clones, especially at the level of adenylation (**Figure 35B**).

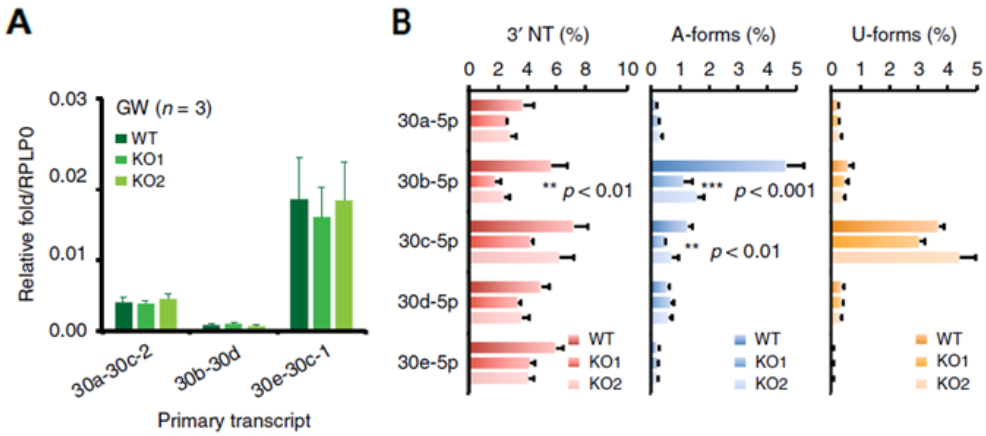

Figure 35. Pri-miRNAs and tailing modifications measurement. (A) Pri-miRNAs for miR-30 family were measured by RT-qPCR in WT or MRE-KO clones (n = 3). (B) % of tailing events (3′NT), adenylated (A-forms) or uridylated isomiRs (U-forms) were measured by sRNA-seq in both WT (n =4) or MRE-KO clones (n = 3) conditions.

To be sure that the increase in miR-30b/c was not due to clonal selection, we performed RT-qPCR to absolute compare the levels of miR-30c in the MRE-KO clones with those measured in wild type clones or in clones exposed to Cas9 but not carrying MRE deletion (No-del clones). We found increased levels of miR-30c only in MRE-KO clones (**Figure 36**).

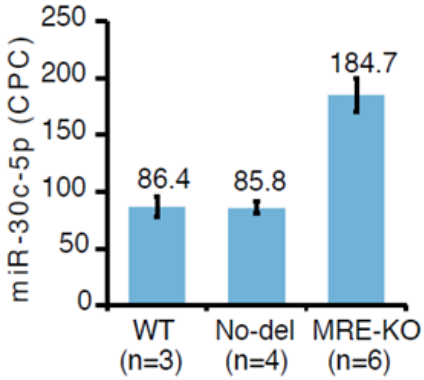

Figure 36. Quantitative analysis of miR-30c after CRISPR experiment. Absolute quantification of miR-30c in WT cells, clones exposed to sgRNA+Cas9 but not carrying MRE deletion (no-del) and MRE-KO clones by RT-qPCR. Bar graph shows the average and the SEM of independent experiments.

In addition, we also evaluated the effect of serum stimulation on MRE-KO cells compared to parental cells. In the latter, the serum determined a downregulation of miR-30b/c levels with a rapid increase of 3' tailing forms (4-8 hrs post stimulation), as expected (**Figure 37A and Figure 37B**). In contrast, in MRE-KO cells, miR-30b/c undergoes no downregulation, but remains consistently highly expressed.

Hence, it can be inferred that in both growing cells (stationary) and after serum stimulation (dynamic) conditions, the levels of miR-30b/c are controlled by Serpine1 via TDMD.

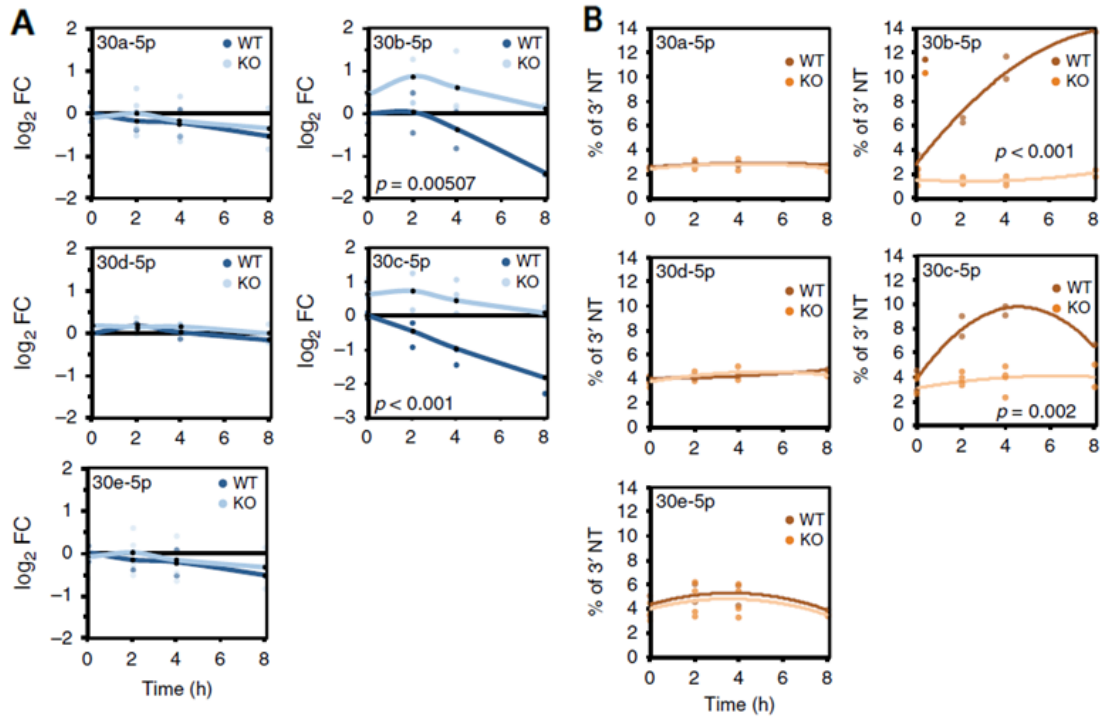

Figure 37. Evaluation of miR-30 expression after CRISPR experiment. Expression of miR-30 family members measured by sRNA-seq after serum stimulation in WT and MRE-KO cells. For each miRNA, expression regulation (A, log2 FC) and tailing events (B, % 3′NT) are reported.

2.1.4 Wild-type but not mutant MRE rescues TDMD

To directly verify the occurrence of TDMD, we subsequently tried to rescue the interaction between miR-30 and Serpine1 3'UTR in MRE-KO cells. We generated three adenoviral constructs expressing the red fluorescent tracking protein (RFP) fused with the Serpine1 3'UTR (**Figure 38**).

Figure 38. Strategy to re-express Serpine1 MRE. Scheme of the recombinant adenoviral constructs used to rescue the expression of Serpine1 WT form of the 3′UTR fused to an RFP reporter and two mutants (the first where miR-30 MRE had been completely eliminated (MUT) and the second where the 3′ complementary site had been replaced but the seed sequence left intact (SEED).

Specifically, three different Serpine1 sequences were used: a wild-type sequence (SE1-WT), which includes the miR-30 MRE, and two mutant sequences, in which the miR-30 MRE was completely abolished (SE1-MUT) or mutated only at the level of the 3 'complementary region, leaving the match with the miRNA seed (SE1-SEED) (**Figure 38**).

By monitoring the effects of the constructs by RT-qPCR, it was observed that RFP-SE1-WT resulted in a significant reduction in the levels of miR-30c and, to a lesser extent, miR-30b, but not of the other family members or the unrelated miRNA let-7b (**Figure 39**).

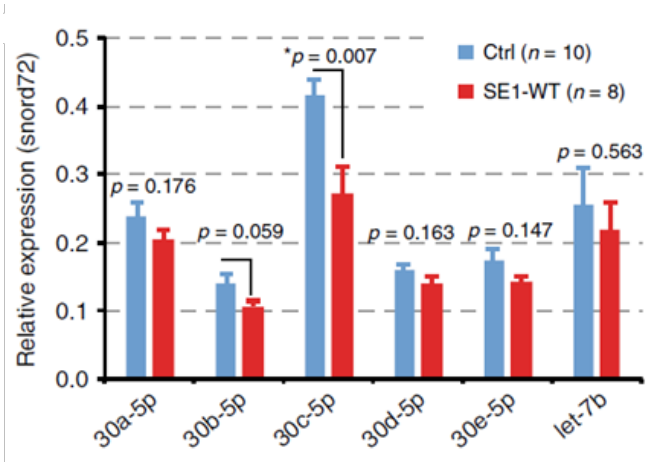

Figure 39. Re-expression of Serpine1 MRE rescues TDMD. Bar plot showing the expression of miR-30 family members and Let-7b as a control by RT-qPCR in cells transduced with control virus (Ctrl) or with RFP-SE1-WT adenoviruses (p-values by Welch's t-test).

In particular, when the construct was expressed at moderate levels (~1000 CPC with a transduction efficiency of ~ 30%, judged by RFP + cells), a moderate decrease (~20%) in miR-30c was observed. On the other hand, a high expression of the construct (~10,000 CPC; nearly 100% RFP + cells) resulted in a significantly greater reduction of about 3 times

(**Figure 40A, Figure 40B**). In contrast, the two mutant constructs, SE1-MUT and SE1-SEED, did not cause any variation in miRNA levels, demonstrating that mutations at the 3' end, by altering the complementarity of the sequence, do not allow target-directed degradation (**Figure 40A, Figure 40B**). These data were also confirmed by sRNA-seq analyses (**Figure 40C**).

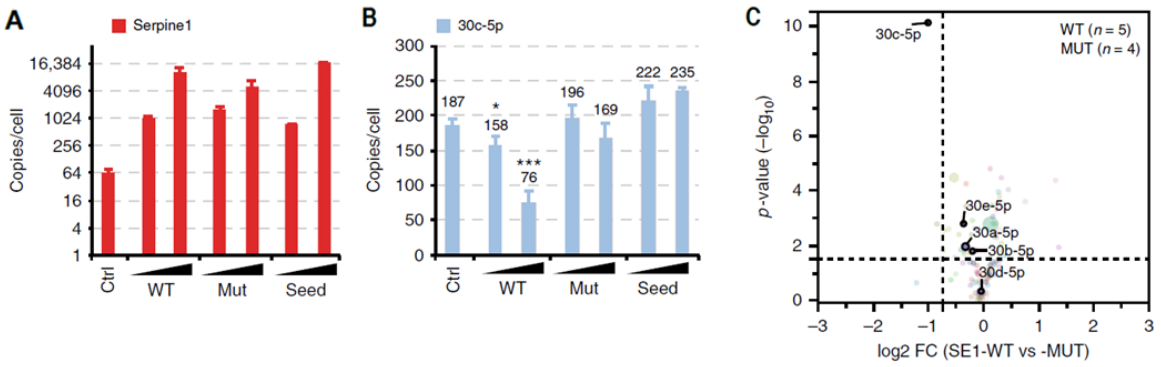

Figure 40. Absolute quantification of Serpine1 3'UTR and miR-30c in the rescue experiment. (A, B) Absolute expression (copies\cells) of Serpine1 3′UTR mRNA and miR-30c determined by RT-qPCR. Adenoviruses were expressed at two different multiplicities of infection (MOI ~1 and ~5). *p < 0.05, ***p < 0.001, Welch's t-test. (C) sRNA-seq was performed to measure miRNA expression in MRE-KO cells that express both a WT (n = 5) and a MUT (n =4) 3′UTR of Serpine1. The graph shows the average log2 FC (x-axis) and the p-value (–log10, y-axis) by Welch's t-test. Colour coding represents different miRNA families.

Furthermore, the RFP-SE1-WT construct also altered the level of the tailing variants, especially increasing the adenylated fraction of miR-30c and miR-30b (**Figure 41**).

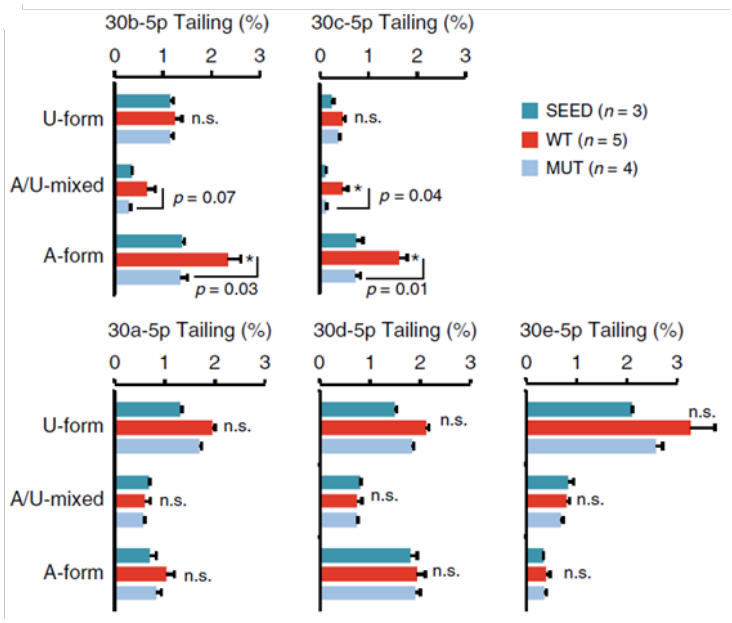

Figure 41. Evaluation of tailing events in the rescue experiment. % of tailing events, distinguished as adenylated (A-form), uridylated (U-form), or mixed isomiRs (A/U-mixed), as measured by sRNA-seq. p-values by Welch's t-test.

We then studied the 3’ pairing between Serpine1 and miR-30c in the context of ectopic MRE expression, using different Serpine1 mutants. We observed that the TDMD was almost completely abolished with four mismatches in the 3' end, while it underwent only a limited reduction when the central bulge size was increased up to seven nucleotides (**Figure 42A, Figure 42B**), suggesting that the 3C type is one of the crucial features for TDMD to occur.

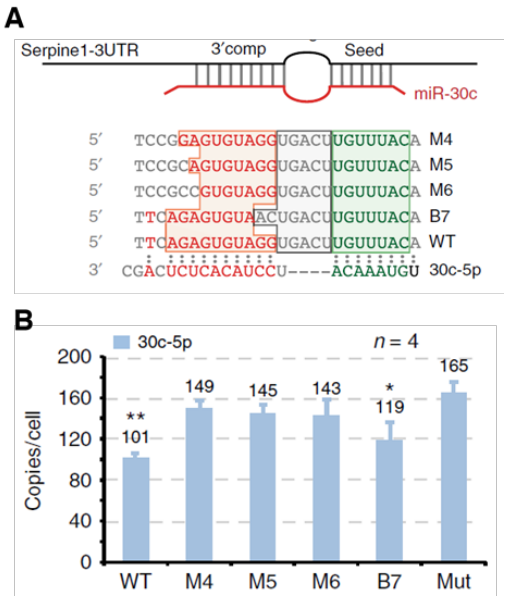

Figure 42. Expression of mutant binding sites for miR-30. (A) Scheme of the mutant Serpine1 3’UTR constructs (see Methods) that were designed to dissect TDMD 3′ pairing rules. Seed in green and 3′ complementary pairing in red. (B) Absolute expression (copies\cells) of miR-30c measured by RT-qPCR after over-expression of Serpine1 3’UTR mutants. *p < 0.05, ***p <0.01, Welch’s t-test.

2.1.5 miR-30 activity is modulated by Serpine1

We hypothesized that the endogenous targets involved in TDMD should control the global activity of miRNAs by inducing de-repression of shared targets, similarly to ceRNA competition (Bosson et., al 2014; Denzler et al., 2014). Instead, blocking TDMD, as we did in MRE-KO cells, should lead to an increase in miRNA activity (**Figure 43**).

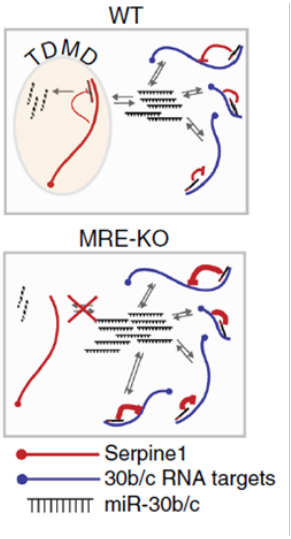

Figure 43. Scheme representing expected miR-30c activity of WT and MRE-KO cells. Canonical targets are in blue and TDMD transcripts in red. When TDMD is suppressed by removing the MRE from a TDMD target, miRNA increases in quantity and it is redistributed on their targets thus increasing its activity of repression.

To study miR-30c activity on endogenous targets at a global level, the complete transcriptome of parental cells and MRE-KO was measured, both in steady state (growing - GW) and after stimulation with serum (TC). By focusing our attention on the genes that were expressed in both conditions (n=9619), we defined miR-30 targets based on TargetScan7.1 computational predictions and we found 897 conserved (CS) and 1793 non-conserved (NCS) interactions. First the dynamics of miR-30 predicted targets in wild-type cells was evaluated. As shown in **Figure 26**, miR-30b/c expression strongly decreases 4hrs after serum stimulation. Conversely, predicted targets were more induced after 8 and 12h upon serum stimulation (**Figure 44**).

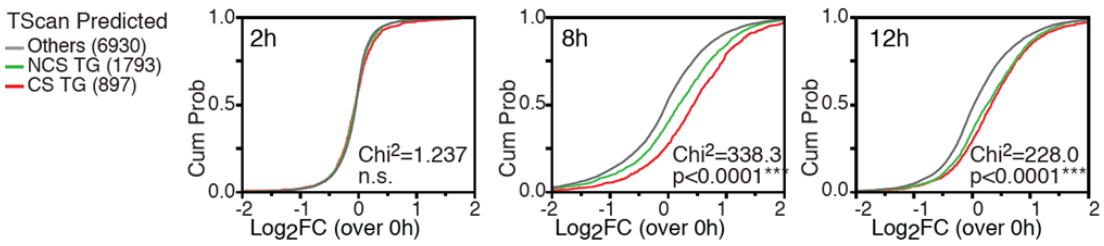

Figure 44. Analysis of the dynamics of targets after serum stimulation in WT 3T9 cells. Cumulative distribution functions (CDF) of log2FC over starved cells are shown for TargetScan predicted mir-30 targets conserved (CS) or not conserved (NCS).

Subsequently, the target repression in MRE-KO and wild type cells was compared. After serum stimulation, we previously demonstrated that the reduction of miR-30b/c was

abrogated in MRE-KO cells (see **Figure 37**). As expected, we observed a significant repression of miR-30c predicted targets either in asynchronously growing MRE-KO cells (**Figure 45A**) or in serum-stimulated cells at 8 and 12 hours (**Figure 45A, Figure 45B**). Taken together, these data substantiate the role of Serpine1:miR-30b/c interaction in control the activity of miR-30 targets.

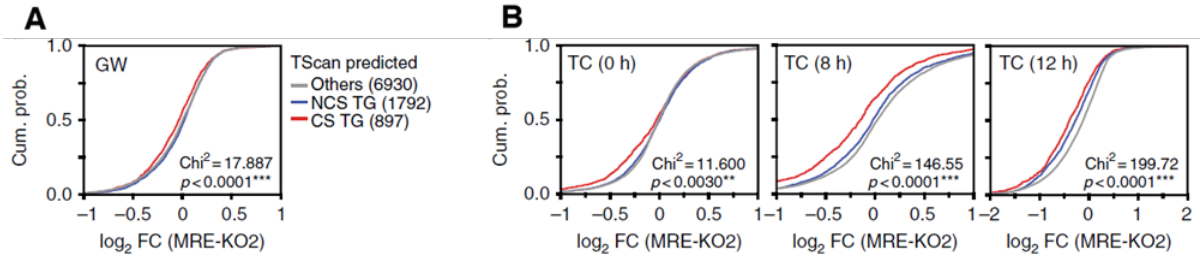

Figure 45. miR-30 activity increases in MRE KO cells. (A, B) Cumulative distribution functions (CDF) of log2 FC of mRNA (MRE-KO vs WT) for CS, NCS targets and genes not predicted as targets (Other).

2.2 Identification of TDMD pairs in human and mouse transcriptomes

In the previous chapter, we provided molecular evidence that the endogenous transcript Serpine1 controls the expression levels of miR-30b-5p and miR-30c-5p through TDMD mechanism in mouse fibroblasts (Ghini et al., 2018). Additional TDMD interactions has been described by other groups, one between the endogenous RNAs libra / Nrep and miR-29b-3p and the other between Cyrano and miR-7-5p (Bitetti et al., 2018; Kleaveland et al., 2018). Remarkably, these independent studies suggest that endogenous TDMD is widely involved in sculpting the levels of many miRNAs in several cellular contexts. Anyway, it is still unknown how many endogenous TDMD interactions exist. Indeed, the commonly used target predictive algorithms, such as TargetScan, miRanda or miRDB, that provide information about possible miRNA targets, rely on a scoring system (e.g. context score) that focuses on the seed region and, therefore, does not allow to specifically search for TDMD triggers. Therefore we decided to attempt a genome-wide identification of the potential TDMD interactions, by performing an integrative bioinformatics analysis on all the TargetScan predicted miRNA:target pairs. We focused on the structural features shared by all TDMD pairs so far reported (Cazalla et al., 2010; Bitetti et al., 2018; Kleaveland et al., 2018; Ghini, Rubolino et al., 2018) (**Figure 46A, Figure 46B**), as: i) the number of consecutive nucleotides pairings at the miRNA 3' end (3C pairing), ii) the size of the central bulge and iii) the miRNA:target hybridization energy (minimal free energy, MFE).

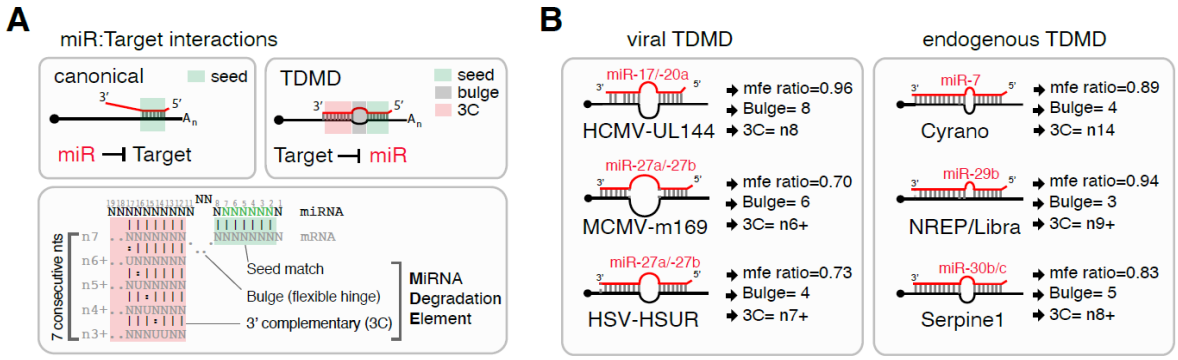

Figure 46. miRNA:TDMD trigger interactions. (A) On the top, the different types of miRNA:target interactions (canonical and TDMD) are shown. Below, panel describes the MDE (miRNA Degradation Element) and the nomenclature used to classify 3' complementarity (3C) types. (B) Schematic representation of the MDEs of known viral (on the left) and endogenous (on the right) TDMD targets. Their structural and thermodynamic features are described: minimal free energy (MFE) of the interaction, bulge and 3C type. MFE is reported as a ratio over an optimal TDMD duplex.

We implemented a pipeline, based on a custom R function, to compute these parameters for miRNA:target pairs (**Figure 47A**). Briefly, we performed pairwise sequence alignments

between miRNAs and targets based on a seed-anchoring approach, using as input all transcripts reported in the TargetScan7.2 database (human and mouse). For each miRNA:target pair, we then extracted structural information on its potentially TDMD-like structure by computing all the relevant quantitative parameters of the bipartite duplex (seed, 3C pairing and central bulge, altogether forming the "miRNA Degradation Element" or MDE, **Figure 46A**).

More than 10 million of miRNA:target pairs were analyzed for each of the two genomes. Then, a set of "Predicted TDMD-pairs" was defined based on the following rules (**Figure 47A**): *i*) a 3C pairing region at least 7 consecutive bases long, tolerating only one G:U wobbles (**Figure 46A** "3C type") *ii*) the presence of a bulge from 2 to 8 nucleotides, and *iii*) a miRNA:target hybridization energy at least 0.7 times greater than that of a theoretically perfect TDMD duplex ("MFE ratio" ≥ 0.7) in order to eliminate energetically unstable pairs generated by the alignment. Overall, the Predicted TDMD set includes 0.8% (**Figure 47B**) of all interactions either in human or in mouse, with a total of ~2,000 conserved (CS) and over 100,000 non conserved (nCS) interactions. Data are available online on the TDMD*finder* webtool, where users can freely explore and query the full dataset for TDMD predictions on a specific transcript and/or miRNA.

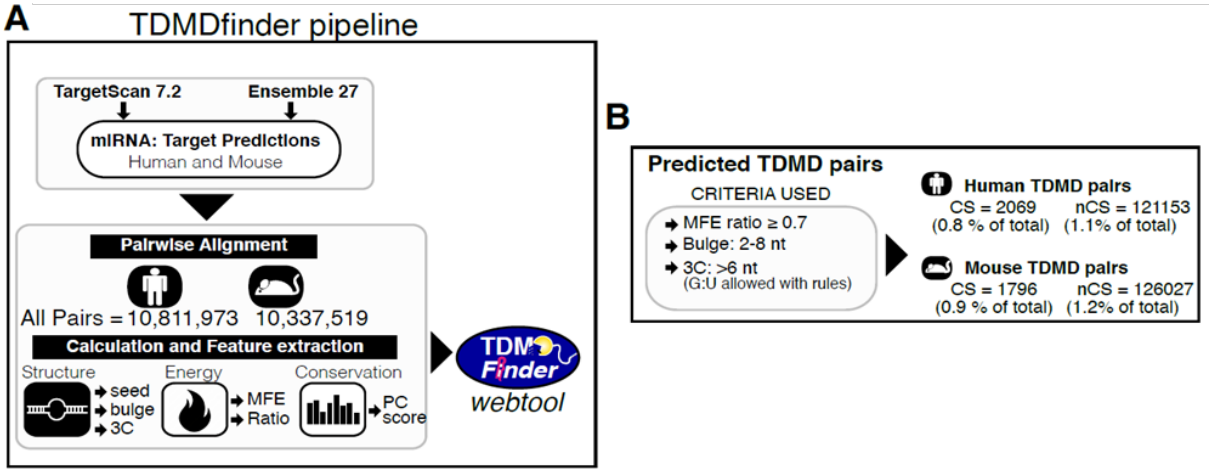

Figure 47. Identification of TDMD interactions in human and mouse transcriptome. (A) The schemes illustrate the workflow used to identify and investigate TDMD interactions: TDMD*finder* pipeline. (B) The criteria used to classify "Predicted TDMD" interactions are reported.

2.2.1 Features of the predicted TDMD-pairs

Of the criteria used to select for TDMD, the MFE ratio and the 3C consecutive pairing type resulted to be more stringent (**Figure 48**). In the case of the conserved human transcripts, 19% of pairs showed a MFE ratio > 0.7, while only 2.9% of pairs met the 3C consecutive match requirement (**Figure 48A, Figure 48B, Figure 48C**). Although TDMDs were selected without considering what type of match their seed regions formed, predicted TDMDs were slightly enriched for 8mer and 7mer-m8 types and depleted for 7mer-1A (**Figure 48D).**

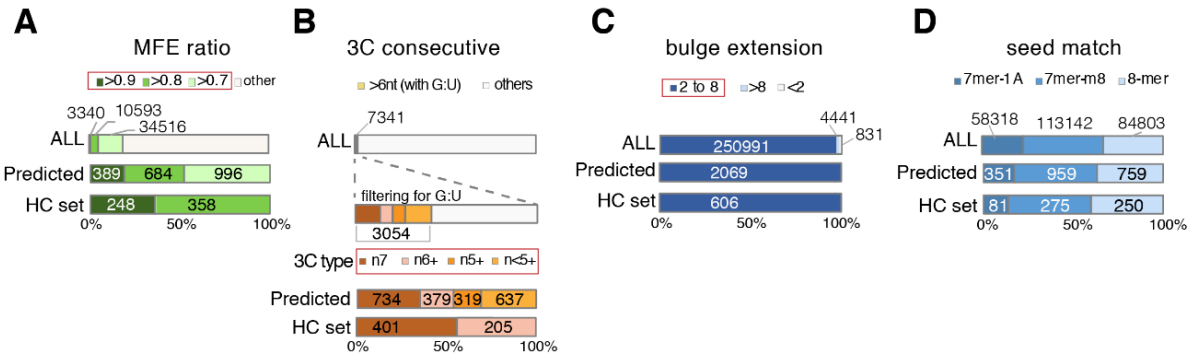

Figure 48. TDMD interactions features. (A-D) Features of genes and miRNAs involved in predicted endogenous TDMD. Bar plots describes the distribution, across all human conserved TargetScan predictions (ALL), the Predicted and the HC TDMD pairs, of the TDMD pair features. Predictions by TDMD*finder* were based on: MFE ratio class (A), 3C type (B), bulge extension (C) and seed match (D).

Analyzing the predicted sets for both humans and mouse, n7 was the most represented 3C type (about 25% of the predicted pairs) with at least 7 consecutive bases without G:U (**Figure 49A**). We annotated experimentally validated direct interactions either reported in the Human TarBase (Helwak et al., 2013) or obtained from intramolecular ligation-based approaches (CLEAR-SEQ and CLASH) (Moore et al., 2015; Pawlica et al., 2016). Globally, more than 20% of predicted TDMDs were found to correspond to validated interactions (**Figure 49B**). The overlap with each of the three validated data sets was significantly enriched (**Figure 49C**).

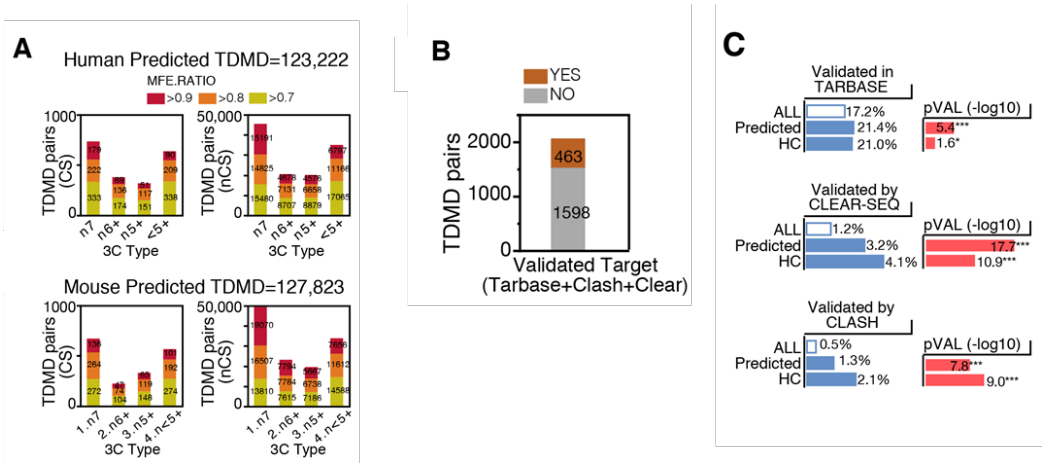

Figure 49. Characteristics of predicted TDMD pairs. (A) Number of Predicted TDMD pairs identified in the conserved (CS) and non-conserved (NCS) target groups. Data are stratified according to their 3C-type and MFE ratio class. (B) Human Conserved Predicted TDMDs are shown. Data are stratified according to their target validation status. (C) The frequency (%) of the validated transcripts was computed in the TargetScan database (ALL) and in the Predicted and High Confidence (HC) TDMD pairs sets (p-values by Chi-test).

Phylogenetic conservation, generally limited to the seed pairing region, is a key feature of miRNA target sites which are biologically functional (Bartel, 2018). However, we observed that in previously known endogenous TDMD triggers, such as Serpine1 and Nrep (Bitetti et al., 2018; Kleaveland et al., 2018), phylogenetic conservation extended also to the 3C pairing region (**Figure 50A)**. Overall, when compared to canonical MREs, the 3C pairing regions in MDEs of both Predicted and HC TDMDs were only marginally more phylogenetically conserved (**Figure 50B)**. When the conservation score (PhyloP) was individually assigned to predicted MDEs, 40% (829/2069) of them showed significant phylogenetic conservation (PhyloP score ≥ 2, which means P-value ≤ 0.01 in $-\log_{10}$ scale), suggesting a probable selective pressure (**Figure 50C**). Phylogenetically Conserved predicted TDMDs are also reported online, in the *TDMDfinder* tool.

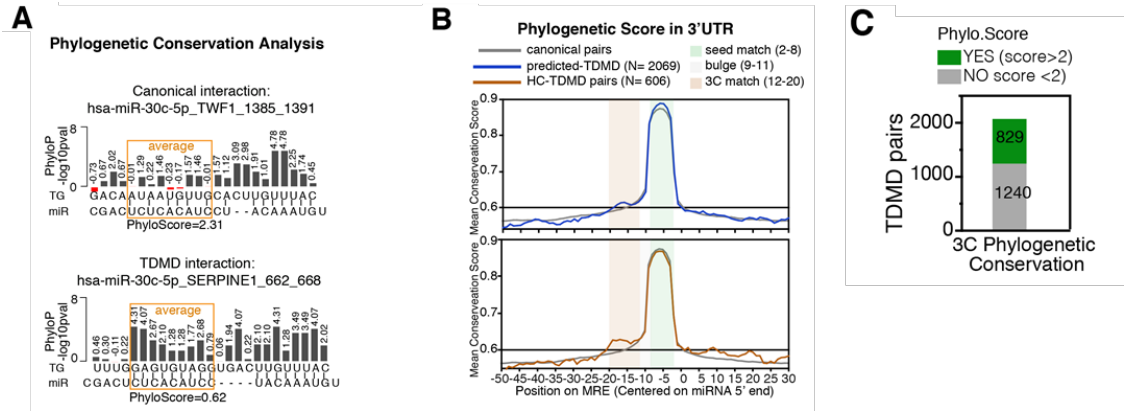

Figure 50. Phylogenetic conservation analysis. (A) A typical phylogenetic conservation analysis is shown. On the top, there is an example of PhyloP scores for a canonical interaction between miR-30c and TWF1, a canonical target with a non-conserved MRE. Below, the same analysis was performed for miR-30c and SERPINE1, a TDMD transcript with a conserved MDE. (B) Representation of the mean PhyloP conservation score at single nucleotide level. The analysis was performed for Predicted and HC MDEs and for control MREs. The conservation score is provided for 50 bases upstream from the 30 bases downstream from the nucleotide matching miRNA 5' end. (C) Phylogenetic Conservation of Predicted TDMD pairs measured by PhyloP scores (average conservation over the whole 3C pairing region).

2.2.2 Features of genes and miRNAs predicted to be involved in TDMD

Human-predicted TDMD interactions consist in a total of 1457 different TDMD genes (i.e. 11.8% of genes with at least one preserved MRE) and 324 different miRNAs (87.6% of 370 miRNAs with at least one CS target). Therefore, most miRNAs are probably susceptible to TDMD degradation, instead a relatively small group of genes is potentially capable of triggering TDMD. On average, each miRNA reported 5 CS Predicted MDEs and 36 NCS Predicted MDEs (**Figure 51**).

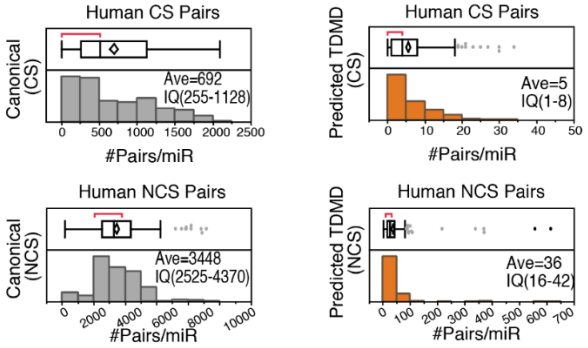

Figure 51. Number of transcripts per miRNA. Canonical targets (on the left) or Predicted TDMD (on the right) are considered and divided according to conserved (on the top) and non-conserved (below) targets. Average values (Ave) and interquartile ranges (IQ) are reported.

We performed a correlation analysis to evaluate and compare the number of conserved MREs (canonical transcripts predicted by TargetScan) and that of MDEs (TDMD triggers predicted by TDMD*finder*). For some of the miRNA families, for example miR-15, miR-17, miR-302, miR-28, known to include several members and/or to have a complex genomic organization, a larger number of CS TDMD interactions was predicted (**Figure 52A)**. As for the NCS TDMD pairs, they were found to be unusually over-represented in the miR-17 family (**Figure 52B, Figure 52C**).

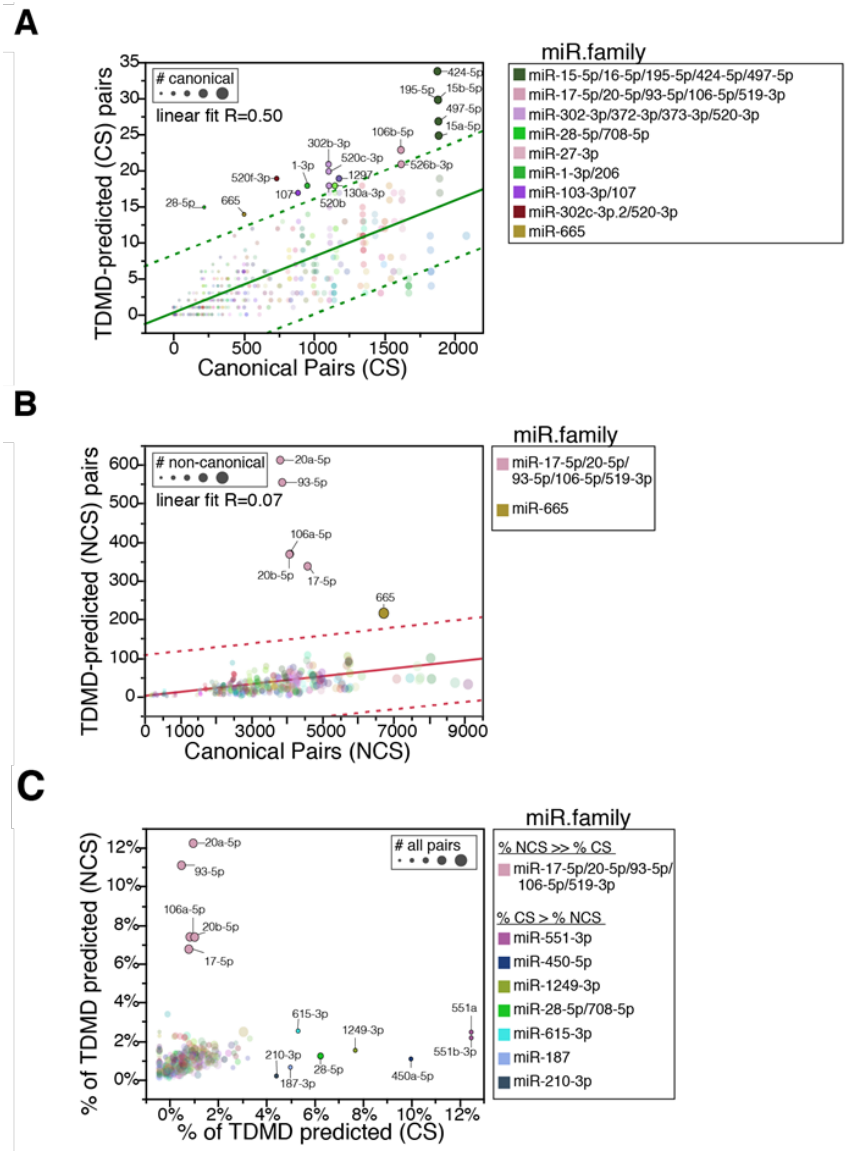

Figure 52. Correlation analysis to compare the number of canonical targets and TDMD transcripts. (A, B) Correlation between the number of canonical and TDMD targets for conserved (A) and non-conserved pairs (B) is described in a bivariate analysis with linear fitting. Outlier families are highlighted. (C) Bivariate analysis correlating the frequencies of TDMD transcripts calculated over total conserved (CS) and non-conserved (NCS) interactions. Outlier families are reported.

The genes predicted to establish TDMD interactions (TDMD genes) showed some particular characteristics. Compared to canonical target genes, they exhibited significantly longer 3' UTRs and remarkably more MREs, which were also at a higher density (**Figure 53A**). MRE and MDE were similarly positioned within the 3'UTRs (**Figure 53B**) and had similar inclusion rates in alternative transcription isoforms (**Figure 53C**).

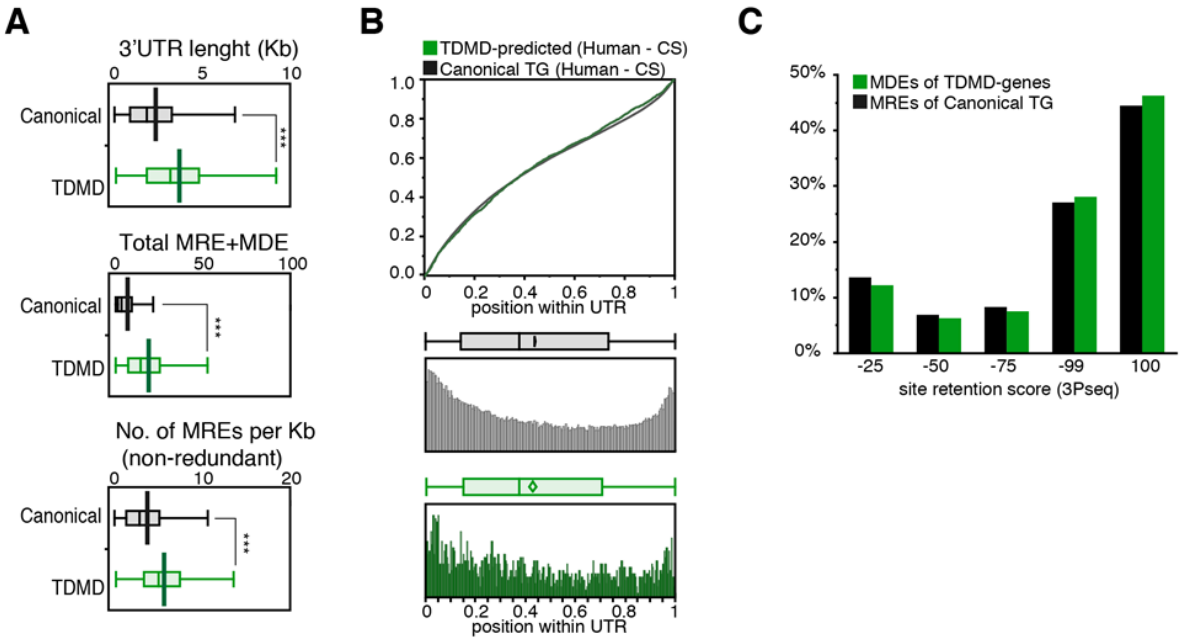

Figure 53. Main features of Predicted MDEs. (A) 3'UTR region length (Kilobase) (top), number (Total MRE+MDE) (center) and density (number of MREs per Kilobase) in conserved canonical target and TDMD genes are reported (***p < 0.001, Wilcoxon test). (B) Cumulative distribution function (CDF) plot of MREs and MDEs relative positions (0-100 scale) within their 3'UTR regions. The data are evaluated in canonical targets and TDMD predicted genes, respectively. (C) The plot shows the frequency (%) of site retention among alternative isoforms, measured for both MREs and MDEs. 3Pseq data from TargetScan 7.2 were used to estimate affected isoform ratios (AIR, 0-100).

Regarding their biological functions, TDMD genes were enriched both for development related ontologies, with particularly overrepresented neuronal functions, and for pathways and upstream regulators that are frequently altered in human cancer, such as estrogen, P53, WNT and TGF-β signaling (**Figure 54A, Figure 54B, Figure 54C**). By performing tissue-specific expression analysis, it was observed that most of the TDMD genes were expressed in several tissues, while 99 of them were highly specific for the brain (**Figure 54D**). This might reflect the higher propensity of TDMD mechanism to occur in the brain, where it was primarily described as being particularly active (de la Mata et al., 2015; Ghini, Rubolino et al,. 2018).

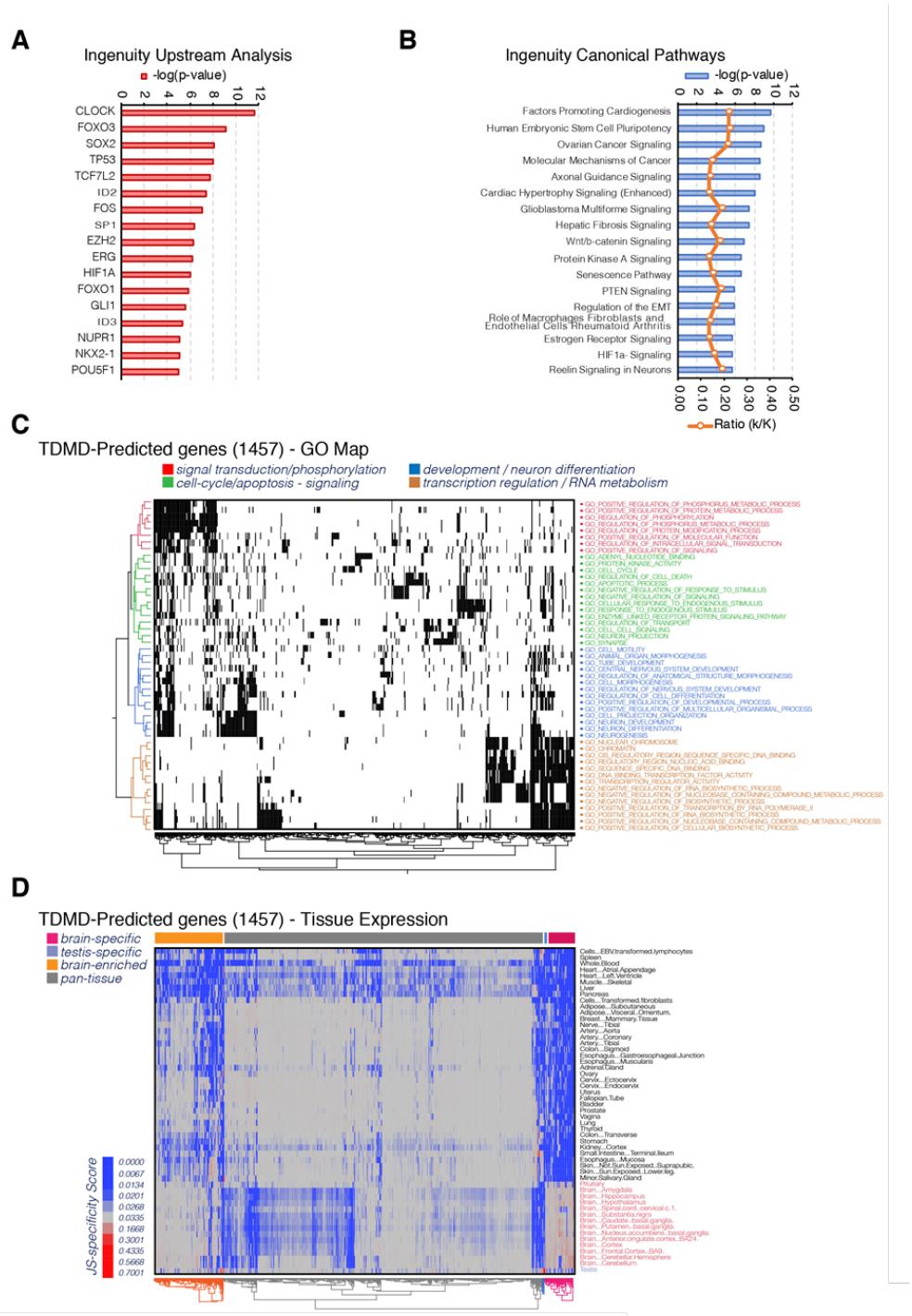

Figure 54. Features of Predicted TDMD genes. (A) Upstream regulators enriched among the 1457 Predicted TDMD genes (IPA, Qiagen). The pathways with a -log10 pValue > 5 are reported. (B) Canonical pathways enriched among the Predicted TDMD genes (IPA, Qiagen); k indicates the fraction of genes in the intersection of predicted genes with indicated pathways, while K indicates the total number of genes in each set. (C) Two-way clustering of Predicted TDMD genes (columns) and enriched Gene Ontologies (rows); statistically significant GOs, as determined through the "compute overlaps'" tool at MSigDB, are shown in black. Clustering highlights group of GO which are functionally related, as reported in the legend above the graph. (D) Two-way cluster (ward method) showing the specificity score (JS Score) of Predicted TDMD genes in different tissues. The higher is the JS score, the stronger is the specific expression of a gene only in a fraction of the samples under examination. Expression data were obtained from GTEx dataset. The cluster in red highlights brain derived samples.

2.2.3 Strategy for the experimental validation of predicted TDMD-pairs

In order to experimentally verify the accuracy of the TDMD*finder* predictions, we selected 38 predicted TDMD interactions, related to 25 different TDMD-genes and 9 miRNA families (**Figure *55***).

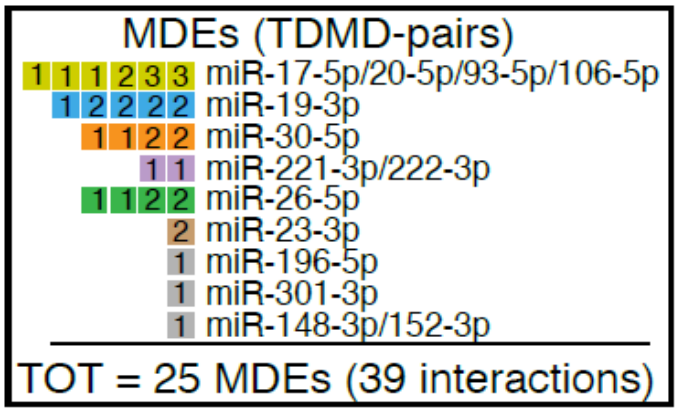

Figure 55. List of the predicted TDMD pairs tested. Each square represents a miRNA degradation element (MDE). MDEs that target the same miRNA family are grouped. The number reported in the squares describes the total number of interactions. Colored squared indicate that at least one of the corresponding TDMD pairs has been positively validated.

We focused our attention on miRNA families that have i) phylogenetically conserved seed region, ii) whose miRNA members are expressed in HeLa cells (used for the experimental validation) and iii) have been reported as relevant for human cancer (according to the literature). As positive control, we used the SERPINE1:30c interaction, which we have previously identified and validated in mouse fibroblasts (Ghini, Rubolino et al., 2018). To verify the occurrence of TDMD we used an approach, named 'TDMD assay', based on the ectopic overexpression of GFP reporter plasmids containing in their 3'UTRs the MDEs of the predicted TDMD transcripts with high (>90%) transfection efficiency (**Figure 56A, Figure 56B**).

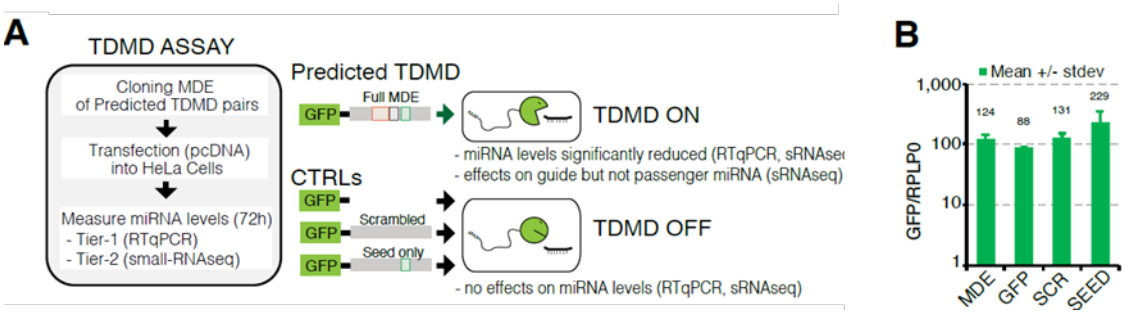

Figure 56. Strategy for the validation of TDMD interactions: the TDMD assay. (A) Summary procedure of the TDMD-assay. For each candidate, a region (~100bp or ~400bp depending on the construct) containing the predicted MDE was cloned into a GFP vector and transiently overexpressed in HeLa cells. (B) The bar chart shows the relative expression of the different constructs using RPLP0 as reference.

To prove the specificity of the observed effect, negative controls were used: i) the empty GFP vector (CTRL_GFP), the GFP vector encoding either ii) a scramble sequence (SCR) or iii) a mutant form of the MDE of interest, obtained by deleting the 3C pairing region while leaving the seed pairing sequence (SEED) intact. The expression levels of the target miRNAs were measured by RT-qPCR and small RNA-sequencing (sRNA-seq). sRNA-seq was used to monitor the expression levels of guide and passenger miRNAs. In fact, TDMD is acting at post-transcriptional level and, therefore, we expect that each tested MDE should be able to repress the expression of the cognate guide miRNA only, with no effects on the passenger miRNA. Indeed, when using the MDE of SERPINE1, miR-30c and -30b were significantly reduced, as predicted (**Figure 57A, Figure 57B, Figure 57C**) and sRNA-seq confirmed that the passenger strands for both miR-30c and -30b did not significantly change (**Figure 57C, Figure 57D**). Also, two additional controls were designed for miR-106b and miR-26a, namely "Optimal TDMD" MDEs, *ad hoc* sequences pairing with all bases of the miRNA sequence, except in position 9-10-11. When we tested these two artificial "optimal TDMD", we found that TDMD uncouples the expression of the two miRNAs strands by targeting specifically the guide strand (**Figure 57E, Figure 57F).** Hence, these data demonstrated that the "TDMD assay" is an effective strategy for testing TDMD*finder* predictions.

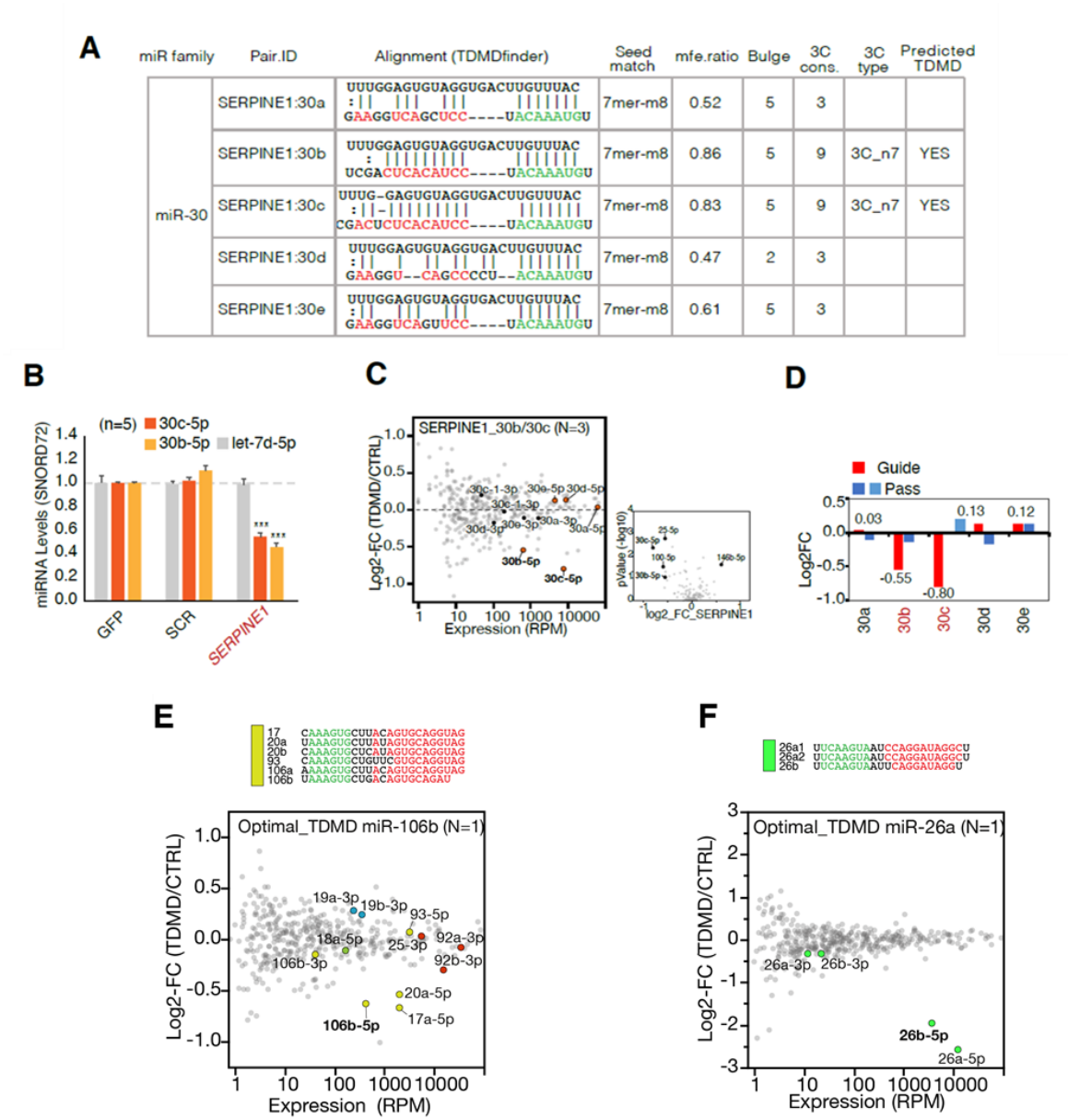

Figure 57. TDMD assay on SERPINE1:miR.30b/c pairs. (A) TDMD*finder* predictions output for SERPINE1 trigger and miR-30 family. (B) Results of TDMD assays, for SERPINE1 and miR-30 family. The bar chart shows the mature miRNAs levels measured by performing RT-qPCR (+/- SEM, N=biological replicates) and normalized over CTRL_GFP. The unrelated Let-7d miRNA was also measured. SNORD72 was used as normalizer. p-values were calculated by Dunnet's t-Test, using the SCR group as reference. (C) Small-RNA sequencing results of the TDMD assays. On the left, the scatter plot of the regulations (log2 fold changes of MDE vs CTRL, y axis) over the expression (reads per million, x-axis) of all detected miRNAs is shown. The colored dots represent the members of the targeted miR-family (guide and passenger miRNAs). On the right, it is shown the volcano plot highlighting the miRNAs statistically deregulated (p-values by Student's t-test < 0.05 and log2FC > |0.5|). (D) sRNA-seq measurement of mature miRNAs levels upon SERPINE1 assay for the entire miR-30 family, with guide and passenger miRNAs is shown. CTRL_GFP is used as normalizer. (E, F) Small-RNA sequencing results related to two control TDMD transcripts ("Optimal_TDMD") that were designed in order to promote the specific decrease in miRNAs belonging to the miR-17 family (E) and the miR-26 family (F).

2.2.4 Validation of the predicted TDMD pairs

Next, we applied the same strategy to measure the effects of 37 predicted TDMD interactions that were selected for the validation. By using either RT-qPCR or sRNA-seq, we observed a significant reduction in the levels of the predicted guide miRNAs and negligible differences in the levels of the passenger miRNAs in 20 of the 37 tested pairs (**Figure 58**).

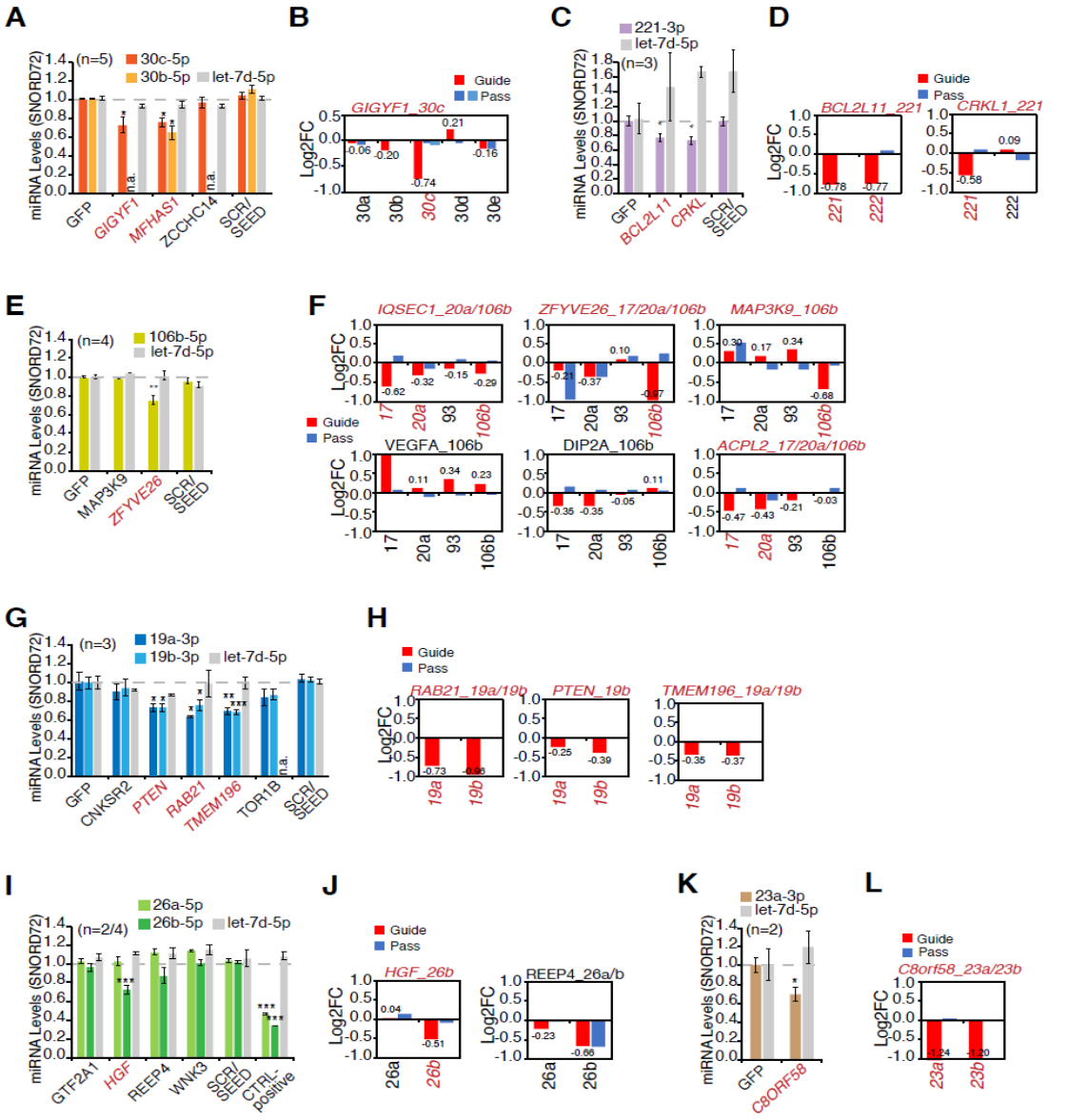

Figure 58. Experimental validation of predicted TDMD interactions. (A-L) Results of TDMD assay, divided for miRNA family. The plots (A, C, E, G, I, K) show mature miRNAs expression levels (+/- SEM, N= number of replicates) measured by performing RT-qPCR and normalized over CTRL_GFP. The unrelated miRNA, Let-7d, was also measured. SNORD72 was used as housekeeping gene. P-values were calculated by Dunnet's t-Test, using the SCR/SEED group as reference. Plots (B, D, F, H, J, L) show mature miRNAs levels for the all miRNA family, with guide and passenger miRNAs) measured by sRNA-seq and normalized over CTRL_GFP. Above each bar graph are indicated the predicted interactions (gene:miRNA, in red when the prediction was confirmed).

Besides finding a new trigger for miR-30c (GIGYF1:30c, **Figure 58A, Figure 58B**), a member of a family already known to be regulated by TDMD, five other families were found: miR-221 (CRKL:221, BCL2L11:221, **Figure 58C, Figure 58D**), miR-17 (IQSEC1:20a/106b, ZFYVE26:106b, MAP3K9:106b, ACPL2:17 **Figure 58E, Figure 58F**), miR-19 (RAB21:19a/b, PTEN:19b, TMEM196:19a/b, **Figure 58G, Figure 58H**), miR-26 (HGF:26b, **Figure 58I, Figure 58J)** and miR-23 (C8orf58:23a/b, **Figure 58K, Figure 58L**). Three TDMD pairs were excluded from the set of validated interactions as they showed differences in the levels of the passenger miRNAs by sRNA-seq: REEP4:26b, ACPL2:20a and ZFYVE26:20a (**Figure 58F, Figure 58J).** Three other families (miR-196 miR-148, miR-301) were tested, but their predicted MDEs did not trigger significant effects (**Figure 59A, Figure 59B**).

To further confirm that the miRNA levels decrease was due to a post-transcriptional mechanism, the primary transcript levels (pri-miRNAs) for two of the miRNA families (miR-30 and miR-19, **Figure 59C, Figure 59D**) were measured. In both cases, the expression levels of pri-miRNAs are unable to explain the observed change in miRNA levels. In conclusion, these results showed that 17 out of the 37 tested interactions and six distinct miRNA families are susceptible to TDMD when MDEs are overexpressed in HeLa cells.

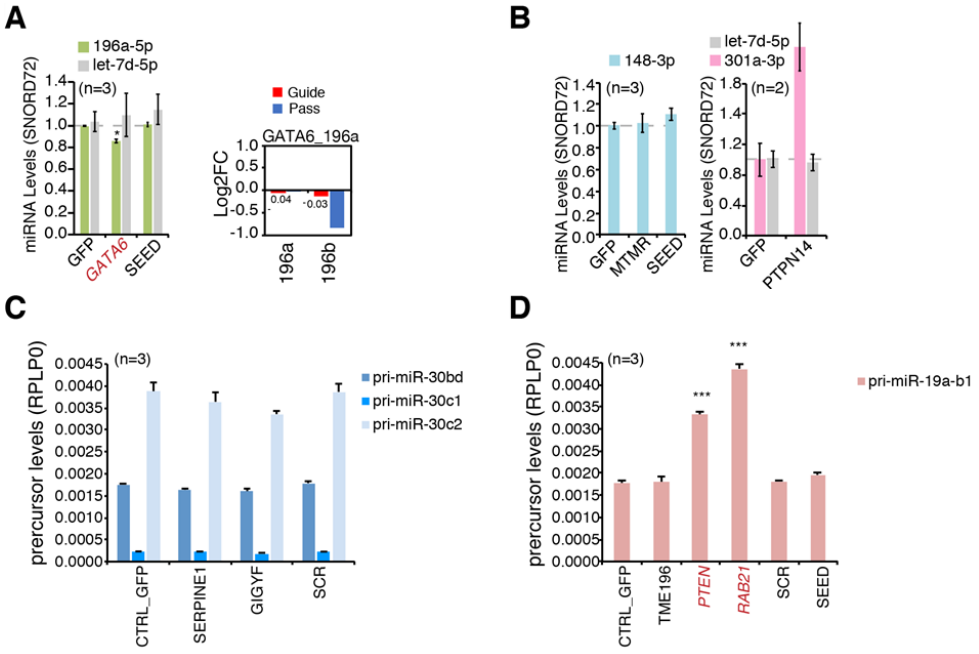

Figure 59. Experimental validation of predicted TDMD interactions. (A, B) Results of TDMD assays for miR families that were not validated. (A) The bar chart shows mature miR-196a relative expression (+/- SEM) using SNORD72 as reference. Expression levels were measured by RT-qPCR (on the left) or by small-RNA-seq (on the right). (B) The bar charts show mature miR-148a and miR-301a relative expression (+/- SEM) using SNORD72 as reference, measured by RT-qPCR. (C, D). The bar chart shows miR-30b/c and miR-19a/b primary transcripts relative expression (+/- SEM) using RPLP0 as reference, measured by RT-qPCR. Pri-miR-19b-2 was not detected in HeLa cells and it is not shown.

2.2.5 Identification of High-Confidence (HC) TDMD pairs

To correct for any transcriptional effect on miRNA levels that might have been caused by the assay, we calculated the "TDMD net effect" by normalizing the reduction in the expression of each guide miRNA for the regulation (if any) in the levels of its passenger. Eight MDEs, corresponding to 10 interactions, displayed a strong TDMD net effect (-0.5 log_2 normalized decrease; **Figure 60A**): GIGYF1 and SERPINE1 (miR-30c), MAP3K9 and ZFYVE26 (miR-106b), RAB21 (miR-19a/b), BCL2L11 and CRKL (miR-221) and C8orf58 (miR-23a/b). Through a contingency analysis, we compared the "net TDMD effect" with the predicted TDMD interactions features. Stronger TDMD effects were significantly related to MDE characterized by extensive (n7) 3C pairings, high binding energy (MFE ratio ≥ 0.8) and with bulges larger than 4 nucleotides. (**Figure 60B**).

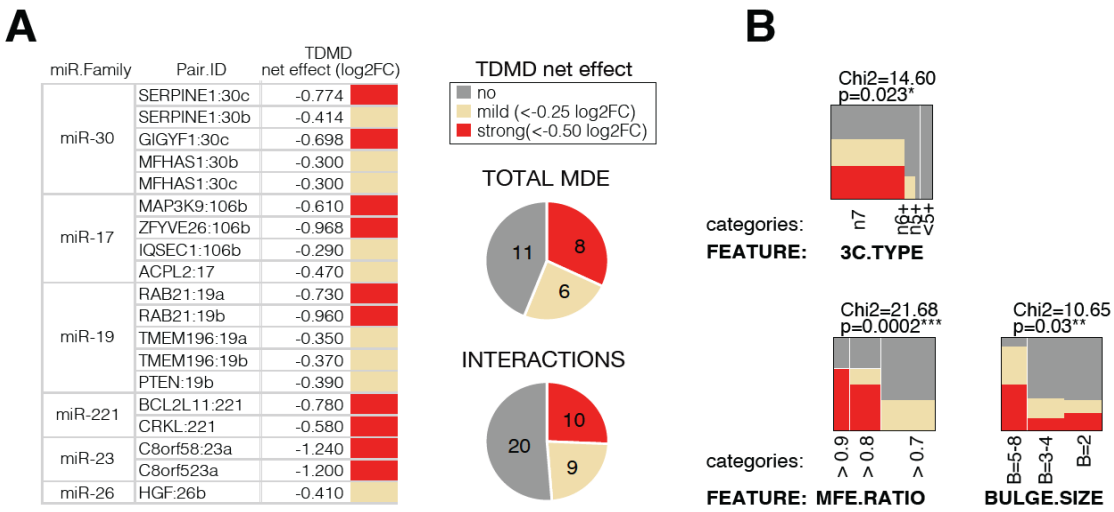

Figure 60. Summary of validation results. (A) The validation results are summarized in the table (on the left) and in the pie charts (on the right). The results were expressed as "TDMD net effect", normalizing the log2FC (MDE vs CTRL) of the guide over the associated passenger miRNA by sRNA-seq. (B) Contingency analysis are shown. The "TDMD net effect" classes are correlated to TDMD predictions features (p-values by Chi-test).

No significant associations were found with the level of phylogenetic conservation, the number of matches at the miRNA 3' end or with whether or not the miRNA:target interaction of interest had been experimentally verified (according to Tarbase) (**Figure 60B**). However, a positive trend was found in all of the above features. Notably, all the strongest interactions belonged to either the n7 or the n6+ 3C type and had a MFE ratio of at least 0.8 (**Figure 61A**), and for this reason they have been grouped into a "High Confidence TDMD" set (HC TDMD), including miRNA:target interactions with the highest probability of being actual TDMD couples. The HC set consists in the ~0.2% of all interactions, with 606 and 521 CS

pairs in human and mouse, respectively. About 29% of the Human Predicted TDMD Set is retained in the HC set (**Figure 61B)**. All HC TDMD interactions have been annotated in the TDMD finder webtool.

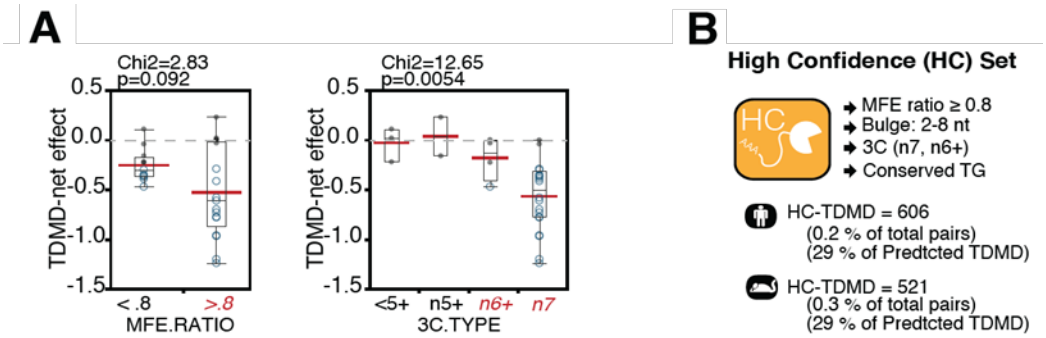

Figure 61. High Confidence set definition. (A) Box plots of the "TDMD net effects". TDMD interactions are grouped according to MFE ratio (on the left) or 3C type (on the right) (p-values and Chi-square by Wilcoxon test). (B) Criteria used to classify High-Confidence TDMD pairs in human and mouse are shown.

2.2.6 TDMDfinder predicts selective TDMD effects for miRNA families

sRNA-seq data were used to evaluate if TDMD*finder* could selectively predict the effect of several MDEs on different members of the same miRNA family, which share the same seed sequence and therefore are associated with similar sets of canonical targets, but often display different 3' ends and therefore are in theory susceptible to post-transcriptional regulation by different sets of MDEs. For example, TDMD*finder* predicts that the members of the miR-30 family are differently susceptible to TDMD, due to the different pairing conformations they adopt when binding their triggers (**Figure 62)**.

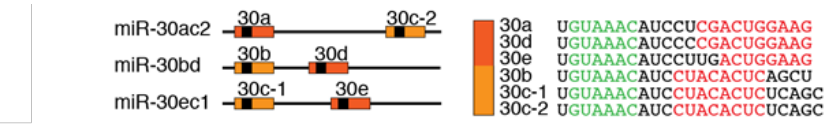

miR family	Pair.ID	Alignment (TDMDfinder)	Seed match	mfe.ratio	Bulge	3C cons.	3C G:U	3C type	Predicted TDMD
miR-30	SERPINE1:30a	UUUGGAGUGUAGGUGACUUGUUUAC GAAGGUCAGCUCC----UACAAAUGU	7mer-m8	0.52	5	3	3		
	SERPINE1:30b	UUUGGAGUGUAGGUGACUUGUUUAC UCGACUCACAUCC----UACAAAUGU	7mer-m8	0.86	5	9	9	3C_n7	YES
	SERPINE1:30c	UUUG-GAGUGUAGGUGACUUGUUUAC CGACUCUCACAUCC----UACAAAUGU	7mer-m8	0.83	5	9	9	3C_n7	YES
	SERPINE1:30d	UUUGGAGUGUAGGUGACUUGUUUAC GAAGGU--CAGCCCCU--ACAAAUGU	7mer-m8	0.47	2	3	3		
	SERPINE1:30e	UUUGGAGUGUAGGUGACUUGUUUAC GAAGGUCAGUUCC----UACAAAUGU	7mer-m8	0.61	5	3	3		

miR family	Pair.ID	Alignment (TDMDfinder)	Seed match	mfe.ratio	Bulge	3C cons.	3C type	Predicted TDMD
miR-30	GIGYF1:30a	CUUCUGAGAGUGGUCAAUGUUUACA GAAG---GUCAGCUCCUACAAAUGU	8mer	0.66	3	4		
	GIGYF1:30b	CUUCUGAGAGUGGUCAAUGUUUACA UCGACUCACAUC--CUACAAAUGU	8mer	0.76	3	5		
	GIGYF1:30c	CUUCUGAGAGUGGUCAAUGUUUACA CGACUCUCACAUCCUACAAAUGU	8mer	0.87	4	9	3C_n7	YES
	GIGYF1:30d	CUUCUGAGAGUGGUCAAUGUUUACA GAAG---GUCAGCCCCUACAAAUGU	8mer	0.62	3	4		
	GIGYF1:30e	CUUCUGAGAGUGGUCAAUGUUUACA GAAG---GUCAGUUCCUACAAAUGU	8mer	0.74	5	4		

Figure 62. Schematic summary of miR-30 family predictions selected for the experimental validation. On the top, the guide miRNA sequences and the genomic cluster organization are shown. The seed and 3C pairing regions are highlighted. Below, the TDMD*finder* predictions of miRNA:target alignment are reported in the tables. The scores for MFE ratio, Bulge extension, 3C and 3C type are also shown. Alignment and features are available in the online tool.

sRNA-seq results from the TDMD assay experiments confirmed that validated miR-30 TDMD targets (SERPINE1, GIGYF1) significantly altered the expression levels of only few miRNAs and exhibited a clear specificity. Specifically, SERPINE1 repressed both miR-30b and miR-30c levels (**Figure 63A),** instead GIGYF1 acted only on miR-30c (**Figure 63B**).

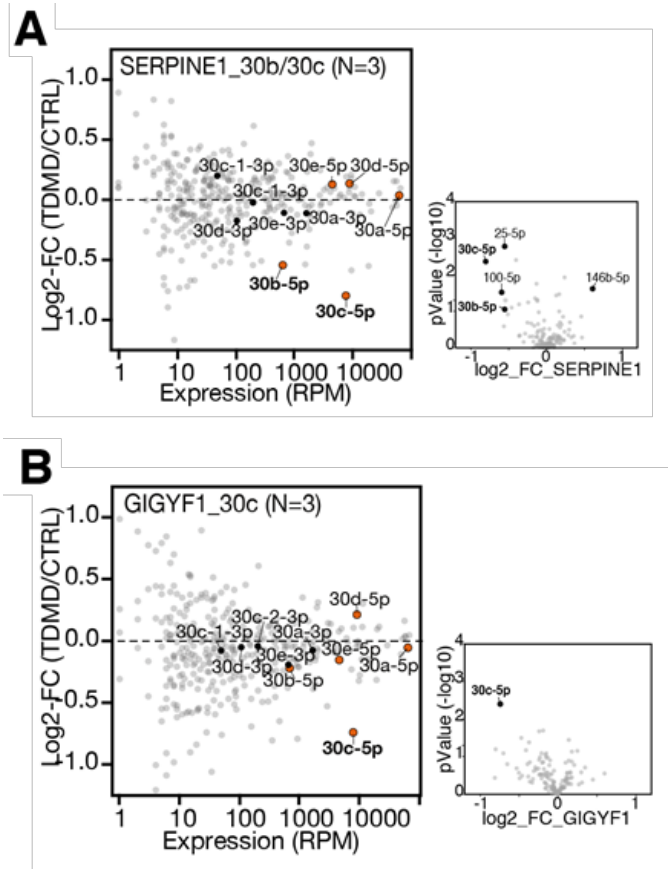

Figure 63. sRNA-seq results of miR-30 family predictions by TDMD assay. (A, B) On the left, the scatter plot shows the fold changes (log2 of MDE vs CTRL, y axis) over the expression levels (reads per million, x-axis) of all the detected miRNAs. The colored dots represent the members of the targeted miR-family (guide and passenger miRNAs) and the co-clustered miRNAs (if any). On the right, the volcano plots highlight miRNAs regulated in a statistically significant manner (p-values by Student's t-test <0.05 and log2FC >|0.5|).

In the case of the miR-221 and miR-26 families, TDMD*finder* also predicted different susceptibility to TDMD because of a very different type of 3C pairing and energetic stability (**Figure 64A, Figure 64B**).

Figure 64. Representation of miR-222 and miR-26 family predictions selected for the experimental validation. (A, B) On the top, guide miRNAs sequences and genomic cluster organization are reported. The seed and 3C pairing regions are highlighted. Below, the TDMD*finder* predictions of miRNA:trigger alignment are showed in the tables. The scores for MFE ratio, Bulge extension, 3C and 3C type are also shown.

Coherently, CRKL1 is able to discriminate between miR-221 and miR-222 (**Figure 65A**) and HGF discriminated miR-26b from miR-26a (**Figure 65B**). On the contrary, BCL2L11, which had been predicted to interact only with miR-221 (**Figure 64A**), could significantly repress miR-222 too (**Figure 65A**). Notably, we observed that a different alignment with a 3C pairing, made up of 6 consecutive nucleotides at the miRNA 3' end, is also possible and might explain this effect (**Figure 64A**).

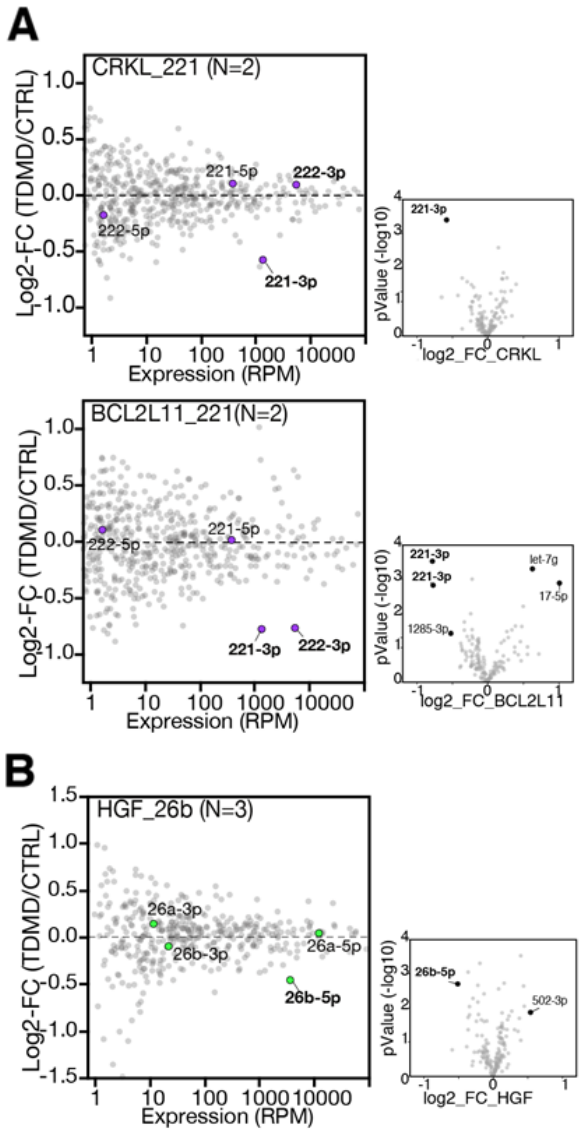

Figure 65. sRNA-seq results of miR-222 and miR-26 family predictions by TDMD assay. (A, B) The scatter plot shows the fold changes (log2 of MDE vs CTRL, y axis) over the expression levels (reads per million, x-axis) of all the detected miRNAs. Above each panel the predicted TDMD pairs and number of replicates (N) are showed. The colored dots represent the members of the targeted miRNA family (guide and passenger) and the co-clustered miRNAs (if any) (p-values by Student's t-test < 0.05 and log2FC >|0.5|). On the right, the volcano plots highlight miRNAs statistically significant regulated (p-values by Student's t-test < 0.05 and log2FC >|0.5|).

Regarding the miRNAs belonging to each of the remaining families (miR-17, miR-19 and miR-23), similar 3' end sequences have been observed, so TDMD*finder* predictions were less selective, with the same MDE directed to different family members (**Figure 66A, Figure 66B, Figure 66C)**.

Figure 66. Representation of miR-17, miR-19 and miR-23 family predictions selected for the experimental validation. (A, B, C) Guide miRNAs sequences and genomic cluster organization for miR-17 (A), miR-19 (B) and miR-23 (C) families. The seed and 3C pairing regions are highlighted. TDMD*finder* predictions of miRNA:target alignment are reported in the tables. The scores for MFE ratio, Bulge extension, 3C and 3C type are also shown. Alignment and features are available in the online tool.

Coherently, sRNA-seq results were more widely distributed, with multiple members of the predicted miRNA families being repressed **(Figure 67A, Figure 67B Figure 67C)**.

In the case of some MDEs (i.e. ZFYVE26, RAB21, TMEM196 and PTEN), unrelated miRNAs were also regulated, possibly as a result of secondary effects in these TDMD tests. Interestingly, as predicted by TDMD*finder,* miR-106b, whose 3C region is the most divergent within the miR-17 family, was specifically repressed by MAP3K9 **(Figure 66A and Figure 67A)**.

In conclusion, TDMD*finder* predictions could point out if TDMD selectively affects different members of the same miRNA family. This could happen in the case of miRNAs whose 3C regions are sufficiently different.

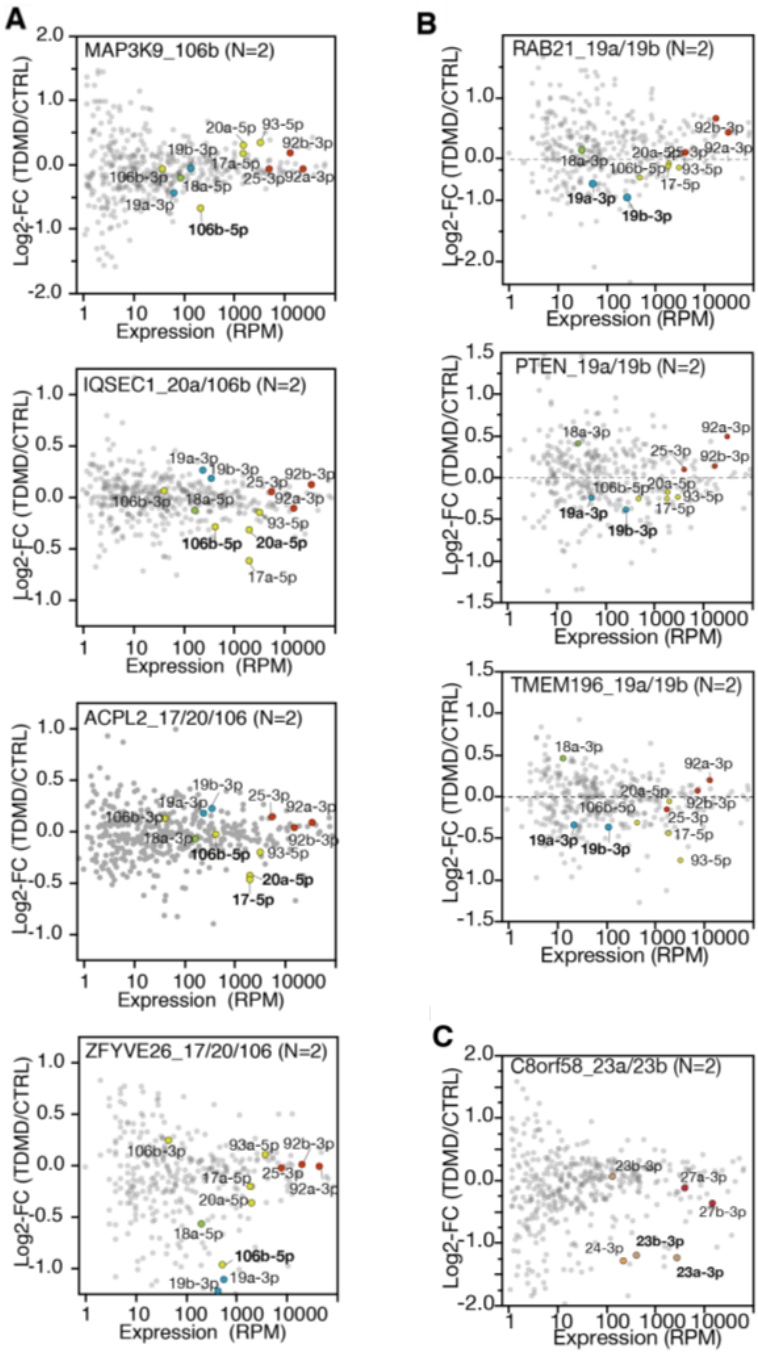

Figure 67. sRNA-seq results of miR-17, miR-19 and miR-23 family predictions by TDMD assay. (A, B, C) sRNA-seq results of the TDMD assays experiments. The scatter plot shows the fold changes (log2 of MDE vs CTRL, y axis) over the expression levels (reads per million, x-axis) of all the detected miRNAs. Above each panel the predicted interactions and the number of replicates (N) are reported. The colored dots represent the members of the considered miRNA family (guide and passenger) and the co-clustered miRNAs (if any) (p-values by Student's t-test < 0.05 and log2FC >|0.5|).

2.3 Analysis of TDMD interactions in cancer datasets

In Chapter 2, we identified TDMD triggers by a predictive tool based on sequence alignment and structural features calculations. Nonetheless, the TDMD mechanism depends also on quantitative parameters, primarily the expression levels of both the miRNA and the target (Bitetti et al., 2018; Sheu-Gruttadauria et al., 2019; Han et al., 2020), which were not taken into consideration. We used the multi-omic molecular landscape of human tumors provided by The Cancer Genome Atlas (TCGA) to retrieve miRNA and mRNA expression data in 21 cancer datasets for a total of 8572 tumor samples (**Figure 68A**). We focused on the High Confidence TDMD subset, which contained 606 miRNA:target pairs. For each of these pairs we retrieved information about miRNA expression and target expression (**Figure 68B, Figure 68C**) and performed a series of correlation analysis to investigate which TDMD interactions might be relevant in human cancer.

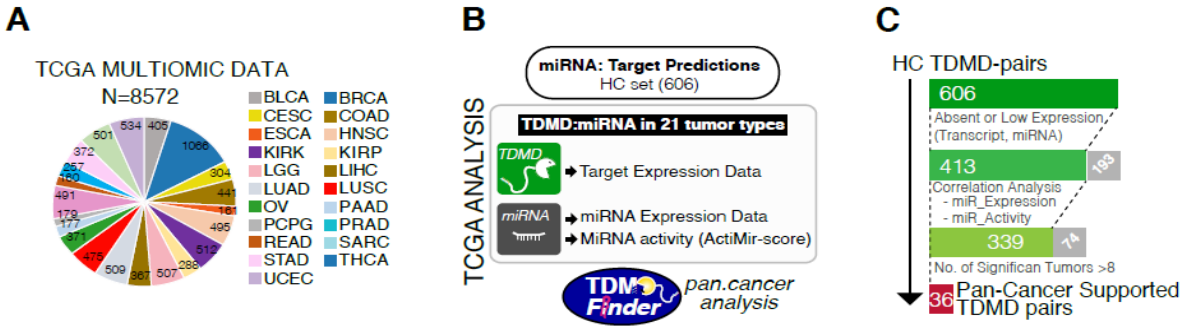

Figure 68. "Pan-cancer" analysis. (A) Number of samples used in the correlation analysis, divided considering the tumor type. (B) Scheme of the strategy used to analyze HC TDMD pairs in human cancer. (C) Steps followed to identify Pan-cancer supported TDMD interactions, with number of pairs that passed the filtering process and of those that did not (grey bars).

We hypothesized that if TDMD is occurring, there should be a negative correlation in cancer samples between the TDMD trigger (i.e. the transcript) and its associated miRNA ("miRNA Expression Test"). For example, in the case of SERPINE1:miR-30c interaction, a significant Spearman negative correlation was observed in multiple (N=18) cancer types (**Figure 69A**). The reduction of miRNA expression levels by TDMD should also produce effects on miRNA activity (i.e. the ability of a given miRNA to repress its canonical targets), as observed for previous endogenous TDMDs (see Chapter 1 and Ghini, Rubolino et al., 2018). Therefore, we exploited the "ActMiR score" (Lee et al., 2016), a computational method for explicitly inferring the activity of miRNAs based on the changes in the expression levels of target genes in cancer datasets and measured the correlation between the TDMD-transcript and miRNA activity ("miRNA Activity Test"). Indeed, we observed a significant negative

Spearman correlation in many cancer types (N=15) between SERPINE1 expression and miR-30 activity (**Figure 69B**), confirming that this TDMD interaction is potentially occurring in human cancers.

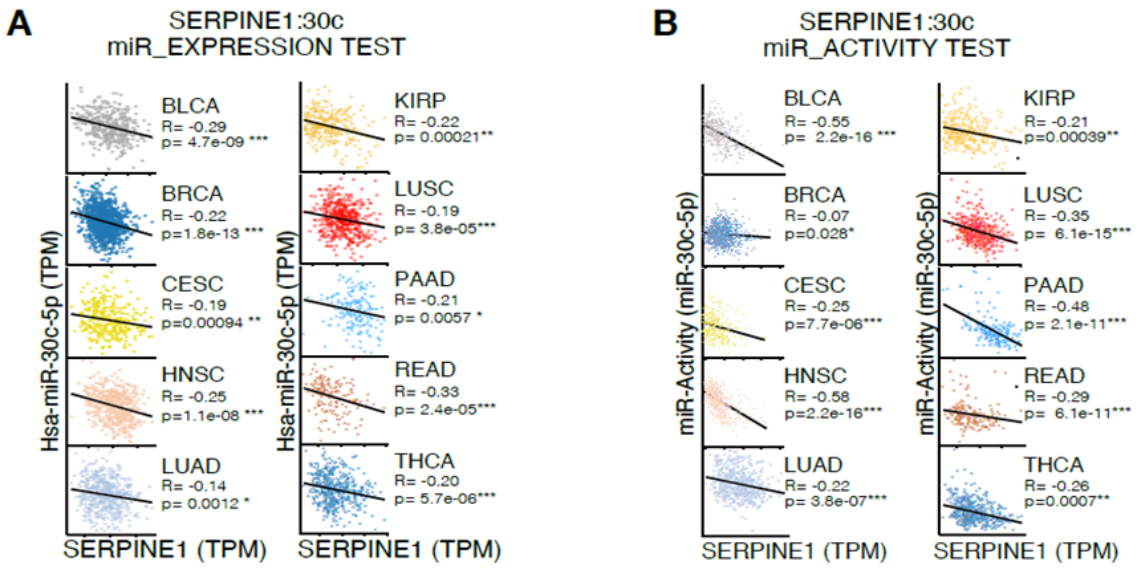

Figure 69. Spearman correlation analysis. (A, B) Bivariate analysis, linear fitting and Spearman correlation results (R and p-values), between the TDMD target and the expression (A) or the activity (B) (TPM, transcripts per million) of its associated miRNA. Reported are the tumor types with significant anti-correlation for both the miRNA Expression and the miRNA Activity test.

We considered as relevant those TDMD interactions that showed significant anti-correlation in both the miRNA Expression and miRNA Activity tests in the same cancer type. To avoid any possible bias from individual tumor datasets (e.g., tumor purity, molecular subtypes, genetic events), we focused on TDMD pairs that gave significant and consistent scores in 9 or more cancer types (**Figure 70A, Figure 70B**). These TDMD pairs were named as "Pan-cancer supported" and comprised 36 interactions, 28 triggers and 30 MDEs. This list includes previously known endogenous TDMDs, such as SERPINE1 and NREP, and others validated by the TDMD assay (ZFYVE26, RAB21, PTEN, IQSEC1, BLC2L11) (see chapter 2 and Simeone, Rubolino et al., 2022). Interestingly, the predicted miRNAs well-known oncogenic (miR-19, miR-17) and tumor-suppressor families (let-7, miR-30, miR-34, miR-33), suggesting TDMD as a new potential oncogenic mechanism.

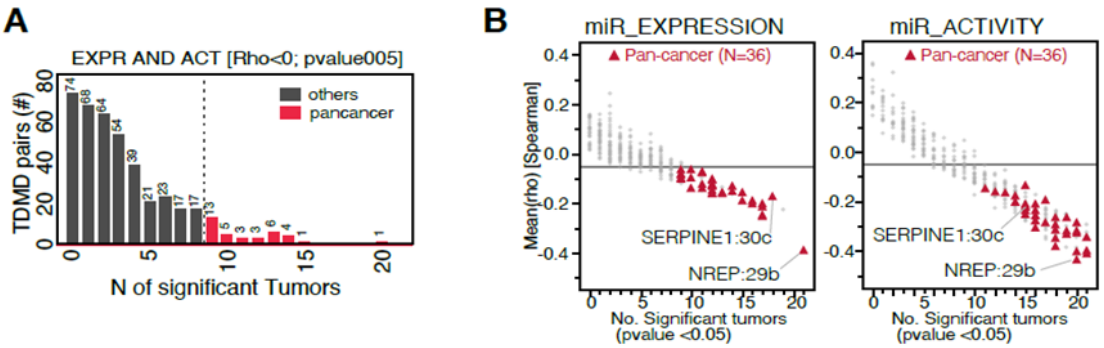

Figure 70. Identification of "Pan-cancer" TDMD interactions. (A) Bar chart with the distribution of TDMD interactions that ranked positively (Rho < -0.05 and p < 0.05) for both miRNA Expression and miRNA at least in one tumor. 36 pairs were named "Pan-cancer supported" TDMD interactions (in red), as they scored positively for both tests in at least 9 different tumors. (B) Scatter plots reporting, for all TDMD pairs, the mean Spearman correlation across the 21 tumors (y-axis) against the total number of tumor types with a significative anti-correlation (x-axis) by using the miRNA Expression (left) or Activity test (right). The 36 Pan-cancer supported TDMD interactions are in red.

2.3.1 Additional tests in support of Pan-cancer TDMD pairs

Anti-correlation between the target and the miRNA is necessary but not sufficient to prove that TDMD is occurring. Therefore, to provide further evidence that TDMD is taking place, we performed an additional test, named "Passenger Test", based on the correlation between either the guide or the passenger miRNA and the TDMD trigger.

The Passenger Test is based on the assumption that the TDMD mechanism is able to uncouple the expression of guide and passenger miRNAs, as showed in the previous chapters. Therefore, the miRNA and target correlation in tumors was normalized for the passenger correlation, to get rid of the transcriptional effects that are in common between guide and passenger miRNA (**Figure 71A**). As we expected, and supporting the validity of our test, known TDMD pairs, such as SERPINE1:30c and NREP: 29b, were only modestly affected by this normalization (**Figure 71A**). Globally, 20 out of the 36 TDMD interactions of Pan-cancer supported group maintained a negative anti-correlation in several tumor types after the normalization by the "Passenger Test" (**Figure 71B and Figure 71C**). For the 16 other TDMD interactions, both guide and passenger miRNAs were found to be similarly correlated with the TDMD transcript, by suggesting that the correlation measured in cancer datasets primarily occurred at the transcriptional level. The results of Passenger Test are also included in TDMD*finder* and can help in the selection of TDMD interactions potentially relevant in human cancer and therefore worthy of additional investigation by functional studies.

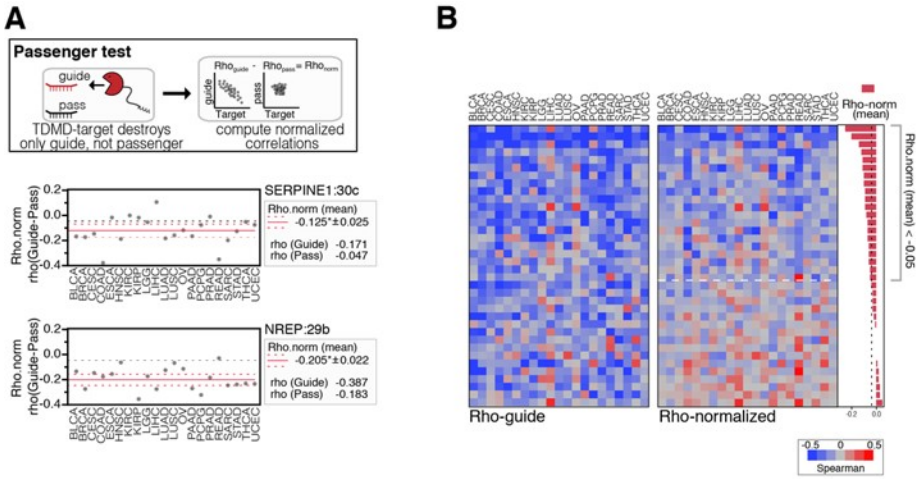

C

miR.family	PAIR.ID	Significant Cancers	Passenger.TEST Rho mean	Rho.norm	Result
miR-29	**NREP:29b-3p**	20	-0.39	-0.20	YES
	ROBO1:29b-3p	13	-0.20	-0.08	YES
miR-33	ABCA1:33a-5p	15	-0.20	-0.07	YES
	HADHB:33a-5p	9	-0.08	-0.01	NO
miR-30	**SERPINE1:30c-5p**	14	-0.17	-0.11	YES
	TMCC1:30b-5p	14	-0.16	-0.10	YES
	SERPINE1:30b-5p	9	-0.14	0.03	NO
miR-200	ZFPM2:429-3p	14	-0.25	-0.25	YES
	SRP72:200b-3p	9	-0.08	-0.03	NO
miR-96	DAB2:96-5p	14	-0.24	-0.14	YES
	SDC2:96-5p	11	-0.16	-0.10	YES
miR-17	**ZFYVE26:106b-5p**	13	-0.13	-0.09	YES
	ZFYVE26:17-5p	12	-0.12	-0.05	YES
	DSTYK:106b-5p	10	-0.15	-0.11	YES
	ZFYVE26:106a-5p	9	-0.10	-0.06	YES
	IQSEC1:106b-5p	9	-0.16	-0.07	YES
	PLEKHM1:106a-5p	9	-0.10	-0.05	YES
	PLEKHM1:17-5p	12	-0.13	-0.03	NO
	ATXN1:93-5p	9	-0.14	0.02	NO
	ATXN1:20a-5p	13	-0.19	-0.02	NO
miR-19	**RAB21:19b-3p**	13	-0.16	-0.09	YES
	RAB21:19a-3p	13	-0.16	-0.12	YES
miR-21	KLF9:590-5p	13	-0.21	-0.04	NO
	THRB:21-5p	9	-0.15	0.01	NO
miR-27	CPEB3:27a-3p	11	-0.19	-0.09	YES
	RC3H1:27a-3p	12	-0.10	-0.06	YES
miR-493	MAP7:493-5p	11	-0.07	0.00	NO
let-7	SMCR8:let-7d-5p	10	-0.09	-0.06	YES
	ZNF322:let-7d-5p	9	-0.06	0.00	NO
miR-135-5p	RAB33B:135b-5p	10	-0.11	-0.03	NO
miR-34	ZNF207:34a-5p	10	-0.13	-0.07	YES
miR-376c	PHIP:376c-3p	10	-0.06	0.05	NO
miR-145-5p	RTKN:145-5p	9	-0.12	0.03	NO
miR-23	ISCA2:23b-3p	9	-0.08	0.00	NO
miR-130	MCTP1:301a-3p	9	-0.13	0.00	NO
	PTPN14:301a-3p	9	-0.10	0.02	NO

Figure 71. Additional test in support of Pan-cancer TDMD interactions. (A) Top: scheme of the Passenger test: a normalized Spearman correlation coefficient for each TDMD interaction was calculated as Rho-norm = Rho-guide – Rho-passenger; the normalization was performed for each tumor type and only if the Rho of the passenger strand was < 0, to avoid artifacts. Bottom: Passenger test results for SERPINE1:miR-30c and NREP:miR-29b. (B) Heatmaps reporting the results of the Passenger test (Rho-guide and Rho-norm) in all tumor types for the Pan-cancer supported TDMD interactions. (C) Table showing Pan-cancer supported TDMD interactions and Passenger Test results.

2.3.2 TDMD confers selective advantages to breast cancer cells

Since we identified in silico a set of cancer-relevant TDMD interactions, we decided to directly explore the hypothesis that the TDMD mechanism in cancer cells regulates the levels of key miRNAs. We focused on breast cancer, whose mechanisms for controlling cellular transformation, cell identity and differentiation were already well-known to us (Culurgioni et al., 2018; Bonetti et al., 2019; Panebianco et al., 2019; Tordonato et al., 2021), and choose to study the validated SERPINE1:30c pair. This couple scored among the top hits in all previous *in silico* tests (correlation analysis, activity test and passenger test), with SERPINE1 also being the most expressed TDMD transcript for miR-30c both in breast cancer cell lines with basal-like features (**Figure 72**). In particular, in TNBC/basal tumors, typically characterized by a very aggressive behavior, poor outcome, high rate of metastasis and high content of cancer stem cells (Dent et al., 2007; Shibue and Weinberg, 2017), SERPINE1 is highly expressed (**Figure 72**), suggesting that TDMD might be used to keep low the levels of miR-30c, which is known to have a tumor-suppressor role in breast cancer, by increasing the sensitivity to chemotherapy drugs and inhibiting the growth of cancer stem cells (CSC) (Bockhorn et al.; 2013; Yu et al.; 2010; Chao et al; 2015).

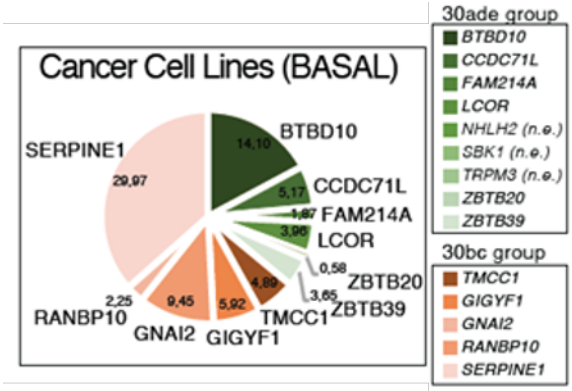

Figure 72. Distribution of TDMD-genes for miR-30 family. Pie charts showing the distribution of TDMD-genes for miR-30 family based on their expression in cancer cell lines of the basal subtype. Expression was measured by RNA-seq and normalized as TPM. (n.e. = not expressed).

We investigated this hypothesis by exogenously manipulating the miR-30c:SERPINE1 interaction in a TNBC/basal cell line, SUM159PT with high expression of SERPINE1 and measuring the corresponding molecular and cellular phenotypes (**Figure 73**).

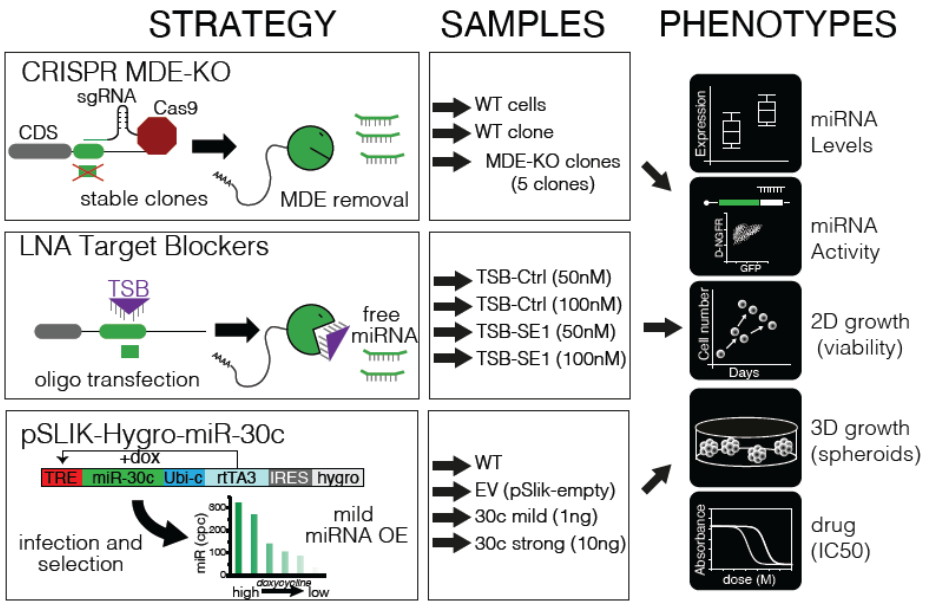

Figure 73. Strategies to investigate phenotypes related to SERPINE1:miR-30c interaction. Schematic representation of the different methodological strategies used to investigate the phenotypes that depend on the SERPINE1:miR-30c interaction.

In particular, we were able to affect the TDMD mechanism by either i) deleting the SERPINE1 MDE by CRISPR, with the same approach that we used in 3T9 fibroblasts (see chapter 1) (**Figure 74**); or ii) using an LNA Target-Protector molecule, which, upon transfection, can obstruct the interaction between SERPINE1 mRNA and miR-30c.

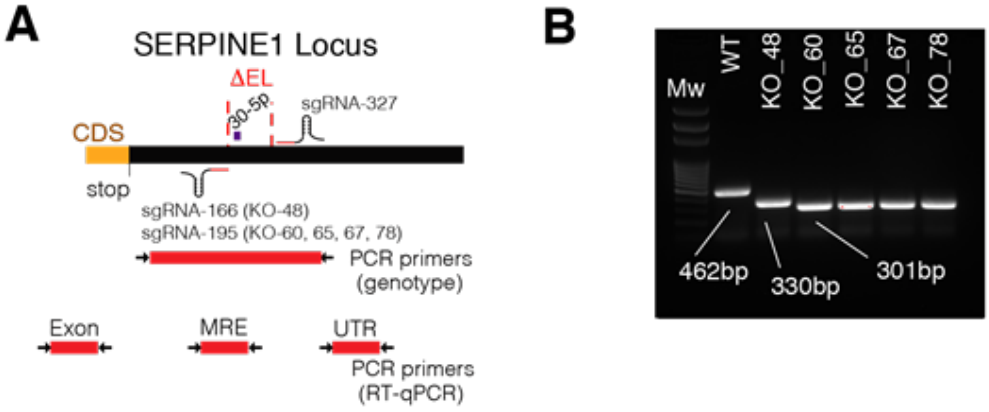

Figure 74. CRISPR-Cas9 technology for the removal of miR-30 MDE from 3′UTR of SERPINE1. (A) Human SERPINE1 3'UTR is depicted, with the position of the sgRNAs used to remove miR-30 MDE and of the PCR primers used in the characterization of MRE-KO clones. (B) End-point PCR from genomic DNA of parental cells and MRE-KO clones confirms the expected deletions.

The levels and activity of miR-30c increased in both cases (**Figure 75**), further validating SERPINE1 as an endogenous TDMD for miR-30c in human breast cancer cells.

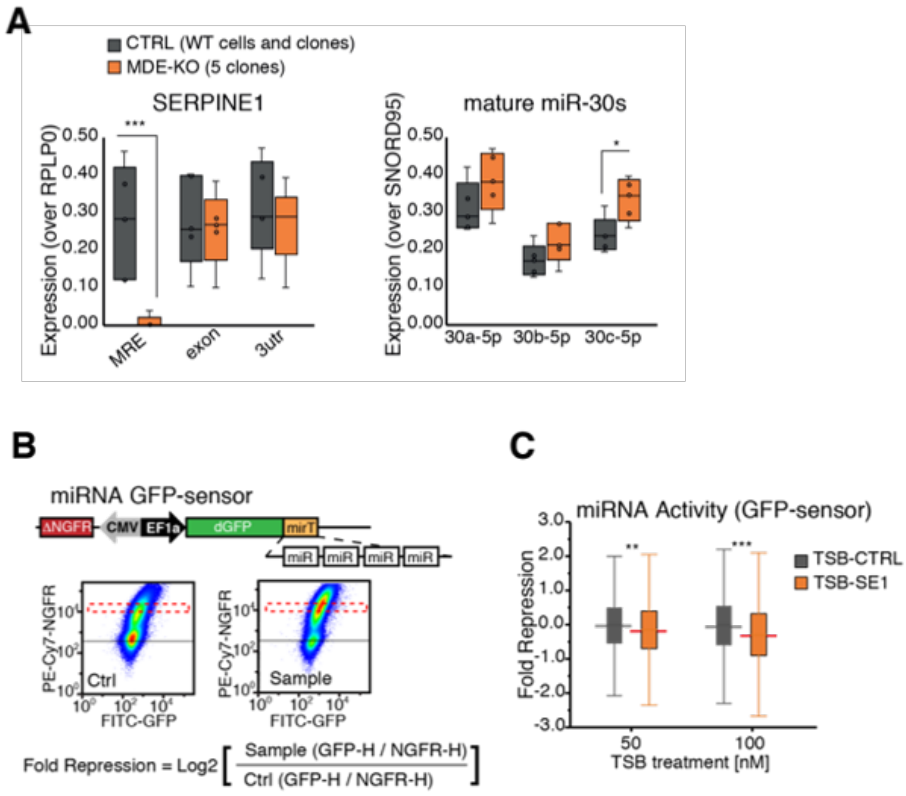

Figure 75. Evaluation of SERPINE1 expression and miR-30c level and activity upon TDMD disruption. (A). RT-qPCR of SERPINE1 transcript (left), mature miRNAs of the miR-30 family (right). Data are normalized over the appropriate house-keeping gene (reported on Y-Axes). P-values by Welch T-test. Controls include parental cells (in bulk) and two individual undeleted clones. (B) Scheme of the single cell reporter system used to evaluate miR-30c activity. A bidirectional promoter is used to transcribe identical levels of a control NGFR and a targeted destabilized GFP, which contains in its 3'UTR four miR-30c MREs (4X_30). By FACS we measured NGFR and dGFP expression in each cell, and we subdivided sorted cells into bins with similar NGFR expression (dotted red box). Finally, fold repression exerted by miR-30c (a proxy of miR activity) was calculated in different biological samples with the indicated formula. (C) SUM159PT were transfected with Target Site Blockers (TSB, Qiagen) designed to block SERPINE1:miR-30 interaction (TSB-SE1) or negative control (TSB-CTRL) at the indicated concentration. After 72hrs miRNA activity was measured.

In agreement with previous observations in other systems (Bitetti et al., 2018; Ghini et al., 2018), TDMD affected miR-30c levels in a relatively mild manner in range with the changes previously observed with the Serpine1:miR-30c pair in mouse fibroblasts (Ghini, Rubolino et al. 2018) (2-fold increase upon TDMD disruption). As a further approach, we used a tunable (doxycycline dependent) system to mildly over-express (2 to 3-fold) miR-30c in SUM159PT cells and obtain a TDMD-like effect (**Figure 76**).

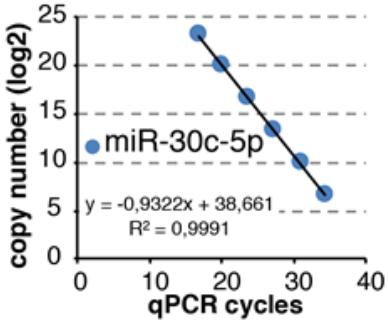

SUM159PT	miR-30c (copies/cell)
N. I. (not infected)	55
N.T. (not treated)	202
Mild OE (1ng/ml)	277
Strong OE (10 ng/ml)	12,327

Figure 76. Absolute quantification of miR-30c in SUM159PT. On the left, the titration curve used for the absolute quantification of miR-30c is reported. On the right, a table summarizes miR-30c level as copies/cells. (N.T.) stands for cells infected but not treated with doxycycline and (N.I.) for not infected cells.

Neither mild over-expression of miR-30c nor MDE-KO by CRISPR had a consistent effect on proliferation when cells were grown on plastics ("2D", **Figure 77A**, **Figure 77B**), though we observed variability among the different MDE-KO clones.

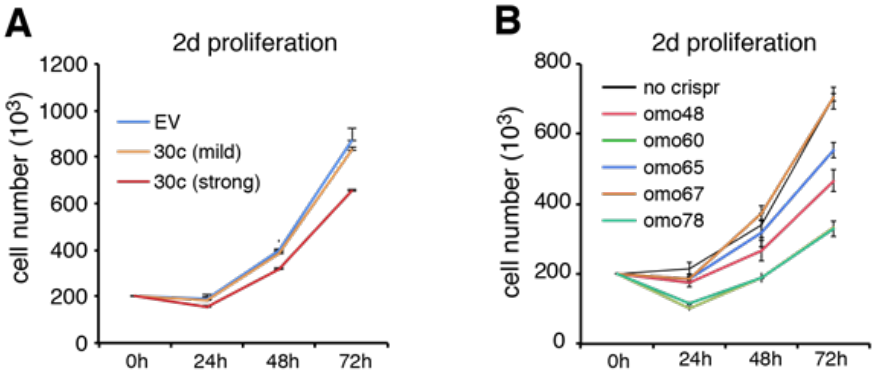

Figure 77. Characterization of SUM159 MDE KO clones (A) Growth curve of SUM159PT cells expressing miR-30c at different levels, as indicated. N=3. (B) Growth curve of SUM159PT clones bearing a deletion in SERPINE1 3'UTR. N=3.

We exploited the mammosphere assay to look at cancer stem cell (CSC) properties (Dontu et al., 2003). The number of mammospheres, which is a proxy measure of the number of cancer stem cells in the initial population, decreased when miR-30c was induced, even at low doses (**Figure 78A**), and was similarly reduced upon transfection of Target-Protector molecules and in each of the different MDE-KO clones (**Figure 78B, Figure 78C**).

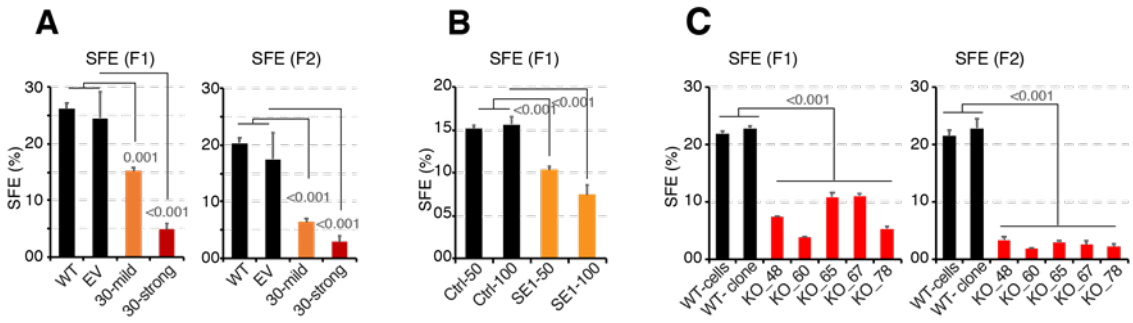

Figure 78. Interference of Serpine1:miR30c TDMD affects mammosphere growth. Bar charts reporting the results of the mammosphere assay performed in SUM159PT following different perturbations of the SERPINE1:miR-30c interaction. In panel A, miR-30c was mildly or strongly overexpressed. In panel B, Target-Protector molecules were used at two different concentrations (50 or 100 nM) to prevent the SERPINE1:miR-30c interaction. In panel C, CRISPR/cas9 system was used to remove the MDE for miR-30c from SERPINE 3'UTR, thus generating 5 independent clones. Shown is the sphere forming efficiency (SFE %, average and SEM from three replicates) measured at the first (F1) and at the second generation (F2). Data are from one of two independent experiments. P-values by Student's T-test.

This effect was maintained also in the second generation (F2, **Figure 78A, Figure 78C**), implying that miR-30c stabilization has a direct impact on CSCs, as only the cells with stem-cell properties could be propagated under these conditions. We then evaluated the sensitivity of breast cancer cells to chemotherapy drugs by using Paclitaxel, an anti-microtubule agent used in the treatment of various cancers including breast (Manfredi et al., 1984; Foa et al., 1994). Following miR-30c mild over-expression, SUM159PT cells became sensitized to Paclitaxel (**Figure 79A**, **Figure 79D**). Very similar results were obtained when TDMD was disrupted either through Target-Protector molecules (**Figure 79B, Figure 79E**) or in MDE-KO cells (**Figure 79C, Figure 79F**). Together these data show that SERPINE1-directed miR-30c degradation in breast cancer cells does play a role in modulating cancer phenotypes, affecting cancer stem cell properties (as assessed by mammosphere formation) and drug (paclitaxel) sensitivity.

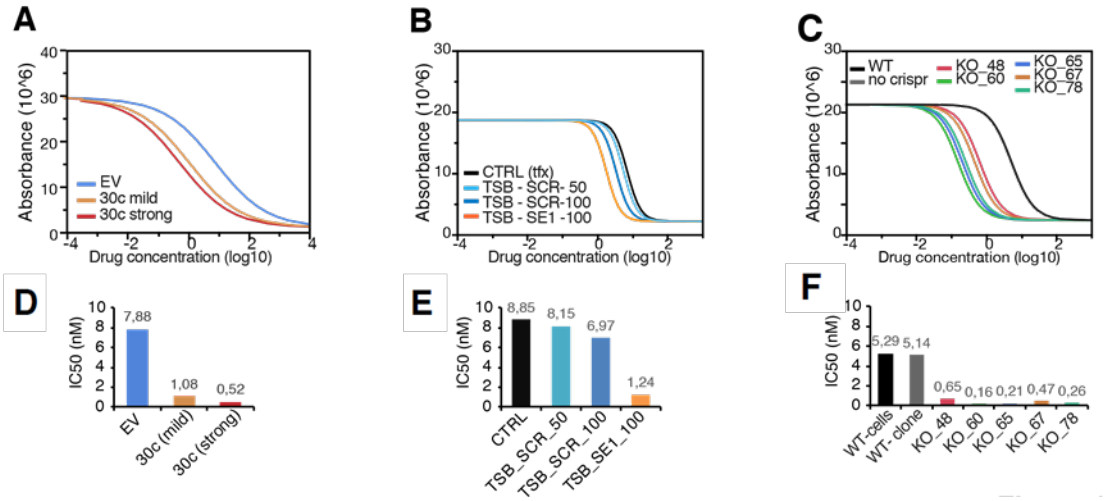

Figure 79. Interference of Serpine1:miR30c TDMD affects paclitaxel sensitivity. (A, B, C) Cell viability was measured by ADP-Glo Max Assay in SUM159PT cells treated for 3 days with Paclitaxel at different concentrations (panels D, E and F) and used to calculate IC50 values (panels D, E, F) upon different perturbations of the SERPINE1:miR-30c interaction. The results shown are from one of two independent experiments.

2.4 Identification of TDMD substrates relevant for Breast Cancer

In the previous chapter, we showed computational analyses supporting TDMD as a potential oncogenic mechanism. Furthermore, we focused on the SERPINE1:miR30b/c interaction, as proof of principle validation in support of TDMD role in tumorigenesis. Further efforts are needed to highlight the specific miRNAs that are under the control of TDMD in cancer and to elucidate, at endogenous level, the involvement of the predicted TDMD triggers. Recently, the ZSWIM8 Cullin-RING E3 ubiquitin ligase substrate adaptor has been implicated in the TDMD mechanism (Shi et al., 2020; Han et al., 2020). ZSWIM8 is recruited by the TDMD conformation and induces the degradation of AGO, thus resulting in miRNA release and decay. Importantly, ZSWIM8 is essential for TDMD to occur, providing a powerful biochemical and genetic tool for unveiling miRNAs that are under TDMD regulation. In order to block the ZSWIM8 expression, we exploited an approach, based on CRISPR interference (CRISPRi), where the catalytically dead-Cas9 nuclease (dCas9) is fused with a Krüppel-associated-box transcriptional repressor protein (KRAB). The fusion protein inhibits the expression of selected genes according to the sequence-complementarity of sgRNAs designed around the Transcription Start Site (TSS) of the target genes in a doxycycline-inducible fashion **(Figure 80)**.

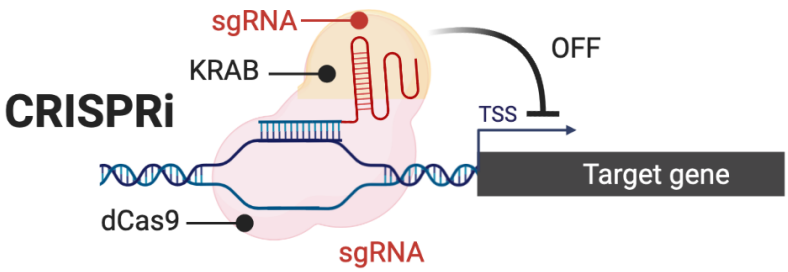

Figure 80. Schematics of dCas9-KRAB system. The knock-down is achieved by directing an enzymatically dead Cas9 conjugated with a KRAB repressive domain to a target locus (Created in Biorender.com).

The inducibility of the system offers the advantages of *i*) obtaining an acute repression of the targeted genes limited to the experimental setting; *ii*) avoiding unwanted or uncontrolled phenotypic effects when handling the cellular population before the experiment and *iii*) decreasing chances of silencing and counterselection of the transgene during culture. We generated a set of 8 different CRISPRi breast cancer cell lines, comprising Luminal- (MCF-7, T47D), Her2- (SKBR3, MDA- MB361) and TNBC- subtypes (SUM159PT, MDA-MB231, BT459, MDA-MB436) **(Figure 81)**.

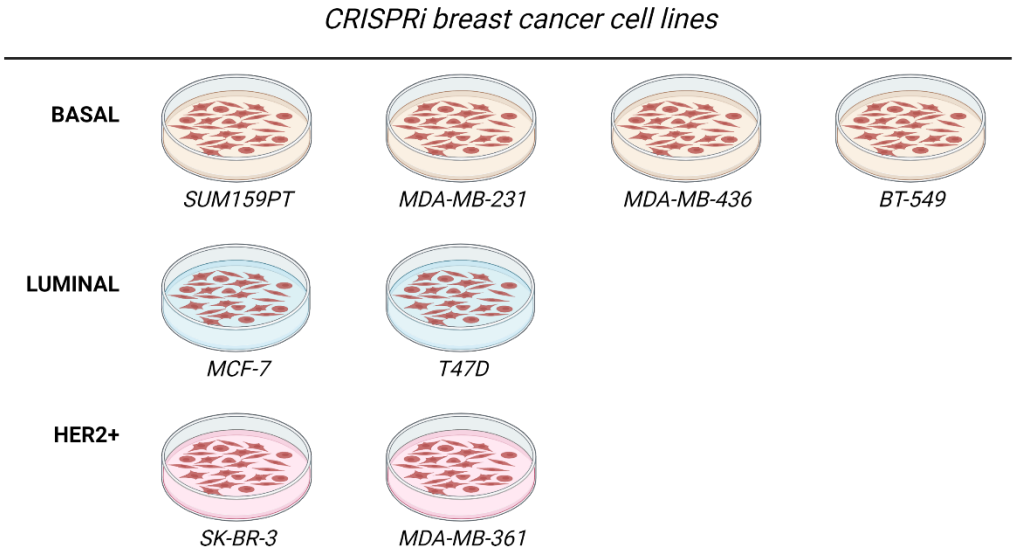

Figure 81. CRISPRi breast cancer cell lines. The BC cell lines used in the work belong to three subtypes: luminal, HER2 amplified (HER2+), and basal subtype (Triple-Negative Breast Cancer - TNBC). CRISPRi panel has been generated in collaboration with Bianca Giuliani (Created in Biorender.com).

In each cell line, the expression of dCas9-KRAB was in a range suggestive of a strong dCas9-KRAB activity, according to previous data available in the lab (**Figure 82)**.

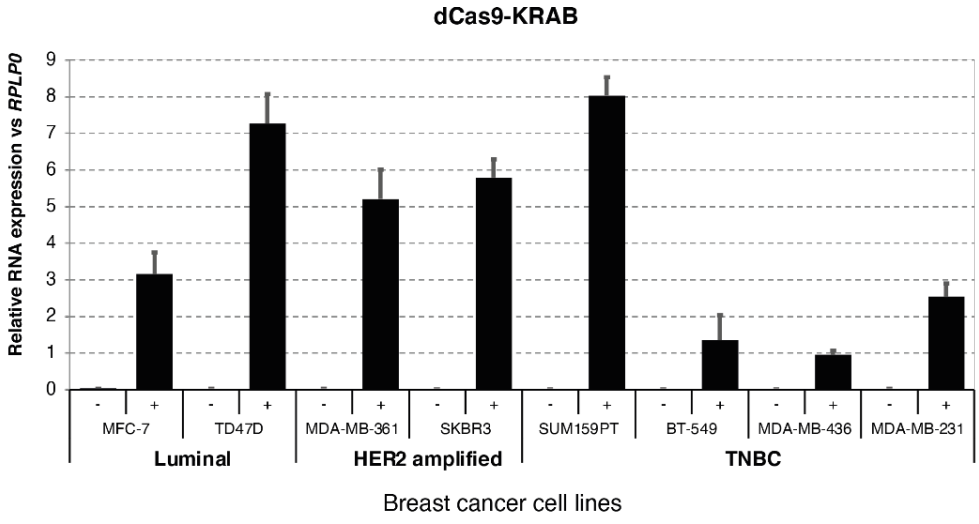

Figure 82. dCas9-KRAB expression in BC cell lines. RT-qPCR was performed in all the 8 cell lines after treatment with 1 µg/ml of Doxycycline (+) for 72h. The bar chart shows the relative RNA expression (+/- SEM) using RPLP0 as reference.

Hence, we designed three sgRNAs targeting several positions of the ZSWIM8 promoter (sgRNA28, sgRNA34, sgRNA42) and three different negative control sgRNAs (Empty Vector (EV), sgRNALacZ, sgRNAGAL4) that are not predicted to target any human gene. We first tested the system in SUM159PT, where we found that, in presence of doxycycline,

each of the targeting sgRNAs produced a knock down of ZSWIM8 by more than 90% **(Figure 83A).**

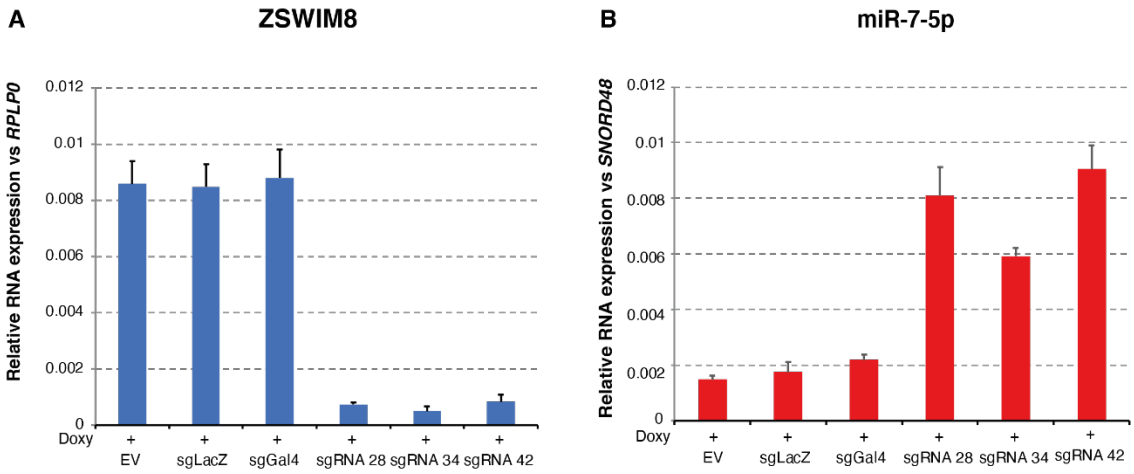

Figure 83. ZSWIM8 and miR-7 expression upon ZSWIM8 Knock-Down in SUM159PT. (A, B) RT-qPCR was performed after treatment with 0.5 µg/ml of Doxycycline (+) for 7 doublings. The bar charts show the relative expression (+/- SEM) using RPLP0 (A) and SNORD48 (B) as normalizer, respectively.

Furthermore, since the TDMD mechanism was previously established to regulate miR-7 expression (Kleaveland et al., 2018) and miR-7 was found upregulated upon loss of ZSWIM8 (Shi et al., 2020; Han et al., 2020), we decided to use it as a positive control to monitor the effectiveness of ZSWIM8 removal. In SUM159PT, miR-7 was strongly induced when TDMD process was impaired (**Figure 83B**). Then, we measured ZSWIM8 and miR-7 expression in all the other BC cell lines. ZSWIM8 was repressed more that 70% in presence of the 3 different sgRNAs 28, 34 and 42 (**Figure 84**) and miR-7 was induced in a statistically significative manner in all the tested cell lines (**Figure 85 and Table 1**).

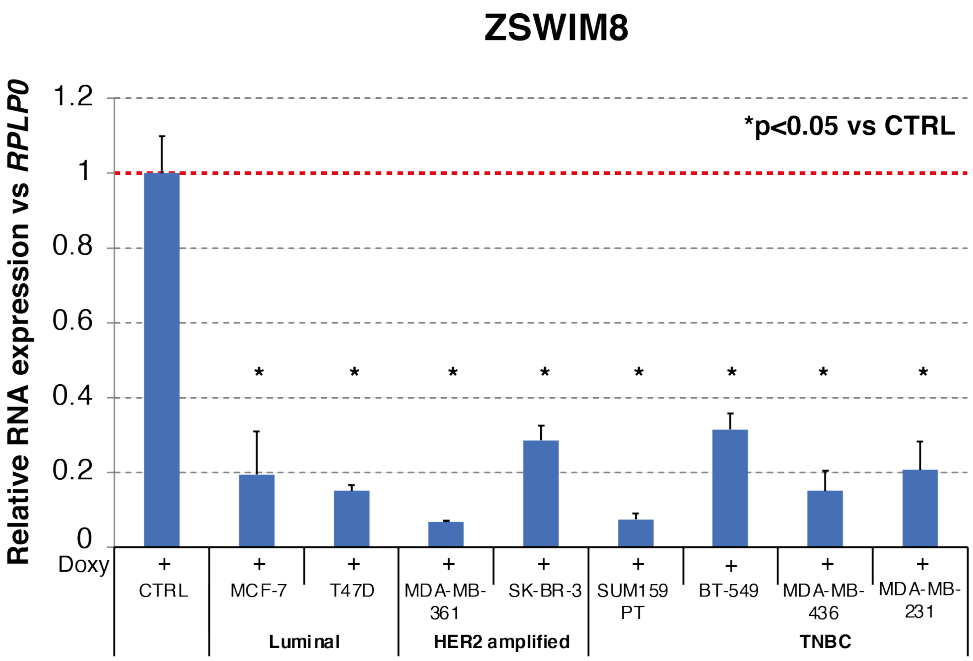

Figure 84. ZSWIM8 Knock-Down in BC cell lines. RT-qPCR was performed in all the 8 cell lines after treatment with 0.5 µg/ml of Doxycycline (+) for 7 doublings. The bar chart shows the relative RNA expression (+/- SEM) using RPLP0 as normalizer (Student's test, $p<0.05$).

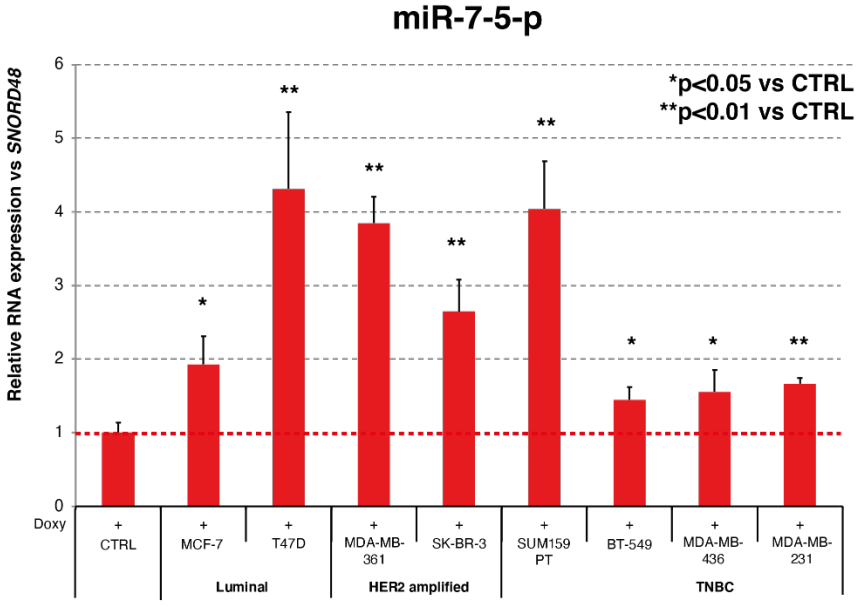

Figure 85. miR-7 expression upon ZSWIM8 Knock-Down in BC cell lines. RT-qPCR was performed in all the 8 cell lines after treatment with 0.5 µg/ml Doxycycline (+) for 7 doublings. The bar chart shows the relative RNA expression (+/- SEM) using SNORD48 as normalizer (Student's test, $p<0.05$ and $p<0.01$).

CELL LINE	ER	HER2	SUBTYPE	% ZSWIM8 KD	L2FC MIR-7	STUDENT'S T-TEST
SUM159PT	-	-	TNB	92%	1.87	p=0.0015
MDA-MB-231	-	-	TNB	80%	0.73	p=0.0003
BT-549	-	-	TNB	69%	0.55	p=0.0496
MDA-MB-436	-	-	TNB	86%	0.62	p=0.0367
T47D	+	-	LUMINAL A	85%	2.08	p=0.0055
MCF-7	+	-	LUMINAL A	83%	0.95	p=0.0157
MDA-MB-361	+	+	HER2 amplified	93%	1.87	p=0.0003
SK-BR-3	-	+	HER2 amplified	71%	1.41	p=0.0042

Table 1. Summary of RT-qPCR data upon ZSWIM8 KD in BC cells. The presence of ER and HER2 receptors, the BC subtype molecular, the percentage (%) of ZSWIM8 KD, the regulation for miR-7 in Log2FoldChange and the p-value from the Student's T-test are shown for each cell line.

2.4.1 sRNA seq analysis

To unveil the entire landscape of miRNAs acting as TDMD-substrates in breast cancer, we performed small RNA-seq (sRNA seq). We produced sRNA libraries from three independent biological replicates (one with each of the three ZSWIM8 sgRNAs or the three ctrl sgRNAs). Cells were collected after seven doublings in presence of 0.5 μg/ml of Doxycycline. We focused on miRNAs that were significantly upregulated after ZSWIM8-KD. In total, we found 119 miRNAs that were sensitive to ZSWIM8-KD.

Notably, the positive control miR-7-5p was found upregulated in a statistically significant manner in all the cell lines, with an induction level in the same range of that found by performing RT-qPCR (see **Figure 85**), thus confirming the quality of our sRNA seq experiments.

We divided all the results according to the cell line or to the BC subtype. Four cell lines belong to the triple-negative subtype: SUM159PT with 25 miRNAs significantly upregulated, BT-549 with 19, MDA-MB-436 with 21 and MDA-MB-231 cells with 14 **(Figure 86)**. Among the most upregulated microRNAs in TNBC we found miR-7-5p and miR-335-5p. We summarized the significant upregulated miRNAs in a Venn diagram (**Figure 87**): only miR-7-5p was significantly upregulated in all the four TNBC cell lines, miR-335-3p and miR-3529-3p were upregulated in 3 out of 4 cell lines and nine miRNAs were induced in at least two cell lines. Of note, the known TDMD substrate miR-29b-3p was found in this latter group (up in SUM159PT and BT-549).

For what concerns the cell lines of the luminal subtype (**Figure 88**), 38 miRNAs were upregulated in MCF-7 cells and 25 miRNAs were identified in T-47D cells. Six miRNAs were upregulated in both cell lines (**Figure 89**), including miR-7-5p and miR-1180-3p that were highlighted also in the TNBC subtype.

Finally, regarding the HER2+ subtype, the number of upregulated miRNAs was lower than for the other cell lines, with 17 miRNAs identified in MDA-MB-361 and only 8 in SK-BR-3 cells **(Figure 90)**. Only three miRNAs were found in common between the two cell lines, miR-335-3p, miR-3529-3p and miR-7-5p (**Figure 91**), none of which is specific only for the HER2+ subtype.

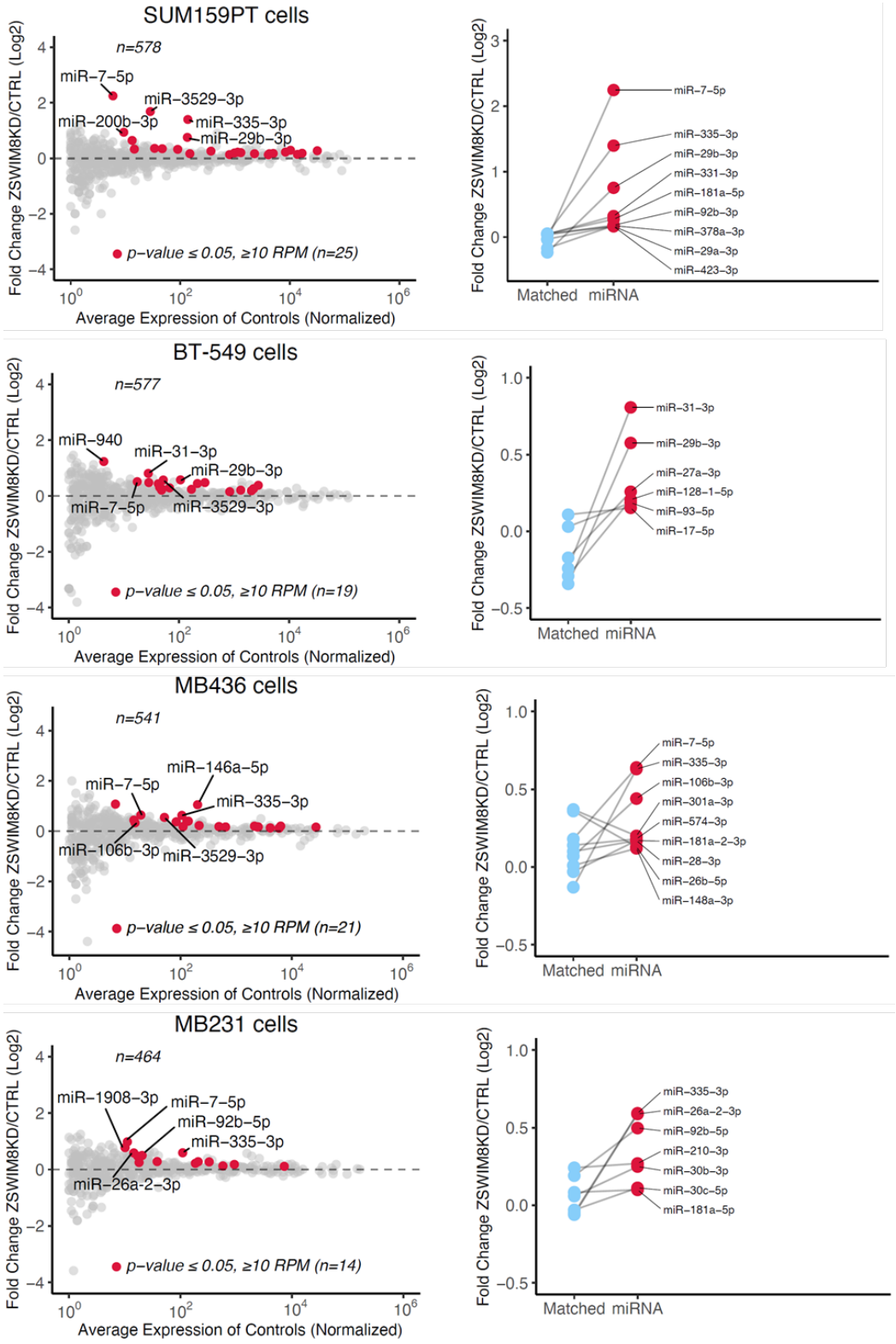

Figure 86. Schematics of sRNAseq results in the four cell lines of the basal subtype. On the left, for each cell line, the graphs show the fold change in miRNA levels observed upon KD of ZSWIM8 against the average expression of CTRLs. The red dots represent the significant upregulated miRNAs (Student's t-test p-value ≤ 0.05) and expressed above a threshold ($\geq$ 10 ReadsPerMillion, RPM). The grey points represent remaining miRNAs. On the right, the influence of ZSWIM8 on those significant miRNAs that have an expressed matched strand is shown. The red dots are for miRNAs significantly regulated upon ZSWIM8-KD, blue dots represent their matched strand.

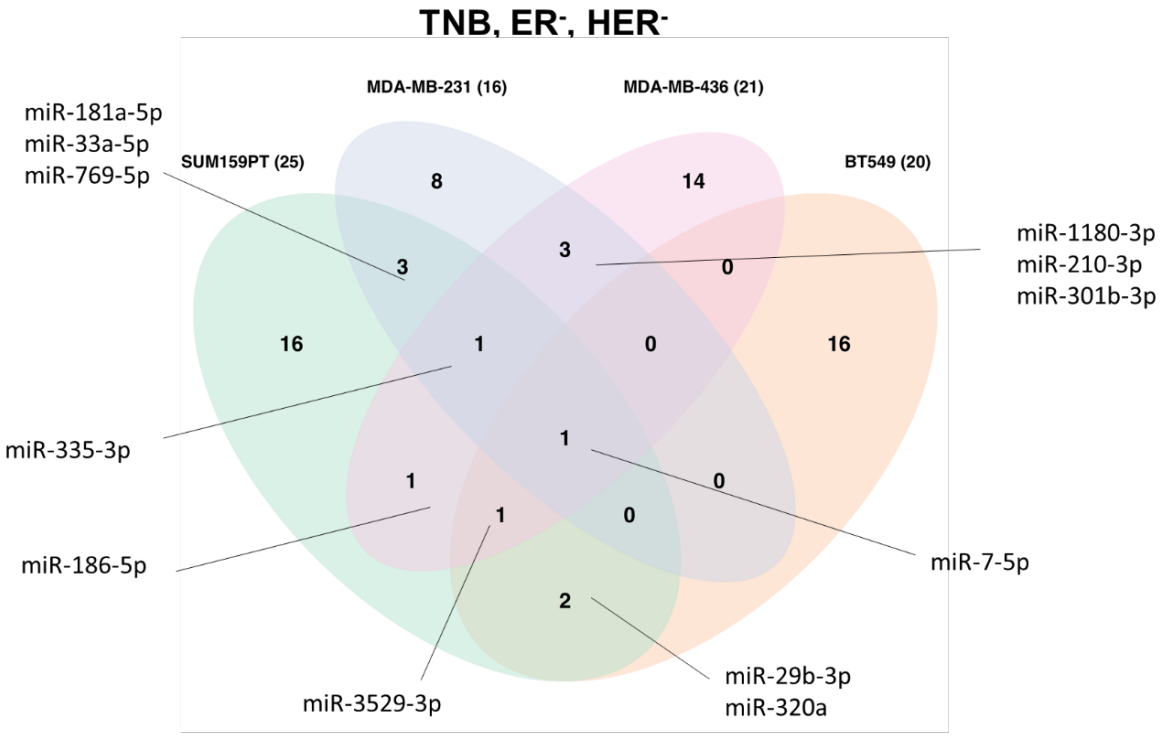

Figure 87. Summary of upregulated miRNAs in the TNB subtype. The Venn diagram shows all the significant upregulated miRNAs in the four basal cell lines analyzed. Each cell line corresponds to a specific set color. MiRNAs that are commonly upregulated in multiple cell lines are listed.

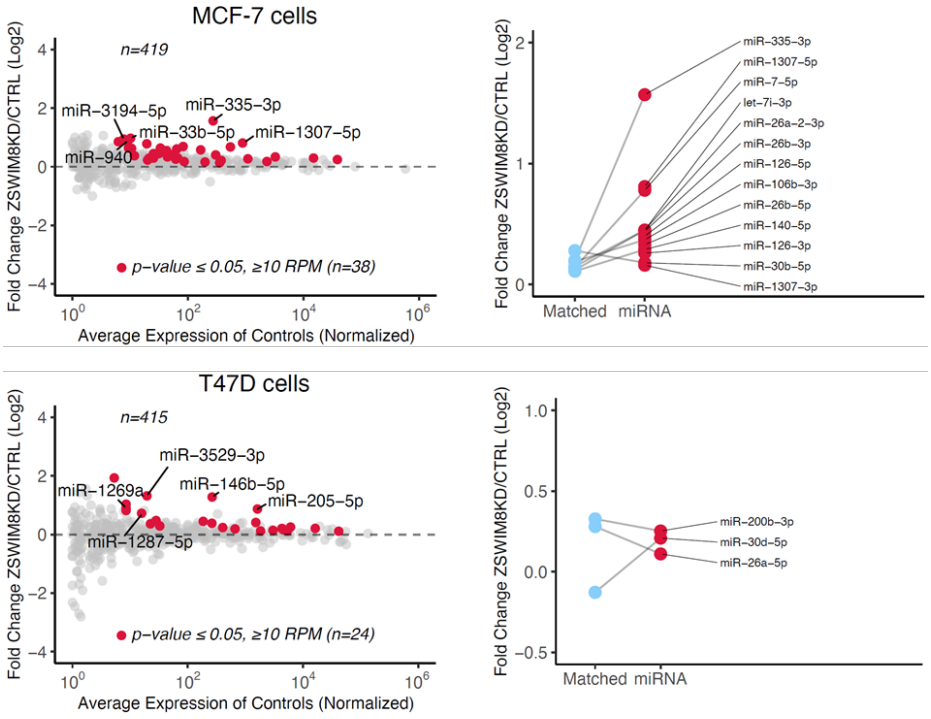

Figure 88. Schematics of sRNAseq results in the two cell lines of the luminal subtype. On the left, for each cell line, the graphs show the fold change in miRNA levels observed upon polyclonal KD of ZSWIM8 against the average expression of CTRLS. The red dots represent the significant upregulated miRNAs (Student's t-test p-value ≤ 0.05) and expressed above a threshold ($\geq$ 10 ReadsPerMillion, RPM). The grey points represent remaining miRNAs. On the right, the influence of ZSWIM8 on those significant miRNAs that have an expressed matched strand is shown. The red dots are for miRNAs significantly regulated upon ZSWIM8-KD, blue dots represent their matched strand.

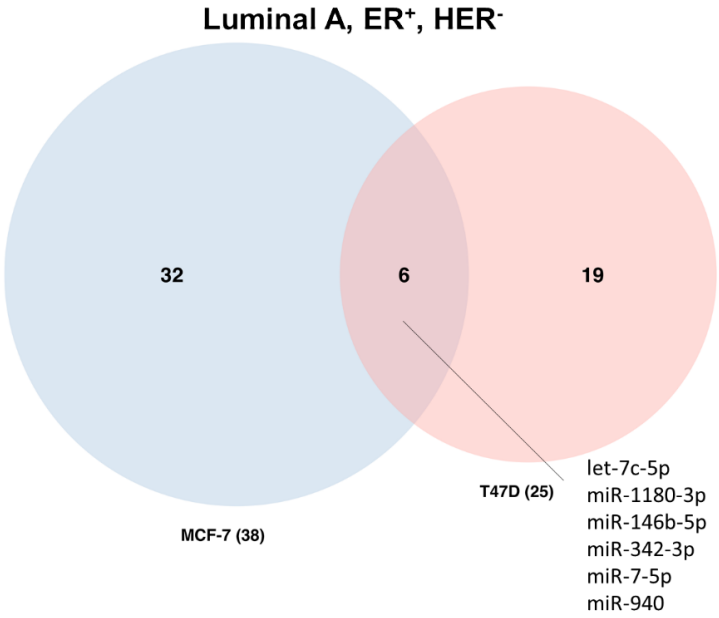

Figure 89. Summary of upregulated miRNAs in the luminal subtype. The Venn diagram shows all the significant upregulated miRNAs in the two luminal cell lines analyzed. Each cell line corresponds to a specific set color. MiRNAs that are common to multiple cell lines are listed.

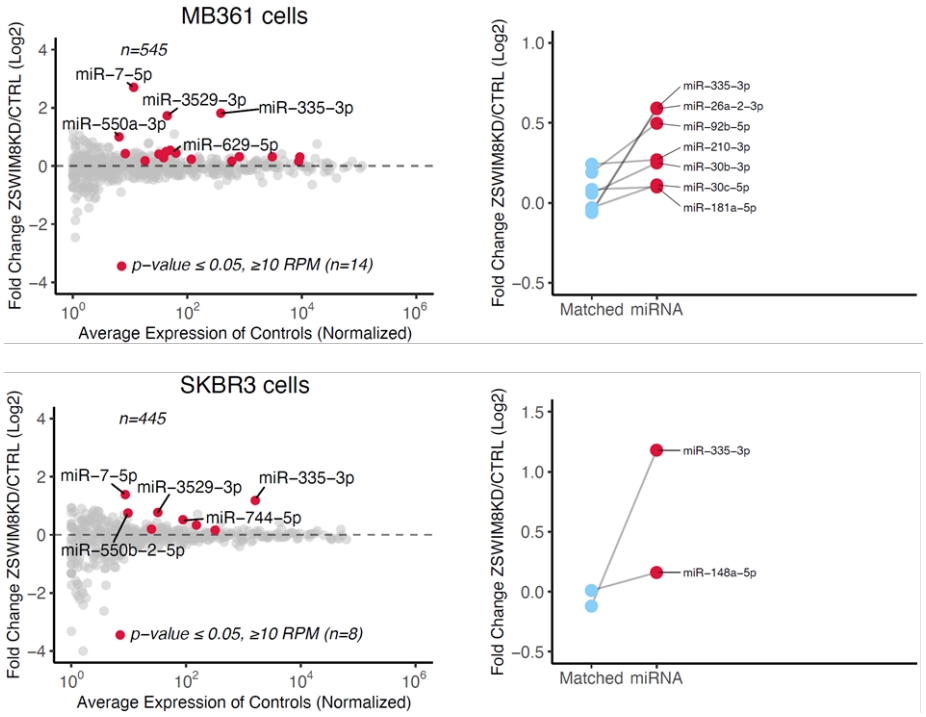

Figure 90. Schematics of sRNAseq results in the two cell lines of the HER2+ subtype. On the left, for each cell line, the graphs show the fold change in miRNA levels observed upon polyclonal KD of Zswim8 against the average expression of CTRLS. The red dots represent the significant upregulated miRNAs (Student's t-test p-value ≤ 0.05) and expressed above a threshold (≥ 10 ReadsPerMillion, RPM). The grey points represent remaining miRNAs. On the right, the influence of ZSWIM8 on those significant miRNAs that have an expressed matched strand is shown. The red dots are for miRNAs significantly regulated upon ZSWIM8-KD, blue dots represent their matched strand.

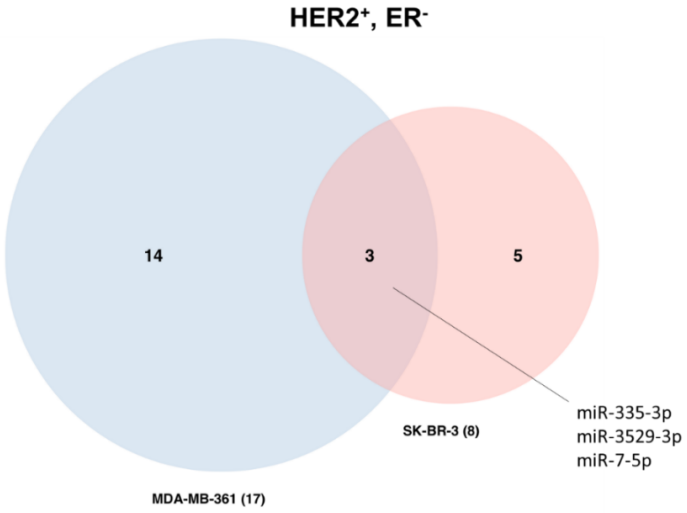

Figure 91. Summary of upregulated miRNAs in the HER2+ subtype. The Venn diagram shows all the significant upregulated miRNAs in the two cell lines analyzed. Each cell line corresponds to a specific set color. MiRNAs that are common to multiple cell lines are listed.

In summary, among all BC subtypes, 119 miRNAs were identified as potentially under ZSWIM8-dependent TDMD control (**Figure 92**). Interestingly, most of the significant miRNAs were specific for each individual cell line. In fact, we found that only 6 miRNAs were in common among TNB, luminal and HER2+ subtypes (namely miR-7-5p, miR-181b-5p, miR-744-5p, miR-335-3p, miR-3529-3p and miR-26b-5p), 11 miRNAs were shared among TNB and luminal, 2 miRNAs among luminal and HER2+ and 1 among TNB and HER2+. 55 out of 119 miRNAs were named "BC TDMD miRNAs" and prioritized for further studies as they i) showed a consistent regulation upon ZSWIM KD (> 0.3 Log2FC), often in more than one cancer cell type; ii) had a medium to high level of expression in breast, which suggested these miRNAs to be biologically active.

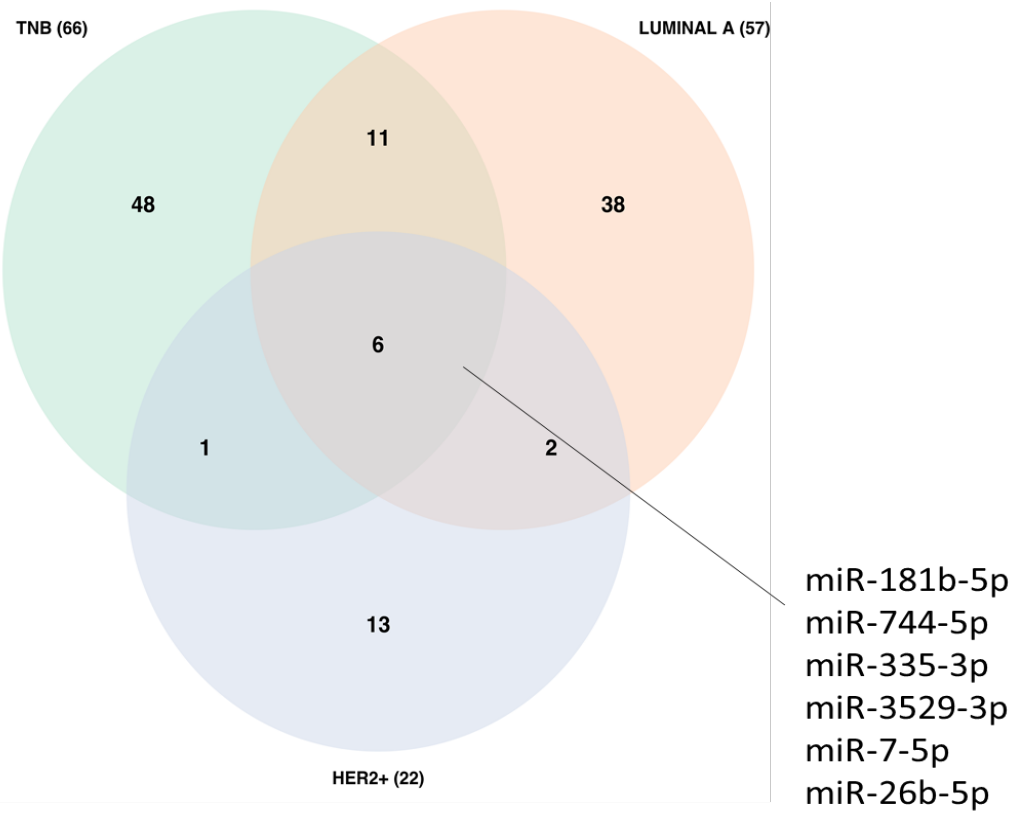

Figure 92. Schematic summary of upregulated miRNAs in all the BC subtypes. The Venn diagram shows all the significant upregulated miRNAs in the three subtypes analyzed. Cell lines were grouped into the corresponding subtypes. MiRNAs that are common to all the subtypes are listed.

2.4.2 Additional tests in support of BC TDMD miRNAs

Upon repression of ZSWIM8, we identified a set of miRNAs that are potentially TDMD substrates. We observed that most of the regulated miRNAs were only mildly induced and that most of the candidates were found only in a single cell line. In these conditions, it is important to be cautious in the interpretation of the results. In particular, the perturbation of ZSWIM8 for a prolonged period (7 doublings) might produce cell-line specific secondary effects. We tried to quantify the amount of primary and secondary effects by evaluating the number of miRNAs that were upregulated (possibly TDMD related) or downregulated (attributable to secondary effects) after ZSWIM8 KD in each cell line. We expected that the more there was an equal balance between miRNAs going up and miRNAs going down after ZSWIM8 KD the more likely it was that some of the observed effects were secondary effect of ZSWIM8 KD. In BT-549, SK-BR3 and MDA-MB-361 down-regulated miRNA largely exceeded up-regulated ones, suggesting the presence of stronger secondary effects. Conversely, in MCF-7, T47-D, SUM159PT, MDA-MB-231, MDA-MB-436 the number of upregulated miRNAs exceeded that of downregulated ones, suggesting an enrichment for primary TDMD-related effects (**Figure 93**).

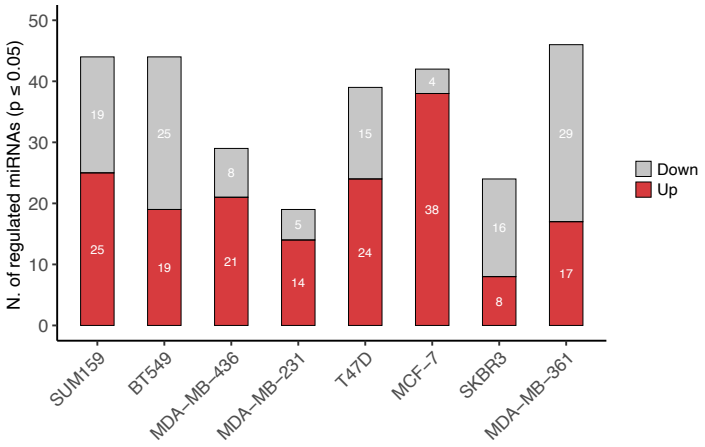

Figure 93. Number of upregulated and downregulated miRNAs upon ZSWIM8 KD. The number of significantly upregulated (red) and downregulated (grey) miRNAs upon ZSWIM8 KD in every cell line (Student's t-test p-value ≤ 0.05) is reported.

TDMD is a post-transcriptional mechanism that acts on a specific miRNA strand, without an increase in the abundance of the corresponding strand. When we performed sRNA seq analysis, we observed that, for some miRNAs, both strands showed similar regulation, suggesting a transcriptional effect on miRNA levels caused by ZSWIM8 KD. Unfortunately, in many cases the matched strands were not detected by sRNA-seq and the analysis could

not be performed systematically. To circumvent this issue, we measured the expression level of primary precursor molecules (pri-miRNAs) for all the 55 BC TDMD miRNAs. The analysis was carried out by RT-qPCR on the same samples that were used for sRNA-seq.
Given that pri-miRNA transcripts are not systematically annotated, we designed multiple RT-qPCR assays, considering 500 base pairs upstream and downstream the mature miRNA of interest. For each intronic miRNA, we also designed an additional primer pair within the host gene, while for miRNAs of interest within a cluster we avoided the design over other miRNAs not involved in the analysis (**Figure 94**).

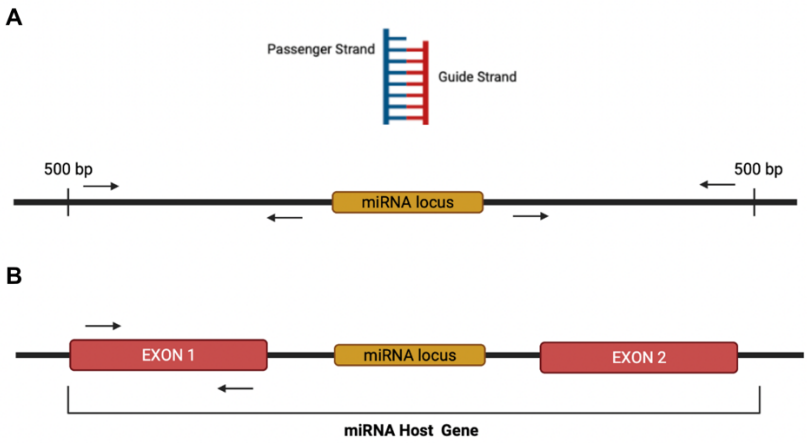

Figure 94. Schematics of Primer design for pri-miRNA expression analysis through RT-qPCR (A) For miRNAs whose locus falls in an intergenic region (intergenic miRNAs), the primer design regions were set about 500 bp upstream and downstream the miRNA locus (see arrows) (B) For miRNAs whose locus falls inside a host gene (intragenic miRNAs), primers were also designed within exonic regions of the host gene to assess also the expression of host gene. (Created in Biorender.com).

We analyzed primary transcripts by RT-qPCR in each cell line where a statistically significative up-regulation of the mature miRNAs was observed upon ZSWIM KD. Then, to get rid of any transcriptional effects triggered by ZSWIM8 KD, we calculated a "TDMD net effect" by normalizing the regulation of each candidate TDMD miRNAs (L2FC calculated from sRNA-seq) over the regulation of the test assay showing the highest induction level (for pri-miRNAs the L2FC from RT-qPCR; for matched miRNA strands the L2FC from sRNA-seq; **Figure 95A**). This normalization strategy takes into consideration the "worst case scenario" and has been selected to minimize the false positive rate. In the end, we considered as TDMD BC miRNA only those miRNAs that retained a TDMD net effect $\geq$ 0.3 Log2FC after compensating the transcriptional component.
For example, in the case of SUM159PT, we tested the nine miRNAs that by sRNA seq showed an induction $\geq$ 0.3 Log2FC upon ZSWIM8 KD (**Figure 95B**): 5 out of 9 tested miRNAs (miR-200b-3p, miR-29b-3p, miR-335-3p, miR-3529 and miR-7) passed the test,

while 4 out of 9 (miR-331-3p, miR-33a, miR-1260b and miR-641) were defined as transcriptionally regulated.

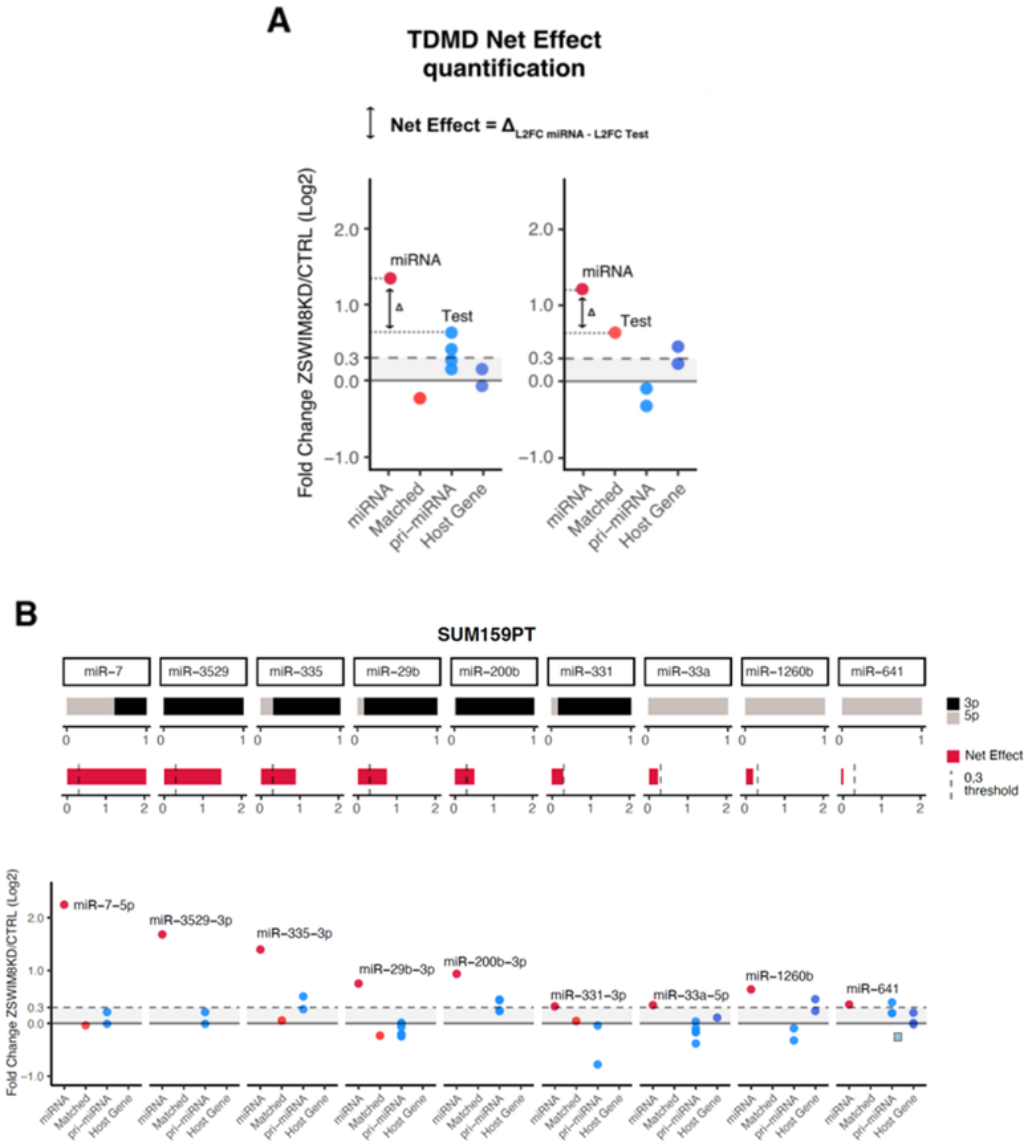

Figure 95. Primary transcripts analysis. (A) Schematics of the strategy for the TDMD Net Effect calculation. As TDMD regulation acts at post-transcriptional level, the "net effect" represents the regulation upon ZSWIM8-KD devoid of any transcriptional contribution, considering the 'worst case scenario'. Shown are two examples in which the "net effect" was calculated by either subtracting the regulation of the primary transcript (or the host gene), on the left side, or subtracting the regulation of matched miRNA, on the right side. (B) Representation of the regulations (L2FC values upon ZSWIM8-KD) for candidate miRNAs (in red) and for their matched strands (light red), pri-miRNAs (blue) and host genes (dark blue), respectively, in SUM159PT cells. In the upper part of the figure, it is reported: i) the name of the miRNA, ii) the expression (as percentage) of the 5p and 3p strands, and the values of the "net effect" (red bar). A dashed bar indicates the threshold for "net effect" (≥ 0.3 L2FC). Values for candidate miRNA (red) and its matched strand (light red) were obtained by small RNA sequencing analysis. Values for pri-miRNA (blue) and Host Gene (dark blue) were obtained by RT-qPCR, as shown in Figure 95, normalized with either RPLP0 or GADPH (two or more dots are shown, considering the two normalizations and different pairs of primers used).

Overall, we sorted the 55 miRNAs according to the Net Effect: known endogenous TDMD substrates, such as miR-7-5p and miR-29b-3p, ranked among the top 10 upregulated miRNAs (**Figure 96**). The set of 31 miRNAs with a Net Effect greater than 0.3 L2FC was termed High Confidence (HC) Breast Cancer TDMD substrates. The HC BC TDMD set was further investigated in order to unveiling the associated endogenous triggers.

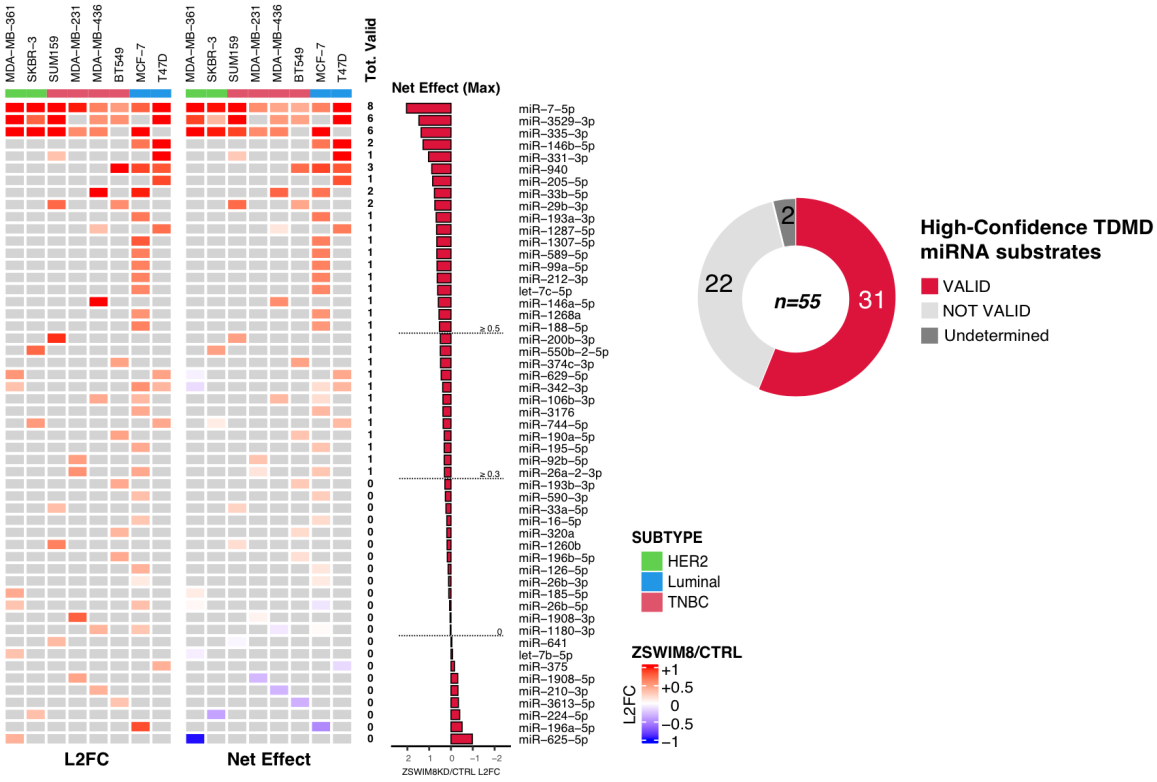

Figure 96. Final representation of candidate miRNA substrates and their regulation in BC cell lines. The ZSWIM8/CTRL L2FC (on the left) and the net effects (on the right) are shown for each candidate miRNA in the heatmaps. A red bar represents the maximum of the net effects calculated across the 8 cell lines for a specific miRNA. The dashed lines define thresholds for selecting max net effects equal or greater than 0.5 or 0.3, respectively. The high confidence (HC) set of TDMD substrates is shown in the donut chart, considering as valid the miRNAs with a maximum net effect equal or greater than 0.3 (31 miRNAs). 22 miRNAs do not pass the threshold and 2 miRNAs were undetermined.

2.4.3 Experimental validation of potential BC TDMD triggers

We defined a set of High Confidence (HC) BC miRNAs. For each HC BC miRNA substrate, we will retrieve the set of predicted TDMD triggers, combining the TDMD*finder* pipeline predictions with the in-house generated BC expression profiles (sRNA and RNA seq data). Once we will have identified all the potential TDMD triggers expressed in BC cell lines, we aim to experimentally confirm a small set of biologically relevant TDMD triggers by repressing their expression through the CRISPRi system and monitoring if the miRNA substrate level increases (**Figure 97**).

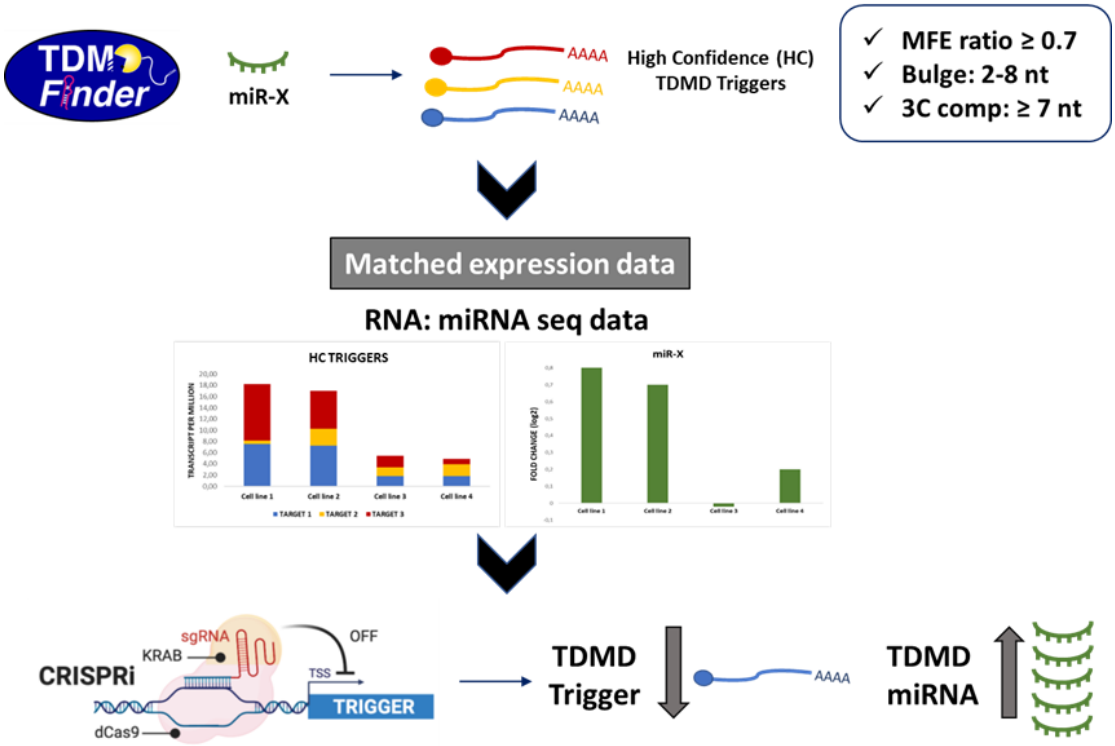

Figure 97. Schematic representation of the strategy to select and verify TDMD triggers. For each of the high-confidence TDMD miRNA substrate the TDMD*finder* pipeline can be exploited to obtain predictions of the potential TDMD triggers. In-house generated expression profiles of BC cell lines (sRNA and RNA seq data) can be used to compare the expression of the potential TDMD triggers in the different BC cell lines and correlate their level (as individual transcripts and as cumulative levels) with the observed TDMD effects obtained upon ZSWIM8 KD. Selected TDMD triggers can be validated experimentally through CRISPRi according to the following hypothesis: repression of the "true" trigger is expected to rescue miRNA levels.

As proof-of principle validation of this approach, we started with miR-29b-3p, a BC relevant TDMD substrate significantly upregulated after ZSWIM8 KD in SUM159PT and BT-549 cells (**Figure 98A**). miR-29b-3p is an interesting miRNA due to its role as tumor suppressor (Chou et al., 2013). In particular, Chou et al., showed that miR-29b-3p is deregulated in BC

and its alteration is related with tumor development and metastasis. Furthermore, in our pan cancer analysis, described in the chapter 3, we showed that NREP:miR-29b interaction was the strongest anticorrelated pair across all tumors (Simeone, Rubolino et al., 2022). Therefore, we used the TDMD*finder* pipeline to search for HC TDMD triggers and identified 3 potential candidates: ROBO1, NREP and CBX6.

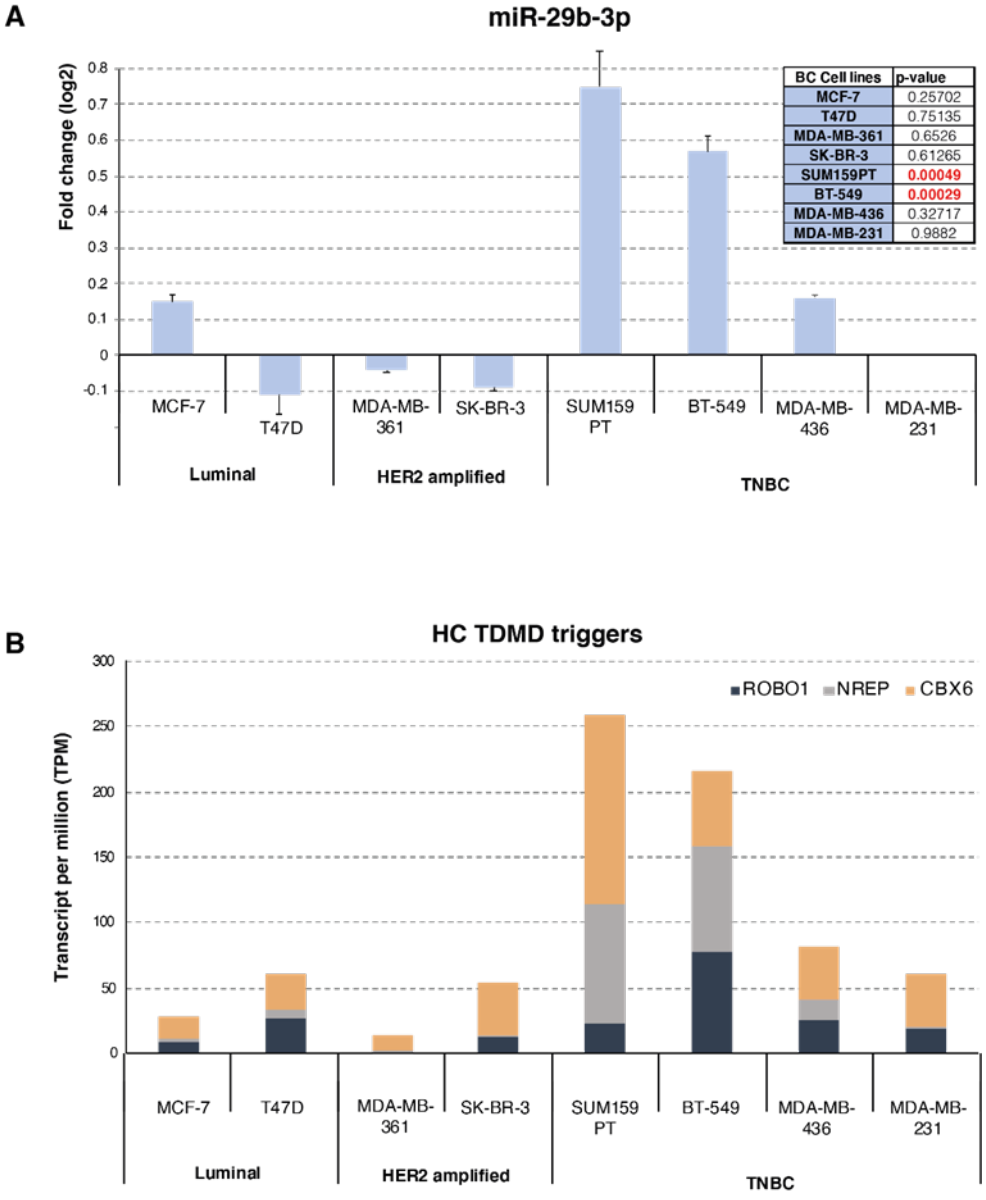

Figure 98. miR-29b-3p case. (A) miR-29b-3p expression upon ZSWIM8 KD in the different BC cell lines by RT-qPCR. The plot shows the average of log2 fold changes +/- SEM (Student's test, $p<0.05$). A table representing the p-values is shown on the right. (B) Cumulative plot (by using RNA seq data) represents the three high-confidence TDMD triggers for miR-29b-3p: ROBO1, NREP and CBX6.

Notably, ROBO1, NREP and CBX6 were cumulatively more expressed in SUM159PT and BT-549 cells compared to the other cell lines, with NREP resulting as the more selectively expressed gene (**Figure 98B**). In this light, we decided to KD the NREP gene by using the CRISPRi system in SUM159PT e BT-549 cells, expecting an increased expression of the substrate miR-29b-3p (**Figure 97)**.

Employing 5 sgRNAs against NREP and the 3 sgRNAs controls previously used in all the experiments related to ZSWIM8 KD, we observed a strong KD of NREP gene (**Figure 99A**) and a significant induction of miR-29b-3p with all the tested sgRNAs (**Figure 99B**).

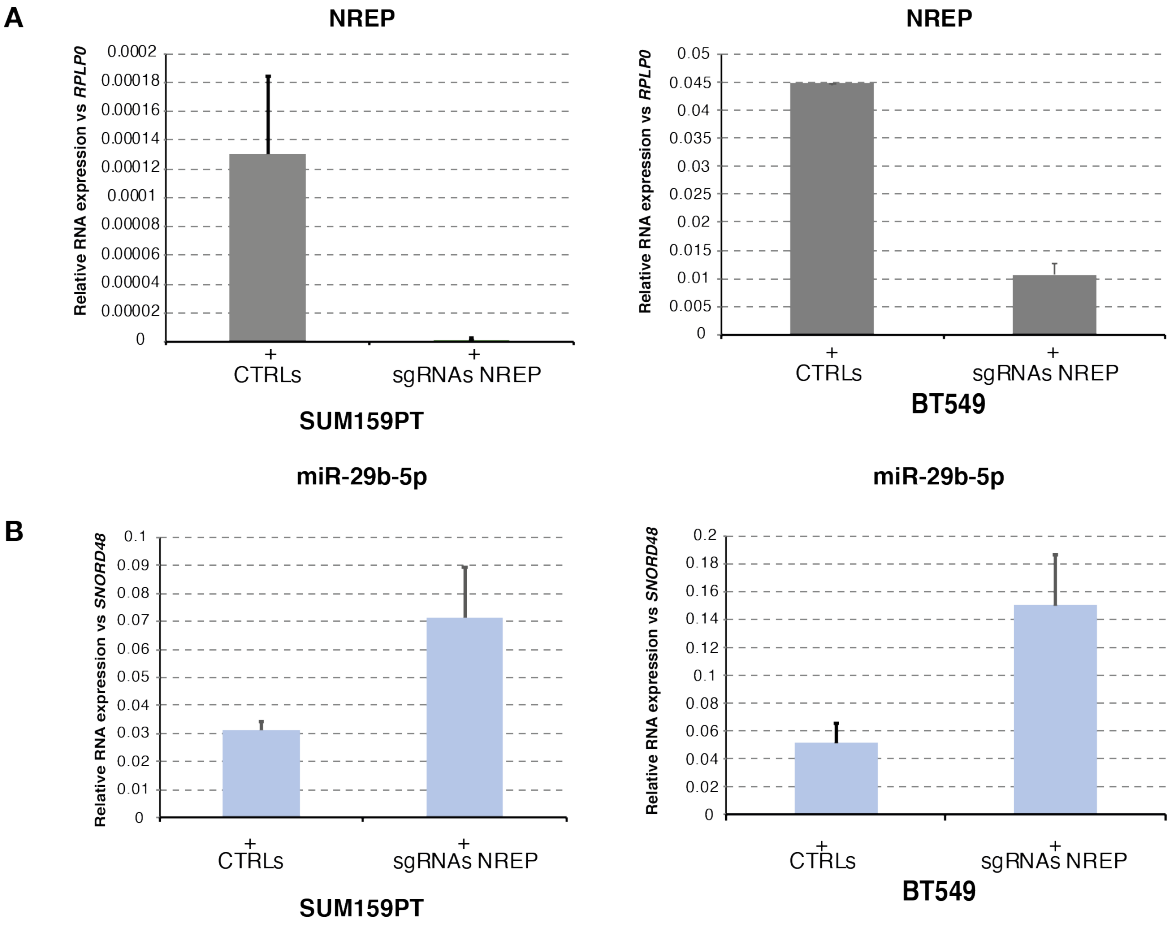

Figure 99. NREP KD and miR-29b-3p expression in SUM159PT and BT-549 cell lines. (A, B) RT-qPCR was performed after treatment with 0.5 µg/ml of Doxycycline (+) for 7 doublings. The bar chart shows the relative RNA expression vs RPLP0 (A) or SNORD48 (B) as normalizers. Bars represent the mean values (+/- SEM) calculated in three controls and five sgRNAs, respectively (Student's test, $p<0.05$).

To confirm that the induction of mir-29b-3p was due to a post-transcriptional mechanism, we measured the primary transcripts (pri-miRNAs) expression of miR-29b-3p which is transcribed in two different genomic loci (pri-miR-29b1 and pri-miR-29b2). We observed no significant differences in pri-miRNAs expression for both pri-miR-29b1 and pri-miR-29b2 (**Figure 100**).

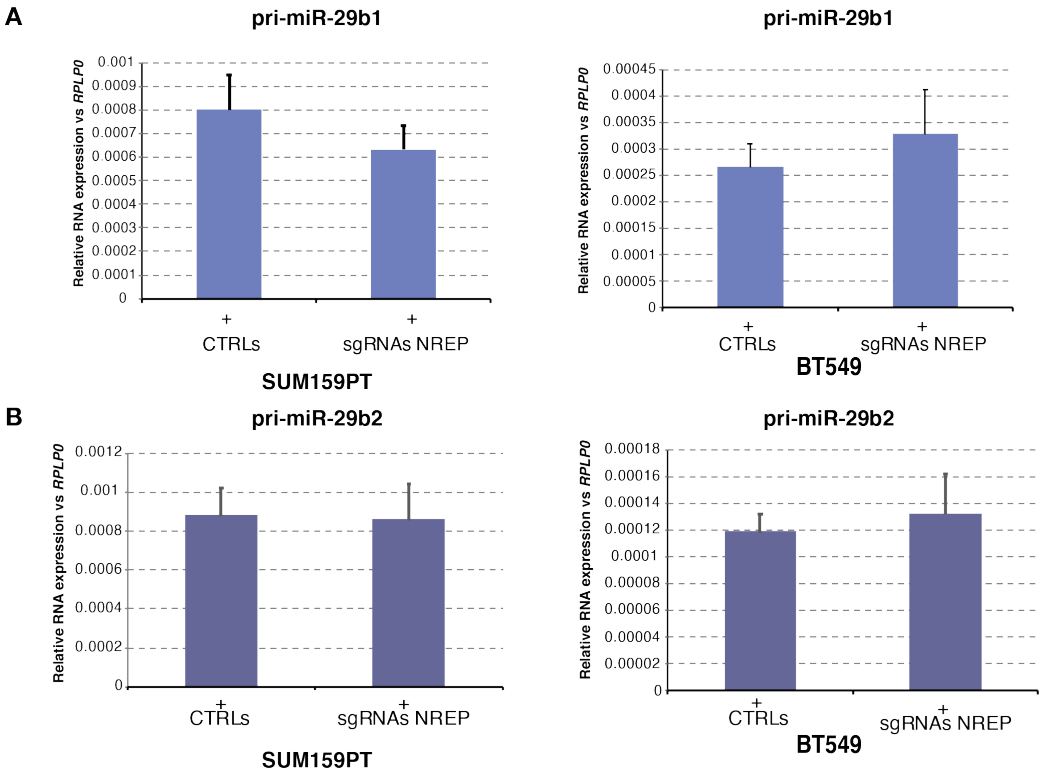

Figure 100. PrimiR-29b-3p expression upon NREP KD in SUM159PT and BT-549 cell lines. RT-qPCR was performed for two different genomic loci, pri-miR-29b1 (A) and pri-miR-29b2 (B) after treatment with 0.5 µg/ml of Doxycycline (+) for 7 doublings. The bar chart shows the relative RNA expression using RPLP0 as normalizer. Bars represent the mean values (+/- SEM) calculated in three controls and five sgRNAs, respectively (Student's test, $p<0.05$).

Finally, by comparing the data obtained after ZSWIM8 KD and after NREP KD in SUM159PT and BT-549 cells, we observed a similar induction of miR-29b-3p (in terms of Log2 FC) (**Figure 101**), suggesting that NREP is the main TDMD trigger for miR-29b-3p in SUM159PT and BT-549 cells. In conclusion, our data showed that the strategy we devised is effective to quickly identify TDMD substrates and triggers and we will use it to validate predicted TDMD triggers for other HC miRNA substrates.

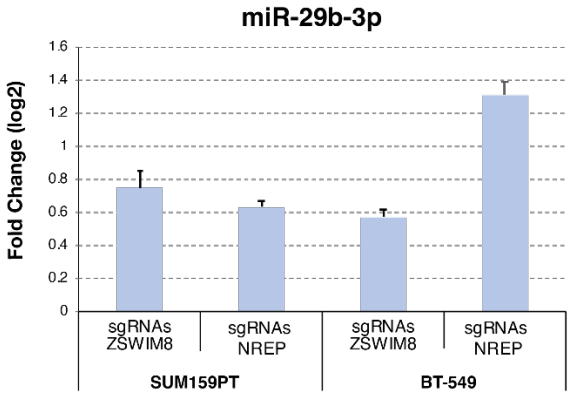

Figure 101. Comparison between data of miR-29b-3p expression after ZSWIM8 KD (sRNA seq data) and after NREP KD (RT-qPCR data) in SUM159PT and BT-549 cells. The plot shows the average of log2 fold changes (+/- SEM).

2.4.4 TDMD ZSWIM8-independent mechanisms

We previously showed that the endogenous RNA trigger Serpine1 controls the degradation of miR-30b-5p and miR-30c-5p in mouse fibroblasts and in human cells (Ghini, Rubolino et al., 2018, Simeone, Rubolino et al., 2022). Shi et al., and Han et al., revealed that TDMD required the ZSWIM8 Cullin-RING E3 ubiquitin ligase substrate adaptor. Moreover, in these studies ZSWIM8 was shown to control the degradation of several miRNAs in cells of mammals, flies and nematodes, but miR-30b-5p and miR-30c-5p were never observed among the ZSWIM8-sensitive miRNAs. Similarly, when we knocked-down ZSWIM8 in our panel of BC cells, miR-30b-5p and miR-30c-5p were never found among the significantly upregulated miRNAs as a consequence of TDMD disruption. Hence, we hypothesized the existence of a ZSWIM8-independent TDMD mechanism. To gain a deeper understanding of miR-30b-5p and miR-30c-5p degradation through TDMD, we decided to couple the knock-down of ZSWIM8 with the overexpression of SERPINE1 miRNA degradation element (MDE). We expected that, if miR-30b/c TDMD was controlled in a ZSWIM8 independent manner, then SERPINE1 MDE should have retained its ability to trigger miR-30b/c degradation even upon ZSWIM8 knock-down (**Figure 102**).

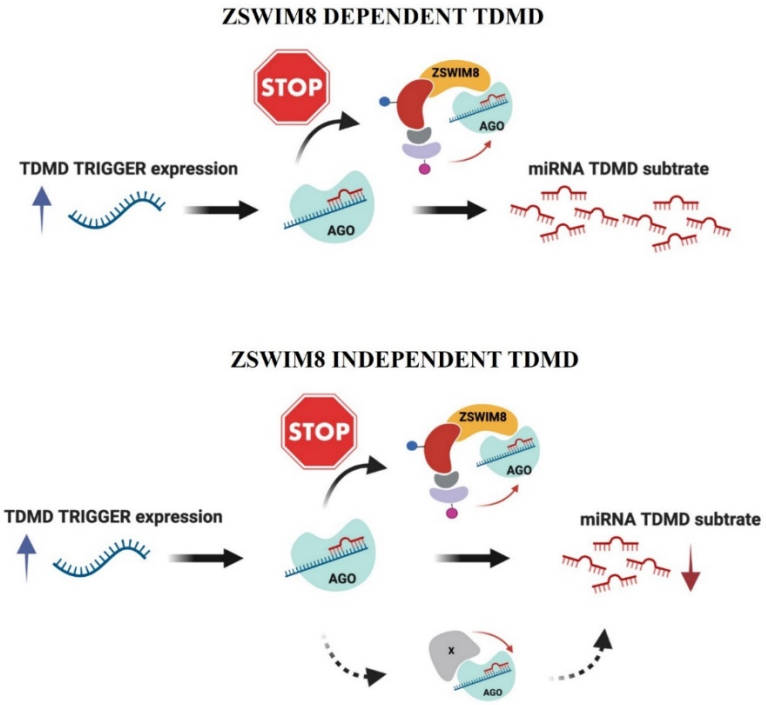

Figure 102. Schematic representation of TDMD models. On the top, a ZSWIM8 dependent model is shown, in which TDMD effects are completely dependent on a functional ZSWIM8 protein: TDMD effects induced upon TDMD trigger overexpression are abrogated upon genetic impairment of ZSWIM8 (i.e. by CRISPRi). Shown below is the TDMD ZSWIM8-independent model: TDMD effects induced upon TDMD trigger overexpression are insensitive to genetic impairment of ZSWIM8 (i.e. by CRISPRi).

To perform this experiment, we chose HeLa cells, a well-known cellular system particularly easy to manipulate. Moreover, a polyclonal Knock-out of ZSWIM8 in HeLa cells had already been done (Shi et al., 2020) and this gave us the advantage of being able to compare the data obtained in the same cell line. We generated the HeLa-dCas9-KRAB cell line (**Figure 103**), with the same strategy shown in **Figure 80** and we transduced the cells with the sgRNAs targeting ZSWIM8 (sgRNA28, sgRNA34, sgRNA42).

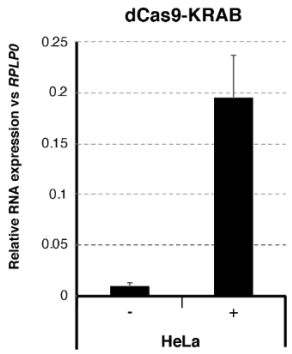

Figure 103. dCas9-KRAB expression in HeLa cell line. RT-qPCR was performed after treatment with 1 µg/ml of Doxycycline (+) for 72h. The bar chart shows the relative RNA expression (+/- SEM) vs RPLP0 as normalizer.

ZSWIM8 expression decreased more than 70% in presence of the sgRNAs 28, 34 and 42 after doxycycline induction for 7 days (**Figure 104A)**. Concomitantly, RT-qPCR showed an increased expression of miR-7, by confirming that the TDMD process was impaired in these cells upon ZSWIM8 depletion (**Figure 104B**). As previously observed also by Shi et al., the expression of miR-30c didn't change after the KD of ZSWIM8 (**Figure 104C**).

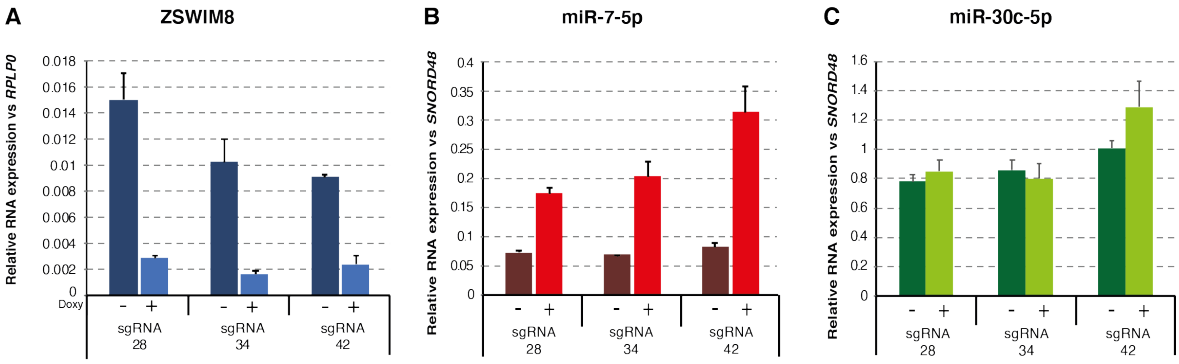

Figure 104. ZSWIM8 Knock-Down, miR-7-5p and miR-30c-5p expression in HeLa cells. (A, B, C) RT-qPCR was performed after treatment with (+) or without (-) 0.5 µg/ml of Doxycycline for 7 doublings in presence of the three sgRNAs (sgRNA28, sgRNA34 and sgRNA42) against ZSWIM8. The bar chart shows the relative RNA expression (+/- SEM) using RPLP0 (A) and SNORD48 (B, C) as normalizer (Student's test, $p<0.05$).

As an additional control, we tested NREP:miR-29b pair. MiR-29b-3p was found to be upregulated upon loss of ZSWIM8 (Shi et al, 2021) in HeLa cells and we also confirmed in SUM159PT and BT-549 cells that NREP is the main TDMD trigger for miR-29b-3p (see **Figure 99** and **Figure 100**). Therefore, we decided to use this interaction as a positive ctrl of TDMD impairment after ZSWIM8 KD. We used either the wild type sequence or a scramble one (NREP WT MDE and NREP SCR MDE). As expected, NREP WT MDE construct triggered miR-29b degradation in presence of ZSWIM8 WT, but the effect was almost completely abrogated upon ZSWIM8 KD, thereby confirming that NREP driven TDMD is ZSWIM8 dependent (**Figure 105A**).

Concomitantly, we infected Hela-dCas9-KRAB cells with SERPINE1 (SERP1) MDE or SERPINE1 scramble constructs. After SERP1 WT MDE expression, miR-30b-5p and miR-30c-5p were downregulated either in presence or absence of ZSWIM8, showing that miR-30b-5p and miR-30c-5p degradation through TDMD was unaltered after ZSWIM8 depletion **Figure 105B**).

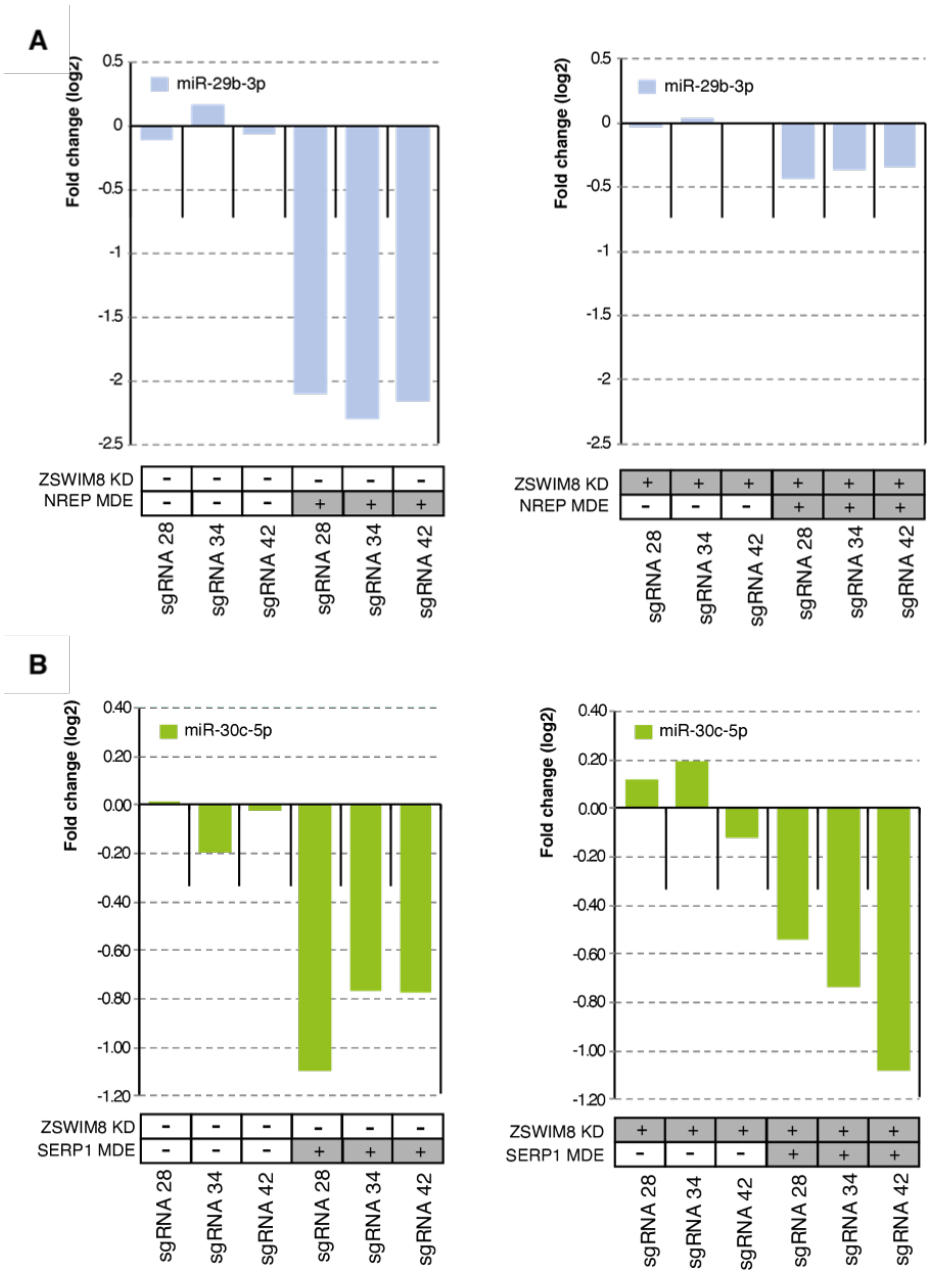

Figure 105. ZSWIM8 KD coupled with the overexpression of NREP MDE. (A) On the left, it is shown the Log2 Fold change in levels of miR-29b-3p in absence of doxycycline (ZSWIM8 WT) upon the overexpression of a Control sequence or NREP-MDE, used as RNA trigger, and indicated in the graph as either NREP MDE (-) or (+) conditions, respectively. On the right, it is shown the Log2 Fold change in levels of miR-29b-3p in presence of doxycycline (ZSWIM8 KD). The difference in regulation highlights the ZSWIM8 dependency of the effects. (B) On the left, it is shown the Log2 Fold change in levels of miR-30c-5p in absence of doxycycline (ZSWIM8 WT) upon the overexpression of a Control sequence or SERPINE1-MDE, used as RNA trigger, and indicated in the graph as either SERP1 MDE (-) or (+) conditions, respectively. On the right, it is shown the Log2 Fold change in levels of miR-30c-5p in presence of doxycycline (ZSWIM8 KD). The regulation is maintained, highlighting ZSWIM8 independent TDMD effects.

In conclusion, by coupling the KD of ZSWIM8 with the overexpression of NREP MDE and/or SERPINE1 MDE, we supported the existence of a ZSWIM8 independent TDMD pathway in addition to the ZSWIM8 dependent TDMD pathway. (**Figure 106**).

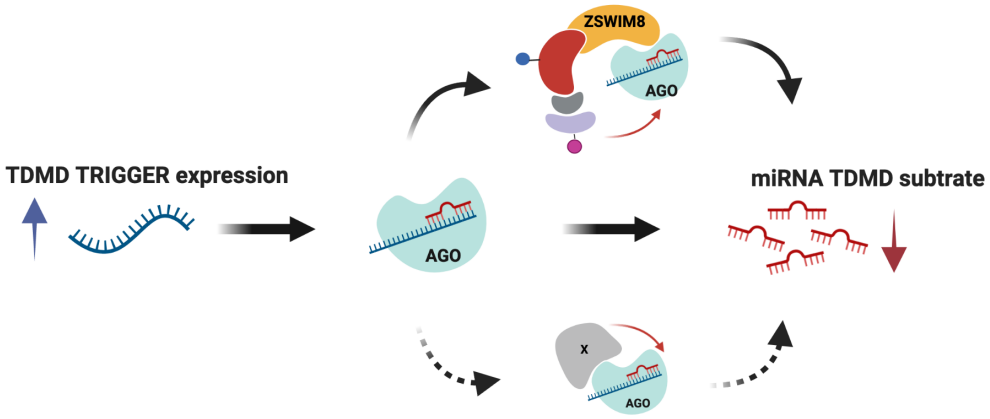

Figure 106. Final representation of TDMD models. The coexistence of a ZSWIM8 dependent TDMD pathway and a ZSWIM8 independent TDMD pathway is plausible.

3. Discussion

3.1 New Insights into TDMD

TDMD molecular bases and physiological role are still obscure. Endogenous RNA targets implicated in TDMD and the role they play in modulating miRNAs activity need to be further investigated, especially in non-neuronal cells. When we started to study TDMD, back in 2017, the evidence of miRNA decay was derived from studies on viral RNA targets (Cazalla et al., 2010; Marcinowski et al., 2012) and on artificial transcripts (Denzler et al., 2014; Baccarini et al., 2011). Therefore, we decided to provide evidence that this mechanism existed in mammalian cells, identifying endogenous TDMD triggers in control of miRNA level and activity. We chose to study Serpine1 since it was one of the top candidates in a list of targets showing ideal TDMD structural features: a 8-mer or 7-mer-8 seed, a bulge from 2 to 5 nucleotides and high complementarity at the 3' end (3C-score). We showed that, both in growing fibroblasts and during cell cycle re-entry of quiescent cells stimulated with serum (physiological conditions), Serpine1 transcript is able to post-trascriptionally control the levels of two related miRNAs, miR-30c and miR-30b, by triggering their degradation. Degradation involves some specific post-transcriptional modifications at the 3'end of the miRNA, as higher levels of adenylation. All the members of miR-30 family can interact with Serpine1 through their seed sequence which is shared among miRNAs of the same family, but only miR-30b/c present an extended 3C pairing to Serpine1. Hence, we showed that the extended 3' end complementarity, as previously observed *in vitro* and with artificial transcripts (de la Mata et al., 2015; De et al., 2013) is crucial for a TDMD mechanism driven by endogenous transcripts. Coherently, Serpine1 showed stronger effects on miR-30c degradation than on miR-30b, as miR-30c presents additional 3' base pairings with Serpine1. The 3C pairing is essential also in the reconstitution experiments. In particular, some mismatches can be tolerated in proximity of the bulge, instead, if the mismatches are located close to the miRNA 3'end, TDMD is completely impaired. The extended 3' end complementarity is not the only feature for TDMD occurrence, which also needs several context-dependent and quantitative requirements. Hence, we performed absolute quantification of miRNA and target expression copies per cells and calculated the correspondent target per miRNA value (TPM) in order to examine the stoichiometry of the miRNA:target interaction. Serpine1 was strongly induced after serum stimulation of quiescent fibroblasts, so as to widely exceed the levels of expression of miR30b/c (TPM>10) and halve their levels in about 4 hours. Therefore, a dramatic upregulation of a TDMD trigger could have a role in accelerating TDMD in a specific time window. Indeed, a longer

half-life of miR-30b/c (12 and 16 hours, respectively) was previously estimated in growing cells (Marzi et al.; 2016). In the same period, also Bitetti et al., provided a case of endogenous TDMD, named NREP. NREP is able to promote degradation of miR-29b in neuronal cells. Interestingly, NREP:miR-29b and Serpine1:miR-30b/c interactions present the same structural characteristics. Notably, NREP is primarily expressed in the brain and the disruption of NREP:miR-29b interaction produced and impaired motor functions in mouse and fish. Anyway, the impact of NREP on miR-29b targets was not clarified. Endogenous TDMD transcripts should influence the canonical miRNA-mediated repression. By investigating Serpine1:miR-30 example, we provided evidence in support of this hypothesis. Indeed, we have demonstrated that MRE-KO clones have a significant and consistent increase in miR-30 activity, as showed by using the miR-sensor, a synthetic reporter directly measuring the activity of the miRNA or endogenous transcripts identified by prediction algorithms and monitored by RNA-seq. At steady-state (growing conditions), the effects on endogenous transcripts are mild, with about a 5% of increase in repression. In the context of serum-stimulated cells, miR-30 targets were strongly (about 20%) and specifically repressed. In particular, miR-30b/c targets were preferentially repressed, compared to shared miR-30 targets. Interestingly, two independent studies have suggested that miR-30b and miR-30c preferentially bind targets with additional pairing in the 3' region (Moore et al., 2015; Helwak et al., 2013). To conclude, we provided evidence that endogenous targets can control miRNA level through TDMD and thus modulate the activity of miRNAs on their targets in mammalian cells.

3.2 TDMDfinder, an inventory of human and mouse TDMD pairs

It is still unknown how many endogenous TDMD targets exist. We provided the first inventory of miRNA:target interactions with the potential of generating TDMD effects. *TDMDfinder* is a computational pipeline and webtool that, using both quantitative and qualitative parameters, measures the likelihood of any miRNA:target interaction resulting into TDMD. When applied to the human and mouse genomes, our pipeline identified thousands of pairs that display structural features that are compatible with TDMD. According to our predictions, about 1% of all miRNA:target interactions could induce target-directed miRNA degradation. Thus, virtually, every miRNA might be regulated by several and independent transcripts via TDMD, suggesting a pervasive role of this mechanism in miRNA biology. In order to verify the accuracy of TDMD*finder* predictions, we performed an extensive experimental validation in HeLa cells. We validated a set of potential TDMD

interactions related to 9 different miRNA families and achieved a 45.9% validation rate (17 validated pairs out of 37), a performance which is in range with that of the computational tools usually used to predict canonical miRNA targets (Baek et al, 2008). Interestingly, some of the tested interactions were chosen from the Pan-cancer set and four out of seven of them were validated with the TDMD assay, by confirming the possible existence of cancer-relevant TDMD interactions. Two peculiar features, such as the thermodynamic stability (MFE ratio) and the number of consecutive nucleotides in the 3' region of the miRNA (3C type), were found to be significantly associated with validated interactions and were used to define a set of high-confidence (HC) TDMD pairs. All the "Predicted" or "HC" TDMD predictions can be easily recovered from the *TDMDfinder,* a webtool that provides the structural information on all TDMD-like interactions involving a specific miRNA and its targets. Importantly, the users are encouraged to customize *TDMDfinder* selection criteria. Indeed, the criteria to assess if a miRNA:target pair forms a TDMD-like structure are not rigid and could be customized in case of miRNA:target interactions with specific features. We measured the effects on miRNA decay with the "TDMD assay". In principle, in the TDMD assay, the levels of miRNAs of interest are measured following the ectopic overexpression of any selected MDE. This is a procedure widely used to study TDMD effects (de la Mata et al., 2015; Sheu-Gruttadauria et al., 2019; Pawlica et al., 2016; Ghini, Rubolino et al. 2018). The specificity for TDMD effects was determined by using MDE mutant constructs where the seed regions were left intact but the 3C pairing sequences were deleted. An additional verification test consisted in measuring the levels of guide and passenger miRNAs, since TDMD mechanism acts at post-transcriptional level and affects selectively one of the two miRNA strands.

3.3 TDMD mechanism in the miRNA biology

TDMD is a mechanism acting at post-transcriptional level and it is capable of diversifying the expression of miRNAs that are associated from a transcriptional point of view. By analyzing through small RNA sequencing the set of TDMD assays performed in our validation studies, we were able to experimentally verify that many MDEs can discriminate between different members of the same miRNA family, if these have sufficiently different 3C pairings. Hence, TDMD can function as a fine-tuning mechanism in the regulation of the expression of miRNAs organized in clusters or families. In addition, TDMD is a mechanism that, impacting on shared targets, influences also the miRNA activity (Ghini, Rubolino et al., 2018; Kleaveland et al., 2018; Bitetti et al., 2018). In fact, TDMD can be defined a new

mechanism in control of non-coding RNA biology that involves peculiar RNA molecules and regulates gene expression in trans (Kopp et al., 2018).

It must be pointed out that the capability of a specific transcript to trigger TDMD, which can be predicted by *TDMDfinder*, does not imply that the degradation of the miRNA also happens in a physiological and/or pathological scenario, even for the interactions validated by the TDMD assay. In fact, the TDMD assay has the limit of ectopically overexpress MDE regions outside of their full 3'UTR structures. For example, an MDE site could not be able to bind the miRNA, as RNA binding proteins (RBPs) mask the region and/or the specific 3'UTR structure. Furthermore, the experimental validation of a specific MDE by performing the TDMD assay is not sufficient to prove that the regulation by TDMD occurs *in vivo* and at endogenous level, because other factors, as the availability and the expression levels of either the target or the miRNA, also play a role in this process. Actually, the quantitative requirements for TDMD to take place have been investigated only in a limited context (Ghini, Rubolino et al., 2018; Kleaveland et al., 2018) and cannot be easy accounted for by a computational tool based on predictions. Further studies are needed to show in which specific landscape each of the predicted MDEs play a part.

3.4 TDMD pairs in human cancer

Human cancer is an interesting biological landscape for evaluating the implications of the TDMD pairs predicted by the *TDMDfinder* pipeline. We used the large TCGA datasets to extract quantitative information for whether miRNAs or targets in thousands of samples and investigate the relevance of TDMD couples at endogenous levels. Based on a set of correlation analyses that took into account TDMD effects on miRNA levels and miRNA activity, we speculated that TDMD might occur in human cancer. Indeed, miRNA levels are often deregulated in human cancer (Lujambio and Lowe., 2012) and this dysregulation cannot be justified in all cases by alterations in the biogenesis of miRNAs. Modulation of cancer relevant genes and pathways or chromosomal rearrangements, including amplifications and/or deletions, may cause dramatic changes in the expression of TDMD transcripts, thus contributing to alterations of miRNAs expression in cancer. Notably, we isolated a number of strongly supported interactions, namely "pan-cancer supported" TDMD pairs, that passed through additional tests, as the "Passenger test" (see chapter 3), and so reinforced the hypothesis that TDMD could take place in such cases. Importantly, these "pan-cancer supported" TDMD interactions include previously demonstrated endogenous TDMD transcripts, NREP and SERPINE1, and several of those that were experimentally validated by performing the TDMD-assay (ZFYVE26, RAB21, PTEN, IQSEC1,

BCL2L11), here analyzed at their endogenous expression levels. In order to provide a proof-of-concept example of TDMD as a relevant mechanism in cancer, we dissected the miR-30c:SERPINE1 interaction in the context of breast cancer. In TNBC/basal tumors, SERPINE1 endogenous expression is extremely high, suggesting that TDMD might be used to keep low levels of miR-30c, which is known to have a tumor-suppressor function in breast cancer, by increasing the sensitivity to chemotherapy drugs and inhibiting the growth of cancers stem cells (CSC) (Bockhorn et al.; 2013; Yu et al.; 2010; Chao et al; 2015). Our lab has acquired long-standing experience in breast cancer cellular models and in particular of TNBC cell lines, among which SUM159PT represents a versatile and useful model for cancer studies. We were able to interfere with the TDMD mechanism by either deleting the SERPINE1 MDE by CRISPR or using a LNA Target-Protector molecule, which obstructs the interaction between SERPINE1 mRNA and miR-30c. The levels and the activity of miR-30c increased in both cases, further validating SERPINE1 as an endogenous TDMD for miR-30c in human breast cancer cells. In agreement with previous observations in other systems, TDMD affected miR-30c levels in a relatively mild manner (2-fold increase upon TDMD disruption). As a further approach, we used a tunable (doxycycline dependent) system to mildly over-express (2 to 3-fold) miR-30c in SUM159PT cells and obtained a TDMD-like effect. Using these three independent and complementary experimental approaches we showed that two specific cancer phenotypes, namely the resistance to drug treatment (i.e. paclitaxel, frequently used in chemotherapy regimens) and the ability to survive in non-adherent conditions, which is associated to cancer stem cells, were both dependent on a fully functioning TDMD mechanism. This is just a proof of principle validation of TDMD role in human breast cancer. In-depth characterization studies on several TDMD pairs, tumor types and phenotypes of cancer are required to completely unveil the function of TDMD in the mechanisms of cancer initiation and/or evolution.

3.5 ZSWIM8 regulates miRNA expression in breast cancer

A deeper understanding of the TDMD pathway would benefit from the identification of factors required for this mechanism. Although TDMD process was first discovered more than ten years ago, until 2020 the mechanistic model for miRNA degradation through TDMD remained elusive. Many candidates, such as terminal nucleotidyltransferases and nucleases were tested for roles in both TDMD and miRNA turnover (Rissland et al., 2011; Haas et al., 2016; Mansur et al., 2016; Kleaveland et al., 2018; Shukla et al, 2019; Pawlica et al., 2020; Burroughs et al., 2010). Recently, an unbiased genetic screening approach was set up to identify proteins involved in the TDMD machinery, revealing the ZSWIM8 culling-

RING ubiquitin ligase substrate adapter as an essential mediator of this mechanism (Shi et al., 2020; Han et al., 2020). The discovery of ZSWIM8 as a crucial factor for TDMD provided us the opportunity to study the broad role of endogenous TDMD in breast cancer. Hence, we performed a CRISPRi based ZSWIM8 KD in a set of 8 different breast cancer cell lines, representing the entire spectrum of breast cancer subtypes, comprising Luminal- (MCF-7, T47D), Her2- (SKBR3, MDA- MB361) and TNBC- subtype (SUM159PT, MDA-MB231, BT459, MDA-MB436). In total, we found 119 miRNAs that were significantly increased after ZSWIM8-KD, 55 of which were named "Breast cancer (BC) miRNA" and selected for additional test as they showed a consistent regulation upon ZSWIM8 KD (≥ 0.3 L2FC), often in more than one cancer cell type, and had a medium to high level of expression in breast, which suggested these miRNAs to be active in this context.

To get rid of any transcriptional effect triggered by ZSWIM8 KD, we performed a transcriptional analysis of precursor molecules (pri-miRNAs) to validate the "true" BC TDMD substrates. Globally, our analyses showed that loss of ZSWIM8 caused significantly increased accumulation of 31 miRNAs without any evidence of transcriptional regulation. We termed this "High Confidence (HC) BC miRNA". Similarly, sRNA seq of ZSWIM8-deficient MEFs, neurons or human cancer cell lines (HeLA, A549 and MCF7) revealed 32 miRNAs that were upregulated after the impairment of TDMD (Shi et al., 2020; Han et al., 2020). Interestingly, several HC BC miRNAs, such as miR-7, miR-335, miR-29b, miR-33 and miR-744, showed increased accumulation also in MEFs, neurons or cancer cell lines (Shi et al., 2020; Han et al., 2020) suggesting that these miRNAs are substrates of endogenous TDMD triggers in multiple cellular contexts.

Notably, most of HC BC miRNAs were cell line specific, while 9 out of 31 were strongly upregulated in more than one cell line. Among these 9 HC BC miRNAs, we found some that had been previously associated to breast cancer progression, such as miR-29-3p, miR-146b-5p and miR-33b-5p. Specifically, the anti-metastatic role of miR-29b is known in breast cancer and the direct targets of this miRNA include a number of pro-metastatic factors involved in angiogenesis and remodeling of the tumor microenvironment, such as VEGFA, ANGPTL4, PDGF, LOX and MMP9 (Chou et al., 2013). Similarly, it was shown that miR-33b, in addition to its role in the regulation of lipid, cholesterol homeostasis and glucose metabolism, inhibits breast cancer metastasis by targeting HMGA2, SALL4 and TWIST1 (Yancheng et al., 2015). Furthermore, our group has linked miR-146b depletion to reduced pharmacological resistance in breast cancer (Tordonato et al., 2021). We still have much to learn about how TDMD impacts on miRNA activity in various cell types and in different biological contexts. In particular, we envision that different TDMD triggers might control

the level and the activity of their miRNA substrates either in steady state conditions or in response to specific stimuli, generating a complex scenario of miRNA levels.

Looking ahead, identifying the TDMD triggers is crucial to validate the expanded role of TDMD mechanism in miRNA biology. To this aim, we designed an effective strategy based on the combined use of *TDMDfinder* predictions and experimental tools, such as CRISPRi. We exploited ZSWIM8 KD to identify the set of miRNAs under the control of TDMD in a given cell line. Then, we exploited *TDMDfinder* to identify potential TDMD triggers, and used RNA-seq information to define their expression levels. Finally, we inhibited the candidate TDMD-trigger by using CRISPRi system. We performed a proof-of-concept validation of the strategy on a candidate TDMD pair (NREP:miR-29b) by generating NREP KD SUM159PT and BT549 cells and observing stabilization of the mature miR-29b. No effects were found on the primary transcripts levels, proving NREP as the endogenous TDMD triggers of miR-29b in human BC cells. In the near future, we will select a small set of BC relevant TDMD interactions to test. By using the CRISPRi system, we will validate additional endogenous TDMD triggers for their ability to control miRNA level and activity.

3.6 TDMD ZSWIM8 independent mechanisms

The discovery of ZSWIM8 ubiquitin ligase substrate adaptor as an essential factor in TDMD pathway allowed us, for the first time, the identification of miRNA substrates that are regulated in breast cancer revealing more than 30 miRNAs significantly upregulated upon TDMD impairment. Similarly, previous studies focusing on a panel of ZSWIM8-deficient mammalian cell lines identified 32 miRNAs under the control a ZSWIM8-dependent TDMD mechanism (Shi et al., 2020; Han et al., 2020). Additional studies in Drosophila S2 cells knock-out for the ZSWIM8 homolog Dora and in *C. elegans* deficient of the ZSWIM8 homolog EBAX-1 showed several miRNAs under the control of TDMD in these species (Shi et al., 2020). Interestingly, miR-30b-5p and miR-30c-5p, known endogenous TDMD substrate in mouse and human (Ghini, Rubolino et al., 2018, Simeone, Rubolino et al., 2022), were never found among the significantly upregulated miRNAs as a consequence of a ZSWIM8-dependent TDMD disruption. Here, by coupling the knock-down of ZSWIM8 with the overexpression of SERPINE1 miRNA degradation element (MDE), we showed that miR-30b-5p and miR-30c-5p degradation through TDMD was unaltered after ZSWIM8 depletion. Interestingly, ZSWIM8 transcript is widely expressed in human tissues with a median of 45.2 transcript per million (TPM) in a human transcript-expression atlas (Consortium et al., 2013) by suggesting that it could cause TDMD in many cell types. Nonetheless, three potential paralogs of ZSWIM8 in mammalian cells (ZSWIM4, 5, 6),

although less expressed than ZSWIM8 (median TPM 4.3 for ZSWIM4, 3.3 for ZSWIM5 and 12.9 for ZSWIM6) might also drive TDMD, maybe recognizing peculiar miRNA-AGO-transcript complexes. Actually it is still unknown how ZSWIM8 specifically recognize the AGO:miRNA complex. Structural studies revealed that base-pairing of a miRNA with a TDMD transcript promotes conformational changes of human AGO2, including opening of the central cleft (Sheu-Gruttadauria et al., 2019). It is possible that this configuration unveils a site that enables ZSWIM8 recruitment. Perhaps there are alternative mechanisms for the association of ZSWIM8 beyond extended 3' complementarity, such as RNA binding proteins linked to the target and able to interact with ZSWIM8. It could be possible that specific RNA binding proteins have higher affinity for a given miRNA:target complex (i.e. miR:30b/c:SERPINE1) and they are prone to interact with proteins displaying ZSWIM8-like functions. Coherently with this hypothesis, the F-box protein HAWAIIAN SKIRT, which functions as a cullin-RING ubiquitin ligase adapter protein, has been shown to be required for target directed miRNA degradation in *Arabidopsis* (Zhang et al., 2017; Lang et al., 2018; Mei et al., 2019). Further investigation about ZSWIM8 independent TDMD mechanisms are needed. Since the miR:30 family consist of five members who share the same seed sequence, it is very cumbersome to create a sensor that specifically monitor the decay of miR:30b/c. For this reason, as opposed for the TDMD pair miR-7:CYRANO (Shi et al., 2020; Han et al., 2020), it was not feasible for us to perform a genome-wide CRISPR-Cas9 screen to identify the factors that are required for miR-30b/c TDMD.

Moreover, despite the recent findings, many points should be clarified also in the current TDMD model. Specifically, in the new TDMD E3 model, ZSWIM8 senses the conformational changes that occur when the target RNA pairs with the 3' region of the miRNA. Then, AGO2 is polyubiquitinated and degraded exposing the miRNA to the action of some not yet identified cellular exonucleases, while the trigger is released undamaged, as it is protected by the presence of the 5 'cap and the 3' poly (A) tail. It is relevant that the half-live of AGO2 protein is usually longer than the half-live of most miRNAs, by suggesting that, for numerous miRNA-AGO complexes, the miRNA is firstly degraded while AGO2 protein is recycled (Kingston and Bartel, 2019).

To conclude, the degradation of AGO-miRNA complexes through the ubiquitin-proteasome machinery might be a common mechanism to regulate the decay of miRNAs in several species, even if we still have a lot to learn about the molecular mechanisms underlying TDMD.

4. Materials and Methods

4.1 Cell cultures and reagents

Mouse 3T9 fibroblasts were cultured in DMEM (Dulbecco's modified Eagle's medium) supplemented with 10% fetal bovine serum (FBS), 100 U/mL penicillin and 100 mg/mL streptomycin. Cells were routinely checked for mycoplasma contamination and resulted negative. 3T9 cells were induced to quiescence in a serum-deprived medium (0.1% FBS) for 3 days. Cell cycle re-entry was stimulated by adding fresh medium with 10% FBS.

HeLa cells (Human cervical carcinoma, ECACC No. 96112022) were cultured in DMEM supplemented with 10% FBS, 100 U/mL penicillin and 100 mg/mL streptomycin. Cells were routinely checked for mycoplasma contamination and always tested negative. HeLa cells carrying the PB-TRE-dCas9-KRAB construct, referred in the text as Hela-KRAB (see PiggyBac transposition) were cultured in the same media of parental HeLa cell line with 10% TETFREE FBS and 100 µg/mL Hygromycyn B.

SUM159PT, triple negative human BC cells, were cultured in Ham's F12 medium, supplemented with 5% FBS (South American origin), 2mM Glutamine, 5 µg/mL insulin, 1 µg/mL hydrocortisone, 10mM HEPES, 100 µg/mL of Penicillin/Streptomycin and were cultured under an atmosphere of 10% CO2 at 37°C.

Other BC cell lines

List of BC Cell lines PB-TRE-dCas9-KRAB transposed:

CELL LINE	ER	HER2	SUBTYPE	MEDIUM	HYGROMICIN SELECTION
SUM159PT	-	-	TNBC	Ham's F12, 5% Fetal Bovine Serum (FBS), 2mM Glutamine, 5 µg/ml insulin, 1 µg/ml hygrocortisone, 10 mM HEPES, 100 µg/ml P/S	200 µg/ml
MDA-MB-231	-	-	TNBC	DMEM + 10% FBS + 2 mM L-Glutamine + 1% P/S	200 µg/ml
BT-549	-	-	TNBC	DMEM + 10% FBS + 2 mM L-Glutamine + 1% P/S	100 µg/ml
MDA-MB-436	-	-	TNBC	DMEM:Ham's F12 medium (1:1 mixture) supplemented with 2 mM L-Glutamine and 10% FBS + 1% P/S	100 µg/ml
T47D	+	-	LUMINAL A	DMEM + 10% FBS + 2 mM L-Glutamine + 1% P/S	100 µg/ml
MCF-7	+	-	LUMINAL A	DMEM + 10% FBS + 2 mM L-Glutamine + 1% P/S	100 µg/ml
MDA-MB-361	+	+	HER2 amplified	DMEM + 10% FBS + 2 mM L-Glutamine + 1% P/S	100 µg/ml
SK-BR-3	-	+	HER2 amplified	DMEM + 10% FBS + 2 mM L-Glutamine + 1% P/S	100 µg/ml

FBS was substituted with Tetracycline Free FBS after transposition.

4.2 miRNA, Pri-miRNA and mRNA RT-qPCR expression analyses

4.2.1 Total RNA extraction

Total RNA extraction, including small RNAs, was performed with miRNeasy Mini Kit (Qiagen). Samples were prepared according to recommendations in the miRNeasy Handbook. Cells were spun down and resuspended in 700 µL of QIAzol Lysis Reagent and incubated at RT for 5 min; then 140 µL of Chloroform were added. The solution was then vortexed for 15 s and incubated at room temperature for 2-3 min. Each sample was centrifuged for 15 min at 12,000 x g at 4°C and the upper aqueous phase was transferred into a new collection tube. Then 1.5 volumes of 100% ethanol were added. Samples were transferred to RNeasy MinElute spin column and centrifuged at ≥8000xg for 15 s. The flow-through was discarded. Columns were washed with 350 µL of RWT buffer. DNase treatment was performed on columns. DNase I was prepared diluting 10 µL of DNase I (Qiagen) in 70 µL of RDD buffer and incubated at RT for 15 min. 350 µL of RWT were used for washing. Columns were further washed with 500 µL of RPE buffer in two centrifugation steps at ≥8000xg of 15 s and 2 min. Empty columns were further centrifuged to remove residual ethanol. RNA was extracted in RNase free H_2O and quantified by NanoDrop UV-Vis Spectrophotometer (Thermo Scientific). RNA was stored at -80°c.

4.2.2 mRNA retrotranscription

Pri-miRNAs and mRNAs were evaluated by quan3.1titative PCR on total RNA. Total RNA was retro-transcribed in cDNA according to SuperScript® VILO cDNA Synthesis Kit (Life Technologies cat.no. 11754050). The reaction was set-up as follows:

COMPONENT	QUANTITY
RNA	100 – 1 µg
5X Vilo Reaction Mix	4 µl
10X SuperScript Enzyme Mix	2 µg
H_2O	Up to 20 µl

Retro-transcription reaction was carried-out in a thermal cycler with the following conditions:

STEP	TEMPERATURE (°C)	TIME (min)
Annealing	25°C	10
Extension	42°C	60
Enzyme inactivation	85°C	5
Incubation	4°C	Hold

cDNA was stored at -20°c for subsequent amplification.

4.2.3 Real time quantitative PCR

Expression levels of pri-miRNAs and mRNAs were detected by Real-Time quantitative PCR (RT-qPCR) with Fast SYBR Green reagents (Life Technologies). About 25 ng of cDNA were used as the input to detect pri-miRNAs, instead 5 ng of cDNA were used as the input to detect mRNAs. For each cDNA sample, a reaction was set-up as follows:

COMPONENT	QUANTITY
2X Fast SYBR Master Mix	10 µl
Forward and Reverse primers 3.3 µM	2 µl
Template cDNA	1 – 5 ng/µl
Nuclease-free H_2O	Up to 20 µl

Reactions were carried out in BIORAD CFX Real-Time PCR detection system under the following cycling conditions:

STEP	TEMPERATURE (°C)	TIME
Initial Denaturation	95°C	15 min
3-step cycling (39 cycles):		
Denaturation	94°C	15 sec
Annealing	55°C	30 sec
Extension	70°C	30 sec

Regarding the pri-miRNAs, since the exact boundaries of most of them are not precisely known, it was necessary to manually define them. We designed specific pri-miRNA probes by using the UCSC Genome Browser where the sequencing tracks data were manually inspected to define the putative pri-miRNA regions of the miRNAs of interest. For each

intergenic and/or intronic miRNA we assessed the presence of adjacent track signals and then we defined the pri-miRNA design region about 500 base pairs upstream and downstream the miRNA of interest. For each intronic miRNA, we designed also primer pairs falling into the host gene, while for miRNAs of interest within a cluster we avoided the design over other miRNAs not involved in the analysis. Once retrieved the specific sequences, primer pairs were designed through computer assisted primer design software (Primer3 Plus). All primer pairs were tested for the linear amplification of their target with serial dilutions of cDNA.

The complete list of primers used in chapter1, 2 and 3 are available online in the Supplementary data of the associated paper. The complete list of primers used in chapter 4 are available upon request.

Reactions were performed in triplicates. Data were normalized on Ct values of the housekeeping gene RPLP0 and/or GAPDH by calculating their ΔCt. Data in the text are expressed in Relative RNA expression calculated according to the formula $2^{\wedge -\Delta Ct}$.

4.3 MiRNA expression analyses

4.3.1 microRNAs retrotranscription

Mature miRNAs were detected by RT-qPCR with the miScript system (Qiagen) for the experiments described in chapter 1, 2 and 3. Since the miScript system was no longer available, experiments described in chapter 4 were performed by using the miRCURY system (Qiagen), a LNA-based system for sensitive and accurate detection of miRNAs by qPCR.

MiScript protocol

Total RNA was retrotranscribed into cDNA according to miScript II RT Kit. Reverse transcription reaction components are reported in the table below:

COMPONENT	VOLUME/REACTION
5x miScriptHiSpec Buffer	4 µL
10x miScriptNucleics Mix	2 µL
RNase-free water	Variable
miScript Reverse Transcriptase	2 µL
Template RNA (1µg)	Variable
Total volume	10 µL

The protocol consists of the following steps:

STEP	TEMPERATURE (°C)	TIME (min)
Annealing/Extension	37°C	60
Heat-inactivate of miScript Reverse Transcriptase	95°C	5

MiRCURY protocol

The method is based on universal reverse transcription (RT), followed by real-time PCR amplification with LNA-enhanced primers. For the cDNA synthesis with the miRCURY LNA RT KIT, each RNA sample is diluted to 5 ng/µl using nuclease-free water. The reverse transcription reactions were all prepared on ice using 10 ng of RNA for each sample, according to the standard protocol:

COMPONENT	miRNA PCR ASSAY
5x miRCURY SYBR® Green RT Reaction Buffer	2 µl
RNase-free water	5 µl
10x miRCURY RT Enzyme Mix	1 µl
Template RNA	2 µl
TOTAL REACTION VOLUME	10 µl

The reverse transcription reaction protocol consists of the following steps:

STEP	TEMPERATURE (°C)	TIME (min)
Annealing/Extension	42°C	60
Heat-inactivate the Reverse Transcriptase	95°C	5

4.3.2 MicroRNAs Real Time-quantitative PCR (RT-qPCR)

In order to measure expression levels of specific miRNAs, cDNAs were amplified and their levels were detected by Real-Time quantitative PCR (RT-qPCR). Relative to the miSCRIPT system, for each cDNA sample a mix was prepared according to the following volumes:

REAGENT	QUANTITY
2x QuantiTect SYBR Green master mix	10 µL
10x miScript Universal Primer	2 µL
10x miScript Primer Assay	2 µL
RNase-free water	Variable
Template cDNA	1 ng/µL

The amplification reaction protocol consists of the following steps:

STEP	TEMPERATURE (°C)	TIME
PCR initial heat activation	95°C	15 min
3-step cycling (40 cycles):		
Denaturation	94°C	15 sec
Annealing	55°C	30 sec
Extension	70°C	30 sec

miRNAs were detected using miScript Primer Assays available in the Qiagen catalog online.

For the miRNA qPCR showed in the chapter 4, the miRCURY LNA SYBR Green PCR Kit was used. The cDNAs were then diluted 1:60 with nuclease free water and amplified with the specific primer mix according to the following protocol:

COMPONENT	VOLUME
2x miRCURY SYBR® Green Master Mix	5 µl
Resuspended PCR primer mix	1 µl
cDNA template	3 µl
RNase-free water	1 µl
TOTAL REACTION VOLUME	10 µl

The amplification reaction protocol consists of the following conditions:

STEP	TEMPERATURE (°C)	TIME (sec)
PCR initial heat activation	95°C	120
2-step cycling (40 cycles)		
Denaturation	95°C	10
Combined annealing/extension (Fluorescence data collection)	56°C	60
Melting curve analysis	60-95°C	120

miRNAs were detected using miRCURY® miRNA Assays available in a Qiagen online list.

4.4 RNA sequencing and data analysis

Libraries were generated using the TruSeq RNA Library Prep Kit v2 (Illumina). Next, sequencing was performed on an Illumina HiSeq 2000 at 50 bp single-read mode and 50 million read depth (3×). Reads were aligned to the reference genome using the TopHat aligner (version 2.0.6) with default parameters. Differentially expressed genes were identified using the Bioconductor package DESeq2 based on read counts, considering genes whose q value relative to the control was lower than 0.05 and whose maximum expression was higher than RPKM of 1. For miRNA-target analysis, mouse miR-30 targets were downloaded from TargetScan 7.1, including information on conservation and on the type of seed (8-mers, 7-mer-m8, and 7-met-1A).

4.5 sRNA sequencing and data analysis

Small RNA sequencing (sRNA-seq) libraries were prepared with the TruSeq Small RNA Kit (Illumina), following the manufacturer's instructions. Next, sequencing was performed on an Illumina HiSeq 2000 at 50 bp single-read mode and 20 million read depth (8×). Sequencing quality was checked in the FASTQC report, by considering only the experiments with Q30 or above (Phred Quality Score). miRNA counting was performed with the Isomirage tool (Muller et al., 2014). Normalization was performed with the library size (reads-per-million). All the analyses were performed on canonical and templated miRNA reads to exclude miRNA 3' isoforms, which are typically modulated upon TDMD.

4.6 miRNA 3C-target analysis

3C-targets were selected according to criteria outlined in Figure 23. Both the conserved sites (CS) and non-conserved sites (NCS) were used. Targets were then classified according to the 3′ end pairing contribution, a feature that measures the presence of a binding region, in addition to the seed, located at the 3′ end of the miRNA. Those targets containing 3′ end supplementary regions were referred to as "3C target genes" (3C_TGs) and classified in three classes (HIGH, MID, LOW) according to the 3′ pairing contribution score, as shown in chapter 1. Targets expressed in 3T9 mouse fibroblasts were identified by crossing the list of 3C_TGs with RNA-seq data sets (growing cells and serum stimulated cells). Genes with FPKM values < 1 were considered as 'not expressed' and, therefore, excluded. Finally, we selected targets of expressed miRNAs in 3T9 cells, by considering sRNA-seq data and filtering miRNA > 10 cpm.

4.7 Generation of SERPINE1-MRE Knockout

SgRNAs flanking MRE of miR-30 were designed for SERPINE1 transcript, using the CRISPR Design Tool. SgRNAs were cloned into the PX458 vector (Ran et al. 2013). Cells (3T9 fibroblasts and SUM149PT) were co-transfected with two PX458 vectors (sgRNA_1 and sgRNA_2) harboring single sgRNAs sequence (5 μg each construct) together with Cas9-GFP. The transfection efficiency with lipofectamine 3000 was around 30%. At 48 h after the transfection, the top 5% of GFP+ cells were sorted as single cells into 96-well plates. After 2 weeks, deletions in clonal cells were screened by PCR using specific primers to detect bi-allelic deletions. Positive clones were confirmed by DNA sequencing. The protocol efficiency was about 20% for mono-allelic and 2% for bi-allelic deletions in 3T9 fibroblasts, instead 66% for mono-allelic and 17% for bi-allelic deletions for SUM159PT cells. The PCR primers and the sgRNAs used in clone screening were reported in Supplementary Table S5 (Ghini, Rubolino et al., 2018).

4.8 Rescue of MRE expression by adenoviral constructs

In order to re-express MRE of miR-30, recombinant adenoviruses were produced using the AdEasy System (Agilent), following manufacturers' instructions. Briefly, gene synthesis (GenScript) generated a mCherry-Serpine1 (3′UTR) construct that was cloned into pShuttle vector (Agilent) by adding KpnI-NotI sites at the extremities. After homologous recombination in BJ5183-AD-1 cells (Agilent), positive recombinants (isolated by PacI digestion) were used to produce adenoviruses in 239 cells. Viruses were finally concentrated

with Adeno-X maxi purification kit (Takara). The full list of the mCherry-Serpine 3′UTR construct and the oligonucleotides used to produce the adenoviral constructs were reported in the methods of the related paper (Ghini, Rubolino et al., 2018).

4.9 Expression of mutant-binding sites for miR-30

In order to re-express different variants of MRE of miR-30 in MRE-KO clones, we cloned MRE with 20 surrounding bases into EcoRI-XhoI sites that were put after the stop codon of an eGFP cloned in a pcDNA3.1 mammalian expression vector (Thermo Fisher Scientific). Vectors were transfected in MRE-KO clones with Lipofectamine 3000 reagent (Thermo Fisher Scientific). Cells were collected for RT-qPCR analysis after 48 h.

4.10 Measurement of miR-30 activity (miR-sensor) by flow cytometry

A sequence harboring four complementary repeats for miR-30c-5p and a control sequence were purchased from TwinHelix and cloned (XbaI/XmaI) into the 3′UTR of a destabilized GFP (dGFP) of a bidirectional lentiviral vector (BdLV_1370), which also expressed ΔNGFR under the same promoter (a kind gift from Luigi Naldini). Infected cells were analyzed by FACS (MACSQuant Flow cytometer, Miltenyi) to isolate populations with similar ΔNGFR expression. Data analysis was performed with the FlowJo software (TreeStar): for each cell, fluorescence levels of ΔNGFR and dGFP were log-transformed and cells were then divided into bins of 1000 cells each, based on their ΔNGFR level. Finally, dGFP expression was calculated for each bin and repression folds were calculated as the ratio [dGFP(miR-30)] / [dGFP(control)].

4.11 mRNA:miRNA TDMD predictions

All the human and mouse target:miRNA interactions data used (conserved (C) and non-conserved (nC), respectively, N_{human_C} = 257466, N_{human_nC} = 14279806, N_{mouse_C} = 193264, N_{mouse_nC} = 10662819) were downloaded from TargetScan database. The TargetScan database was also used to retrieve the position of all MREs within its 3'UTR region. Then, the ~30 nucleotides upstream the MRE were retrieved from Ensembl database and the pairwise sequence alignments was performed, in a global fashion, by using the *pairwiseAlignment* function in the Biostring library from Bioconductor and as gap penalty and substitution scoring scheme we found in microRNA.org. Only the alignments covering the entire length of the miRNA were further analyzed in order to find the “best alignment”,

defined as the one having i) an alignment score falling between the 50th and the 100th percentile and ii) the smallest number of gaps. For each aligned RNA duplex, information on the number of matches, mismatches, and consecutive aligned characters was extracted using a custom implemented R function, together with additional information, such as dimension of the bulge. In order to identify 3' complementary regions (3C) compatible with TDMD, we identified all the pairs with 7 or more (≥ 7) consecutive pairings (tolerating one G:U wobble).

4.12 Calculation of Minimum Free Energy (MFE)

The RNAhybrid tool (Kruger et al., 2006) was used to calculate the minimum free energy (MFE) of hybridization of each predicted mRNA:miRNA duplex. For each interaction, the ratio between its MFE and the MFE of a "theoretically perfect TDMD" was also calculated. These "perfect TDMD-interactions" were built ad-hoc for all annotated miRNAs, using RNA sequences complementary to the specific miRNA sequence in all positions except for position 9,10 and 11 (i.e. bulge region).

4.13 Predicted and HC TDMD pairs selection and phylogenetic conservation

To define the list of the predicted TDMD pairs, we considered the following criteria: i) alignments with seven or more consecutive 3C matches (≥7), ii) a bulge extension between 2 and 8 nucleotides in total (≥2 and ≤8) and iii) a MFE ratio greater than 0.7 (≥0.7). HC TDMD pairs were selected from the list of predicted TDMD pairs by filtering out those with six or more consecutive 3C matches (≥6), considering canonical pairings only, and a MFE ratio greater than 0.8 (≥0.8). For each predicted TDMD pair, the phylogenetic conservation of the region corresponding to the 3C pairing was measured using the PhyloP scores (retrieved from the UCSC). We used PhyloP scores calculated from multiple sequence alignments of 99 vertebrate genomes with the human genome (hg19/GRCh37).

PhyloP scores were first calculated at single nucleotide level and then averaged over the entire 3C pairing region, defined as a stretch of consecutive base pairs. For non-TDMD, the PhyloP score is calculated by considering a fixed window of 7 bases.

4.14 Pan-Cancer TCGA Analysis

Target mRNA Expression Data

Normalized Genomic Data Commons (GDC) harmonized RNA-seq data [both mRNA and miRNA, respectively FPKM (Fragments Per Kilobase Million) and RPM (Reads Per Million)], of 21 selected TCGA solid primary tumor types (BLCA, BRCA, CESC, COAD, ESCA, HNSC, KIRC, KIRP, LGG, LIHC, LUAD, LUSC, OV, PAAD, PCPG, PRAD, READ, SARC, STAD, THCA, UCEC) were downloaded using the TCGAbiolinks R/Bioconductor package (Colaprico et al., 2016), including 8572 patient samples.

MiRNA expression data

Loci-based isoform quantification txt files, which report counts (raw and normalized to RPM) of every miRNA-seq read observed, were retrieved using TCGAbiolinks.

Target:miRNA and Target:Activity correlations

The correlation between TDMD target expression and miRNA expression was measured for all HC TDMD pairs in each cancer type using the Spearman test ("miRNA Expression Test"). In each tumor sample, the activity of each miRNA of the human HC set was estimated with the ActMir algorithm (Lee et al., 2016), a computational method based on the expression levels of both miRNAs and their predicted target genes. Activity was measured using the list of predicted conserved targets but excluding candidate TDMD transcripts. The correlation between miRNA activity and the expression level of any of its predicted TDMD-targets was evaluated using the Spearman test ("miRNA Activity Test"). For the Pan-cancer interactions we calculated also the correlation between the TDMD target and the passenger strand of the targeted miRNAs in each tumor type. A "Normalized Spearman Correlation" was then computed as (Rho.Guide - Rho.Passenger). For passenger miRNAs with multiple genomic loci (e.g. miR-24-1-5p and miR-24-2-5p), the average correlation was used.

4.15 TDMDfinder tool

TDMD*finder* is a web tool which consists of a user interface frontend implemented in Javascript/Ajax/CSS and a computational backend implemented in PHP 5.5, R 3.3 and MySQL 5.5 for data storage (http://213.82.215.117:9999/TDMDfinder/index.php). The user interface allows to search and visualize the results and to export the results in standard formats, such as Excel/csv for tables and PNG for plots. The computational backend is

designed to dynamically build SQL (Structured Query Language) queries for data retrieval and to perform statistical tests and draw plots using the analysis section.

4.16 TDMD-assay

With the aim of overexpressing the MDEs of the selected TDMD triggers, MDE sequences and controls (mutant seed and scrambled sequences) were sub-cloned into the mammalian expression vector PCDNA 3.1 vector, a gift from Doug Golenbock (Addgene plasmid, #13031), in the 3'UTR of an EGFP reporter gene. For miR-106b and miR-26a were designed two other positve controls, namely “Optimal TDMD” (sequencences pairing with all bases of the miRNA, except for positions 9, 10 and 11).
HeLa cells were transfected by using Lipo3000 (ThermoFisher Scientific) with the PCDNA EGFP-MRE-X constructs in six-wells (400.000 cells/well) and cells were collected 72h after transfection. The full list of constructs is available online in the Supplementary table S2 of the associated paper (Simeone, Rubolino et al., 2022).

4.17 Inducible Expression of miRNAs

Inducible expression of miR-30c was achieved using the pSLIK-Hygro system (Addgene plasmid #25737) containing a fragment of the miR-30c primary transcript had been sub-cloned from Lenti-miR microRNA precursors clones (System Biosciences). As negative control pSLIK-Hygro empty vector has been used. Doxycycline was dissolved in water (10mg/mL stock solution) and used as indicated.

4.18 Mammospheres cultures

In order to obtain first-generation mammospheres, 200 cells were seeded in ultra-low adherent plates in presence of methylcellulose (MethoCult M3236, Stem Cell Technologies), diluted 1:1 in MEBM supplemented with 5 μg/ml insulin, 0.5 μg/ml hydrocortisone, 2% B27 (Invitrogen), 20 ng/ml EGF and bFGF (BD Biosciences), and 4 μg/ml heparin (Sigma). After 7 days, mammospheres were counted. As for the second-generation assays, spheres were mechanically dissociated and 200 cells from disaggregated primary-mammospheres were plated in the same conditions as above.

4.19 Cell viability analysis

SUM159pt cells were seeded in complete medium in 96-well plates (3000 cells/well) and treated with paclitaxel (1000 nM, 100 nM, 10 nM and 1 nM). After 72 hours, cell vitality was measured by ADP-Glo™ Max Assay (Promega, V7001) following the manufacturer's instructions. Measurements were acquired from 8 different wells in each of the biological replicates.

4.20 Target site blockers

miRCURY LNA Target Site Blockers (TSB) were designed by Exiqon. TBS-SE selectively binds a sequence that overlaps the MRE for miR-30 in the SERPINE1 3'UTR. TBS-Ctrl has no significant match to any annotated human 3'UTR. SUM159PT (200.000 cells/well) were in reverse transfected by using Lipo3000 with the miRCURY LNA TSBs (TBS-SE or TBS Ctrl) at two different concentrations (50 nM and 100nM).
Quantity of each reagent is reported in the following table:

CULTURE FORMAT	VOLUME OF MEDIUM ON CELLS (µl)	FINAL VOLUME OF DILUTED TBS(µl)	VOLUME HIPERFECT REAGENT (µl)	FINAL TBS CONC. (nM)
6-well	2300	100	12	30/50/100

After 72hrs miRNA activity was measured.

4.21 Production of stable dCas9-KRAB cell lines and sgRNAs delivery

4.21.1 Cloning of PB-TRE-dCas9-KRAB

The PB-TRE-dCas9-KRAB plasmid was previously generated by Bianca Giuliani in the lab. Specifically, the DNA sequence of KRAB repressor domain was amplified by PCR from the pHAGE TRE dCas9-KRAB (Addgene plasmid #50917) and cloned in frame into the PB-TRE-dCas9-VPR backbone (Addgene plasmid #63800) within the AscI/AgeI sites. The cloning was sequence-verified by Sanger Sequencing.

4.21.2 PiggyBac Transposition

Cells were seeded at 60-70% confluency the day before transposition in six well plates. Cells were transfected according to Lipo3000 protocol with 500 ng of transposon DNA (PB-TRE-dCas9-KRAB) and 200 ng of SuperPiggyBac transposase helper plasmid (Systems Bioscience). Specifically, the DNA was diluted in 125µL of Opti-MEM (ThermoFisher Scientific) and 5µL of P3000 transfection reagent. 7.5 µL of Lipofectamine3000 were diluted in 125 µL of Opti-MEM and vortex thoroughly. The DNA mix and Lipo mix were mixed 1:1 and incubated for 20 min at room temperature, then added dropwise to cells with fresh media. After 72h from transfection, cells were put in selection with 200 µg/mL Hygromycin B.

4.21.3 Lentiguide cloning for sgRNAs delivery

LentiGuide (Addgene#52963) cloning occurs within the Esp3I sites. Restriction digestion was performed as follows:

COMPONENT	QUANTITY
Plasmid	5 µg
Tango buffer (Thermo)	5 µl
Esp3I (Thermo)	3 µl
DTT	20 mM
H_20	Up to 50 µl

The reaction was incubated for at least 2h at 37°C. Digested plasmid was purified from a 1.2% agarose gel and dephosphorylated as follows:

COMPONENT	QUANTITY
Plasmid gel purified	Up to 1 µg
Phosphatase buffer	2 µl
Alkaline phosphatase	1 U
H_20	Up to 50 µl

sgRNAs oligos were purchased by Sigma-Aldrich. Forward and Reverse phosphorylated oligos were annealed:

COMPONENT	QUANTITY
T4 ligation buffer (NEB)	1 µl
T4 Polynucleotide Kinase (NEB)	0.5 µl
Oligo FWD	1 µl
Oligo RV	1 µl
H_20	6.5 µl

Annealed Oligos were diluted 1:200 in H2O for subsequent ligation reaction:

COMPONENT	QUANTITY
Plasmid dephos.	Up to 1 µg
Oligo annealed diluted (1:200)	1 µl
DNA dilution buffer	2 µl
H_20	Up to 10 µl
T4 ligation buffer	10 µl
T4 ligase	5 U

3 µL of ligation mix were used for subsequent transformation in Stbl3 cells. Cloning was sequence-verified by Sanger Sequencing.

4.21.4 Lentiviral production

HEK293T cells were seeded 24 hours before transfection at 70-80% confluency in DMEM media with Glutamax, supplemented with 10% TET FREE FBS and 100 µg/mL of Penicillin/Streptomycin in 6 well plates. The plasmid sgRNAs were packaged with psPAX2 (gag&pol) and VSV-G (envelope) plasmid transfected according to Lipofectamine 3000 protocol. The transfection mix was then added dropwise to cells with 1.5 mL of fresh media that was replaced after 12-16 hours. Supernatant was collected 24 hours after media replacement and centrifuged to remove cell debris, filtered through 0.22 µm syringe filters and used for subsequent infection.

4.21.5 Lentiviral transduction

Cell lines used in chapter 4 were seeded at 50% confluency the day before the transduction. Polybrene was added to the undiluted lentiviral supernatant to a final concentration of 1 µg/mL Transduction was usually carried out over-night and the following morning media was changed. Selection was started 48 hours after the end of infection. Cells were treated with 0.5 µg/mL of Doxycycline for 7 doublings to induce the KD of the gene of interest (ZSWIM8 and NREP). The sgRNAs sequences are reported below:

sgRNA	Forward	Reverse
LacZ	CACCGTGCTGCAAGGCGATTAAGT	AAACACTTAATCGCCTTGCAGCAC
GAL4	CACCGATGTGGTCATTCGTCATGA	AAACTCATGACGAATGACCACATC
ZSWIM8_28	CACCGTGCTGCAAGGCGATTAAGT	AAACACTTAATCGCCTTGCAGCAC
ZSWIM8_34	CACCGATGTGGTCATTCGTCATGA	AAACTCATGACGAATGACCACATC
ZSWIM8_42	CACCGTAGGGCCGGGACGAAGCGCT	AAACAGCGCTTCGTCCCGGCCCTAC
NREP_1	GTCCCAGCCGGGGATAGGAA	TTCCTATCCCCGGCTGGGAC
NREP_2	GGAGTAATCAAGTGTAAGGG	CCCTTACACTTGATTACTCC
NREP_3	GTGCTTCCGAGGGTCTTCTT	AAGAAGACCCTCGGAAGCAC
NREP_4	GAAAGAGTAATCAAGTGTAA	TTACACTTGATTACTCTTTC

Bibliography

Akiyoshi S., Ishii M., Nemoto N., Kawabata M., Aburatani H., Miyazono K., "Targets of transcriptional regulation by transforming growth factor-beta: expression profile analysis using oligonucleotide arrays." (2001); *Jpn J Cancer Res. 92:257-268*. DOI: 10.1111/j.1349-7006.2001.tb01090.x

Ameres S.L., Horwich M.D., Hung J.H., Xu J., Ghildiyal M., Weng Z., Zamore P.D., "Target RNA-directed trimming and tailing of small silencing RNAs." (2010); *Science 328:1534–1539*. DOI: 10.1126/science.1187058

Amodeo V., Bazan V., Fanale D., Insalaco L., Caruso S., Cicero G., Bronte G., Rolfo C., Santini D., Russo A., "Effects of anti-miR-182 on TSP-1 expression in human colon cancer cells: there is a sense in antisense?" (2013); *Expert Opin Ther Targets. 17(11):1249-61*. DOI: 10.1517/14728222.2013.832206

Andersson M.G., Haasnoot P.C.J., Xu N., Berenjian S., Berkhout B., Akusjärvi G., "Suppression of RNA interference by adenovirus virus-associated RNA." (2005); *J. Virol. 79:9556–9565*. DOI: 10.1128/JVI.79.15.9556-9565.2005

Asangani I.A., Rasheed S.A., Nikolova D.A., Leupold J.H., Colburn N.H., Post S., Allgayer H., "MicroRNA-21 (miR-21) post-transcriptionally downregulates tumor suppressor Pdcd4 and stimulates invasion, intravasation and metastasis in colorectal cancer." (2008); *Oncogene. 27(15):2128-36.* DOI: 10.1038/sj.onc.1210856.

Avraham R., Sas-Chen A., Manor O., Steinfeld I., Shalgi R., Tarcic G., Bossel N., Zeisel A., Amit I., Zwang Y., Enerly E., Russnes H.G., Biagioni F., Mottolese M., Strano S., Blandino G., Børresen-Dale A.-L., Pilpel Y., Yakhini Z., Segal E., Yarden Y., "EGF decreases the abundance of microRNAs that restrain oncogenic transcription factors." (2010); *Sci Signal. 3:ra43*. DOI: 10.1126/scisignal.2000876

Babiarz J.E., Ruby J.G., Wang, Y., Bartel D.P., Blelloch R., "Mouse ES cells express endogenous shRNAs, siRNAs, and other Microprocessor-independent, Dicer-dependent small RNAs." (2008); *Genes Dev. 22:2773–2785.* DOI: 10.1101/gad.1705308

Baccarini A., Chauhan H., Gardner T.J., Jayaprakash A.D., Sachidanandam R., Brown B.D., "Kinetic analysis reveals the fate of a microRNA following target regulation in mammalian cells." (2011); *Curr Biol. 21:369–376*. DOI: 10.1016/j.cub.2011.01.067

Baek D., Villén J., Shin C., Camargo F.D., Gygi S.P., Bartel D.P. "The impact of microRNAs on protein output." (2008); *Nature. 455(7209):64-71*. DOI: 10.1038/nature07242.

Bail S., Swerdel M., Liu H., Jiao X., Goff L.A., Hart R.P., Kiledjian M., "Differential regulation of microRNA stability." (2010); *RNA 16:1032-1039*. DOI: 10.1261/rna.1851510

Bak R.O. and Mikkelsen J.G., "miRNA sponges: soaking up miRNAs for regulation of gene expression." (2014); *Wiley Interdiscip Rev RNA. 5(3):317-33.* DOI: 10.1002/wrna.1213.

Ballarino M., Pagano F., Girardi E., Morlando M., Cacchiarelli D., Marchioni M., Proudfoot N.J., and Bozzoni I., "Coupled RNA processing and transcription of intergenic primary microRNAs." (2009); *Mol Cell Biol. 29:5632–5638.* DOI: 10.1128/MCB.00664-09

Balzeau J., Menezes M.R., Cao S., Hagan J. P., "The LIN28/let-7 pathway in cancer." (2017); *Front Genet. 8:31*. DOI: 10.3389/fgene.2017.00031

Barger J.F. and Nana-Sinkam S.P. "MicroRNA as tools and therapeutics in lung cancer." (2015); *Respir Med. 109(7):803–812*. DOI: 10.1016/j.rmed.2015.02.006

Bartel D.P., "Metazoan MicroRNAs." (2018); *Cell. 173:20-51.* DOI: 10.1016/j.cell.2018.03.006

Bartel D.P., "MicroRNAs: target recognition and regulatory functions." (2009); *Cell. 136: 215-233*. DOI: 10.1016/j.cell.2009.01.002

Barth S., Pfuhl T., Mamiani A., Ehses C., Roemer K., Kremmer E., Jaker C., Hock J., Meister G., and Grasser F.A., "Epstein-Barr virus-encoded microRNA miR-BART2 down-regulates the viral DNA polymerase BALF5." (2008); *Nucleic Acids Res. 36:666–675*. DOI: 10.1093/nar/gkm1080

Beg M.S., Brenner A.J., Sachdev J., Borad M., Kang Y. K., Smith S., Bader A., Kim S, Hong D.S. "Phase I study of MRX34, a liposomal miR-34a mimic, administered twice weekly in patients with advanced solid tumors." (2017). *Invest New Drugs. 35(2):180–188*. DOI: 10.1007/s10637-016-0407-y

Bellutti F., Kauer M., Kneidinger D., Lion T., Klein R., "Identification of RISC-associated adenoviral microRNAs, a subset of their direct targets, and global changes in the targetome upon lytic adenovirus 5 infection." (2015); *J Virol. 89:1608–1627*. DOI: 10.1128/JVI.02336-14

Bitetti A., Mallory A.C., Golini E., Carrieri C., Carreño Gutiérrez H., Perlas E., Pérez-Rico Y.A., Tocchini-Valentini G.P., Enright A.J., Norton W.H.J., Mandillo S., O'Carroll D., Shkumatava A., "MicroRNA degradation by a conserved target RNA regulates animal behavior." (2018); *Nat Struct Mol Biol. 25:244–251*. DOI: 10.1038/s41594-018-0032-x

Bockhorn J., Dalton R., Nwachukwu C., Huang S., Prat A., Yee K., Chang Y.F., Huo D., Wen Y., Swanson K.E., Qiu T., Lu J., Park S.Y., Dolan M.E., Perou C.M., Olopade O.I., Clarke M.F., Greene G.L., Liu H., "MicroRNA-30c inhibits human breast tumour

chemotherapy resistance by regulating TWF1 and IL-11." (2013); *Nat Commun. 4:1393*. DOI: 10.1038/ncomms2393.

Boele J., Persson H., Shin J.W., Ishizu Y., Newie I.S., Sokilde R., Hawkins S.M., Coarfa C., Ikeda K., Takayama K., Horie-Inoue K., Ando Y., Burroughs A.M., Sasaki C., Suzuki C., Sakai M., Aoki S., Ogawa A., Hasegawa A., Lizio M., Kaida K., Teusink B., Carninci P., Suzuki H., Inoue S., Gunaratne P.H., Rovira C., Hayashizaki Y., de Hoon M.J., "PAPD5-mediated 30 adenylation and subsequent degradation of miR-21 is disrupted in proliferative disease." (2014); *Proc Natl Acad Sci USA. 111:11467–11472*. DOI: 10.1073/pnas.1317751111

Bohnsack M.T., Czaplinski K., Gorlich D., "Exportin 5 is a RanGTP-dependent dsRNA-binding protein that mediates nuclear export of pre-miRNAs." (2004); *RNA. 10:185–191*. DOI: 10.1261/rna.5167604

Bonetti P., Climent M., Panebianco F., Tordonato C., Santoro A., Marzi M.J., Pelicci P.G., Ventura A., Nicassio F., "Dual role for miR-34a in the control of early progenitor proliferation and commitment in the mammary gland and in breast cancer." (2019); *Oncogene. 38(3):360-374*. DOI: 10.1038/s41388-018-0445-3.

Bosson A.D., Zamudio J.R., Sharp P.A., "Endogenous miRNA and target concentrations determine susceptibility to potential ceRNA competition." (2014); *Mol Cell. 56:347-359*. DOI: 10.1016/j.molcel.2014.09.018

Burroughs A.M., Ando Y., de Hoon M.J., Tomaru Y., Nishibu T., Ukekawa R., Funakoshi T., Kurokawa T., Suzuki H., Hayashizaki Y., Daub C.O., "A comprehensive survey of 3' animal miRNA modification events and a possible role for 3' adenylation in modulating miRNA targeting effectiveness." (2010); *Genome Res. 20(10):1398-410*. DOI: 10.1101/gr.106054.110.

Cai X., Hagedorn C.H., Cullen B.R., "Human microRNAs are processed from capped, polyadenylated transcripts that can also function as mRNAs." (2004); *RNA. 10:1957–1966. DOI: 10.1261/rna.7135204*

Calin G.A. and Croce C.M., "MicroRNAs and chromosomal abnormalities in cancer cells.", (2006); *Oncogene. 25:6202–6210.* DOI: 10.1038/sj.onc.1209910

Calin G.A., Dumitru C.D., Shimizu M., Bichi R., Zupo S., Noch E., Aldler H., Rattan S., Keating M., Rai K., Rassenti L., Kipps T., Negrini M., Bullrich F., Croce C.M., "Frequent deletions and down-regulation of micro- RNA genes miR15 and miR16 at 13q14 in chronic lymphocytic leukemia." (2002); *Proc Natl Acad Sci USA. 99:15524-15529.* DOI: 10.1073/pnas.242606799

Calin GA and Croce C.M. ,"MicroRNA signatures in human cancers." (206); *Nat Rev Cancer. 6(11): p.857-66*. DOI: 10.1038/nrc1997

Cantini L., G. Bertoli C. Cava T. Dubois A. Zinovyev M. Caselle I. Castiglioni E. Barillot L. Martignetti." Identification of microRNA Clusters Cooperatively Acting on Epithelial to Mesenchymal Transition in Triple Negative Breast Cancer, (2019); *47(5):2205-2215.* DOI: 10.1093/nar/gkz016

Carè A., Catalucci D., Felicetti F., Bonci D., Addario A., Gallo P., Bang M.L., Segnalini P., Gu Y., Dalton N.D., Elia L., Latronico M.V., Høydal M., Autore C., Russo M.A., "MicroRNA-133 controls cardiac hypertrophy." (2007); *Nat Med. 13:613–618*. DOI: 10.1038/nm1582.

Carthew R.W. and Sontheimer E.J., "Origins and Mechanisms of miRNAs and siRNAs." (2009); *Cell. 136:642-655*. DOI: 10.1016/j.cell.2009.01.035

Cazalla D., Yario T., Steitz J.A., Steitz J., "Down-regulation of a host microRNA by a Herpesvirus saimiri noncoding RNA." (2010); *Science. 328:1563–1566*. DOI: 10.1016/j.cell.2009.01.035

Chacon-Cortes D., Smith R.A., Haupt L.M., Lea R.A., Youl P.H., Griffiths L.R., "Genetic association analysis of miRNA SNPs implicates MIR145 in breast cancer susceptibility." (2015); *BMC Med Genet. 16:1–11.* DOI: 10.1186/s12881-015-0248-0

Chang T.C., Wentzel E.A., Kent O.A., Ramachandran K., Mullendore M., Lee K.H., Feldmann G., Yamakuchi M., Ferlito M., Lowenstein C.J., Arking D.E., Beer M.A., Maitra A, Mendell J.T., "Transactivation of miR-34a by p53 broadly influences gene expression and promotes apoptosis." (2007); *Mol Cell. 26:745–752*. DOI: 10.1016/j.molcel.2007.05.010

Chang T.C., Yu D., Lee Y.S., Wentzel E.A., Arking D.E., West K.M., Dang C.V., Thomas-Tikhonenko A., Mendell J.T., "Widespread microRNA repression by Myc contributes to tumorigenesis." (2008); *Nat Genet. 40:43-50*. DOI: 10.1038/ng.2007.30

Chao C.C., Kan D., Lu K.S., Chien C.L., "The role of microRNA-30c in the self-renewal and differentiation of C6 glioma cells." (2015); *Stem Cell Res. 14(2):211-223*. DOI: 10.1016/j.scr.2015.01.008

Chen C.Y. and Shyu A.B., "Mechanisms of deadenylation-dependent decay." (2011); *Wiley Interdiscip Rev RNA. 2:167–183*. DOI: 10.1002/wrna.40

Chen L.-L. and Yang L. "Regulation of circRNA biogenesis." (2015); *RNA Biol. 12:381–388*. DOI: 10.1080/15476286.2015.1020271

Cheng C.Y., Hwang C.I., Corney D.C., Flesken-Nikitin A., Jiang L., Öner G.M., Munroe R.J., Schimenti J.C., Hermeking H., Nikitin A.Y., "miR-34 cooperates with p53 in suppression of prostate cancer by joint regulation of stem cell compartment." (2014); *Cell Rep. 6:1000–1007*. DOI: 10.1016/j.celrep.2014.02.023

Chou J., Lin J.H., Brenot A., Kim J.W., Provot S., Werb Z., "GATA3 suppresses metastasis and modulates the tumor microenvironment by regulating microRNA-29b expression." (2013); *Nat Cell Biol. 15:201–213*. DOI: 10.1038/ncb2672

Chou Y.T., Lin H.H., Lien Y.C., Wang Y.H., Hong C.F., Kao Y.R., Lin S.C., Chang Y.C., Lin S.Y., Chen S.J., Chen H.C., Yeh S.D., Wu C.W., "EGFR promotes lung tumorigenesis by activating miR-7 through a Ras/ERK/Myc pathway that targets the Ets2 transcriptional repressor ERF." (2010); *Cancer Res. 70:8822–31*. DOI: 10.1158/0008-5472.CAN-10-0638

Colaprico A., Silva T.C., Olsen C., Garofano L., Cava C., Garolini D., Sabedot T.S., Malta T.M., Pagnotta S.M., Castiglioni I., Ceccarelli M., Bontempi G., Noushmehr H., "TCGAbiolinks: an R/Bioconductor package for integrative analysis of TCGA data." (2016); *Nucleic Acids Res. 44(8):e71*. DOI: 10.1093/nar/gkv1507

Croce C.M. "Causes and consequences of microRNA dysregulation in cancer." (2009); *Nat Rev Genet. 10(10):704–714*. DOI: 10.1038/nrg2634

Culurgioni S., Mari S., Bonetti P., Gallini S., Bonetto G., Brennich M., Round A., Nicassio F., Mapelli M., "Insc:LGN tetramers promote asymmetric divisions of mammary stem cells." (2018); *Nat Commun. 9(1):1025*. DOI: 10.1038/s41467-018-03343-4

Dai X., Cheng H., Bai Z., Li J., "Breast Cancer Cell Line Classification and Its Relevance with Breast Tumor Subtyping." (2017); *J Cancer. 8(16):3131-3141.* DOI: 10.7150/jca.18457

Das S.K., Sokhi U.K., Bhutia S.K., Azab B., Su Z.-Z., Sarkar D., Fisher P.B., "Human polynucleotide phosphorylase selectively and preferentially degrades microRNA-221 in human melanoma cells." (2010); *Proc Natl Acad Sci USA. 107:11948–11953*. DOI: 10.1073/pnas.0914143107

Davis E., Caiment F., Tordoir X., Cavaille´ J., Ferguson-Smith A., Cockett N., Georges M., Charlier C. "RNAi-mediated allelic trans-interaction at the imprinted Rtl1/Peg11 locus." (2005); *Curr Biol. 15:743–749*. DOI: 10.1016/j.cub.2005.02.060

Davis-Dusenbery B.N. and Hata A., "Mechanisms of control of microRNA biogenesis." (2010); *J Biochem. 148:381-392*. DOI: 10.1093/jb/mvq096

de la Mata M., Gaidatzis D., Vitanescu M., Stadler M.B., Wentzel C., Scheiffele P., Filipowicz W., Großhans H., "Potent degradation of neuronal miRNAs induced by highly complementary targets." (2015); *EMBO Rep. 16:500–511*. DOI: 10.15252/embr.201540078

Denkert C., Liedtke C., Tutt A., von Minckwitz G., "Molecular alterations in triple-negative breast cancer–the road to new treatment strategies." (2017); *Lancet. 389:2430–2442*. DOI: 10.1016/S0140-6736(16)32454-0

Denli A.M., Tops B.B.J., Plasterk R.H.A., Ketting R.F., Hannon G.J., "Processing of primary microRNAs by the Microprocessor complex." (2004); *Nature. 432:231–235.* DOI: 10.1038/nature03049

Dent R., Trudeau M., Pritchard K.I., Hanna W.M., Kahn H.K., Sawka C.A., Lickley L.A., Rawlinson E., Sun P., Narod S.A., "Triple-negative breast cancer: clinical features and patterns of recurrence." (2007); *Clin Cancer Res. 13(15 Pt 1):4429-4434*. DOI: 10.1158/1078-0432.CCR-06-3045

Denzler R., Agarwal V., Stefano J., Bartel D.P., Stoffel M., "Assessing the ceRNA hypothesis with quantitative measurements of miRNA and target abundance." (2014); *Mol Cell. 54:766-776*. DOI: 10.1016/j.molcel.2014.03.045

Dueck A., Ziegler C., Eichner A., Berezikov E., Meister G., "microRNAs associated with the different human Argonaute proteins." (2012); *Nucleic Acids Res. 40:9850-9862*. DOI: 10.1093/nar/gks705

Ebert M.S. and Sharp P.A., "Emerging roles for natural microRNA sponges." (2010); *Curr Biol. 20(19):R858-861*. DOI: 10.1016/j.cub.2010.08.052.

Ebert M.S., Neilson J.R., Sharp P.A., "MicroRNA sponges: Competitive inhibitors of small RNAs in mammalian cells." (2007); *Nat Methods. 4:721–726*. DOI: 10.1038/nmeth1079

Elkayam E., Kuhn C.D., Tocilj A., Haase A.D., Greene E.M., Hannon G.J., Joshua-Tor L., "The structure of human argonaute-2 in complex with miR-20a." (2012); *Cell. 150:100-110*. DOI: 10.1016/j.cell.2012.05.017

Esquela-Kerscher A. and Slack F.J., "Oncomirs—microRNAs with a role in cancer." (2006); *Nat Rev Cancer., 6(4):259–269*. DOI: 10.1038/nrc1840

Eulalio A., Huntzinger E., Izaurralde E., "Getting to the root of miRNA-mediated gene silencing." (2008); *Cell. 132:9-14*. DOI: 10.1016/j.cell.2007.12.024

Faehnle C.R., Elkayam E., Haase A.D., Hannon G.J., Joshua-Tor L., "The making of a slicer: activation of human Argonaute-1." (2013); *Cell Rep. 3:1901–1909*. DOI: 10.1016/j.celrep.2013.05.033

Fiedler J. and Thum T., "New Insights Into miR-17-92 Cluster Regulation and Angiogenesis." (2016); *Circ Res. 118(1):9-11.* DOI: 10.1161/CIRCRESAHA.115.307935.

Frank F., Sonenberg N., Nagar B., "Structural basis for 5'-nucleotide base-specific recognition of guide RNA by human AGO2." (2010); *Nature. 465:818–822*. DOI: 10.1038/nature09039

Fridrichova I. and Zmetakova I., "MicroRNAs Contribute to Breast Cancer Invasiveness." (2019); *Cells. 8(11):1361*. DOI: 10.3390/cells8111361.

Fuchs Wightman F., Giono L.E., Fededa J.P., de la Mata M. “Target RNAs Strike Back on MicroRNAs.” (2018); *Front Genet. 9:435*. DOI: 10.3389/fgene.2018.00435.

Galardi S., Mercatelli N., Giorda E., Massalini S., Frajese G.V., Ciafrè S.A., Farace M.G., “miR-221 and miR-222 expression affects the proliferation potential of human prostate carcinoma cell lines by targeting p27Kip1.” (2007); *J Biol Chem. 282:23716–23724*. DOI: 10.1074/jbc.M701805200

Gallouzi I.E. and Wilusz J. “A DIStinctively novel exoribonuclease that really likes.” (2013); *U EMBO J. 32:1799–1801*. DOI: 10.1038/emboj.2013.136

Gantier M.P., McCoy C.E., Rusinova I., Saulep D., Wang D., Xu D., Irving A.T., Behlke M.A., Hertzog P.J., Mackay F., Williams B.R.G., “Analysis of microRNA turnover in mammalian cells following Dicer1 ablation.” (2011); *Nucleic Acids Res. 39:5692–5703*. DOI: 10.1093/nar/gkr148

Gentner B., Schira G., Giustacchini A., Amendola M., Brown B.D., Ponzoni M., Naldini L., “Stable knockdown of microRNA in vivo by lentiviral vectors.” (2009); *Nat Methods. 6:63–66*. DOI: 10.4161/cc.6.16.4526

Ghini F., Rubolino C., Climent M., Simeone I., Marzi M.J., Nicassio F., “Endogenous transcripts control miRNA levels and activity in mammalian cells by target-directed miRNA degradation.” (2018); *Nat Commun. 9:3119*. DOI: 10.1038/s41467-018-05182-9

Gillies J.K. and Lorimer I.A., “Regulation of p27Kip1 by miRNA 221/222 in glioblastoma.” (2007); *Cell Cycle. 6:2005–2009*. DOI: 10.4161/cc.6.16.4526

Gilot D., Migault M., Bachelot L., Journé F., Rogiers A., Donnou-Fournet E., Mogha A., Mouchet N., Pinel-Marie M.L., Mari B., Montier T., Corre S., Gautron A, Rambow F., El Hajj P., Ben Jouira R., Tartare-Deckert S., Marine J.C., Felden B., Ghanem G., Galibert M.D., “A non-coding function of TYRP1 mRNA promotes melanoma growth.” (2017); *Nat Cell Biol. 19(11):1348-1357*. DOI: 10.1038/ncb3623

Golden R.J., Chen B., Li T., Braun J., Manjunath H., Chen X., Wu J., Schmid V., Chang T.C., Kopp F., Ramirez-Martinez A., Tagliabracci V.S., Chen Z.J., Xie Y., Mendell J.T., “An Argonaute phosphorylation cycle promotes microRNA- mediated silencing.” (2017); *Nature. 542:197–202*. DOI: 10.1038/nature21025

Goodall G.J. and Wickramasinghe V.O., “RNA in cancer.” (2021); *Nat Rev Cancer. 21(1):22-36.* DOI: 10.1038/s41568-020-00306-0

Grimson A., Farh K.K.-H., Johnston W.K., Garrett-Engele P., Lim L.P., Bartel D.P., “MicroRNA targeting specificity in mammals: determinants beyond seed pairing.” (2007); *Mol Cell. 27:91–105*. DOI: 10.1016/j.molcel.2007.06.017

Grishok A., Pasquinelli A.E., Conte D., Li N., Parrish S., Ha I., Baillie D.L., Fire A., Ruvkun G., Mello C.C., "Genes and mechanisms related to RNA interference regulate expression of the small temporal RNAs that control C. elegans developmental timing." (2001); *Cell 106:23–34*. DOI: 10.1016/s0092-8674(01)00431-7

Guo Y., Liu J., Elfenbein S.J., Ma Y., Zhong M., Qiu C., Ding Y., Lu J., "Characterization of the mammalian miRNA turnover landscape." (2015); *Nucleic Acids Res 43:2326-2341*. DOI: 10.1093/nar/gkv057

Guo Y.E. and Steitz J.A., "Virus Meets Host MicroRNA: the Destroyer, the Booster, the Hijacker." (2014); *Mol Cell Biol. 34:3780–3787*. DOI: 10.1128/MCB.00871-14

Ha M. and Kim V.N. "Regulation of microRNA biogenesis. " (2014); *Nat Rev Mol Cell Biol. 15:509-524*. DOI: 10.1038/nrm3838

Haas G., Cetin S., Messmer M., Chane-Woon-Ming B., Terenzi O., Chicher J., Kuhn L., Hammann P., Pfeffer S., "Identification of factors involved in target RNA-directed microRNA degradation."(2016); *Nucleic Acids Res. 44:2873–2887*. DOI: 10.1093/nar/gkw040

Hackanson B., Bennett K.L., Brena R.M., Jiang J., Claus R., Chen S.-S., Blagitko-Dorfs N., Maharry K., Whitman S.P., Schmittgen T.D., Lübbert M., Marcucci G., Bloomfield C.D., Plass C. "Epigenetic modification of CCAAT/enhancer binding protein α expression in acute myeloid leukemia." (2008); *Cancer Research. 68(9):3142–3151*. DOI: 10.1158/0008-5472.CAN-08-0483

Hammond S.M., Boettcher S, Caudy A.A., Kobayashi R., Hannon G.J., "Argonaute2, a Link Between Genetic and Biochemical Analyses of RNAi." (2001); *Science. 293:1146–1150*. DOI: 10.1126/science.1064023

Han J., LaVigne C.A., Jones B.T., Zhang H., Gillett F., Mendell J.T., "A ubiquitin ligase mediates target-directed microRNA decay independently of tailing and trimming." (2020); *Science. 370(6523):eabc9546*. DOI: 10.1126/science.abc9546

Hansen T.B., Jensen T.I., Clausen B.H., Bramsen J.B., Finsen B., Damgaard C.K., Kjems J., "Natural RNA circles function as efficient microRNA sponges." (2013); *Nature. 495:384–388*. DOI: 10.1038/nature11993

Hansen T.B., Wiklund E.D., Bramsen J.B., Villadsen S.B., Statham A.L., Clark S.J., Kjems J., "miRNA-dependent gene silencing involving Ago2-mediated cleavage of a circular antisense RNA." (2011); *EMBO J. 30:4414–4422*. DOI: 10.1038/emboj.2011.359

Hauptmann J., Dueck A., Harlander S., Pfaff J., Merkl R., Meister G., "Turning catalytically inactive human Argonaute proteins into active slicer enzymes." (2013); *Nat Struct Mol Biol. 20(7):814-817.* DOI: 10.1038/nsmb.2577

Helwak A., Kudla G., Dudnakova T., Tollervey D., “Mapping the human miRNA interactome by CLASH reveals frequent noncanonical binding.” (2013); *Cell. 153:654-665*. DOI: 10.1016/j.cell.2013.03.043

Henry J.C., Azevedo-Pouly A.C.P., Schmittgen T.D. “MicroRNA replacement therapy for cancer.” (2011); *Pharm Res. 28(12):3030–3042*. DOI: 10.1007/s11095-011-0548-9

Hosseinahli N., Aghapour M., Duijf P.H.G., Baradaran B., “Treating cancer with microRNA replacement therapy: A literature review.” (2018); *J Cell Physiol. 233(8):5574-5588*. DOI: 10.1002/jcp.26514. Epub 2018 Mar 9.

Hu Z., Liang J., Wang Z., Tian T., Zhou X., Chen J., Miao R., Wang Y., Wang X., Shen H., “Common genetic variants in pre-microRNAs were associated with increased risk of breast cancer in Chinese women.” (2009); *Hum Mutat. 30:79–84*, DOI: 10.1002/humu.20837.

Hua Z. and Vierstra R.D., “The cullin-RING ubiquitin-protein ligases.” (2011); *Annu Rev Plant Biol. 62:299–334*. DOI: 10.1146/annurev-arplant-042809-112256

Huang, X., Ding L., Bennewith K.L., Tong R.T., Welford S.M., Ang K.K., Story M., Le Q.T., Giaccia A.J., “Hypoxia- inducible mir-210 regulates normoxic gene expression involved in tumor initiation.” (2009); *Mol Cell. 35:856–867*. DOI: 10.1016/j.molcel.2009.09.006

Hutvàgner G. and Zamore P.D. “A microRNA in a multiple-turnover RNAi enzyme complex.” (2002); *Science. 297:2056–2060*. DOI: 10.1126/science.1073827

Hwang H.-W., Wentzel E.A., Mendell J.T., “A Hexanucleotide Element Directs MicroRNA Nuclear Import.” (2007); *Science. 315:97–100*. https://doi.org/10.1126/science.1136235

Iwasaki S., Kobayashi M., Yoda M., Sakaguchi Y., Katsuma S., Suzuki T., Tomari Y., “Hsc70/Hsp90 chaperone machinery mediates ATP-dependent RISC loading of small RNA duplexes.” (2010); *Mol Cell. 39:292-299*. DOI: 10.1016/j.molcel.2010.05.015

Iyer V.R., Eisen M.B., Ross D.T., Schuler G., Moore T., Lee J.C., Trent J.M., Staudt L.M., Hudson J. Jr, Boguski M.S., Lashkari D., Shalon D., Botstein D., Brown P.O., “The transcriptional program in the response of human fibroblasts to serum.” (1999); *Science. 283(5398):83-87*. DOI: 10.1126/science.283.5398.83.

Jamshidi M., Fagerholm R., Muranen T.A., Kaur S., Potdar S., Khan S., Netti E., Mpindi J.P., Yadav B., Kiiski J.I., Aittomäki K., Heikkilä P., Saarela J., Bützow R., Blomqvist C., Nevanlinna H. “High miR-30 Expression Associates with Improved Breast Cancer Patient Survival and Treatment Outcome.” (2021); *Cancers (Basel). 13(12):2907*. DOI: 10.3390/cancers13122907.

Jiang L. and Hermeking H., “miR-34a and miR-34b/c suppress intestinal tumorigenesis.” (2017); *Cancer Res. 77:2746–2758*. DOI: 10.1158/0008-5472.CAN-16-2183

Jiang S., Miao D., Wang M., Lv J., Wang Y., Tong J., “MiR-30-5p suppresses cell chemoresistance and stemness in colorectal cancer through USP22/Wnt/beta-catenin signaling axis.” . (2019); *J Cell Mol Med. 23(1):630-640.* DOI: 10.1111/jcmm.13968

Jonas S. and Izaurralde E. “Towards a molecular understanding of microRNA-mediated gene silencing.” (2015); *Nat Rev Genet. 16:421–433*. DOI: 10.1038/nrg3965

Jones-Rhoades M.W., Bartel D.P., Bartel B. “MicroRNAs and their regulatory roles in plants.” (2006); *Annu Rev Plant Biol. 57:19–53*. DOI: 10.1146/annurev.arplant.57.032905.105218

Kalinowski F.C., Brown R.A., Ganda C., Giles K.M., Epis M.R., Horsham J., Leedman P.J., “microRNA-7: a tumor suppressor miRNA with therapeutic potential.” (2014). *Int J Biochem Cell Biol. 54:312–317*. DOI: 10.1016/j.biocel.2014.05.040

Kamenska A., Lu W.T., Kubacka D., Broomhead H., Minshall N., Bushell M., Standart N. “Human 4E-T represses translation of bound mRNAs and enhances microRNA-mediated silencing.” (2014); *Nucleic Acids Res. 42:3298–3313*. DOI: 10.1093/nar/gkt1265

Kamenska A., Simpson C., Vindry C., Broomhead H., Bénard M., Ernoult- Lange M., Lee B.P., Harries L.W., Weil D., Standart N., “The DDX6-4E-T interaction mediates translational repression and P-body assembly.” (2016); *Nucleic Acids Res. 44:6318–6334*. DOI: 10.1093/nar/gkw565

Kandettu A., Radhakrishnan R., Chakrabarty S., Sriharikrishnaa S., Kabekkodu S.P., “The emerging role of miRNA clusters in breast cancer progression.” (2020); *Biochim Biophys Acta Rev Cancer. 1874(2):188413*. DOI: 10.1016/j.bbcan.2020.188413

Katoh T., Sakaguchi Y., Miyauchi K., Suzuki T., Kashiwabara S., Baba T. “Selective stabilization of mammalian microRNAs by 30 adenylation mediated by the cytoplasmic poly(A) polymerase GLD-2.” (2009); *Genes Dev. 23:433–438*. DOI: 10.1101/gad.1761509

Khvorova A., Reynolds A., Jayasena S.D., “Functional siRNAs and miRNAs exhibit strand bias.” (2003); *Cell. 115:209–216*. DOI: 10.1016/s0092-8674(03)00801-8

Kim V.N., Han J., Siomi M.C., “Biogenesis of small RNAs in animals.” (2009); *Nat Rev Mol Cell Biol. 10:126-139*. DOI: 10.1093/nar/gkw565

Kingston E.R. and Bartel D.P., “Global analyses of the dynamics of mammalian microRNA metabolism.” (2019); *Genome Res. 29:1777–1790*. DOI: 10.1101/gr.251421.119

Kleaveland B., Shi C.Y., Stefano J., Bartel D.P.,. "A Network of Noncoding Regulatory RNAs Acts in the Mammalian Brain." (2018); *Cell. 174:350-362.e17*. DOI: 10.1016/j.cell.2018.05.022

Kong Y.W., Ferland-McCollough D., Jackson T.J., Bushell M. "MicroRNAs in cancer management." (2012); *Lancet Oncol. 13(6):e249–e258*. DOI: 10.1016/S1470-2045(12)70073-6

Krol J., Loedige I., Filipowicz W., "The widespread regulation of microRNA biogenesis, function and decay." (2010); *Nat Rev Genet. 11:597-610*. DOI: 10.1038/nrg2843

Krüger J. and Rehmsmeier M., "RNAhybrid: microRNA target prediction easy, fast and flexible." (2006); *Nucleic Acids Res. 34:W451-454*. DOI: 10.1093/nar/gkl243

Kuchenbaecker K.B., Hopper J.L., Barnes D.R., et al. "Risks of breast, ovarian and contralateral breast cancer for BRCA1 and BRCA2 mutation carriers." (2017); *JAMA. 317: 2402–16*. DOI: 10.1001/jama.2017.7112

Lagos-Quintana M., Rauhut R., Lendeckel W., Tuschl T. "Identification of novel genes coding for small expressed RNAs." (2001); *Science. 294:853–858*. DOI: 10.1126/science.1064921

Lang P.L.M., Christie M.D., Dogan E.S., Schwab R., Hagmann J., van de Weyer A.L., Scacchi E., Weigel D., "A Role for the F-Box Protein HAWAIIAN SKIRT in Plant microRNA Function." (2018); *Plant Physiol. 176(1):730-741*. DOI: 10.1104/pp.17.01313.

Lau N.C., Lim L.P., Weinstein E.G., Bartel D.P. "An abundant class of tiny RNAs with probable regulatory roles in Caenorhabditis elegans." (2001); *Science. 294:858–862*. DOI: 10.1126/science.1065062

Lee R.C., and Ambros V., "An extensive class of small RNAs in Caenorhabditis elegans." (2001); *Science. 294:862–864*. DOI: 10.1126/science.1065329

Lee R.C., Feinbaum R.L. and Ambros, V. "The *C. elegans* heterochronic gene lin-4 encodes small RNAs with antisense complementarity to lin-14." (1993); *Cell. 75:843–854*. DOI: 10.1016/0092-8674(93)90529-y

Lee S., Song J., Kim S., Kim J., Hong Y., Kim Y., Kim D., Baek D., Ahn K., "Selective degradation of host MicroRNAs by an intergenic HCMV noncoding RNA accelerates virus production." (2013); *Cell Host Microbe. 13:678–690.* DOI: 10.1016/j.chom.2013.05.007

Lee Y., Ahn C., Han J., Choi H., Kim J., Yim J., Lee J., Provost P., Rådmark O., Kim S., Kim V.N., "The nuclear RNase III Drosha initiates microRNA processing." (2003); *Nature. 425:415–419*. DOI: 10.1038/nature01957

Lee Y., Jeon K., Lee J.T., Kim S., Kim V.N. “MicroRNA maturation: stepwise processing and subcellular localization.” (2002); *EMBO J. 21:4663–4670*. DOI: 10.1093/emboj/cdf476

Lee Y., Kim M., Han J., Yeom K.H., Lee S., Baek S.H., Kim V.N., “MicroRNA genes are transcribed by RNA polymerase II.” (2004); *EMBO J. 23:4051–4060*. DOI: 10.1038/sj.emboj.7600385

Lee Y.S. and Dutta A., “MicroRNAs in cancer.” (2009); *Annu Rev Pathol. 4:199-227*. DOI: 10.1146/annurev.pathol.4.110807.092222.

Levati L., Pagani E., Romani S., Castiglia D., Piccinni E., Covaciu C., Caporaso P., Bondanza S., Antonetti F.R., Bonmassar E., Martelli F., Alvino E., D'Atri S., “MicroRNA-155 targets the SKI gene in human melanoma cell lines.” (2011); *Pigment Cell Melanoma Res. 24:538–550*. DOI: 10.1111/j.1755-148X.2011.00857.x

Li C.L., Nie H., Wang M., Su L.P., Li J.F., Yu Y.Y., Yan M., Qu Q.L, Zhu Z.G., Liu B.Y., “microRNA-155 is downregulated in gastric cancer cells and involved in cell metastasis.” (2012); *Oncol Rep. 27:1960–1966*. DOI: 10.3892/or.2012.1719

Li G.C., Cao X.Y., Li Y.N., Qiu Y.Y., Li Y.N., Liu X.J., Sun, X.X., “MicroRNA-374b inhibits cervical cancer cell proliferation and induces apoptosis through the p38/ERK signaling pathway by binding to JAM-2.” (2018); *J Cell Physiol. 233(9):7379–7390*. DOI: 10.1002/jcp.26574

Li P., Sheng C., Huang L., Zhang H., Huang L., Cheng Z., Zhu Q., “MiR-183/-96/-182 cluster is up-regulated in most breast cancers and increases cell proliferation and migration.” (2014); *Breast Cancer Res. 16:473*. DOI: 10.1186/s13058-014-0473-z

Li Y. and Kowdley K.V., “MicroRNAs in common human diseases.” (2012); *Genomics Proteomics Bioinformatics. 10: 246-253.* DOI: 10.1016/j.gpb.2012.07.005

Libri V., Helwak A., Miesen P., Santhakumar D., Borger J.G., Kudla G., Grey F., Tollervey D., Buck A.H., “Murine cytomegalovirus encodes a miR-27 inhibitor disguised as a target.” (2012); *Proc Natl Acad Sci USA. 109:279–284.* DOI: 10.1073/pnas.1114204109

Lim J., Ha M., Chang H., Kwon S.C., Simanshu D.K., Patel D.J., Kim V.N., “Uridylation by TUT4 and TUT7 marks mRNA for degradation.” (2014); *Cell. 159:1365–1376*. DOI: 10.1016/j.cell.2014.10.055

Lim Y.Y., Wright J.A., Attema J.L., Gregory P.A., Bert A.G., Smith E., Thomas D., Lopez A.F., Drew P.A., Khew-Goodall Y., Goodall G.J., “Epigenetic modulation of the miR-200 family is associated with transition to a breast cancer stem- cell-like state.” (2013): *J Cell Sci. 126:2256–2266*. DOI: 10.1242/jcs.122275

Loibl S., Poortmans P., Morrow M., Denkert C., Curigliano G., “Breast cancer.” (2021); *Lancet. 397(10286):1750-1769*. DOI: 10.1016/S0140-6736(20)32381-3.

Long X.B., Sun G.-B., Hu S., Liang G.-T., Wang N., Zhang X.-H., Liu Z., “Let-7a microRNA functions as a potential tumor suppressor in human laryngeal cancer.” (2009); *Oncol Rep. 22(5):1189–1195*. DOI: 10.3892/or_00000554

Lujambio A. and Lowe S.W., “The microcosmos of cancer.” (2012); *Nature. 482(7385):347-355*. DOI: 10.1038/nature10888

Lund E., Guttinger S., Calado A., Dahlberg J.E., Kutay U. “Nuclear export of microRNA precursors.” (2004); *Science. 303:95–98*. DOI: 10.1126/science.1090599

Ma L., Teruya-Feldstein J., Weinberg R.A., “Tumor invasion and metastasis initiated by microRNA-10b in breast cancer.” (2007); *Nature. 449:682–688*. DOI: 10.1038/nature06174

Mahrour N., Redwine W.B., Florens L., Swanson S.K., Martin-Brown S., Bradford W.D., Staehling-Hampton K., Washburn M.P., Conaway R.C., Conaway J.W., “Characterization of Cullin-box sequences that direct recruitment of Cul2-Rbx1 and Cul5-Rbx2 modules to Elongin BC-based ubiquitin ligases.” (2008); *J Biol Chem. 283:8005–8013*. DOI: 10.1074/jbc.M706987200.

Mansur F., Ivshina M., Gu W., Schaevitz L., Stackpole E., Gujja S., Edwards Y.J., Richter J.D., “Gld2-catalyzed 3' monoadenylation of miRNAs in the hippocampus has no detectable effect on their stability or on animal behavior.” (2016); *RNA. 22(10):1492-1499. DOI: 10.1261/rna.056937.116*

Marcinowski L., Tanguy M., Krmpotic A., Radle B., Lisnic V.J., Tuddenham L., Chane-Woon-Ming B., Ruzsics Z., Erhard F., Benkartek C., Babic M., Zimmer R., Trgovcich J., Koszinowski U.H., Jonjic S., Pfeffer S., Dölken L., “Degradation of cellular mir-27 by a novel, highly abundant viral transcript is important for efficient virus replication in vivo.” (2012); *PLoS Path. 8:e1002510*. DOI: 10.1371/journal.ppat.1002510

Martin G. and Keller W., “RNA-specific ribonucleotidyl transferases.” (2007); *RNA 13:1834–1849*. DOI: 10.1261/rna.652807

Marzi M.J., Ghini F., Cerruti B., de Pretis S., Bonetti P., Giacomelli C., Gorski M.M., Kress T., Pelizzola M., Muller H., Amati B., Nicassio F., “Degradation dynamics of microRNAs revealed by a novel pulse-chase approach.” (2016); *Genome Res. 26:554–565*. DOI: 10.1101/gr.198788.115

McCann J.V., Xiao L., Kim D.J., Khan O.F., Kowalski P.S., Anderson D.G., Pecot C.V., Azam S.H., Parker J.S., Tsai Y.S., Wolberg A.S., Turner S.D., Tatsumi K., Mackman N., Dudley A.C., “Endothelial miR-30c suppresses tumor growth via inhibition of TGF-

β-induced Serpine1." (2019); *J Clin Invest. 129(4):1654-1670*. DOI: 10.1172/JCI123106

McCaskill J., Praihirunkit P., Sharp P.M., Buck A.H., "RNA-mediated degradation of microRNAs: a widespread viral strategy?" (2015); *RNA Biol. 12:579–585*. DOI: 10.1080/15476286.2015.1034912

Mei J., Jiang N., Ren G., "The F-box protein HAWAIIAN SKIRT is required for mimicry target-induced microRNA degradation in Arabidopsis." (2019); *J Integr Plant Biol. 61(11):1121-1127*. DOI: 10.1111/jipb.12761

Mekuria A.N., Abdi A.D., Mishore K.M., "MicroRNAs as a Potential Target for Cancer Therapy." (2018); *J Cancer Sci Ther. 10:152-161*. DOI: 10.4172/1948-5956.1000535

Melo S.A., Moutinho C., Ropero S., Calin G.A., Rossi S., Spizzo R., Fernandez A.F., Davalos V., Villanueva A., Montoya G., Yamamoto H., Schwartz S. Jr, Esteller M., "A genetic defect in exportin-5 traps precursor microRNAs in the nucleus of cancer cells." (2010); *Cancer Cell. 18:303–315*. DOI: 10.1016/j.ccr.2010.09.007

Meng F., Henson R., Wehbe-Janek H., Ghoshal K., Jacob S.T., Patel T., "MicroRNA-21 regulates expression of the PTEN tumor suppressor gene in human hepatocellular cancer." (2007); *Gastroenterology. 133:647–658*. DOI: 10.1053/j.gastro.2007.05.022

Mermel C.H., Schumacher S.E., Hill B., Meyerson M.L., Beroukhim R., Getz G., "GISTIC2.0 facilitates sensitive and confident localization of the targets of focal somatic copy-number alteration in human cancers." (2011); *Genome Biol. 12:R41*. DOI: 10.1186/gb-2011-12-4-r41

Mogilyansky E. and Rigoutsos I., "The miR-17/92 cluster: a comprehensive update on its genomics, genetics, functions and increasingly important and numerous roles in health and disease." (2013); *Cell Death Differ. 20(12): p.1603-14*. DOI: 10.1038/cdd.2013.125

Moi L., Braaten T., Al-Shibli K., Lund E., Busund L.T.R., "Differential expression of the miR-17-92 cluster and miR-17 family in breast cancer according to tumor type; Results from the Norwegian Women and Cancer (NOWAC) study." (2019); *J Transl Med. 17:1–20*. DOI: 10.1186/s12967-019-2086-x

Moore M.J., Scheel T.K., Luna J.M., Park C.Y., Fak J.J., Nishiuchi E., Rice C.M., Darnell R.B. "miRNA-target chimeras reveal miRNA 3'-end pairing as a major determinant of Argonaute target specificity." (2015); *Nat Commun. 6:8864*. DOI: 10.1038/ncomms9864

Morales S., De Mayo T., Gulppi F.A., Gonzalez-Hormazabal P., Carrasco V., Reyes J.M., Gómez F., Waugh E., Jara L., "Genetic variants in pre-miR-146a, premiR-499, pre-miR-125a, pre-miR-605, and pri-miR-182 are associated with breast cancer susceptibility in

a south American population." (2018); *Genes (Basel). 9:1–18*. DOI: 10.3390/genes9090427

Mott J.L., Kobayashi S., Bronk S.F., Gores G.J., "mir-29 regulates Mcl-1 protein expression and apoptosis." (2007); *Oncogene. 26:6133–1340*. DOI: 10.1038/sj.onc.1210436

Mourelatos Z., Dostie J., Paushkin S., Sharma A., Charroux B., Abel L., Rappsilber J., Mann M., Dreyfuss G., "miRNPs: a novel class of ribonucleoproteins containing numerous microRNAs." (2002); *Genes Dev. 16:720–728*. DOI: 10.1101/gad.974702

Muller H., Marzi M.J., Nicassio F., "IsomiRage: From Functional Classification to Differential Expression of miRNA Isoforms." (2014); *Front Bioeng Biotechnol. 2:38*. DOI: 10.3389/fbioe.2014.00038

Nakanishi K., Ascano M., Gogakos T., Ishibe-Murakami S., Serganov A.A., Briskin D., Morozov P., Tuschl T., Patel D.J., "Eukaryote-specific insertion elements control human ARGONAUTE slicer activity." (2013); *Cell Rep. 3:1893–1900*. DOI: 10.1016/j.celrep.2013.06.010

Nedaeinia R., Sharifi M., Avan A., Kazemi M., Rafiee L., Ghayour-Mobarhan M., Salehi R., "Locked nucleic acid anti-miR-21 inhibits cell growth and invasive behaviors of a colorectal adenocarcinoma cell line: LNA-anti-miR as a novel approach." (2016); *Cancer Gene Ther. 23(8):246-53*. DOI: 10.1038/cgt.2016.25.

Nguyen D.D. and Chang S., "Development of novel therapeutic agents by inhibition of oncogenic microRNAs." (2017); *Int J Mol Sci. 19(1):E65*. DOI: 10.3390/ijms19010065

Nguyen T.A., Jo M.H., Choi Y.G., Park J., Kwon S.C., Hohng S., Kim V.N., Woo J.S., "Functional Anatomy of the Human Microprocessor." (2015); *Cell. 161(6):1374-1387. DOI: 10.1016/j.cell.2015.05.010*

Nishimura T., Padamsi Z., Fakim H., Milette S., Dunham W.H., Gingras A.C., Fabian M.R., "The eIF4E-binding protein 4E-T is a component of the mRNA decay machinery that bridges the 50 and 30 termini of target mRNAs." (2015); *Cell Rep. 11:1425–1436*. DOI: 10.1016/j.celrep.2015.04.065

Nur U., El Reda D., Hashim D., Weiderpass E., "A prospective investigation of oral contraceptive use and breast cancer mortality: findings from the Swedish women's lifestyle and health cohort." (2019); *BMC Cancer. 19:807*. DOI: 10.1186/s12885-019-5985-6

O'Brien J., Hayder H., Zayed Y., Peng C., "Overview of MicroRNA Biogenesis, Mechanisms of Actions, and Circulation." (2018); *Front Endocrinol. 9:402*. DOI: 10.3389/fendo.2018.00402

Okada N., Lin C.P., Ribeiro M.C., Biton A., Lai G., He X., Bu P., Vogel H., Jablons D.M., Keller A.C., Wilkinson J.E., He B., Speed T.P., He L., "A positive feedback between

p53 and miR-34 miRNAs mediates tumor suppression." (2014); *Genes Dev. 28:438–450*. DOI: 10.1101/gad.233585.113

Okamura K., Hagen J.W., Duan H., Tyler D.M., Lai E.C., "The mirtron pathway generates microRNA-class regulatory RNAs in Drosophila." *Cell. 130:89–100.* DOI: 10.1016/j.cell.2007.06.028

Ozgur S., Basquin J., Kamenska A., Filipowicz W., Standart N., Conti E. "Structure of a human 4E-T/DDX6/CNOT1 complex reveals the different interplay of DDX6-binding proteins with the CCR4-NOT complex." (2015); *Cell Rep. 13:703–711*. DOI: 10.1016/j.celrep.2015.09.033

Palma C.A., Al Sheikha D., Lim T.K., Bryant A., Vu T.T., Jayaswal V., Ma D.D., "MicroRNA-155 as an inducer of apoptosis and cell differentiation in Acute Myeloid Leukaemia." (2014); *Molecular cancer. 13:79*. DOI: 10.1186/1476-4598-13-79

Panebianco F., Climent M., Malvindi M.A., Pompa P.P., Bonetti P., Nicassio F., "Delivery of biologically active miR-34a in normal and cancer mammary epithelial cells by synthetic nanoparticles." (2019); *Nanomedicine. 19:95-105*. DOI: 10.1016/j.nano.2019.03.013

Park J.H., Shin S.Y., Shin C., "Non-canonical targets destabilize microRNAs in human Argonautes." (2017); *Nucleic Acids Res. 45:1569–1583*. DOI: 10.1093/nar/gkx029

Park S.Y., Lee J.H., Ha M., Nam J.W., Kim V.N., "miR-29 miRNAs activate p53 by targeting p85 alpha and CDC42." (2009); *Nat Struct Mol Biol. 16(1):23-9*. DOI: 10.1038/nsmb.1533.

Pasquinelli A.E., Reinhart B.J., Slack F., Martindale M.Q., Kuroda M.I., Maller B., Hayward D.C., Ball E.E., Degnan B., Müller P., Spring J., Srinivasan A., Fishman M., Finnerty J., Corbo J., Levine M., Leahy P., Davidson E., Ruvkun G., "Conservation of the sequence and temporal expression of let-7 heterochronic regulatory RNA." (2000); *Nature. 408:86–89*. DOI: 10.1038/35040556

Passon N., Gerometta A., Puppin C., Lavarone E., Puglisi F., Tell G., Di Loreto C., Damante G., "Expression of Dicer and Drosha in triple-negative breast cancer." (2012); *J. Clin. Pathol. 65:320–326.* DOI: 10.1136/jclinpath-2011-200496

Pawlica P., Moss W.N., Steitz J.A., "Host miRNA degradation by Herpesvirus saimiri small nuclear RNA requires an unstructured interacting region." (2016); *RNA. 22:1181-1189*. DOI: 10.1261/rna.054817.115

Petrovic N. and Ergun S., "MiRNAs as potential treatment targets and treatment options in cancer." (2018); *Mol Diagn Ther. 22(2):157–168*. DOI: 10.1007/s40291-017-0314-8

Piwecka M., Rolle K., Belter A., Barciszewska A.M., Żywicki M., Michalak M., Nowak S., Naskręt-Barciszewska M.Z., Barciszewski J., "Comprehensive analysis of microRNA

expression profile in malignant glioma tissues." (2015); *Mol Oncol. 9:1324–1340*. DOI: 10.1016/j.molonc.2015.03.007

Qin W., Ren Q., Liu T., Huang Y., Wang J., "MicroRNA-155 is a novel suppressor of ovarian cancer-initiating cells that targets CLDN1." (2013); *FEBS letters. 587:1434–1439*. DOI: 10.1016/j.febslet.2013.03.023

Qiu S., Lin S., Hu D., Feng Y., Tan Y., Peng Y., "Interactions of miR-323/miR-326/miR-329 and miR-130a/miR-155/miR-210 as prognostic indicators for clinical outcome of glioblastoma patients." (2013); *J Transl Med. 11:1479–5876*. DOI: 10.1186/1479-5876-11-10

Qiu T., Zhou X., Wang J., Du Y., Xu J., Huang Z., Liu P., "miR-145, miR-133a and miR-133b inhibit proliferation, migration, invasion and cell cycle progression via targeting transcription factor Sp1 in gastric cancer." (2014); *FEBS Letters. 588(7):1168–1177*. DOI: 10.1016/j.febslet.2014.02.054

Qu Y., Zhang H., Sun W., Han Y., Li S., Qu Y., Ying G., Ba Y., "MicroRNA-155 promotes gastric cancer growth and invasion by negatively regulating transforming growth factor-β receptor 2." (2018); *Cancer Sci. 109(3):618–628*. DOI: 10.1111/cas.13472

Rabani M., Levin J.Z., Fan L., Adiconis X., Raychowdhury R., Garber M., Gnirke A., Nusbaum C., Hacohen N., Friedman N., Amit I., Regev A., "Metabolic labeling of RNA uncovers principles of RNA production and degradation dynamics in mammalian cells." (2011); *Nat Biotechnol. 29(5):436-442*. DOI: 10.1038/nbt.1861

Ran F.A., Hsu P.D., Lin C.Y., Gootenberg J.S., Konermann S., Trevino A.E., Scott D.A., Inoue A., Matoba S., Zhang Y., Zhang F., "Double nicking by RNA-guided CRISPR Cas9 for enhanced genome editing specificity." (2013); *Cell. 154(6):1380-1389*. DOI: 10.1016/j.cell.2013.08.021

Reichholf B., Herzog V.A., Fasching N., Manzenreither R.A., Sowemimo I., Ameres S.L., "Time-Resolved Small RNA Sequencing Unravels the Molecular Principles of MicroRNA Homeostasis." (2019); *Mol Cell. 75:756–768.e757*. DOI: 10.1016/j.molcel.2019.06.018

Riaz M., van Jaarsveld M.T.M., Hollestelle A., Prager-van der Smissen W.J.C., Heine A.A.J., Boersma A.W.M., Liu J., Helmijr J., Ozturk B., Smid M., Wiemer E.A., Foekens J.A., Martens J.W.M., "MiRNA expression profiling of 51 human breast cancer cell lines reveals subtype and driver mutation-specific miRNAs." (2013); *Breast Cancer Res. 15(2):R33.* DOI: 10.1186/bcr3415

Rissland O.S. and Norbury C.J., "Decapping is preceded by 3' uridylation in a novel pathway of bulk mRNA turnover." (2009); *Nat Struct Mol Biol. 16:616–623*. DOI: 10.1038/nsmb.1601

Rissland O.S., Hong S.-J., Bartel D.P., “MicroRNA destabilization enables dynamic regulation of the miR-16 family in response to cell-cycle changes.” (2011); *Mol Cell. 43:993–1004*. DOI: 10.1016/j.molcel.2011.08.021

Ruby J.G., Jan C.H., Bartel D.P., “Intronic microRNA precursors that bypass Drosha processing.” (2007); *Nature. 448:83–86*. DOI: 10.1038/nature05983

Rüegger S. and Großhans H., “MicroRNA turnover: when, how, and why.” (2012); *Trends Biochem. Sci. 37:436–446.* DOI: 10.1016/j.tibs.2012.07.002

Rupaimoole R., Ivan C., Yang D., Gharpure K.M., Wu S.Y., Pecot C.V., Previs R.A., Nagaraja A.S., Armaiz-Pena G.N., McGuire M., Pradeep S., Mangala L.S., Rodriguez-Aguayo C., Huang L., Bar-Eli M., Zhang W., Lopez-Berestein G., Calin G.A., Sood A.K., “Hypoxia- upregulated microRNA-630 targets Dicer, leading to increased tumor progression.” (2016); *Oncogene. 35:4312–4320*. DOI: 10.1038/onc.2015.492

Rupaimoole R., Wu S.Y., Pradeep S., Ivan C., Pecot C.V., Gharpure K.M., Nagaraja A.S., Armaiz-Pena G.N., McGuire M., Zand B., Dalton H.J., Filant J., Miller J.B., Lu C., Sadaoui N.C., Mangala L.S., Taylor M., van den Beucken T., Koch E., Rodriguez-Aguayo C., Huang L., Bar-Eli M., Wouters B.G., Radovich M., Ivan M., Calin G.A., Zhang W., Lopez-Berestein G., Sood A.K., “Hypoxia- mediated downregulation of miRNA biogenesis promotes tumour progression.” (2014); *Nat Commun. 5:5202*. DOI: 10.1038/ncomms6202

Saito Y., Liang G., Egger G., Friedman J.M., Chuang J.C., Coetzee G.A., Jones P.A., “Specific activation of microRNA-127 with downregulation of the proto-oncogene BCL6 by chromatin-modifying drugs in human cancer cells.” (2006); *Cancer Cell. 9(6):435–443*. DOI: 10.1016/j.ccr.2006.04.020

Saliminejad K., Khorram Khorshid H.R., Soleymani Fard S., Ghaffari S.H., “An overview of microRNAs: Biology, functions, therapeutics, and analysis methods.” (2019); *J Cell Physiol. 234(5):5451-5465*. DOI: 10.1002/jcp.27486.

Salomon W.E., Jolly S.M., Moore M.J., Zamore P.D., Serebrov V., “Single-Molecule Imaging Reveals that Argonaute Reshapes the Binding Properties of Its Nucleic Acid Guides.” (2015); *Cell. 162:84–95*. DOI: 10.1016/j.cell.2015.06.029

Schirle N.T., Sheu-Gruttadauria J., MacRae I.J. “Structural basis for microRNA targeting.” (2014); *Science. 346:608–613*. DOI: 10.1126/science.1258040

Schreiner W.P., Pagliuso D.C., Garrigues J.M., Chen J.S., Aalto A.P., Pasquinelli A.E., “Remodeling of the Caenorhabditis elegans non-coding RNA transcriptome by heat shock.” (2019); *Nucleic Acids Res. 47:9829–9841*. DOI: 10.1093/nar/gkz693

Schwarz D.S., Hutvágner G., Du T., Xu Z., Aronin N., Zamore P.D., "Asymmetry in the Assembly of the RNAi Enzyme Complex." (2003); *Cell. 115:199–208*. DOI: 10.1016/s0092-8674(03)00759-1

Shah M.Y., Ferrajoli A., Sood A.K., Lopez-Berestein. G., Calin, G.A., "MicroRNA therapeutics in cancer – An emerging concept." (2016); *EBioMedicine. 12:34–42*. DOI: 10.1016/j.ebiom.2016.09.017

Shaham L., Binder V., Gefen N., Borkhardt A., Izraeli S., "MiR-125 in normal and malignant hematopoiesis." (2012); *Leukemia. 26:2011–2018*. DOI: 10.1038/leu.2012.90

Sharma G., Dua P., Agarwal S., "A comprehensive review of dysregulated miRNAs involved in cervical cancer." (2014); *Curr. Genom. 15:310–323*. DOI: 10.2174/1389202915666140528003249

Sheu-Gruttadauria J., Pawlica P., Klum S.M., Wang S., Yario T.A., Schirle Oakdale N.T., Steitz J.A., MacRae I.J. "Structural Basis for Target-Directed MicroRNA Degradation." (2019); *Mol Cell. 75:1243–1255.e7*. DOI: 10.1016/j.molcel.2019.06.019

Shi C.Y., Kingston E.R., Kleaveland B., Lin D.H., Stubna M.W., Bartel D.P., "The ZSWIM8 ubiquitin ligase mediates target-directed microRNA degradation." (2020); *Science. 370(6523):eabc9359.* DOI: 10.1126/science.abc9359

Shibue T. and Weinberg R.A., "EMT, CSCs, and drug resistance: the mechanistic link and clinical implications." (2017) *Nat Rev Clin Oncol. 14(10):611-629*. DOI: 10.1038/nrclinonc.2017.44.

Shimono Y., Zabala M., Cho R.W., Lobo N., Dalerba P., Qian D., Diehn M., Liu H., Panula S.P., Chiao E., Dirbas F.M., Somlo G., Pera R.A., Lao K., Clarke M.F., "Downregulation of miRNA-200c links breast cancer stem cells with normal stem cells." (2009); *Cell. 138:592–603*. DOI: 10.1016/j.cell.2009.07.011

Shin C., Nam J.W., Farh K.K., Chiang H.R., Shkumatava A., Bartel D.P., "Expanding the microRNA targeting code: functional sites with centered pairing." (2010); *Mol Cell. 38:789–802*. DOI: 10.1016/j.molcel.2010.06.005

Shukla S., Bjerke G.A., Muhlrad D., Yi R., Parker R., "The RNase PARN Controls the Levels of Specific miRNAs that Contribute to p53 Regulation." (2019); *Mol Cell. 73(6):1204-1216.e4*. DOI: 10.1016/j.molcel.2019.01.010.

Siegel R.L., Miller K.D., Jemal A., "Cancer statistics, 2020." (2020); *CA Cancer J Clin. 70: 7–30*. DOI: 10.3322/caac.21590

Simeone I., Rubolino C., Noviello T.M.R., Farinello D., Cerulo L., Marzi M.J., Nicassio F., "Prediction and pan-cancer analysis of mammalian transcripts involved in target

directed miRNA degradation." (2022); *Nucleic Acids Res. 50(4):2019-2035*. DOI: 10.1093/nar/gkac057.

Smith K.N., Starmer J., Miller S.C., Sethupathy P., Magnuson T., "Long Noncoding RNA Moderates MicroRNA Activity to Maintain Self-Renewal in Embryonic Stem Cells." (2017); *Stem Cell Reports. 9(1):108-121*. DOI: 10.1016/j.stemcr.2017.05.005.

Sobell H.M., "Actinomycin and DNA transcription." (1985); *Proc Natl Acad Sci USA. 82:5328-5331*. DOI: 10.1073/pnas.82.16.5328

Sossey-Alaoui K., Bialkowska K., Plow E.F., "The miR200 family of microRNAs regulates WAVE3-dependent cancer cell invasion." (2009); *J Biol Chem. 284:33019–33029*. DOI: 10.1074/jbc.M109.034553

Spadotto V., Giambruno R., Massignani E., Mihailovich M., Maniaci M., Patuzzo F., Ghini F., Nicassio F., Bonaldi T., "PRMT1-mediated methylation of the microprocessor-associated proteins regulates microRNA biogenesis." (2020); *Nucleic Acids Res. 48:96–115*. DOI: 10.1093/nar/gkz1051

Sullivan C.S., Grundhoff A.T., Tevethia S., Pipas J.M., Ganem D., "SV40-encoded microRNAs regulate viral gene expression and reduce susceptibility to cytotoxic T cells." (2005); *Nature. 435:682–686*. DOI: 10.1038/nature03576

Sun G., Yan J., Noltner K., Feng J., Li H., Sarkis D.A., Sommer S.S., Rossi J.J., "SNPs in human miRNA genes affect biogenesis and function." (2009); *RNA. 15:1640–1651*. DOI: 10.1261/rna.1560209

Sun Y.M., Lin K.Y., Chen Y.Q., "Diverse functions of miR-125 family in different cell contexts." (2013); *J Hematol Oncol. 6:6*. DOI: 10.1186/1756-8722-6-6

Suzuki H.I., Katsura A., Yasuda T., Ueno T., Mano H., Sugimoto K., Miyazono K., "Small-RNA asymmetry is directly driven by mammalian Argonautes." (2015); *Nat Struct Mol Biol. 22:512–521*. DOI: 10.1038/nsmb.3050

Svoronos A.A., Engelman D.M., Slack F.J. "OncomiR or tumor suppressor? The duplicity of microRNAs in cancer." (2016); *Cancer Res.76(13):3666–3670*. DOI: 10.1158/0008-5472.CAN-16-0359

Terasawa K., Shimizu K., Tsujimoto G. "Synthetic pre-miRNAbased shRNA as potent RNAi triggers." (2011); *J Nucleic Acids. 131579:1–6*. DOI: 10.4061/2011/131579

Tordonato C., Marzi M.J., Giangreco G., Freddi S., Bonetti P., Tosoni D., Di Fiore P.P., Nicassio F., "miR-146 connects stem cell identity with metabolism and pharmacological resistance in breast cancer." (2021) *J Cell Biol. 220(5):e202009053*. DOI: 10.1083/jcb.202009053

Toyota M., Suzuki H., Sasaki Y., Maruyama R., Imai K., Shinomura Y., Tokino T., "Epigenetic silencing of microRNA-34b/c and B- cell translocation gene 4 is associated

with CpG island methylation in colorectal cancer." (2008); *Cancer Res. 68:4123–4132*. DOI: 10.1158/0008-5472.CAN-08-0325

Treiber T., Treiber N., Meister G., "Regulation of microRNA biogenesis and its crosstalk with other cellular pathways." (2019); *Nat Rev Mol Cell Biol. 20:5-20*. DOI: 10.1038/s41580-018-0059-1

Ulitsky I., Shkumatava A., Jan C.H., Sive H., Bartel D.P., "Conserved function of lincRNAs in vertebrate embryonic development despite rapid sequence evolution." (2011); *Cell. 147:1537–1550*. DOI: 10.1016/j.cell.2011.11.055

Van den Beucken T., Koch E., Chu K., Rupaimoole R., Prickaerts P., Adriaens M., Voncken J.W., Harris A.L., Buffa F.M., Haider S., Starmans M.H.W., Yao C.Q., Ivan M., Ivan C., Pecot C.V., Boutros P.C., Sood A.K., Koritzinsky M., Wouters B.G., "Hypoxia promotes stem cell phenotypes and poor prognosis through epigenetic regulation of DICER." (2014); *Nat. Commun. 5:5203*. DOI: 10.1038/ncomms6203

Varilh J., Bonini J., Taulan-Cadars M., "Role of Non-coding RNAs in Cystic Fibrosis." (2015); *Cystic Fibrosis in the Light of New Research. Chapter 12. Edited by Dennis Wat*. DOI: 10.5772/60449

Wang Z., Hou Y., Guo X., van der Voet M., Boxem M., Dixon J.E., Chisholm A.D., Jin Y., "The EBAX-type Cullin-RING E3 ligase and Hsp90 guard the protein quality of the SAX-3/Robo receptor in developing neurons." (2013); *Neuron. 79:903–916*. DOI: 10.1016/j.neuron.2013.06.035

Watson K.L., Jones R.A., Bruce A., Moorehead R.A., "The miR-200b/200a/429 cluster prevents metastasis and induces dormancy in a murine claudin-low mammary tumor cell line." (2018); *Exp. Cell Res. 369:17–26*. DOI: 10.1016/j.yexcr.2018.04.024

Wee L.M., Flores-Jasso C.F., Salomon W.E., Zamore P.D., "Argonaute divides its RNA guide into domains with distinct functions and RNA-binding properties." (2012); *Cell. 151:1055–1067*. DOI: 10.1016/j.cell.2012.10.036

Wu W., Liu S., Liang Y., Zhou Z., Liu X. "MiR-7 inhibitsprogression of hepatocarcinoma by targeting KLF-4 and promises a novel diagnostic biomarker." (2017); *Cancer Cell Int., 17(1):31*. DOI: 10.1186/s12935-017-0386-x

Wu P.H. and Zamore P.D., "To Degrade a MicroRNA, Destroy Its Argonaute Protein." (2021); *Mol Cell. 81(2):223-225*. DOI: 10.1016/j.molcel.2020.12.043.

Wyers F., Rougemaille M., Badis G., Rousselle J.C., Dufour M.E., Boulay J., Régnault B., Devaux F., Namane A., Séraphin B., Libri D., Jacquier A., "Cryptic pol II transcripts are degraded by a nuclear quality control pathway involving a new poly(A) polymerase." (2005); *Cell. 121:725–737*. DOI: 10.1016/j.cell.2005.04.030

Xie J., Ameres S.L., Friedline R., Hung J.-H., Zhang Y., Xie Q., Zhong L., Su Q., He R., Li M., Li H., Mu X., Zhang H., Broderick J.A., Kim J.K., Weng Z., Flotte T.R., Zamore P.D., Gao G., "Long-term, efficient inhibition of microRNA function in mice using rAAV vectors." (2012); *Nat Methods. 9:403–409*. DOI: 10.1038/nmeth.1903

Yamamoto S., Jaiswal M., Charng W.L., Gambin T., Karaca E., Mirzaa G., Wiszniewski W., Sandoval H., Haelterman N.A., Xiong B., Zhang K., Bayat V., David G., Li T., Chen K., Gala U., Harel T., Pehlivan D., Penney S., Vissers L.E.L.M., de Ligt J., Jhangiani S.N., Xie Y., Tsang S.H., Parman Y., Sivaci M., Battaloglu E., Muzny D., Wan Y.W., Liu Z., Lin-Moore A.T., Clark R.D., Curry C.J., Link N., Schulze K.L., Boerwinkle E., Dobyns W.B., Allikmets R., Gibbs R.A., Chen R., Lupski J.R., Wangler M.F., Bellen H.J., "A drosophila genetic resource of mutants to study mechanisms underlying human genetic diseases." (2014); *Cell. 159:200–214*. DOI: 10.1016/j.cell.2014.09.002

Yekta S., Shih I.H., Bartel D.P. "MicroRNA-directed cleavage of HOXB8 mRNA." (2004); *Science. 304:594–596*. DOI: 10.1126/science.1097434

Yi R., Qin Y., Macara I.G., Cullen B.R., "Exportin-5 mediates the nuclear export of pre-microRNAs and short hairpin RNAs." (2003); *Genes Dev. 17:3011–3016*. DOI: 10.1101/gad.1158803

Yoda M., Kawamata T., Paroo Z., Ye X., Iwasaki S., Liu Q., Tomari Y., "ATP-dependent human RISC assembly pathways." (2010); *Nat Struct Mol Biol. 17:17–23*. DOI: 10.1038/nsmb.1733

Yu F., Deng H., Yao H., Liu Q., Su F., Song E., "Mir-30 reduction maintains self-renewal and inhibits apoptosis in breast tumor-initiating cells." (2010); *Oncogene. 29(29):4194-4204*. DOI: 10.1038/onc.2010.167

Yu Q., Xu C., Yuan W., Wang C., Zhao P., Chen L., Ma J., "Evaluation of Plasma MicroRNAs as Diagnostic and Prognostic Biomarkers in Pancreatic Adenocarcinoma: miR-196a and miR-210 Could Be Negative and Positive Prognostic Markers, Respectively." (2017); *Biomed Res Int. 2017:6495867*. DOI: 10.1155/2017/6495867

Yu Y., Wu J., Guan L., Qi L., Tang Y., Ma B., Zhan J., Wang Y., Fang W., Zhang H., "Kindlin 2 promotes breast cancer invasion via epigenetic silencing of the microRNA200 gene family." (2013); *Int J Cancer. 133:1368–1379*. DOI: 10.1002/ijc.28151

Zhang X., Jayaweera D., Peters J.L., Szecsi J., Bendahmane M., Roberts J.A., González-Carranza Z.H., "The Arabidopsis thaliana F-box gene HAWAIIAN SKIRT is a new player in the microRNA pathway." (2017); *PLoS One. 12(12):e0189788.* DOI: 10.1371/journal.pone.0189788.

Zhang X., Wu M., Chong Q.Y., Zhang W., Qian P., Yan H., Qian W., Zhang M., Lobie P.E., Zhu T., “Amplification of hsa-miR-191/425 locus promotes breast cancer proliferation and metastasis by targeting DICER1.” (2018); *Carcinogenesis. 39:1506–1516*. DOI: 10.1093/carcin/bgy102

Zhu Y., Lu Y., Zhang Q., Liu J.-J., Li T.-J., Yang J.-R., Zeng C., Zhuang S.-M., “MicroRNA-26a/b and their host genes cooperate to inhibit the G1/S transition by activating the pRb protein.” (2012); *Nucleic Acids Res. 40:4615–4625*. DOI: 10.1093/nar/gkr1278